

INFLUENCE OF THE PARTICLE SIZE DISTRIBUTION OF CEMENTS WITH DIFFERENT MINERAL ADDITIONS ON ITS PHYSICAL PROPERTIES

Abdelghani Nacéri *

Department of Civil Engineering, University of M'sila, Algeria

Mounir Benia

Department of Civil Engineering, University of Djelfa, Algeria

ABSTRACT

This paper presents the results of an investigation into the influence of particle size distribution (P.S.D) after different times of grinding of two types of cements with various mineral additions (slag and tuff) on its physical properties. This study analyzes the influence of particle size distribution (mean particle diameter "D₅₀") on the consistency and setting time of cement paste. The experimental work shows that cements with different mineral admixtures strongly activated have a faster process of hydration and shorter setting times. The chemical composition and particle size distribution are the process factors affecting the hydraulic reactivity of the cement.

Keywords: Laser granulometry, cement, mineral additions, physical properties.

INTRODUCTION

The fineness of cement is a property, which must be carefully controlled during the manufacturing process [1]. The total specific surface of the cement represents the surface area available for hydration. The usual method to describe the fineness of a cement is the measurement of the specific surface area. This specific surface area is just a factor and gives no information about details of the size distribution of particles of cements. That's why nowadays the particle size distribution analyzed are characterized with laser diffraction [2].

The mineral additions are largely used in the manufacture of cements with mineral additions in the world. From an economic standpoint, they present a very significant factor in the production of Portland cement with mineral admixture, since clinker consumption drops according to the content of addition used [3].

The Portland cement with mineral addition presents a hardening process slowed at its initial period in comparison with an ordinary Portland cement (cement without secondary component). This latent property of cement with mineral addition, requires the use of a efficace activation, chemical, mechanical or thermal [4,5].

The cements with mineral additions have a latent setting times than ordinary Portlands cements, especially in the case of concreting in winter [6]. It is known that setting times can be shortened [7]:

* by high fineness (specific surface) of cement,

* or by the use of accelerating admixtures (sodium hydroxide, potassium hydroxide,.....).

The objective of this study is to evaluate experimentally the influence of particle size distribution (PSD) of cements with mineral additions on the physical properties of cements (hydraulic reactivity).

* Corresponding author
Received Date: 16/10/07
Acceptance Date: 13/8/08

MATERIALS

Fine aggregates (natural sand)

The sand's equivalent measured by the NF P18 standard shows that the dune sand used in this experimental study was clean, siliceous and contains very few fine dust or clayey elements. The fineness modulus calculated was $M_f = 1,73$. This natural sand was taken from M'sila region. The absolute density and porosity were 2,56 Kg/l and 35,94%, respectively. The sand equivalent value (sight/test) was 76/77.

Cements

Two types of Portland cements (CEM II) of various cement factories (cements with various mineral additions : slag and tuff) were used in this experimental study who are :

- * CEM II/A of Sour-El-Ghozlane (clinker : 85%, gypsum : 5% and tuff : 10%).
- * CEM II/B of Hadjar-Soud (clinker : 65%, gypsum : 5% and tuff : 30%).

These two types of cements studied are CEM II/A (CEM II-SG) and CEM II/B (CEM II-HS), which presents different chemical compositions (different clinkers and mineral additions). Each type of the used cement was ground in a grinder in order to obtain various fineness (different specific surfaces) with different particle sizes while varying the time of grinding from 15 to 45 minutes:

- 1st fineness (SSA₁ or F₁): time of grinding 15 minutes.
- 2nd fineness (SSA₂ or F₂): time of grinding 30 minutes.
- 3rd fineness (SSA₃ or F₃): time of grinding 45 minutes.

The chemical composition of the two types of cements used in this research have been determined by the testing method "X-ray Fluorescence Spectrometry (XRF)". Table 1 gives the chemical composition of the oxides present of the two cements used in this experimental work. We used two types of cement (CEM II) manufactured with different mineral additions (slag and tuff), this in the aim of analyzing the influence of the fineness (specific surface area) and particle size distribution of hydraulic cements at various mineral additions on the physical characteristics of hydraulic cements at anhydrous state and the hydrated state. The fineness (specific surface area) of hydraulic cement with mineral admixtures studied was determined by Air Permeability Apparatus. The particle size was measured by means of laser diffraction method. The main parameters that characterize the particle size distribution and the BET specific surface area are shown in Table 2. Figure 1 shows the particle size distribution obtained from laser granulometry at different specific surfaces areas of two cements powders used in this study (CEM II-SG for SSA₁, SSA₂ and SSA₃ and CEM II-HS for SSA₁, SSA₂ and SSA₃).

Table 1: Chemical composition of the two cements studied

Types of cements used	SiO ₂ (%)	Al ₂ O ₃ (%)	Fe ₂ O ₃ (%)	CaO (%)	MgO (%)	K ₂ O (%)	Na ₂ O (%)	SO ₃ (%)
CEM II/A or CEM II-SG	23,48	5,63	3,28	60,60	1,38	0,97	0,19	1,18
CEM II/B or CEM II-HS	24,77	5,81	3,68	64,03	1,19	0,93	0,19	1,19

Table 2: Particle size parameters and specific surface area of the two cements used

Types of cements used	D ₁₀ (μm)	Median size D ₅₀ (μm)	D ₉₀ (μm)	Specific surface area S.S.A (cm ² /g)
				Blaine fineness
CEM II/A or CEM II-SG	0,70	19,14	79,08	3226 for SSA ₁
	0,57	15,72	64,69	4452 for SSA ₂
	0,48	12,72	48,12	5038 for SSA ₃
CEM II/B or CEM II-HS	0.54	16,98	60,28	3442 for SSA ₁
	0,48	14,84	56,93	4484 for SSA ₂
	0,42	12,89	49,53	5068 for SSA ₃

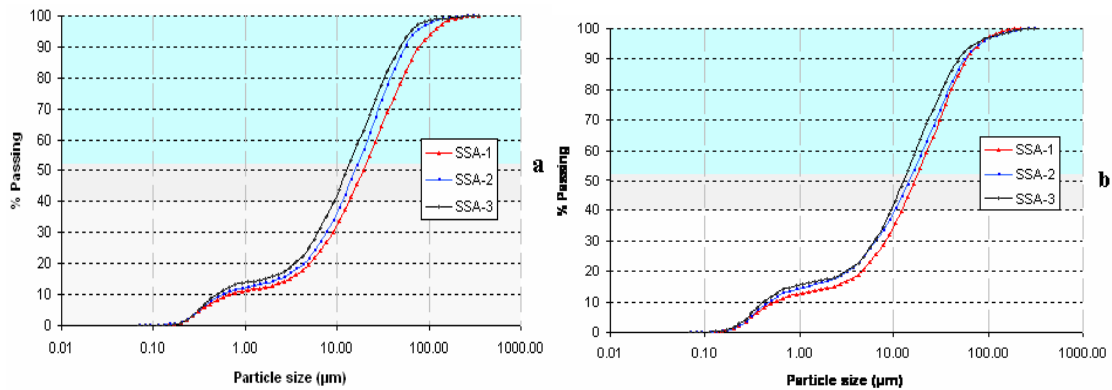


Fig. 1: Particle size distribution of cement studied at different specific surfaces areas
(a) CEM II-SG (SSA₁, SSA₂ and SSA₃)
(b) CEM II-HS (SSA₁, SSA₂ and SSA₃)

RESULTS AND DISCUSSION

Influence of the grinding time on the particle size of cement

The influence of the time of grinding on the different characteristic particles sizes D₁₀, D₉₀ and the mean particle size D₅₀ is shown in Figure 2 of the two cements studied. The D(0.1), D(0.5) and D(9.0) values indicate that 10% (D₁₀), 50% (D₅₀) and 90% (D₉₀) of the particles measured were less than or equal to the size stated.

The increase of the duration of grinding caused the follows :

* for the cement (CEM II/A or CEM II-SG), the D₁₀, the mean particle size (D₅₀) and D₉₀ was between 0.5 to 0.7 μm, 13 to 20 μm and 48 to 79 μm.

* for the cement (CEM II/B or CEM II-HS), the D₁₀, the mean particle size (D₅₀) and D₉₀ was between 0.4 to 0.6 μm, 13 to 17 μm and 50 to 60 μm.

* The increase of the time of grinding causes the decrease of the particle size parameters and the increase of the Blaine fineness for the two cements tested.

This study shows that in case of clinker-natural pozzolan (tuff) mixes and slag-clinker mixes, clinker can grind slightly with natural pozzolan, and slag can grind highly with the clinker. The pozzolanic and grindability properties of the cements were shown to be important for using in blended cement production.

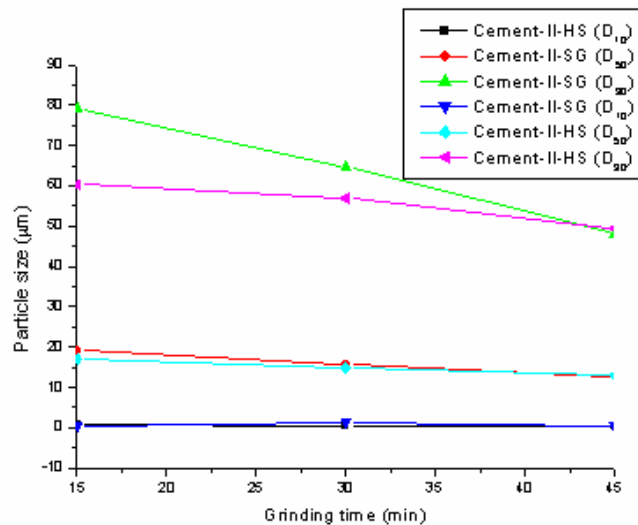


Fig. 2: The effect of the grinding time on the particle size of cements tested

Influence of the mean particle size on the cement paste

Figure 3 presents the effect of mean particle size on the normal consistency (water demand ratio) of cement paste. The cements paste are prepared with three different finenesses (SSA_1 , SSA_2 and SSA_3) and the water demand is measured using the Vicat test. The influence of the mean particle size on the cement paste is expressed by the change in normal consistency (water demand ratio). The variation of the particle sizes affects the water demand ratio (normal consistency).

It is noticed also that the granulometry of cement has a significant influence on the normal consistency of cement paste (water demand ratio), this is translated by increase of the total surface area of the particles when the cement is ground more finely (high fineness).

The initial and final setting times of cements paste according to the mean particle size are shown in figures 4 and 5. When the fineness increased of cement, the initial and final setting times of cement paste are decreased. In general, the setting time of cement paste is shortened with the increase of fineness. The finer particles cause a very short reaction of hydration with a high release of heat during the chemical reaction.

That is explained by the fact that the pozzolanic reactivity is accelerated in the short-term. The kinetics of hydration of the binder becomes increasingly fast according to the increase of the Blaine fineness (specific surface) of cement. Indeed, the very fine particles adhere the some to the others and activate the phenomenon of setting time of cement paste. Thus the effect of the Blaine specific surface on the acceleration of the pozzolanic activity reacts with the calcium hydroxide [$Ca(OH)_2$, Portlandite] to form C-S-H gel crystals.

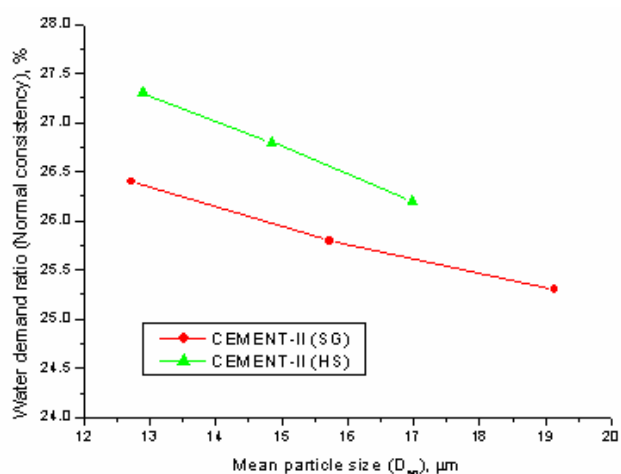


Fig. 3: The effect of the mean particle size on the normal consistency (water demand ratio) of cements studied

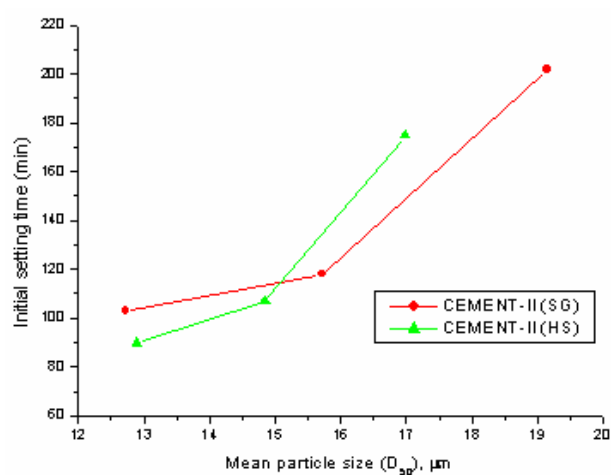


Fig. 4: The effect of the mean particle size on the initial setting time of cements studied

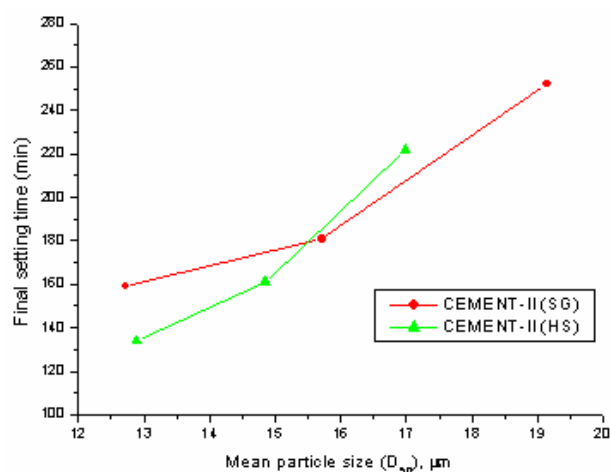


Fig. 5: The effect of the mean particle size on the final setting time of cements studied

CONCLUSION

The particle size of all cements with mineral admixtures (slag and tuff) influence directly the hydration process. The higher specific surface area, produced by the reduction of the particle size of the cement powder, strongly accelerates the reaction kinetics of the cement. This was accompanied with a substantial decrease in setting time.

ACKNOWLEDGMENTS

The authors gratefully acknowledge technical support from the Geomaterials Laboratory of M'sila University and the Cement factories of Sour-El-Ghozlane and Hadjar-Soud.

REFERENCES

1. A.K. SCHINDLER and K.J. FOLLIARD, (2003), "Influence of supplementary cementing materials on the heat of hydration of concrete", Advanced in Cement and Concrete IX Conference, Colorado, pp. 10-14.
2. J. BENSTED, (1981), "Hydratation of Portland cement", Advances in Cement Technology, New York Press, pp. 307-347.
3. A. NACERI and I. MESSAOUDENE, (2006), "The chemical and physical effects of the granulated blast furnace slag on concrete compressive strength", World Journal of Engineering, Vol. 3, No 3, pp. 43-51.
4. S. CAIJUN, (2001), "An overview on the activation of reactivity of natural pozzolans", Canadian Journal of Civil Engineering, pp. 778-786.
5. R. KARA ALI, (2002), "Influence des additions minérales sur le besoin en eau et les résistances mécaniques des mélanges cimentaires", Thèse de Doctorat, Université de Cergy-Pontoise.
6. ABDELRAZIG, BEI., MAIN, SD. and NOWELL, DV. (1992), "Hydration studies of modified OPC pastes by differential scanning calorimetry", Journal of Thermal Analysis, Vol. 38, pp. 495-504.
7. P. TIKALSKY and R.L FREEMAN, (1998), "The effect of pouzzolan and slag on the resistance of concrete", Master's Thesis, University of Texas.

EVALUATION OF MECHANICAL PROPERTIES OF RECYCLED AGGREGATE FOR STRUCTURAL APPLICATIONS

Sherif Yehia*

Associate Professor, Western Michigan University, 1903 W. Michigan Ave, Kalamazoo, MI 49008-5316, e-mail: sherif.yehia@wmich.edu

Sajjad Khan

Project Engineer, Leland Saylor Associates, San Francisco, CA 94105, USA

Osama Abudayyeh

Professor, Western Michigan University, 1903 W. Michigan Ave, Kalamazoo, MI, 49008- 5316, e-mail: osama.abudayyeh@wmich.edu

ABSTRACT

Recycling aggregates from construction and demolition waste can have positive environmental, economical, and engineering benefits if proper quality of the aggregate is assured. One problem with the use of recycled aggregates (RA) from concrete structures is that the quality of the aggregate can vary due to many factors that affect the consistency, properties, and quality such as: 1) the type of concrete that is recycled; 2) the stresses, conditions, and environment it has endured during its lifespan; 3) the way it is crushed and processed; and 4) the cleanliness of the new, recycled product. Many research efforts have demonstrated an inverse relationship between the amount of RA used and the quality of the new concrete mix.

An experimental investigation to determine the optimum volumetric ratio of the recycled aggregates that can be used in concrete mixes for structural applications is conducted. The mechanical properties of the optimized mix are then evaluated and discussed.

Keywords: Recycled Aggregates, Optimization, Physical Properties of RA, Mechanical Properties, Freeze and Thaw, Shrinkage.

RESEARCH SIGNIFICANCE

Several engineering, economical, and environmental benefits may be gained by utilizing recycled aggregate in concrete applications. The main goal of the investigation presented in this paper is to evaluate the feasibility of utilizing recycled aggregate in concrete mixes for structural applications as opposed to accepted non-structural ones. Therefore, the objectives of this research project are to:

- Determine the optimum volumetric ratio of the recycled aggregate that can be utilized in concrete mixes while achieving concrete properties similar to the mixes that use virgin aggregates.
- Evaluate the physical and mechanical properties of the recycled aggregate before use in structural applications.

Properties of Recycled Aggregate

Many research projects have demonstrated an inverse relationship between the amount of RA used and the quality of the new concrete mix. Olorunsogo and Padayachee^[1] studied the durability of concrete made with RA using durability indexes.

* Corresponding author
Received Date:4/6/08
Acceptance Date:30/7/08

They found that the durability index decreased as the percent of RA substituting the natural aggregates increased^[1]. Gómez-Soberón^[2] found that the porosity of concrete increases considerably when natural aggregates are substituted by RA. He also noted a reduction in the mechanical properties when RA is used in place of natural aggregate^[2]. Poon et. al.^[3] studied the influence of RA moisture content on the compressive strength of the concrete. Their results indicated that 50% substitution of natural aggregates by RA in its air-dried state was the optimal moisture state for producing normal strength concrete^[3]. Levy and Helene^[4] analyzed the water absorption, total pore volume, and carbonation of concrete mixes with varying percentages of RA. The behavior of several concrete mixes using a mix design nomogram was evaluated. The nomogram results showed that the concrete mix with the highest pore volume and same compressive strength did not always correspond to the concrete mix with the highest degree of carbonation^[4].

EXPERIMENTAL INVESTIGATION

Recycled aggregate is exposed to many different detrimental environmental conditions. It is essential to evaluate the physical and mechanical properties which include: specific gravity, water absorption, moisture content, size, shape, texture, durability, and strength. In addition, the optimum percentage of recycled coarse aggregates which can be used to place the virgin aggregates while maintaining similar physical and mechanical properties of concrete needs to be determined. Therefore, the experimental program consists of three phases:

1. Phase I: evaluation of the material properties
2. Phase 2: optimization
3. Phase 3: extensive evaluation of the mechanical properties of the optimized mix

Phase I: Evaluation of the Material Properties

Evaluation of the physical properties of recycled aggregate was conducted in phase I. The evaluation included specific gravity, water absorption, moisture content, size, shape, and texture of the recycled aggregate.

- *Materials:* Coarse aggregate used in this study was recycled from a demolished highway (I-69) near Calhoun County, Michigan. Fine materials, soil, and large pieces of rocks were removed during the recycling operation.
- *Shape and texture of aggregate:* The particle shape and outer surface texture of coarse aggregate influence the properties of the concrete mix^[5]. Generally, the rough and angular aggregates require more water and cement for workability to maintain the water-to-cement ratio as compared to round aggregates. Recycled coarse aggregate used for laboratory testing had aggregates of angular and irregular textures.
- *Graduation and particle size:* The un-sieved recycled aggregate contained about 40% of undesired materials, which can affect the results, quality, and durability of concrete. Therefore, the recycled aggregate used in this study was sieved in two stages. In the first, aggregates were sieved between two sieves: 25mm and 9 mm (1 in. and $\frac{3}{8}$ in.) to eliminate coarse aggregates greater than 25mm (1 in.) and fine materials less than 9mm ($\frac{3}{8}$ in.). Figure 1 shows sample of the recycled aggregate before and after sieving. In the second stage, the sieve analysis for recycled and virgin aggregates were performed in accordance with ASTM^[6] C 136 specification. The gradation curve for the first stage shows that recycled aggregate has more fine materials than virgin aggregate as shown in Figure 2. The gradation curve of the sieved recycled aggregate, as shown in Figure 2, was much closer to that of virgin aggregate as compared to the un-sieved recycled aggregate.
- *Specific Gravity, Water Absorption, and Moisture Content:* Specific gravities for both recycled and virgin aggregates were evaluated in accordance with ASTM C 127 specification. These values had small variation when compared to virgin aggregate and were consistent with results found in the literature^[7,8,9]. Values of moisture content and water absorption play important roles in determining the amount of water required for a concrete mix design. Therefore, these properties were calculated and considered during mix design. Moisture content tests for both recycled and virgin aggregates were performed in accordance with ASTM C-566 specification. It was

found that recycled aggregate has a higher absorption rate and higher moisture content than that of the virgin. Table 1 summarizes some of the physical properties for both aggregates.

Table 1: Comparison of Physical Properties of Aggregates

Physical properties	Recycled aggregate	Virgin aggregate
Bulk specific gravity	2.27	2.49
Bulk specific gravity (SSD)	2.33	2.54
Apparent specific gravity	2.55	2.67
Water absorption	6.5 %	3.2 %
Moisture content	10 %	4 %



Fig 1: Recycled Aggregate Before and after Sieving

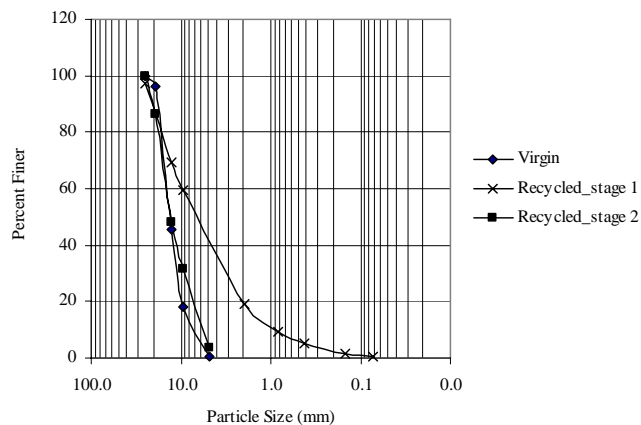


Table 2: Summary of the Optimization Results

Recycled Aggregate (%)	Virgin Aggregate (%)	Fly Ash (%)	Target Strength MPa (psi)	Target Slump mm (in.)	High cement content			Low cement content		
					Slump mm (in)	28-day MPa (psi)	56-day MPa (psi)	Slump mm (in)	28-day MPa (psi)	56-day MPa (psi)
100	0	25	31 (4500)	76 (3) [without fly]	0	41.3 (5989)	42.1 (6109)	63 (2.5)	25 (3633)	26.6 (3856)
75	25	25			51 (2)	44.2 (6405)	44.3 (6418)	63 (2.5)	28 (4058)	29.4 (4261)
50	50	25			76 (3)	51.8 (7446)	51.6 (7490)	76 (3)	41 (5950)	41.9 (6072)
30	70	25			146 (5.75)	53 (7694)	53.6 (7781)	101 (4)	42 (6118)	43.6 (6324)
0	100	25			150 (6.0)	53.5 (7756)	53.9 (7826)	125 (5)	46.6 (6756)	43.6 (6911)
100	0	0			0	29.9 (4342)	30.7 (4452)	N/A	--	--
75	25	0			5 (0.2)	34.8 (5056)	36.4 (5281)	N/A	--	--
50	50	0			40 (1.6)	44.2 (6413)	45 (6572)	N/A	--	--
30	70	0			63 (2.5)	44.6 (6872)	48 (6983)	N/A	--	--
0	100	0			76 (3)	51.9 (7540)	53 (7713)	N/A	--	--

Table 3: The Optimized Mix with Substitution of 50% Recycled Coarse Aggregate

Type I cement	191 kg (421 lbs)
Fine aggregate (Sand)	581 kg (1282 lbs)
Recycled aggregate	406 kg (896 lbs)
Virgin aggregate (Lime Stone)	406 kg (896 lbs)
Fly ash type F	64 kg (143 lbs)
Mixing water	116 kg (256 lbs)

Phase 3: Evaluation of the Mechanical Properties of the Optimized Mix

In this phase, the optimized concrete mix with 50% recycled aggregates has been tested extensively to evaluate its mechanical properties. Two cubic yards were prepared by a local ready mix producer using recycled aggregates from the same source used in the optimization phase. No air-entraining agent or superplasticizers were used with the optimized mix. However, the objective is to evaluate the performance of the recycled aggregate concrete under extreme conditions, especially during the rapid freeze and thaw resistance. Again, all material tests were conducted in accordance with ASTM^[6] specifications and the results were compared with the values found in the literature for recycled aggregates and conventional concrete.

The evaluation of mechanical properties of the optimized concrete mix with recycled aggregate included the determination of the compressive strength, flexural strength, rapid freeze and thaw resistance, drying shrinkage, modulus of elasticity, and alkali silica reactivity. Table 4 provides test names, ASTM number, specimen dimensions, number of specimens, and age of concrete during the test.

Compressive Strength: All specimens were moisture cured till testing dates. Three 150 mm x 300 mm (6 inch x 12 inch) cylinders were tested at every testing age and the average of these results were recorded. Table 5 summarizes the strength development with time. In addition, the results were compared with the available results found in the literature. Results of the compressive strength met the design requirements, and were consistent with the results found in the literature.

Modulus of Elasticity: 150 mm x 300 mm (6 inch x 12 inch) cylinders were tested to compute Chord Modulus of Elasticity of recycled aggregate concrete at 7, 14, 21 and 28 days. The modulus of elasticity (see Table 6) of concrete with 50% recycled aggregates at 28 days was 6% less than that calculated by the ACI equation[13]

$$(E_c = w_c^{1.5} \times 33\sqrt{f_c'})$$

and 3% less than that found in the literature[7,9]. Where f_c' = specified compressive strength of concrete; w_c = Unit weight of concrete lb/ft³ unit weight

Table 4: Summary of Material Testing

Test	Test specifications	Specimen size	No. of specimens per test	Test date since casting
Compressive strength	ASTM C 39-99	Cylinder 150 mm x 300 mm (6 in x12 in)	3	3,7,14 and 28 days
Modulus of elasticity	ASTM C 469-94	Cylinder 150 mm x 300 mm (6 in x12 in)	3	7,14 and 28 days
Stress-strain relation	ASTM C 469-94	Cylinder 150 mm x 300 mm (6 in x12 in)	3	7,14 and 28 days
Flexural strength	ASTM C 78-94	Beam 530 mm x140 mm x 140 mm (5.5 in x5.5inx 21in)	3	7,14 and 28 days
Drying shrinkage	ASTM C 157-99	Prism 610 mm x 100 mm x 100 mm (4 in x 4 in x24 in)	4	Starts after 7 days
Rapid freeze and thaw resistance	ASTM C 666-97 Procedure "A"- Freezing and thawing in water	Prism 76 mm x 100 mm x 406 mm (3 in x 4 in x16 in)	8	Starts after 14 days
Alkali Silica Reactivity	ASTM C 1260	Prism (25 mm x 25 mm x 285 mm) (1in x 1 in x 11.25 in)	9	Starts after 24 hrs

Table 5: Development of Compressive Strength with Time

Age of concrete (days)	Strength recycled aggregate specimens MPa (psi)	Values found in literature MPa (psi)	Strength of conventional concrete MPa (psi)
3	27 (3928)	N.A.	N.A.
7	29 (4220)	N.A.	N.A.
14	34 (4960)	29.8 (4326) ^[2]	N.A.
28	43 (6280)	33.3 (4824) ^[2] to 38 (5520) ^[1]	46.6 (6756)

Table 6: Modulus of Elasticity of Recycled Aggregate

Age of concrete (days)	Chord modulus of Elasticity GPa (103 psi)	ACI ^[13] equation $E_c = w_c^{1.5} \times 33 \sqrt{f_c}$ GPa (103 psi)	Values found in literature GPa (103 psi)
7	27.4 (3978)	25.8 (3743)	N.A.
14	28.8 (4187)	27.9 (4058)	N.A.
28	29.7 (4305)	31.5 (4566)	30 (4420) ^[7]

Flexural Strength: Three beams with dimensions 530 mm x 140 mm x 140 mm (21 inch x 5.5 inch x 5.5 inch) were subjected to third point loading at 7, 14 and 28 days. All beams started to crack within the middle third of the span length in the tension surface. Table 7 summarizes the results of the flexural strength with time and provides a comparison with ACI equation and available data from the literature. The results show that the flexural strength of the 50% recycled aggregate is 30% higher than that predicted by the ACI equation ($7.5 \sqrt{f_c}$).

Table 7: Summary of the Flexural Strength for Recycled Aggregate Concrete with Time

Age of Concrete (days)	Modulus of Rupture MPa (psi)	Values found in literature MPa (psi)	ACI ^[13] equation $R = 7.5 \sqrt{f_c}$ MPa (psi)
7	4.6 (665)	N.A.	3.35 (487)
14	4.9 (710)	N.A.	3.64 (528)
28	5.5 (793)	4.5 (653) ^[7]	4.02 (595)

Drying Shrinkage: Four 610 mm x 100 mm x 100 mm (24 inch x 4 inch x 4 inch) prisms were cast and moisture cured for 7 days. Demac points, spaced at approximately 203 mm (8 inch), were mounted along the longitudinal direction on two perpendicular faces of each sample to monitor shrinkage, as shown in Figure 3. Specimens were kept in room temperature of approximately 23.3 °C (74 °F) and relative humidity of 70 %. Strain readings were recorded everyday for the first week, three times for the second week, and once a week after that for about two months. Shrinkage strain for the first three weeks was higher than the values predicted using ACI-209^[14]. However, after the third week the measured strain was less than that predicted by the ACI Equation, as shown in Figure 4. These results were consistent with that found in the literature^[15]. Higher absorption rate of the recycled aggregate might be the reason of higher drying shrinkage strain. This will require a detailed investigation to confirm this finding.

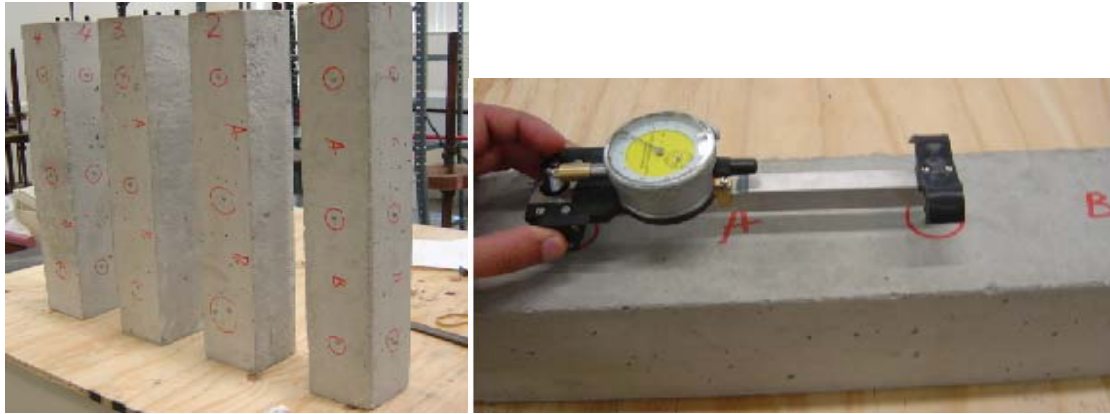


Fig 3: Measurements of Drying Shrinkage Strain

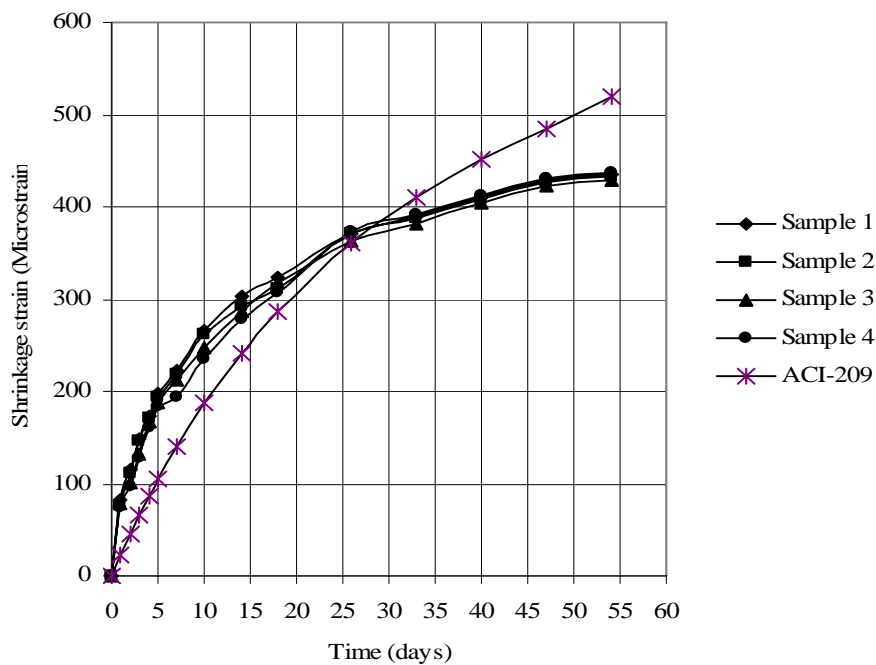


Fig 4: Shrinkage Strain for Recycled Aggregate Concrete with Time

Resistance to Rapid Freezing and Thawing: Eight samples of dimensions 76 mm x 100 mm x 406 mm (3 inch x 4 inch x 16 inch) were evaluated for resistance of rapid freeze and thaw in accordance with ASTM C 666-97 Procedure “A”- Freezing and Thawing in water. Weight, dimension, and transverse frequency were measured for each sample after every 28 to 36 cycles. No significant changes were found up to 124 cycles. However, between 156 and 222 cycles the samples started losing bond between particles and significantly losing weight, as shown in Figure 5. Four samples failed after 222 cycles, while the other four samples failed after 252 cycles.

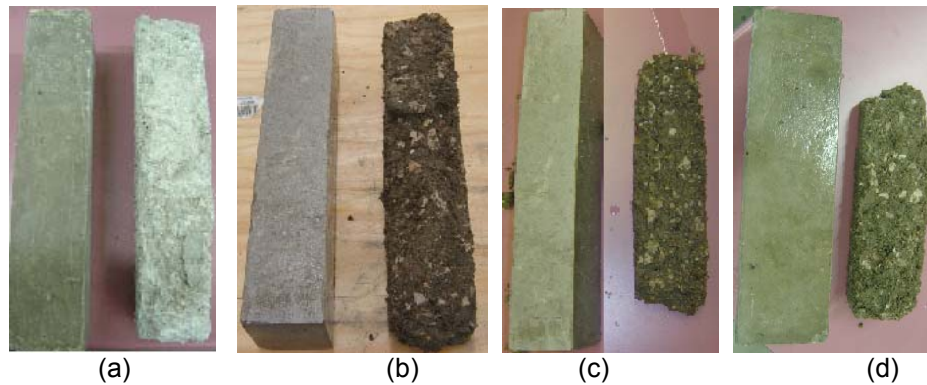


Fig 5. Concrete Samples after Certain Cycles (a): 94 cycles, (b):156 cycles (c): 222 cycles and (d):252 cycles

Evaluation of Alkali Silica Reaction: ASTM C 1260 was followed to evaluate the recycled aggregate from the same source for potential alkali silica reaction (ASR). The evaluation was conducted in four stages:

- Stage I – evaluation of ASR in recycled aggregate concrete without adding fly ash.
- Stage II and III – two percentages, 15 % and 25%, of fly ash class F were added to the mix to evaluate mitigation ability of the fly ash.
- Stage IV - a repeat of stages I, II and III with the addition of 3% deicing salt to the mixing water to simulate other environmental conditions.

Table 8 summarizes the results of the ASTM C 1260 experiments. (A detailed discussion of the results can be found elsewhere^[16].) The results indicate that recycled aggregates used in this research have higher potential for ASR. Adding 25% of fly ash F was able to mitigate the effect of ASR. Similar results were obtained from Stage IV of the study.

Table 8: Summary of Results of ASTM C 1260

Mix Description	Average Expansion (%)			Overall Average	ASTM Range
	1st set	2nd set	3rd set		
Recycled aggregate (RA)	0.272	0.245	0.242	0.253	>0.2%
RA + 15% fly ash	0.211	0.199	0.205	0.205	>0.2%
RA + 25% fly ash	0.084	0.089	0.097	0.090	<0.1%
RA + 3% salt-Normal	0.214	0.203	0.211	0.209	>0.2%
RA + 3% salt + 15 % fly ash	0.225	0.224	0.274	0.241	>0.2%
RA + 3% salt + 25% fly ash	0.112	0.063	0.098	0.091	<0.1%

DISCUSSION AND CONCLUDING REMARKS

Recycled concrete aggregates may provide another source of coarse aggregates suitable for structural applications. Table 9 summarizes the evaluation of the mechanical properties compared with the available data found in the literature.

Results from the experimental evaluation indicated that:

1. Gradation curve of the recycled aggregate needs to be evaluated to ensure having the right gradation for concrete applications. It is also important that recycled aggregate be clear from dust, fine particles, and other impurities like glass, bitumen, and wood particles.
2. Physical properties of recycled aggregates must be evaluated to adjust the mixture proportioning.
3. A 50% recycled aggregates content was found to be the optimum amount that can be used in a concrete mix for structural applications.

4. The optimized mix with 50% recycled aggregates met the design compressive and flexure strength, and modulus of elasticity specified by most DOTs. However, all samples showed higher drying shrinkage at early age, higher potential to ASR and all specimens failed at 252 cycles during the rapid freeze and thaw resistance. In addition, these properties need to be evaluated every time the source of RA is changed.
5. Using 25% of fly ash 'class F' replacement of cement by weight is an effective measure of mitigation of the ASR that does not affect other physical and mechanical properties of the concrete mixture.

Generally, recycled aggregate has the potential to be an alternative source of coarse aggregates in structural concrete mixes.

ACKNOWLEDGEMENT

The authors wish to thank Mr. Dennis Randolph, Consultant, WadeTrem, Grand Rapids and Mr. Steve Cronkite and Mr. Keith Davis of STATLER Ready Mixed Concrete in Kalamazoo, Michigan for providing timely assistance and valuable feedback during this project. Also, the authors would like to acknowledge Mr. Shadi Bajjali, former graduate student at Western Michigan University, for his contribution to the experimental investigation of this research.

Table 9: Summary of Evaluation of Mechanical Properties

Property	Behavior of recycled aggregate concrete	Comparisons with literature and conventional concrete
Compressive strength	It is in the desirable and design limits	28-day strength for concrete with 50% recycled aggregate is 43.3 MPa (6280 psi). This value is about 46.8 (6800 psi) for conventional concrete
Modulus of elasticity	Comparable to the values found in literature	28-day modulus of elasticity for the concrete with 50% recycled aggregate is 29.7 GPa (4305x103 psi.) This value is up to 30.5 GPa (4420x103 psi) found in literature and 4566x103 psi for the same concrete according to ACI ^[13] equation.
Flexural strength	Comparable to other concretes	28-day modulus of rupture value for the concrete with 50% recycled aggregate is up to 5.5 MPa (793 psi) which is comparable to the value of 4.5 MPa (653 psi) for 75% recycled aggregate found in literature
Drying shrinkage	High tendency in the early stages	High shrinkage strain compared to ACI -209 ^[14] predicted strains. But this value is lower after 33 days than the ACI limits.
Rapid freezing and thawing	Satisfactory results in the earlier stages	Good resistance up to 200 cycles of rapid freeze and thawing. In alter stage, segregation of aggregates occurred. No data found for this test of recycled aggregate in literature

REFERENCES

1. Olorunsogo, F.T. and Padayachee, N. "Performance of recycled aggregate concrete monitored by durability indexes," *Cement and Concrete Research*, 32(2), 179-185, Feb 2002.
2. Gómez-Soberón, José M.V. "Porosity of recycled concrete with substitution of recycled concrete aggregate: An experimental study," *Cement and Concrete Research*, 32(8), 1301-1311, Aug 2002.

3. Poon, C.S., Shui, Z.H., Lam, L., Fok, H., and Kou, S.C. "Influence of moisture states of natural and recycled aggregates on the slump and compressive strength of concrete." *Cement and Concrete Research*, 34(1), 31-36. (Jan 2004).
4. Levy, Salomon M. and Helene, Paulo. "Durability of recycled aggregates concrete: a safe way to sustainable development," *Cement and Concrete Research*, Emsford: Pergamon Press, v.34, n.11, p.1975-1980, (Nov. 2004).
5. Kosmatka, S., Kerkhoff, B., Panarese, W. "Design and control of concrete mixtures, 14th edition". Portland cement association, 2001.
6. American Society for Testing and Materials (ASTM), "Concrete and Aggregates," Section 4, V. 04.03, 2007.
7. Ali, M., Ansari, F., Luke, A., Zhang, G., Szary, P. (2000). "Recycled Materials in Portland Cement Concrete".
 - a. <<http://www.cait.rutgers.edu/finalreports/FHWA-NJ-2000-003.pdf>>
8. Chini, A., Kuo, S., Armaghani, J. (2001). "Tests of Recycled Concrete Aggregate in Accelerated Test Track". *Journal of Transportation Engineering* 27(6), pp 486-492.
9. Kuo, S., Chini, A., Ammaghani, J. "Testing and Evaluation of Recycled Concrete Aggregate (RCA) as Mixture and Base Material," *Materials and Construction: Exploring the Connection 1999*, ASCE, pp 704-711, March 1999.
10. Khan, S., Yehia, S., Abudayyeh, O., Jrade A., and Randolph, D., "Evaluation of Mechanical Properties of Recycled Aggregate Concrete (RCA)," Technical Report Number CEM-05-012, Western Michigan University, October 2005.
11. Verbyla, M., Khan, S., and Yehia, S., "An Investigation of Concrete Made With Recycled Concrete Aggregates From Southwest Michigan," Technical Report Number CEM-04-06, Western Michigan University, July 2004.
12. Eighmy, T., Magee, B. (2001). "The Road to Reuse". *Journal of Recycled Materials Resource Center*, University of North Hampshire, Durham, NH, 71 (9), pp 71-81.
13. American Concrete Institute (ACI 318-05), "Building Code Requirements for Structural Concrete," American Concrete Institute, Detroit, MI, 2005.
14. American Concrete Institute, ACI Committee 209R, "Creep and Shrinkage in Concrete," 1992.
15. Soberon, G., Jose, "Relationship between Gas Adsorption and the Shrinkage and Creep of Recycled Aggregate Concrete," paper ID: CCA11386, V. 25, issue 2, ASTM, (Dec 2003).<<http://journalsip.astm.org/JOURNALS/CEMENT/PAGES/102.htm>>
16. Bajjali, S., Yehia, S., and Abudayyeh, O., "Alkali Silica Reaction in Virgin and Recycled Aggregates: State of the Art and Experimental Investigation Using ASTM C 1260 and the Staining Method," Technical Report Number CEM-05-03, Western Michigan University, July 2005.

COMBINED EFFECTS OF SILICA FUME AND SLAG AGGREGATE ON MATRICES USED FOR SOLIDIFICATION OF WASTES

A. El- Dakroury*, I.S. Ibrahim , I. E. Iyob
Hot lab. Center

Atomic Energy Authority, Hot Laboratories and Center, 13759 Cairo Egypt

ABSTRACT

This paper presents a laboratory study on the influence of combining Portland cement (PC) with silica fume and ground granulated blast – furnace slag. This study includes setting times, density, compressive strength, and long- term leaching rates of the radionuclide which used as indicator of immobilization radioactive. The leaching is carried out according to the ANSI/ANS-16.1-2003 test”, The study indicates that the mechanical properties of high strength matrices were improved to a great extent at later ages when cement used in matrix was replaced by silica fume and slag by 25% by weight. The results were compared with those obtained from the blank cement that does not contain slag and silica fume

Keywords: Silica fume, blast – furnace slag, Solidification, Wastes,

INTRODUCTION

This paper is the continuation of an extensive investigation on the efficiency of different cemented matrices for immobilization radioactive liquid wastes. Each type of nuclear power plants is producing a nuclear waste stream of different salt concentration and composition. Cement is used as solidification material for the storage of these wastes. However, the retention of radionuclides, especially cesium, in the cement matrix is negligible. The sorption of cesium on cement is low and diffusivity of cesium in the hydrated cement is high only when cement is mixed with a material having a significant sorption capacity, normally bead or powder ion exchange resins. The leachability of cesium and cobalt from the cement matrix is low enough to be acceptable [1-2]. The objectives of immobilization are to convert the waste into forms which are leach resistant so that the release of radionuclides will be slow even through flowing water may contact them and mechanically, physically and chemically stable for handling, transport and disposal. Although cement has several unfavorable characteristics as a solidifying material, i.e. low volume reduction and relatively high leachability, it possesses many practical advantages: good mechanical characteristics, low cost, easy operation and radiation and thermal stability . it is generally assumed that the cement leachability of ¹³⁷Cs and other radionuclides can be reduced by adding minerals like bentonite, vermiculite ,zeolite, silica fume and the pozzolanic materials such as ground blast- furnace slag and fly ash that can react with the hydrated of cement [3-4]. Blast furnace slag has been widely used as a successful replacement material for Portland cement, improving some properties and bringing environmental and economic benefits. The production of the pig iron production has increased progressively in the recent years. Considering that approximately 300 kg of slag are produced per ton [5-7] Silica fume exhibits superior pozzolanic properties compared with other materials. This is due to its higher percentage of reactive silica and its higher surface area of its particles. The extreme of the fume allows it to react almost immediately with the calcium hydroxide formed during hydration reactions to produce additional amounts the cementing agent, dicalcium and tricalcium silicate hydrates [6 - 9] In the present study ,

* Corresponding author
Received Date:10/6/08
Acceptance Date:23/10/08

silica fume and ground blast furnace slag are simultaneously used in cement for a synergistic effect and some physical, mechanical and chemical properties of cement, including density, compressive strength, and the efficiency of the matrix for immobilizing ¹³⁷Cs as radioactive liquid. The leaching test was carried out according to ANSI / ANS-16.1-2003 test [10]

EXPERIMENTAL

Samples of cementations formulation containing content (w/c ratios of 0.40), three levels of silica fume content (5%,10%and 15%),three levels of ground granulated blast – furnace slag (GGBS)content (5%,10%and 15%) and there are two types of substitution :

15 % silica fume plus 10 % slag, and10 % silica fume plus 15 % slag. The dimensions of cement specimens are cubic specimen of 10 x10 x 10 cm for testing compressive strength and specimen of 2 x2 x 2 cm for test leaching. The cement matrices were mixed in a drum mixture and specimens were molded by vibration. After being placed at the room temperature for 24 hours, the specimens were demouled and then cured in water at the temperature of 25 ±2°C. at 3 ,7 ,28 ...and 180 days, the specimens were taken out from water for testing mechanical properties. The blank cement that did not contain slag and silica fume was marked as cement as cement. The combined blenders of silica fume and slag were used in cement at the total dosage of 25 % while replacing the same amount of cement to keep the weight of bonding materials in cement unchanged.

Materials

The cement used in this work was Normal Portland cement, manufactured by Suez Cement Company. The chemical and physical characteristic of the silica fume is given in table1. The chemical and physical characteristics of the ground granulated blast – furnace slag is given in table2.The chemical and physical characteristics of the cement are given in Table 3. Table (4) shows the cement mixture proportions. Cement mixtures were proportioned using the following materials : The specific surface area of cement ,silica fume and ground granulated blast – furnace slag were 3500 cm² / g , 18460 cm² / g and 5990 cm² / g , respectively .

Table (1) The chemical and physical characteristics of the silica fume

Chemical composition	Percentage by weight (%)
SiO ₂	90 %
Al ₂ O ₃	0.80%
Fe ₂ O ₃	1.10%
CaO	3.30%
MgO	1.70%
Physical data	
Light gray fine powder	
Specific gravity m ² / kg	was in the range of 15,000 to 25,000
Bulk density	2.20 g/cm ³

Table(2) Chemical and Physical Characteristics of Blast furnace slag(GGBS)

Chemical composition	Percentage by weight (%)
CaO	42.28
SiO ₂	33.08
MgO	6.90
Na ₂ O	0.22
K ₂ O	0.31
Al ₂ O ₃	13.93
SO ₃	2.61

Table (3)The chemical and physical characteristics of the cement

Chemical composition	Percentage by weight (%)
SiO ₂	22.7%
Al ₂ O ₃	3.3%
Fe ₂ O ₃	3.3%
CaO	63.9%
MgO	2.3%
SO ₃	2.0%
Potential compound composition	
Tricalcium silicate	52%
Dicalcium silicate	26%
Tricalcium aluminate	3%
Tetracalcium aluminoferrite	12%
Physical data	
Blaine fineness (m ² /kg)	363
Normal consistency (%)	25.6
Vicat set times (min)	
Initial	110
Final	25.6
False set	87.8%
Autoclave expansion	0.05

Table (4) Cement mixtures proportions

Batch	Mix (PC/SF/GGBS)	Label	Cement(kg/m ³)	SF(kg/m ³)	GGBS(kg/m ³)
1	100/0/0	PC	377	0	0
2	95/5/0	5F.	358	19	0
3	90/10/0	10F	339	38	0
4	85/15/0	15F	320	57	0
5	95/0/5	5G	358	0	19
6	90/0/10	10G	339	0	38
7	85/0/15	15G	320	0	57
8	90/5/5	5F+5G	339	5	5
9	80/10/10	10F+10G	300	38	38
10	70/15/15	15F+15G	263	57	57
11	75/10/15	10F+15G	282	38	57
12	75/15/10	15F+10G	282	57	38

LEACHING TEST

Several standard methods and empirical formulas used to calculate the rate of release of radionuclides into the environment have been proposed in the literature: Among these the leaching test was the ANSI/ANS-16.1-2003 test[10]. The leachant was demineralized water with a conductivity of <5μ Ohm / cm the volume of leachant to external geometric surface area of the specimen ratio of 10 cm. specimens were immersed in individual plastic containers. The leachant analyses were carried out on cubic specimens. , All prepared samples; cubic mouldes 2X2x2 cm dimension was mixed with ¹³⁷ Cs is one of the major constituents of the waste water effluents from nuclear reprocessing units. Due to long half- lives and high solubility, radioisotopes of cesium are among the most hazardous nuclides in radioactive wastes.

Samples stored in laboratory at ambient temperature for 28 days curing time. Each sample was immersed in beaker containing 80 ml time intervals. The gamma spectra of studied nuclides were measured using a gamma spectrometer with 4"x4" NaI crystal activated with thallium. A considerable amount of experimental data obtained from the samples, which maintained their dimensional integrity during leaching; indicate that internal bulk diffusion was the most likely rate- determining mechanism during the initial phases of the leaching process. Although additional mechanisms probably did occur to some extent, they are more likely to become rate determining only during later ages of leaching (19, 47 and 90 days) thus, the recommended data handling procedure of the standard was permissible, due to simplification of mass transport theory (second Fick's law at non- stationary state) , for the purpose classifying and ranking solidified wastes, according to leachability. The solution of the mass- transport equations (second Flick's law at non- stationary state), for a specimen that may be considered as a semi-infinite medium, permit the effective diffusivity to be computed by:

$$1. D_e = \pi [C_n / C_o / (\Delta t)_n]^2 [V/S]^2 T$$

$$2. T = [1/2 (t_n^{1/2} + t_n^{1/2})]^2$$

Where:

C_n = is the activity of concentration released from the specimen during the leaching interval;

C_o = is the total activity or concentration of a given ion at the beginning of the first leaching interval ;

$(\Delta t)_n$ = is the duration of the nth leaching interval in seconds;

V = is the volume of the specimen in cm³;

S = is the geometric surface area of the specimen in cm²;

T = is the cumulative leaching time representing the " mean time " of the leaching interval for a semi-infinite medium.

Generally, this method to calculate D_e is valid up to 5 days of leaching time (abbreviated test), where diffusion is the rate- determining mechanism. At this point in the test, the specimen acts like a semi infinite medium. After 5 days, the specimens, generally, acts a finite medium, being the cumulative fraction leached higher than 20 %, and other methods to calculate "D" must be used. So, for example a graphical method or interpolation. So, for example a graphical "G" can be obtained, in this case:

$$3. D_e = Gd^2 / (\Delta t)_n$$

Where

d = is the diameter of the specimen in cm, ;

G = is the dimensionless factor

As far as the leachability index 'l' is concerned, it is a normalization factor , which is related to the specific material tested :

$$4. L = \log (\beta / D_e)$$

Where

" β " is a defined constant (1.0 cm² / s). ("L")also depends on the leaching conditions and the leachant renewal schedule. Leachability studies, therefore, consider all these variables the results are applicable only to cases where all these factors are the same within certain error ranges.

RESULTS AND DISCUSSION

Compressive strength

Table (5) gives the compressive strength values of all cement mixtures. It is indicated in table 5 that at the early age (3 days) for which samples are blended with slag and silica fume, all displayed lower compressive than blank cement (PC), after 7 days of curing, these samples reached a nearly equal level of compressive strength; sample (10F+15G) had the highest strength, followed by sample (10F+10G). When silica is incorporated, the rate of cement hydration increases at the early hours due to the release of CH- ions and alkalis into the pore fluid. The increased rate of hydration may be attributed to the ability of silica fume to improve nucleating sites to precipitating hydration products like lime, C-S-H, and entraining. It has very

significant that non - evaporable water content decreases between 90 and 550 days at low water / cement ratio with the addition of silica fume. The presence of slag in mortars acts as a sink for crystallized Ca (OH)₂ and lowers the permeability of the cement paste. It has been generally that the strength development in the cement composites incorporated with silica fume is due to mainly to the pore size refinement and matrix deification, reduction of Ca (OH)₂ content, and strong cement paste-gel and more homogeneous product at the interfacial zone leads to the rapid strength development of mortar at the early ages . This has been due mainly to the nucleation of CH crystals around silica fume particles around slag. The pore structure of cement paste the silica fume cementations product increases as the slag content increases [6-11]

Table (5) Compressive strength (MPa) of cement

Batch	Mix (PC/SF/GGBS)	Label	3 days	7days	28 days	60 days
1	100/0/0	PC	43.1	51.5	64.5	73.2
2	95/5/0	5F.	32.1	52.3	69	73
3	90/10/0	10F	38.3	56	71	76.1
4	85/15/0	15F	34.4	49	63	72
5	95/0/5	5G	33.2	52.7	66	75
6	90/0/10	10G	34.3	54.1	68	77
7	85/0/15	15G	39.2	55	67	78.1
8	90/5/5	5F+5G	35.1	55.9	71	78
9	80/10/10	10F+10G	37.3	58	73	79
10	70/15/15	15F+15G	38.2	56	69.2	84
11	75/10/15	10F+15G	39.3	60	75.1	87.2
12	75/15/10	15F+10G	37.3	56.2	70	82

Leaching analyses

The effective diffusion coefficients (De), together with other measured parameters for each leaching interval are given in the table (6-7). The cumulative fraction leached of cesium is presented in the fig 2, where it has been included, for comparison, between PC and (10F+15G). As can be seen, the matrix PC has, during the abbreviated test (up 5 to days), lower values of cumulative fraction leached (CFL) values of ¹³⁷Cs than those of matrix (10F+15G). Nevertheless, after 5 days a plateau of stabilization of (CFL) values of the M1 matrix increase along leaching time following a straight line (up to 90 days), which seems to show that the only leaching mechanism of ¹³⁷Cs is diffusion controlled . The mean effective diffusion coefficient (De), up to 90 days, is 2.7 e-09 cm²/ s for PC matrix and that of (10F+15G), matrix during 5 days of leaching was 1.8e-08 cm²/s. The kinetic of the process is lower at longer leaching time , decreasing the corresponding De values up to 5.7 e-12 cm²/s , for the (10F+15G), matrix at 180 days of leaching . The mean leachability index (L) is used to catalogue the efficiency of a matrix material to solidify a waste , being the value of 6 a the threshold to accept a given matrix as adequate for the immobilization of nuclear wastes (ANSI/ANS-16.1, 2003) As it is shown in table (7), the mean leachability index (L) is 7.8 (during the first 5 days) consequently Leaching analyses of matrixes , (10F+15G); (75/10F/15G) and Leaching analyses of PC: (100/0/0) were show in tables(7, 8), the matrix can be catalogued as an efficient material for immobilization cesium from nuclear wastes [13-15].Silica Fume (SF) active mineral admixture used in cement concrete products. It has a good effect on the mechanical properties of the cement. However, SF blended cement has a poorer fluidity compared to PC under the condition which used the same amount of superplactisizer. However, this can be improved by adding ultra-fine slag. By incorporating 15% (GGBS) and 10% (SF) into PC, not only the fluidity of blended cement was improved, but also the 28-day compressive strength of the cements was enhanced and higher decreasing in leachability of ¹³⁷ Cs ion . SF is a high active pozzolanic mineral admixture and slag is a latent hydraulic mineral. The former can prompt the hydration of PC, shorten the setting time of cement, increase the water requirement, and increase the fluidity losing of the fresh paste. However, (GGBS) can defer the reaction of cement hydration and prolong the setting time of cement paste. Both SF and (GGBS) can react with CH released by cement

hydration to produce secondary C-S-H gel inside the cement paste. The secondary formed C-S-H gel improves the microstructure of cement paste matrix; therefore, the macroscopic property of cement was also improved. Than obtained from these studies, the effect of a double activator was found to be better than a single one, causing "the complementary advantage for each other.

Effect of ground granulated blast – furnace slag (GGBS)

The slag that is used in blended cements is a non-metallic mineral byproduct formed when iron is produced in a blast furnace. It does not come from steel or non-ferrous material production. It is produced simultaneously with iron at around 1500 °C It is taken off and cooled in a controlled manner. If cooled slowly it forms a material that is useful for aggregate but of no practical use for cement. If rapid quenching with water is applied it solidifies into a glassy material which, when ground, results in a product that possesses latent hydraulic similar to Portland cements. The end product is a complex material consisting mainly of calcium silicates and calcium aluminates. Putting it simply, it is used to produce hydraulic cement which can be used in the same way as other Portland Cements. The calcium hydroxide which is produced as a by product of Ordinary Portland. Cement hydration reaction is used as the activating component in ground blast furnace slag. One interesting feature which is worthy of highlighting is the fact that the lime formed by the cement hydration is the weakest link in the hydrated cement matrix. The maximum level of ground granulated blast – furnace slag (GGBS) is 15 % by total solid mass used in this study was restricted by workability of the final product. The result shown in Fig (1) illustrates that little reduction in ¹³⁷Cs leachability is achieved by increase (GGBS) up to 15% these due to glassy reaction of GGBS)[10-14]

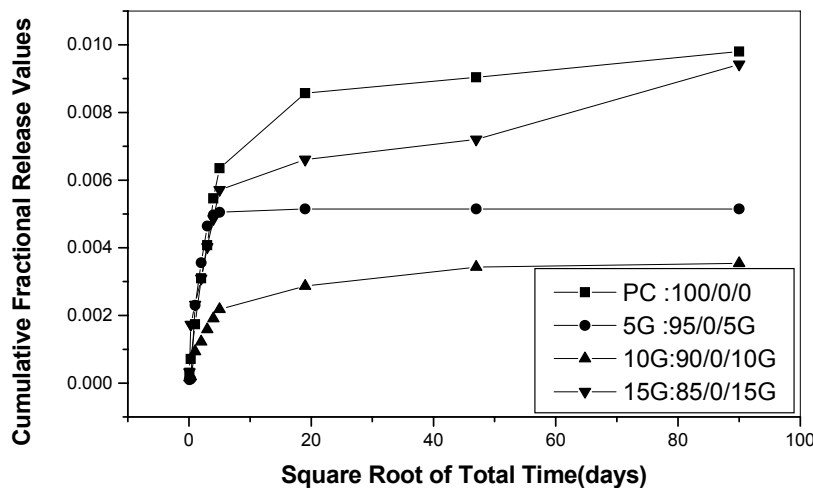


Fig (1) Effect of (GGBS) content on the leachability of ¹³⁷Cs

Effect of silica fume (SF)

The results show a decrease in ¹³⁷Cs leachability of a cement formulation this effect, as illustrated in Fig (2). Due to extreme fineness and high silica content, silica fume is a highly effective pozzolanic material. Silica Fume is used in concrete to improve its properties. It has been found that silica fume improves compressive strength, bond strength, and abrasion resistance, reduces permeability, and therefore helps in Protecting reinforcing steel from corrosion .The superfine size of the condensed silica fume particles , 100 times finer than cement, combined with the very high content of reactive silica (> than 85% by weight) , gives a powerful pozzolanic effect . The pozzolanic reaction of the condensed silica fume increases the calcium silicate hydrates (C-S-H) in the hardened concrete. There is a distinct change in the refinement of the pore structure in the condensed silica fume concrete giving less of the capillary pores and more of finer gel pores due to the void filling action. Although the nature of the hydration products of [15] and its influence on cement hydration are not fully understood at

present, the effect is a refinement of the pore structure when is added to the cementations system. This leads to a reduction in permeability and hence the enhancement of the mechanical properties and durability of concrete containing silica fume. Silica fume has been used as an addition to concrete up to 15 percent by weight of cement, although the normal proportion is 7 to 10 percent. With an addition of 15 percent, the potential exists for very strong and brittle concrete. It increases the water demand in a concrete mix, however, dosage rates of less than 5 percent will not typically require a water reducer. High replacement rates will require the use of a high range water reducer. Concrete incorporating more than 10% silica fume becomes sticky,

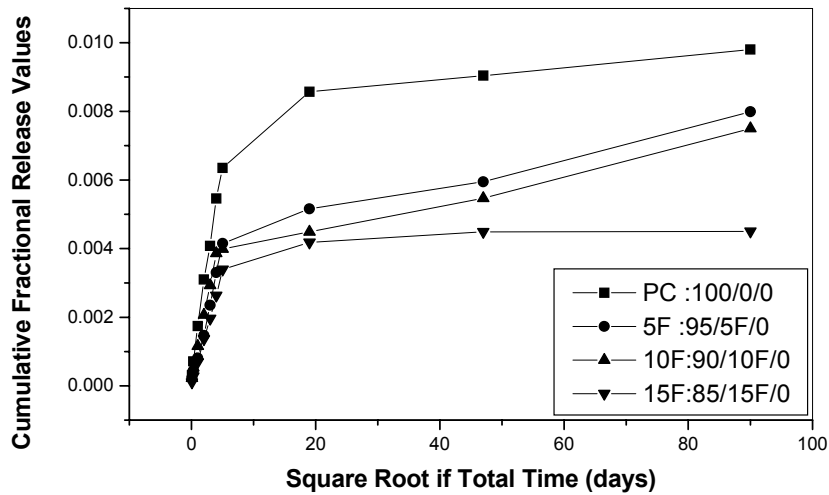


Fig (2) Effect of (SF) content on the leachability of ¹³⁷Cs

Effect a Combined Effects of Silica Fume (SF) and ground granulated blast – furnace slag (GGBS)

Decreasing in leachability of ¹³⁷ Cs ions with increasing the content of (SF) up to 10 % and (GGBS) up to 15 % it is occurs and clear from show the result in Fig (3) and table (6) From the result obtained from these studies, the effect of a double activator was found to be better than a single one, causing the complementary advantage for each other.

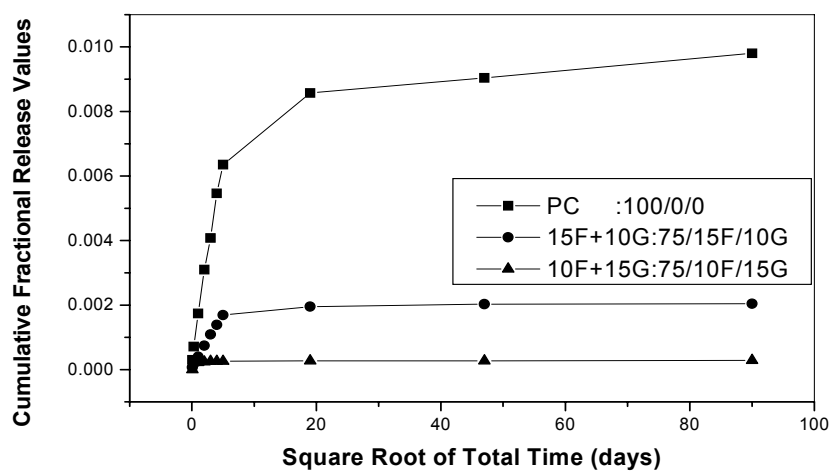


Fig (3) Effect of combined (SF) and (GGBS) content on the leachability of ¹³⁷Cs

Table (6) Leaching analyses of ;(75/10F/15G)

$(\Delta t)_n$	C_n	F_n	F	D_e	L	R ng/cm ² .day
0.08	0.17	0.01	.010	1.0e-08	8.0	1.3e-06
0.29	0.20	0.012	.022	1.9e-08	7.7	6.2e-07
1	0.46	0.027	.049	3.3e-08	7.5	4.5e-07
2	0.42	0.025	.073	3.3e-08	7.5	2.9e-07
3	0.22	0.013	.086	1.5e-08	7.8	1.5e-07
4	0.15	0.009	.095	1.0e-08	8.0	1.0e-07
5	0.08	0.005	.100	3.5e-08	8.5	5.3e-08
18	0.11	0.007	0.106	9.6e-11	10.0	5.8e-08
29	0.04	0.002	0.109	3.0e-11	10.5	2.2e-09
60	0.05	0.003	0.111	1.4e-11	10.9	1.1e-09
90	0.04	0.002	0.114	1.7e-11	10.8	9.3e-10
180	0.05	0.003	0.117	5.7e-12	11.3	4.0e-10

Mean leachability index , $L_i = 7.8$

Confidence range (99.9%)

Correlation coefficient, $r = 0.1$

Standard deviation, $\sigma: 0.3$

Table (7) Leaching analyses of PC: (100/0/0)

$(\Delta t)_n$	C_n	F_n	F	D_e	L	R ng/cm ² /day
0.08	0.052	0.0031	0.0031	1.0e-09	9.0	1.3e-07
0.29	0.063	0.0037	0.0068	2.1e-09	8.7	6.2e-07
1	0.13	0.0074	0.014	2.3e-09	8.6	4.5e-07
2	0.13	0.0077	0.022	3.2 e-09	8.5	2.9e-08
3	0.12	0.0071	0.029	4.5e-09	8.3	1.5e-08
4	0.12	0.0068	0.042	5.8 e-09	8.2	1.0e-08
5	0.11	0.0062	0.067	6.1e-09	8.2	5.3e-08
18	0.44	0.0062	0.068	1.5 e-09	8.8	5.8e-08
29	0.32	0.019	0.116	2.5 e-09	8.6	2.2e-08
60	0.50	0.030	0.139	1.4 e-09	8.9	1.1e-08
90	0.39	0.023	0.139	1.6 e-09	8.8	9.3e-09
180	0.52	0.031	0.169	5.5 e-10	9.3	4.0e-09

Mean leachability index , $L_i = 8.5$

Confidence range (99.9%)

Correlation coefficient, $r = 0.9$

Standard deviation, $\sigma: 0.3$

Where

$(\Delta t)_n$: days

C_n : g/kg is the activity released from the specimen during the n the leaching interval

C_0 : is the total activity of given ion at the beginning of the first leaching interval = 17 g/kg for two masteries

F_n : C_n/C_0

F : $\sum C_n/C_0$

D_e : The diffusion coefficient cm²/s;

L : mean leachability index, = 7.8 for matrix M11 .8.5 for matrix M1

R_n : leaching rate g / cm² / day

CONCLUSIONS

- The incorporation of silica fume in concrete mixes resulted in finer pore structure thus producing low permeability concrete. The superfine size of the condensed silica fume particles of reactive silica (>than 85% by weight), gives a powerful pozzolanic effect. The pozzolanic reaction of the condensed silica fume increases the calcium silicate hydrates (CSH) in the hardened concrete.

- The use of ground granulated blast furnace slag as a supplementary cement material improved the characteristics of the pore structure when appropriate water curing was carried out. The longer curing durations reduces permeability and results in finer pore structure. This is very important for concrete directly exposed to aggressive environments
- Generally the addition of silica fume to ground granulated blast furnace slag was increased, the strength of concrete and increase the CSH leads to a reduction in capillary pores and increased impermeability. This effect gives a concrete with increased resistance to chemical attack; water penetration, sulphates, chlorides, organic materials and acids, then decreases the leaching rate of ^{137}Cs ions in comparison to different matrices
- More than one mineral admixture are usually used together and combined with chemical admixtures to produce concrete with various strength and durability levels.

REFERENCES

- 1- Andersson K, Torstenfelt B and Allard B, 1981 " Diffusion of cesium in concrete , " in Scientific for nuclear waste management (New York: Plenum Press) PP, 235- 242
- 2- M. Atkins and F.P. Glasser ,1992, " Application of portland cement – based materials to radioactive waste immobilization " waste management vol. 12 PP.,105- 131
- 3- Plecas I Peric A, Kostandinovic A A , Drljaca and Glodic1995 , " Effect of curing time on the fraction of ^{60}Co and ^{137}Cs leached from cement matrix " cement and concrete research Vol, 25 pp, 311-313
- 4- I B plecas , R S pavlovic and S D Pavlovic 2003, " leaching of 60 Co and 137 Cs from spent ion exchange resins in cement – bentonite clay matrix " Indian academy of sciences pp,26-32
- 5- J.I Escalante and etal 2001, " Reactivity of blast - furnace slag in Portland cement blends hydrated under different conditions " cement and concrete research vol.31 pp,1403- 1409
- 6- Li Dongxu and etal 2000 , " Study of properties on fly ash - slag complex cement " cement and concrete research vol. ,30 pp,1381- 1387
- 7- M. Oner, K. Erdogu, A. Gunlu 2003, "Effect of components fineness on strength of blast furnace slag cement " cement and concrete research vol.,33 pp, 463-469
- 8- J.A.Larbi, A.L.A. Fraay, J.M.J.M.Bijen, 1990 , "The chemistry of the pore fluid of silica fume blended cement system". cement and concrete research vol.,20issues4, pp, 506-516
- 9- I. G. Richardson, G.W. G roves, 1992, "Microstructure and microanalysis of hardened cement pastes involving ground granulated blast furnace slag cement " ,J. Mater. Sci. vol.,27 pp, 6204-6212
- 10- ANSI/ANS-16.1, 2003, 1998, 1986. "Measurement of the leachability of solidified low – level radioactive waste by a short - term test procedure." ANSI/ANS 16.1 American Nuclear Society
- 11- I.G.Richardson , C. R. Wilding , M.J. Dickson, 1989," The hydration of blast furnace slag cements " Advanced cement based materials vol 2 ,pp, 147-157
- 12- J.S.Lumley, R.S. Gallop, G.K. Moir, H.F.W.Taylor, 1996 "Degrees of reaction of the slag in some blends with Portland cement " cement and concrete research vol.,26 pp, 139-151
- 13- G.Appa Rao,2000 "Influence of silica fume on long - term strength of mortars containing different aggregate fraction " cement and concrete research vol.,31 pp, 7-12
- 14- M.H.Zhang,O.E., Gjorv2000." Effect of silica fume on cement hydration in low porosity cement paste, cement and concrete research vol., 21 pp, 800-808
- 15- Wang Ling, Tian Pei, And Yao Yan. 2004,pplication Of Ground Granulated Blast Furnace Slag In High-Performance Concrete In China," International Workshop on Sustainable Development and Concrete Technology, Beijing, China Building Materials Academy,,pp 309-317.
- 16- Wang Ling, Tian Pei, And Yao Yan. 2004, Application Of Ground Granulated Blast Furnace Slag In High-Performance Concrete In China," International Workshop on Sustainable Development and Concrete Technology, Beijing, China Building Materials Academy, pp 309-317..
- 17- U.S. Department of Transportation, Federal Highway Administration 2005. "High Performance Concrete Structural Designers" Guide . Atlanta: FHWA.pp 11-42

EFFECT OF TIME DELAY AFTER MIXING ON RHEOLOGICAL PROPERTIES OF SELF-COMPACTING CONCRETE

Hossam S. Khalil*

*Materials Engineering Department, Faculty of Engineering, Zagazig University, Egypt,
E-mail: hossamkhalil_m@yahoo.com*

ABSTRACT

Self-compacting concrete (SCC) has been described as "the most revolutionary development in concrete construction for several decades". The present work gives attention to an effect, which can affect the rheological performance of an SCC mix adversely, and hence, its hardened properties also. This effect is the 'time delay' or the time elapsed since the end of the mixing process and the start of the placement of concrete process (or even its end) in situ. An eight SCC mixes were made in this study, in which three values of this time delay were considered: 0, 15 and 30 minutes, and tests were applied on SCC mixes without and with a retarding admixture. The slump flow, V-funnel and L-box tests were applied for the rheological properties, and the compressive and splitting tensile strength tests at 7, 28 and 56 days were carried out for the strength properties of the SCC mixes used. Results showed that a gradual decrease in the rheological properties of the SCC mix occurred as the time delay after mixing increased. At 30 minutes time delay some of the SCC limits were not satisfied. However, the addition of 0.5 % retarding admixture to the SCC mix could attain the rheological properties of the mix within the SCC limits even at 30 minutes time delay.

KEYWORDS: Self-compacting concrete; rheological properties; fresh tests; open time; silica fume; retarder.

INTRODUCTION

Self-compacting concrete (SCC) has been described as "the most revolutionary development in concrete construction for several decades". Originally developed to offset a growing shortage of skilled labor, it has proved beneficial economically because of a number of factors, including: faster construction, reduction in site manpower, better surface finishes, easier placing, improved durability, greater freedom in design, thinner concrete sections, reduced noise levels and absence of vibration, and safer working environment [1].

Practical application has been accompanied by much research into the physical and mechanical characteristics of SCC and the wide range of knowledge generated has been sited and combined in different guideline and specification documents [1, 2]. There have been much researches published concerning the rheological properties of fresh SCC mixes and the mechanical properties and durability of the hardened SCC mixes, and how to enhance such properties. Optimization of the concrete mix constituents [3] and the addition of different mineral admixtures [4] were approaches among others to achieve these goals. On the other hand, the study of the distribution of the in-situ strength along the length of a structural element such as a beam or a column was considered and found to be more uniform in the case of SCC than in the case of normal concrete (NC). In addition, the in-situ strength of SCC was closer to the standard cube strength than that of NC [5].

* Corresponding author
Received Date:9/11/08
Acceptance Date:23/11/08

The present work gives attention to an effect, which can influence the rheological performance of an SCC mix adversely, and hence its hardened properties also. This effect is the 'time delay' or the time elapsed since the end of the mixing process and the start of the placement of concrete process (or even its end) in situ. Researches assumed no delay time as the rheological tests were applied immediately after the mixing process to reflect the rheological properties of the SCC mix, which should satisfy the specification limits of SCC in order to insure proper placement of concrete.

Petersson and Billberg [6] found that when using viscosity agents, the workability by time was decreased compared to mixes with only fillers. The slump flow decreased as the measuring time after mixing increased. With regard to this delay time factor guideline and specification documents [1,2] states that the 'open time' or the time during which the SCC maintains its desired rheological properties is very important to obtain good results in the concrete placing. This time can be adjusted by choosing the right type of superplasticizers or the combined use of retarding admixtures. Different admixtures have different effects on open time, and they can be used according to the type of cement and the timing of the transport and placing of the SCC.

Therefore, the aim of this work is to highlight the effect of the time delay on the rheological and strength properties of an SCC mix. Furthermore, the role of using a retarding admixture with the SCC mix as a means to overcome any resulting adverse effects is considered.

EXPERIMENTAL PROGRAM

The experimental program of this study consisted of eight SCC mixes and was divided into two phases. The purpose of phase (1) was to obtain a proper SCC mix with good SCC rheological and strength properties and it included three mixes. The three mixes were performed with a total powder content for each (cement + supplementary mineral admixture) of 400 Kg/m³, as shown in Table 1. The total powder content of the first mix (M₁) was OPC. The other two mixes (M₂ and M₃) were prepared using silica fume as a 10 % partial replacement of the cement content and as a 10 % addition, respectively. In all mixes the water/total powder ratio (W/P) was kept constant at 0.45, the sand/dolomite ratio was kept constant at 1, and the viscosity enhancing admixture percentage was kept constant at 2% by weight of the total powder content.

The second phase of the work included 6 mixes, including a mix from phase (1), and the purpose of this phase was to study the effect of the time elapsed since mixing of the concrete constituents till applying the rheological tests (time delay), and therefore the effect of the time delay, in placing SSC in situ, on the rheological and strength properties of SCC. The first three mixes of phase 2 (M₃, M₄, and M₅) had the same mix proportions as those of mix M₃, which was adopted based on the results of phase (1). Mix M₃ was tested for its fresh properties immediately after stopping mixing, while mixes M₄ and M₅ had a time delay of 15 and 30 minutes, respectively before applying the tests. The remaining three mixes of this phase (M₆, M₇, and M₈) were similar to the previous three mixes in content and work procedure, respectively, but they contained a 0.5 % retarding admixture by weight of the cement as an attempt to counteract the effect of the time delay on the fresh and hardened properties of the SCC mix (see Table 2).

Ordinary Portland cement (OPC) conforming to the Egyptian standards No. 373-1991 was used. The mineral admixture used was silica fume with a specific gravity of 2.15. Dolomite coarse aggregate was used with a nominal maximum size (NMZ) of 14 mm, specific gravity of 2.78. Local well-graded sand with specific gravity of 2.50 and fineness modulus of 2.2 was used. The chemical admixture used in all mixes with a constant percentage of 2 % of the total powder content was a viscosity enhancing admixture (VEA) that meets the ASTM standard C-494 type G and F. It has a dual action, where it gives excellent flowability and in the same time enhances the stability (viscosity) of concrete. The retarder admixture used in mixes M₆–M₈ with a constant percentage ratio of 0.5 % of the total powder content complies with the ASTM C-494 Type A+B+D and BS 5075 Part 1. It is used as a powerful concrete plasticizer and retarder, where high quality concrete is required in difficult climatic conditions.

Table 1: Concrete mix proportions

Mix type	Cement content (kg/m ³)	Mineral admixture			W/P	Water	Sand	Dolomite	VEA
		Type	%	Content (kg/m ³)					
M ₁	400	-	-	-	0.45	180	905.5	905.5	8
M ₂	360	SF rep.	10	40	0.45	180	898.0	898.0	8
M ₃	340	SF add.	10	40	0.45	180	898.0	898.0	8

Concrete mixes were prepared in a pan mixer. The sand and mineral admixture were added to the coarse aggregate and all were dry mixed till obtaining a homogenous mix (about 60 seconds). Then two-thirds of the mixing water was added gradually while the mixer was rotating, and the concrete was mixed for 120 seconds. The VEA was then added to the remaining water and introduced gradually within 30 seconds, and the concrete was mixed for another 120 seconds. The fresh properties of the tested concrete were the slump flow, V-funnel and L-box tests. Procedure details of these tests were mentioned earlier in Refs. [1-3].

A total number of at least 18 test specimens were cast for each of the eight mixes: 9 cubes of 100×100×100 mm dimensions for measuring the compressive strength, and 9 cylinders of 100×200 mm for measuring the splitting tensile strength. All specimens were demolded after 48 hours and cured in water until the test dates. The concrete cubes and cylinders were tested for each mix at the ages of 7, 28, and 56 days (at least three specimens at each age).

RESULTS AND DISCUSSION

The first phase of this work was to obtain a suitable SCC mix, which would give good rheological properties when compared to the SCC limits in addition to satisfactory strength results. Table (2) and Figs. (1 - 5) show the results of the rheological tests applied on the three mixes of phase (1), M₁, M₂ and M₃, to measure their slump flow and the T_{50 cm} time of the slump flow test, the flow time (T) and the flow time at 5 minutes (T_{5min}) of the V-funnel test, and the blocking ratio (H₂/H₁) of the L-bob test, respectively. These results show that a gradual enhancement in the SCC rheological properties occurred when moving from mix M₁ to mix M₂ to mix M₃, respectively. This is reflected in getting a higher slump flow, a shorter T_{50 cm} time, a shorter flow time, a shorter flow time at 5 minutes, and a larger blocking ratio. Therefore, mix M₃ showed the best performance among the three mixes and could satisfy the SCC limits of these tests. Results obtained can be explained as follows: The use of SF as a partial replacement of the cement content in mix M₂ resulted in a better rheological performance when compared to mix M₁ as SF is well known to be much finer than the cement and this can improve rheology of the mix. The use of SF as an addition in the third mix (m₃) resulted in an even increase in the powder content leading to an even higher rheological performance.

Table 2: Results of the rheological tests for the different mixes

Mix type	Time delay, min	Slump flow		V-funnel		L-box
		mm	T _{50cm} , sec	T, sec	T _{5min} , sec	H ₂ /H ₁
M ₁	0	600	4.12	19.73	Blocking	Blocking
M ₂	0	680	2.28	4.53	40.00	Blocking
M ₃	0	730	1.67	1.12	9.30	1.00
M ₄	15	650	1.32	4.75	12.67	0.83
M ₅	30	500	3.94	5.96	6.47	Blocking
M ₆	0	615	0.98	3.10	3.50	0.86
M ₇	15	615	1.41	3.09	4.93	0.86
M ₈	30	570	5.17	7.47	8.49	0.73

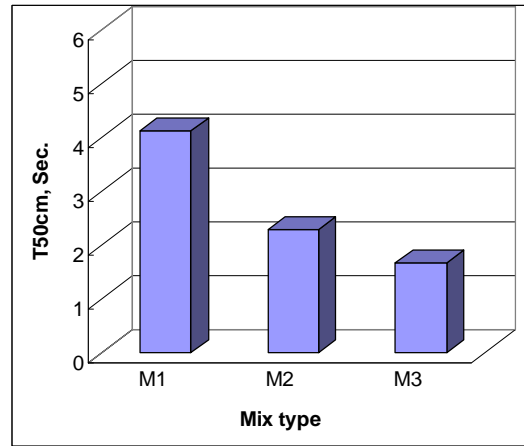
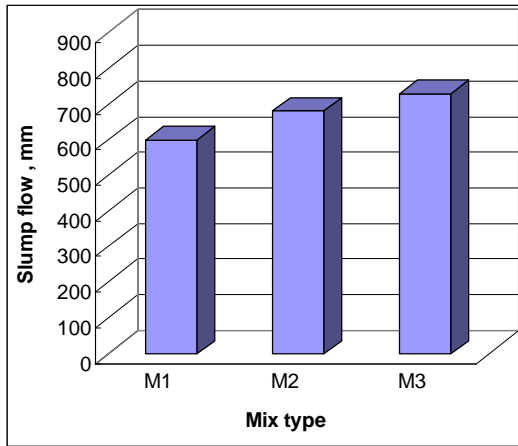


Fig. 1: The slump flow for the different mixes Fig. 2: The T50cm time for the different mixes

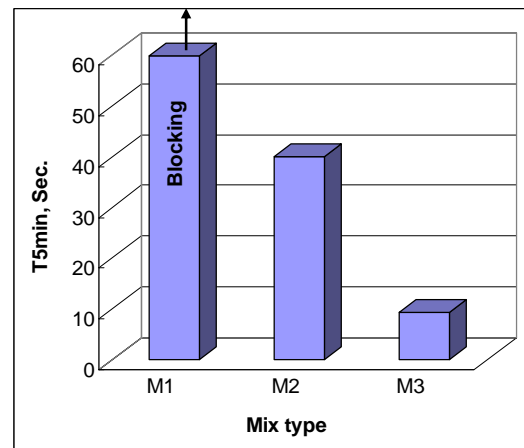
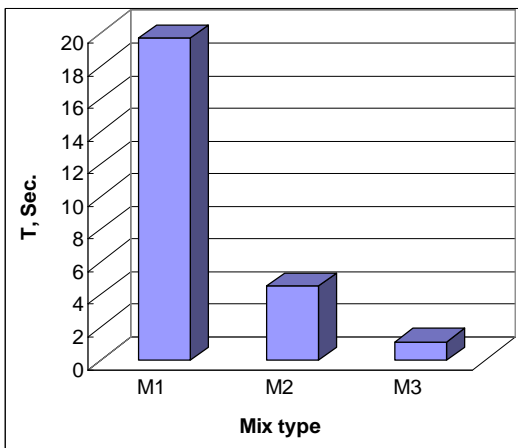


Fig. 3: The flow time for the different mixes Fig. 4: Flow time at 5 min. for different mixes

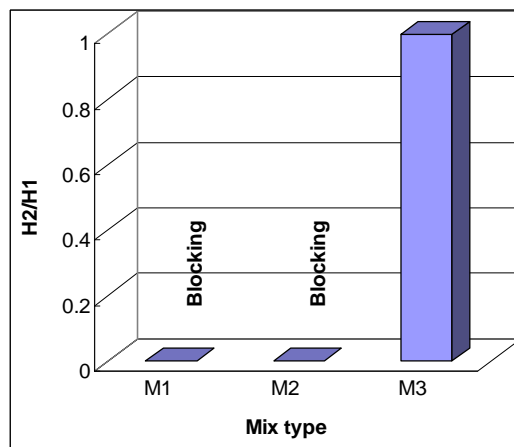


Fig. 5: The blocking ratio for the different mixes

Table (3) and Figs. (6, 7) show the strength results of the hardened concrete of the three mixes considered, $M_1 - M_3$, in terms of the compressive and indirect splitting tensile strengths, respectively. Results of the compressive strength test show clearly the increase in strength of the three mixes as the test age increased from 7 days to 56 days passing through the 28 days

strength. This is well known to be due to the cement hydration process. Results also show the role of using SF in concrete mixes as a replacement or even with more effect as an addition in increasing the strength of a concrete mix. This can be related to its physical and chemical effects. However, the compressive strength of mix M_2 was less than that of mix M_1 , and that can be related to the fact that the chemical effect of SF was not yet reflected as it needed more time to occur, and therefore, it appeared at 28 and 56 days. The physical effect, however, was present at all ages. Results of the splitting tensile strength test also show the increase in strength with time. However, the trend of the results of the three mixes at each age was not clear enough as in the compressive strength test, and this can be related to the variations in the experimental test results, particularly that values of the splitting tensile strength are actually small, relatively.

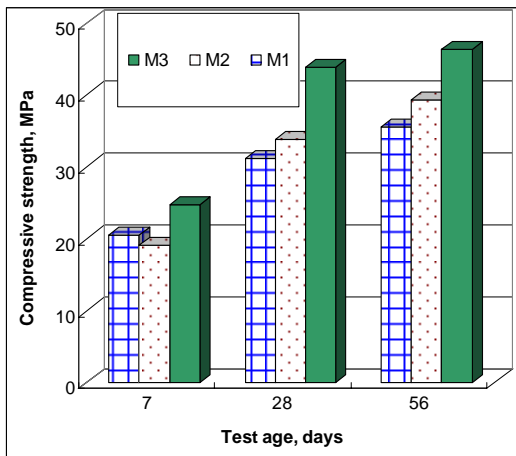


Fig. 6: The compressive strength of the different mixes

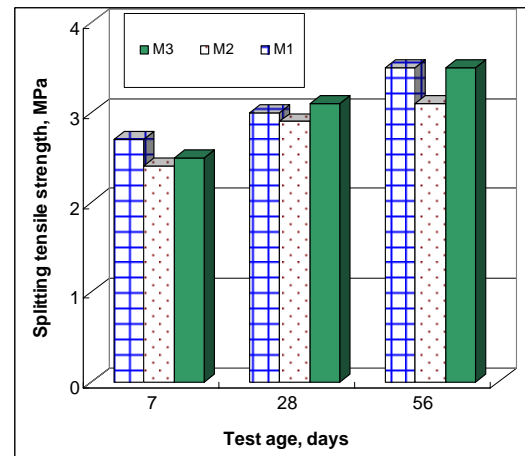


Fig. 7: The splitting tensile strength of the different mixes

Table 3: Results of the strength tests for the different mixes

Mix type	Time delay, min	Compressive strength, MPa			Splitting tensile strength, MPa		
		@ 7 days	@ 28 days	@ 56 days	@ 7 days	@ 28 days	@ 56 days
M_1	0	20.5	31.2	35.5	2.7	3.0	3.5
M_2	0	19.2	33.8	39.3	2.4	2.9	3.1
M_3	0	24.8	43.8	46.4	2.5	3.1	3.5
M_4	15	32.4	55.6	56.3	2.5	3.6	4.4
M_5	30	33.6	45.2	48.1	3.0	3.3	4.2
M_6	0	33.0	50.7	51.5	2.7	4.4	5.6
M_7	15	32.6	43.5	53.0	2.6	3.6	4.0
M_8	30	34.0	43.0	49.6	3.0	3.1	4.0

Results of the second phase of this work are shown in Tables (2, 3), and Figs. (8 - 14), where the effect of the time delay after mixing in performing the rheological tests, and therefore, the effect of the time delay in placing SCC in situ, on the rheological and strength properties of SCC is reflected. The first curve in Figs. (8 - 12) (without a retarder) represents the adopted SCC mix from phase (1) and was subjected to delay time intervals after mixing of 0, 15, 30 minutes before applying the rheological tests, mixes M_3 , M_4 and M_5 , respectively. Results show that a gradual decrease in the rheological properties was obtained as the time delay increased. The SCC limits for each test [1] are also shown on these figures. Although mixes M_3 - M_5 satisfied most of the SCC limits, some limits were exceeded in the slump flow and blocking ratio values for mix M_5 , when tests were performed after 30 minutes from the time of mixing. This is believed to be resulting from the cement hydration process taking action at a higher rate in the beginning, relatively, and leading to the setting of the cement and losing of workability of the mix gradually. Therefore, the time delay did have an effect in reducing the SCC rheological properties

required. This conclusion agrees with the finding of Petersson and Billberg [6], which was mentioned earlier.

Furthermore, this conclusion is highlighted taking into consideration the following two points: The Egyptian Code of Practice states that ordinary concrete should be placed within 30 minutes from the time of mixing in normal weather conditions with an ambient temperature not greater than 30° C, otherwise proper admixtures should be used and proper tests are done before starting the placing process [7]. This can also be related to the code requirement that the initial setting of Portland cement should be at least 45 minutes except low heat Portland cement, for which a minimum of 60 minutes is required [7]. Second, tests applied in this experimental work were made in the laboratory under ideal conditions at a temperature of about 25° C, while SCC in situ is actually subjected to more realistic environmental conditions at even higher ambient temperatures in some regions such as Egypt and the Middle East, which would make the effect of time delay more serious and severe.

The second curve in these figures, Figs. (8 - 12), (with a retarder) represents mixes M₆, M₇ and M₈, which were similar to mixes M₃, M₄ and M₅, respectively, but were having a retarding admixture with 0.5 % ratio by weight of the cement. Results show that the retarding admixture could attain the rheological properties of the SCC mix even with a time delay of 15 minutes (mix M₇) and 30 minutes (mix M₈), and all results were within the SCC limits except the slump flow and the H₂/H₁ ratio of mix M₈, which were a little bit less than the SCC limits. However, this can be overcome by increasing the dose of the retarder in the mix. Few points were discarded in these figures as they were considered unacceptable due to the experimental error. Therefore, the use of a retarder and taking other precautional measures is believed to be a solution in order to insure attainment of the rheological properties of the mix until the whole placing process is completed. The proper dose can be adopted for each case and tests can be applied for the quality control of the SCC mix. This conclusion also agrees with the recommendation of the guideline and specification documents [1,2] with regard to the open time of the SCC mix, which was mentioned earlier.

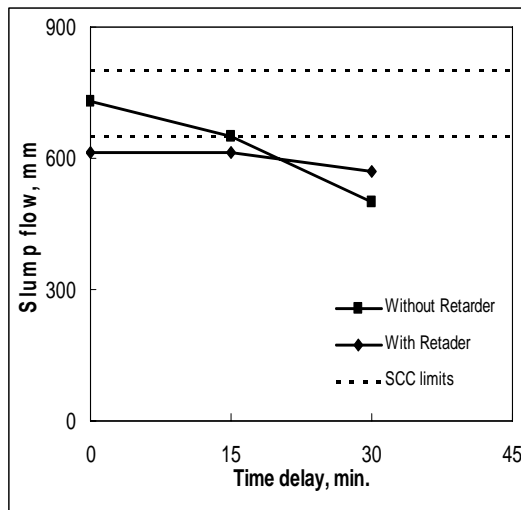


Fig. 8: The effect of time delay after mixing on the slump flow of SCC mixes

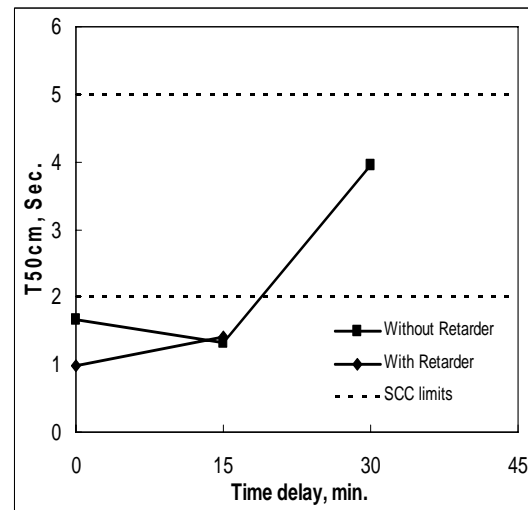


Fig. 9: The effect of time delay after mixing on the T50cm time of SCC mixes

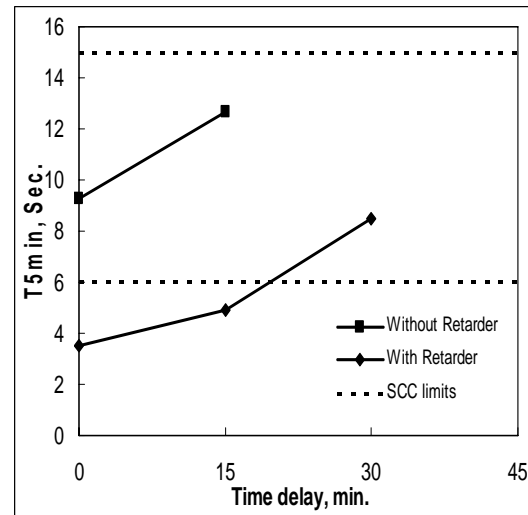
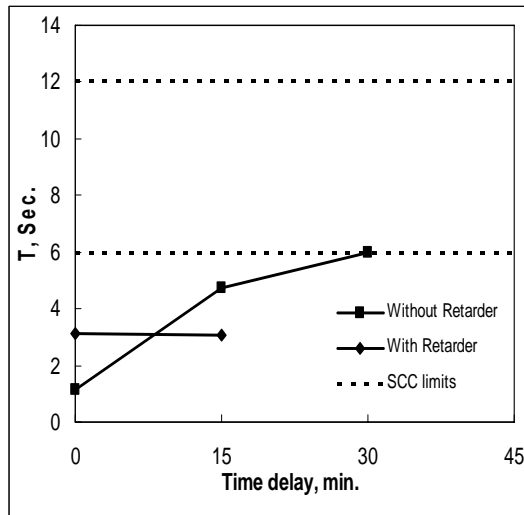


Fig. 10: The effect of time delay after mixing on the flow time of SCC mixes

Fig. 11: The effect of time delay on the flow time @ 5 min of SCC mixes

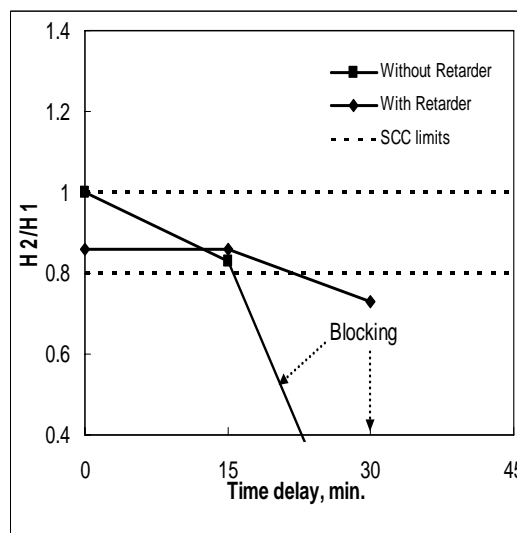


Fig. 12: The effect of time delay on the blocking ratio of SCC mixes

With regard to the hardened properties, Table (3) and Figs. (13, 14) show the compressive and splitting tensile strengths of SCC mixes without and with a retarder, which were subjected to 0, 15 and 30 minutes time delay before rheological tests were applied and followed by pouring concrete in the cube and cylinder molds. The first remark one can notice is that strength results at 28 and 56 days are closer to each other than those at 7 days, as expected. However, results do not show a clear trend when comparing mixes without a retarder to those with a retarder at the different applied delay times and at the same age. This may be related to the variations that might be expected due to the experimental error, which might have interacted with the effects of the considered variables, particularly that the specimens used were of a small size of 100 mm cubes and 100X200 mm cylinders, and the values of ultimate loads in the case of the splitting tensile strength test were typically small. Finally, it is believed that the reduction in the rheological properties of the SCC mix due to the delay time factor will have its effect, in turn, on the quality and strength of the hardened concrete, and more precautional measures are required to detect such effect.

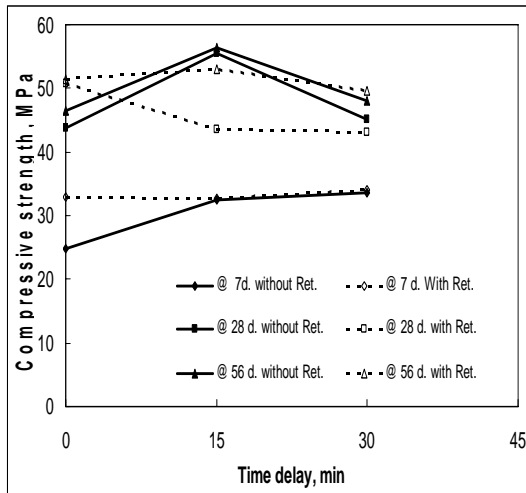


Fig. 13: The effect of time delay on the compressive strength of SCC mixes

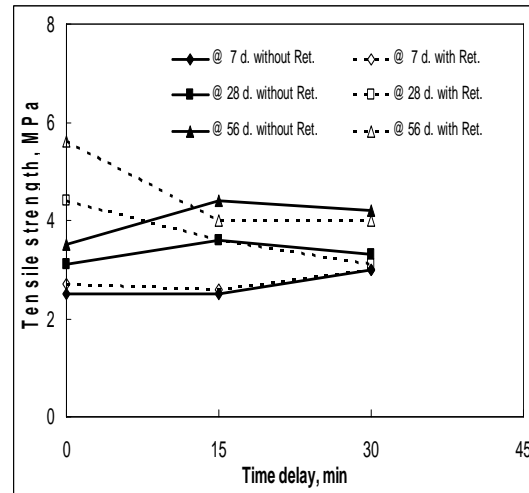


Fig. 14: The effect of delay time on the splitting tensile strength of SCC mixes

CONCLUSIONS

Based on the outcome of this study the following conclusions can be drawn:

1. The use of SF in the SCC mix as 10 % partial replacement of the cement content resulted in an enhancement in the rheological and strength properties of the mix. Use of SF as a 10 % addition led to an even higher enhancement.
2. A gradual decrease in the rheological properties of the SCC mix occurred as the time delay after mixing increased. At 30 minutes time delay some of the SCC limits were not satisfied.
3. As this study was applied in the laboratory, the effect of the time delay is believed to be more harmful on the rheological and hence hardened properties of SCC in situ.
4. The addition of 0.5 % retarding admixture to the SCC mix could attain the rheological properties of the mix within the SCC limits even at 30 minutes time delay.
5. The use of a retarding admixture in the SCC mix is considered one solution, which agrees with the guideline and specification documents, to insure attainment of the required rheological properties of the SCC mix until the placement of concrete is complete.

REFERENCES

1. EFNARC (2002), "Specification and Guidelines for Self-Compacting Concrete", <http://www.efnarc.org/>.
2. Egyptian Code of Practice Committee for SCC (2008), "Technical Specifications for Self-Compacting Concrete", Building and Housing Research Centre, Cairo, Egypt (in Arabic).
3. Ahmed, S.A., Khalil, H.S. and Elmalky, A.A. (2006), " Optimum Mix Constituents of High Strength Self-Compacting Concrete", Civil Engineering Research Magazine, Al-Azhar University, Cairo, Egypt, Vol. 28, No. 1, PP. 365 - 378.
4. Ahmed, S.A., Khalil, H.S. and Elmalky, A.A. (2007), " Use of Ground Glass Powder in Self-Compacting ", Proceedings of the 12th International Colloquium on Structural & Geotechnical Engineering, Cairo, Egypt, PP. 1147-1156.
5. Ahmed, S.A., Khalil, H.S. and Elmalky, A.A. (2007), " Performance of Structural Elements Cast with Self-Compacting Concrete", Proceedings of the Sixth Alexandria International

Conference on Structural and Geotechnical Engineering, Alexandria, Egypt, PP. MT49–MT62.

6. Petersson, Ö., Billberg, P. (1999), "Investigation on Blocking of Self-Compacting Concrete with Different Maximum Aggregate Size and Use of Viscosity Agent instead of Filler", Proceedings of International RILEM Conference on Self-Compacting Concrete, Stockholm, Sweden, edited by RILEM Publications, Cachan, FRANCE (Monographie), PP. 333-344.
7. Egyptian Code of Practice Committee for Design and Construction of Concrete Structures (2007), "The Egyptian Code for Design and Construction of Concrete Structures", Building and Housing Research Centre, Cairo, Egypt (in Arabic).

STABILIZATION OF CEMENTED COLLAPSING-SWELLING CLAY

Adel H. Hammam*

Researcher, Housing & Building National Research Center, Cairo, Egypt

ABSTRACT

Soil stabilization is sometimes considered the best solution to overcome unfavorable properties in the foundation soil. The target of stabilization is to improve one character or more that affects the behavior of foundation and hence the structure can be exposed to failure. The most challenge character that always disturbs the engineer is the sensitivity of unsaturated soil to water and its volume change under immersion conditions. Collapsing and swelling soils are considered the most famous in between the unsaturated problematic soil and although they were exposed to numerous investigations and researches they are still problematic soils. Hammam, A.H et al, 2007, published a research about some properties of cemented collapsing-swelling clay that has been found in Al-Madinah Al-Munawarah, Saudi Arabia. This type of unsaturated soil was the main reason to demolish a new building due to the excessive differential settlement and in turn excessive inclination. After demolishing the building, it was decided to stabilize the site soil with lime additive. Lab program was designed to carry out Atterberg limits, free swell, modified proctor, unconfined compressive strength and consolidation tests. The ratio of lime was chosen to be 8% by weight of dry soil. Comprehensive comparison was achieved between lab tests of un-treated and lime-treated soils to conclude the soil improvement and to support field stabilization which was executed by deep grouting method. Samples were extracted by drilling boreholes after field grouting and the above lab tests were carried out again to compare between the characteristics of lab lime-treated and field lime-treated soils. The results indicated that cemented collapsing-swelling clay has been significantly improved by lime additive and it changed to water-stable soil.

Keywords: Collapsing-swelling clay, lime stabilization, soil improvement.

INTRODUCTION

Ground improvement is considered a geotechnical technique to the solution of problems in the ground for both new and existing civil engineering projects. The main target of ground improvement is to increase the bearing capacity of soil, which can be achieved by altering the soil properties of shear angle Φ , cohesion c , or density γ . Swelling or collapsing potential of soil could be also improved by decreasing its volume change as a result of alteration of moisture content. There are several methods of improving soils; among them are surface or deep compaction, drains with or without preloading, stabilization, grouting and stone or sand columns. Each method includes several sub-procedures, i.e. stabilization can be divided to lime stabilization, cement stabilization, lime-fly ash stabilization and cement-lime stabilization. Also grouting itself can be considered a sub-group of stabilization.

Stabilization is the process of surface or deep mixing admixture materials with a soil to improve certain properties of the soil. The process may include the blending of soils to achieve a desired gradation or the mixing of commercially available additives that may alter the gradation, texture or plasticity, reduce volume-change potential or act as a binder for cementation of the soil. Additive stabilization is achieved by the addition of proper percentages of cement, lime, fly ash, bitumen, or combinations of these materials to the soil.

* Corresponding author
Received Date:23/6/08
Acceptance Date:15/10/08

The selection of type and determination of the percentage of additive to be used is dependent upon the type of soil and the degree of improvement in soil quality desired. Generally, smaller amounts of additives are required when it is simply desired to modify soil properties such as gradation, workability, and plasticity. When it is desired to improve the strength, durability and significantly reduce volume-change, larger quantities of additive are used.

The action of lime in fine soil was explained in Canadian Foundation Engineering Manual, 1992 [2] as follows. When un-slaked lime is mixed into moist soil, four reactions take place such as hydration, ion exchange, cementation (pozzolanic reaction) and carbonation. Hydration and ion exchange start immediately after mixing and finish within a short time. They are responsible for the increasing of soil shear strength and low compressibility. The pozzolanic reaction is comparatively slow and continues for long time and it is responsible for the increasing of shear strength with time. While the carbonation is a reaction between lime and void air and results in a strength reduction, its effect is minimized with decreasing void air especially below ground water table.

Abdel Hady, H [5] measured the properties of treated expansive soil using sand-lime cushion and mixing soil with lime. She concluded that, i) the swelling potential of expansive soil-lime mix decreased with increasing lime content for laboratory model test, and the free swell of expansive soil-lime mix decreases with increasing the lime content. ii) The effect of lime content on the swelling pressure of expansive-lime mix is more significant for lime content $\leq 5\%$ (oedometer and laboratory model). iii) The clay content, liquid limit and plasticity index of expansive soil-lime decrease as the lime content increases, while the plastic limit and shrinkage limit of expansive soil-lime increase as the lime content increases, variation of activity with increasing lime content is small up to 10% and then increased.

Abdel-Aziz A.A [6] used hydrated high calcium lime - $\text{Ca}(\text{OH})_2$ - admixture to investigate its effect on the properties of compacted sandy soil. He found that the best value of lime/soil ratio is about 10%. Shear strength factors Φ and c increased with the increase of lime ratio till 10% at which the maximum value of maximum dry density was achieved.

Awad, T. and Abdel-Hady, H. [7] determined the final heave of the laboratory footing models resting on untreated and treated expansive soil using sand-lime cushion and concluded that, i) the measured final heave of the footings and ground surface decreases as lime content of the cushion increases up to lime content = 10% then, it increases, ii) treatment of swelling soils using sand-lime cushion should be limited to lime content up to 10%, and iii) the distribution of moisture content through the treated expansive soil is not affected by lime content $\leq 10\%$.

El-Hoseiny, Youssef and Samaan [8] found that the best amount of mixing lime to be used in stabilization of the investigated expansive soil is about 6%.

Mountohar, A.S [9] used lime-rice husk ash (RHA) to study the improvement of the bearing of two types of soil, MH & CH. He concluded that lime and RHA added to soil in adequate amounts has a beneficial effect on the soil strength. It has the potential to significantly increase the soil strength and decrease the swell in a relatively short time.

Moseley, M.P. reported [10] that the average water content reduced by 15% when 10% quick lime was mixed with soft clay has an initial water content of about 60%. For inorganic clays with low plasticity ($W_L < 50$) the maximum increase of shear strength is generally obtained with 6-8% quicklime with respect to the dry weight of the soil. The optimum lime content increases with increasing water content and plasticity index of the soil. The stabilized soil is normally firm to hard with low compressibility compared with that of the un-stabilized soil. A significant shear strength increment can be observed with one to two hours after soil treatment. The un-drained shear strength of the stabilized clay can be as high as 0.5MPa to 1.0MPa after one year. Approximately one-third of the final shear strength is obtained after one month and about 75% after three months.

Mohamed, A.M.O et al [11] investigated the improvement of clay properties by using lime treatment. He concluded approximately as results as that of Mountohar, A.S (2002) and Abdel-Aziz A.A (2006).

Bowels [12] stated that lime will reduce the plasticity of most clays (by an ion exchange mechanism, usually Ca for Na), which in return reduces or eliminates volume-change potential. Manual of Soil Stabilization for Pavements has been prepared by Department of the Army, NAVY and Air Force [13] for improving the engineering properties of soils used for pavement. This manual is considered comprehensive study prescribes the appropriate type or types of

additive to be used with different soil types, procedures for determining a design treatment level for each type of additive, and recommended construction practices for incorporating the additive into the soil. The most common improvements achieved through stabilization include better soil gradation, reduction of plasticity index or swelling potential, and increases in durability and strength. If it has been determined that a soil has potential for excessive swell, lime treatment may be appropriate. Lime will reduce swell in an expansive soil to greater or lesser degrees depending on the activity of the clay minerals present. The amount of lime to be added is the minimum amount that will reduce swell to acceptable limits.

Chemical stabilization technique has also been used by several researchers to investigate the improvement of behavior of collapsible soil [14]. Phosphoric acid and lime had been used for the stabilization of collapsible loess that is characterized by having considerable percentage of clay content. Evans and Bell [15] studied the use of phosphoric acid and lime to minimize the erodibility of collapsible soils (Loess) in New Zealand. They concluded that a non-erodible material is produced after seven days of curing with phosphoric acid additions between 0.5 and 3.0% by weight of dried soil, and un-immersed unconfined compressive strength is maximized at about 5%. Also, they concluded that the addition of hydrated lime to loess in concentrations as low as 0.5% by weight of dried soil results in an erosion resistant material given adequate curing; at 2% lime addition, swelling potential is minimized, and the coefficient of permeability (k) has increased by about two orders of magnitude; and at about 5% lime addition, un-immersed unconfined compressive strength is maximized.

El Sakhawy [16 - 17] studied the treatment of collapsing soils of 6th of October City, Egypt using iron slag and cement kiln dust (CKD).

Al-Hamoud et al. [18] investigated the effectiveness of bitumen as a soil stabilizing agent for collapsible soils obtained from Northern Jordan.

From the above literature review it is obvious that stabilization with lime is famous and is considered acceptable method from technical and economical point of view. Technically, lime has the ability to alter the behavior of problematic soil to a desired behavior. At the same time lime is cheaper than the traditional competitor of cement.

Accordingly, to carry this investigation we used the conclusions of the existing researches to stabilize a very interesting practical case of cemented collapsing-swelling clay. Collapsing-swelling clay was found at Al-Madinah Al-Munawrah in Saudi Arabia that it was the reason to demolish a new hotel founded on this soil as soon as water reached to soil beneath the foundations [3]. Laboratory program was achieved to investigate the improvement of soil behavior after mixing with lime. This investigation included the effect of lime on atterberg limits, unconfined compressive strength, void ratio, free swell, compression index and unit weight. This laboratory program was achieved especially to support the field stabilization to improve in-situ soil properties. After stabilizing in-situ soil through controlled field program, samples were collected and tested. Comparison was established between lab results and that from filed samples.

EXPERIMENTAL LAB TESTS

A new building was constructed in the Madinah Munawarra, Saudi Arabia and after several years it suffered excessive differential settlement. Due to critical tilting the building which was consisting of basement and eight stories, was demolished by the local governorate of the city. It was discovered - depending on previous soil investigation - that soil of the site consisted of problematic clay which was called cemented collapsing-swelling clay [4]. After demolishing the building the owner requested AL-JAZZAR office about the suitable recommendations of foundations. AL-JAZZAR office decided to improve the properties of collapsing-swelling clay by using lime treatment [1]. Bulk samples were collected from a depth ranged between 1.0m and 2.0m below foundation level (foundation depth was about 5.0m below ground surface level) through open-pits. All the samples were brought to the Geotechnical & Materials Testing Laboratory of Omar Jazzar Consulting Engineers for further examination in accordance to ASTM D2488. Selected samples were subjected to the physical and mechanical tests in accordance to relevant ASTM Standards. The tests which were carried out included the following:

1. Moisture content (ASTM D2216-98)
2. Liquid limit, Plastic limit and Plasticity Index (ASTM D4318-00)
3. Shrinkage limit (ASTM D-00)
4. Free swell
5. Sieve analysis and hydrometer (ASTM D422-98)
6. Modified Proctor (ASTM, D1557-00)
7. Unconfined compressive strength (ASTM, D2166-00)
8. Consolidation test (ASTM, D2435-96)

Table (1) shows some of soil properties for natural bulk samples.

Table 1: Soil properties of natural bulk samples

Soil Properties	Test results	Soil Properties	Test results
Moisture Content, W %	40 % to 58 %	Free swell %	60 % to 120 %
G _s	2.55 to 2.62	Clay %	36 % 45 %
Liquid Limit, W _L %	65 % to 85 %	Silt %	39 % 55 %
Plastic Limit, W _P %	28 % to 35 %	Sand %	7 % 16 %
Shrinkage Limit, W _S %	13 % to 15 %	Bulk Density, kN/m ³	14.0 to 15.0

Laboratory program was carried out to investigate the improvement of soil behavior after treatment with 8 % of hydrated high calcium lime -Ca (OH)₂. Two types of tests were carried out, un-treated and treated tests. For un-treatment soil, W_L, W_P, W_S and free swell tests were carried out on remolded samples, while unconfined and consolidation tests were carried out on samples prepared using modified Proctor (ASTM, D 1557 method A). The same tests were carried out by the same manner on the lime treatment soil.

Laboratory Preparation of Soil-Lime Mixture (ASTM D 3551 - 96)

Bulk samples (several tens of kilo-grams) were oven-dried, crushed, grinded and sieved on No. 40 sieve. The soil was dry-mixed with 8 % by weight of lime and backed in containers for different tests. For a certain test, suitable weight should be taken and mixed with the suitable quantity of water.

• Effect of Lime on Atterberg Limits and Free Swell

To investigate the effect of the lime on the physical properties of the collapsing-swelling clay, Atterberg limits were performed on un-treated soil without lime additive and the results are shown in table (1). Figure (1) shows a comparison between Atterberg limits of un-treated soil and lime-treated soil. It can be seen that liquid limit ranged between 65% & 85% and 45% & 55% for un-treated and lime-treated soil respectively. Plasticity index ranged between 30% & 45% and 30% & 35% for un-treated and lime-treated soil respectively. The values of shrinkage limits ranged between 13% & 15% and 15% & 18% for un-treated and lime-treated soil respectively. These values could be analyzed that lime additive changed the gradation of soil to a large size by dividing clay particles agglomerate into coarser particles and hence decrease the liquid limit and plasticity index. Chemically, lime has the ability to overcome and decrease the swelling properties of montmorillonite mineral which is considered responsible for clay volume change, by decreasing significantly the surface area of this mineral. This phenomenon can be observed from the results of shrinkage limit values which obviously decreased by lime treatment. This phenomenon could be also observed from figure (2) that shows the relationship between free swell values for un-treated and lime-treated soil. So, the lime additive with a ratio 8 % was capable to neutralize the swelling potential of clay.

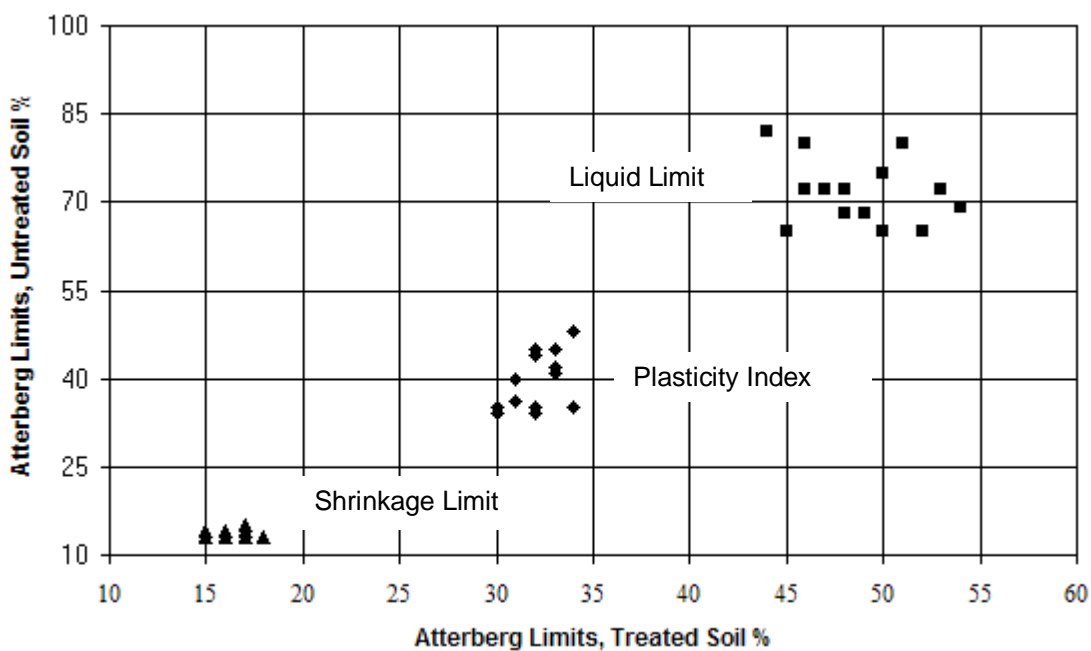


Fig. 1: Comparison between Atterberg limits for treated and un-treated soil

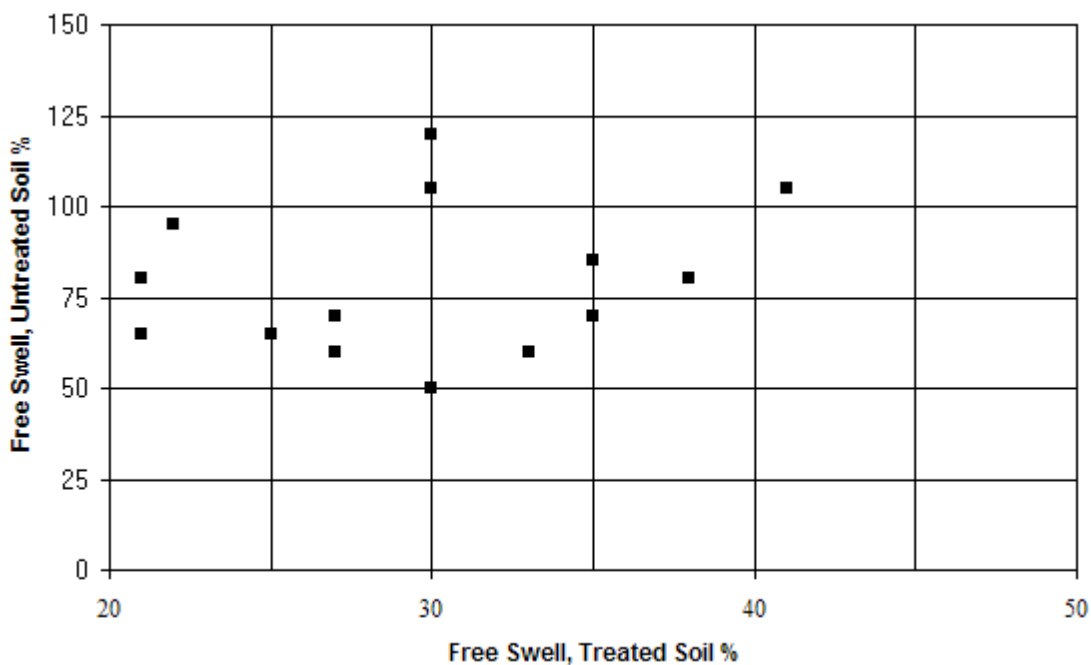


Fig. 2: Comparison between free swell for treated and un-treated soil

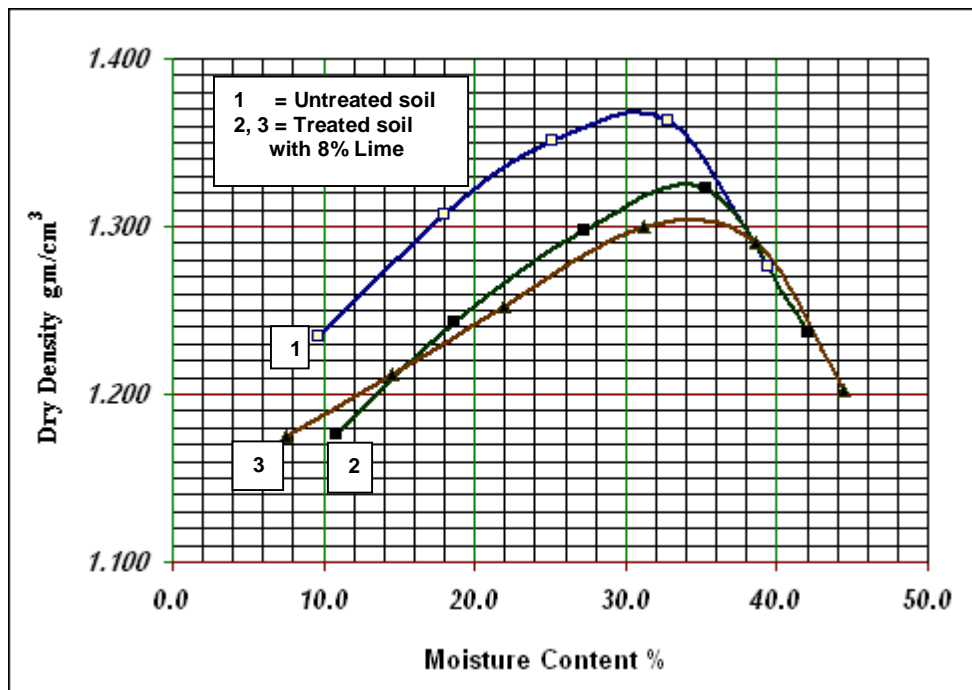


Fig. 3: Relationship between density & moisture content

• Effect of Lime on the Characteristics of the Cemented Collapsing-Swelling Clay

The most important property of this type of soil is its unit weight that is considered the main problem and it should be solved. The bulk unit weight of natural soil was ranged between 1.4 and 1.5g/cm³ with very high void ratio that ranged between 1.59 and 1.91 [4]. In spite of these critical characteristics, the shear strength of soil ranged between stiff to medium stiff according to unconfined compressive strength and standard penetration tests. To investigate this type of cemented collapsing-swelling clay, moisture-density relationship was obtained according to modified proctor (ASTM D-1557, method A). The natural bulk samples were prepared and mixed with the suitable water content to construct the relationship between moisture and dry density for un-treated soil, as shown in figure (3). It can be seen that the density property was significantly improved by remolding process. Remolding or re-compaction of the cemented clay altered the inter-structure from open or flocculated into dispersed structures and hence the void ratio decreased. In general the remolding process affects adversely the shear strength properties of the clay so that the sensitivity of the clay is measured by the comparison between the shear strength for undisturbed and remolded samples at same conditions. This comparison was carried out for the cemented collapsing-swelling clay between unconfined compressive strength, q_c , for undisturbed un-treated and remolded un-treated soil, as shown in figure (4). The remolded samples were prepared at the optimum moisture content according to modified proctor and figure (3) curve-1 represents the compaction curve of these samples. After compaction, samples with dimensions 100mm / 50mm - length / diameter - were extracted in proctor mould. The average values of q_c for undisturbed un-treated samples ranged between 0.40 and 1.10 kg/cm² while q_c for remolded un-treated samples ranged between 1.40 and 1.80 kg/cm². There is a significant improvement for q_c due to remolding or re-compaction of cemented collapsing-swelling clay which refers mainly to the improvement of its bulk and dry density. Also the effect of remolding or re-compaction can be noticed on the consolidation characteristics of soil. Figure (5) shows a semi log relationship between pressure and void ratio for undisturbed un-treated and remolded samples. The remolded samples were prepared as the way as for unconfined test but with oedometer dimensions to be complied with (ASTM, D2435-96). The clay after remolding and compacting was completely different from the original cemented clay and all the properties were obviously improved especially the density, void ratio and compression index. However, although the advantages of remolding and compacting of cemented collapsing-swelling clay are

very obvious, there are two disadvantages prevent the benefit of field-application. First, this type of clay has higher swelling pressure after remolding due to the increase of its density and the decrease of its void ratio. Figure (5) shows that swelling pressure for remolded un-treated soil is twice that for undisturbed soil. The second disadvantage is that re-compaction can only be carried out for shallow depths, so for deep or thicker strata it will not be practical solution. To investigate the effect of the lime on properties of cemented collapsing-swelling clay, modified proctor, unconfined compressive strength and consolidation tests were carried out. After preparing lime-soil treatment as mentioned above (article 2.1) enough samples were taken to perform the tests according to the relevant ASTM standards.

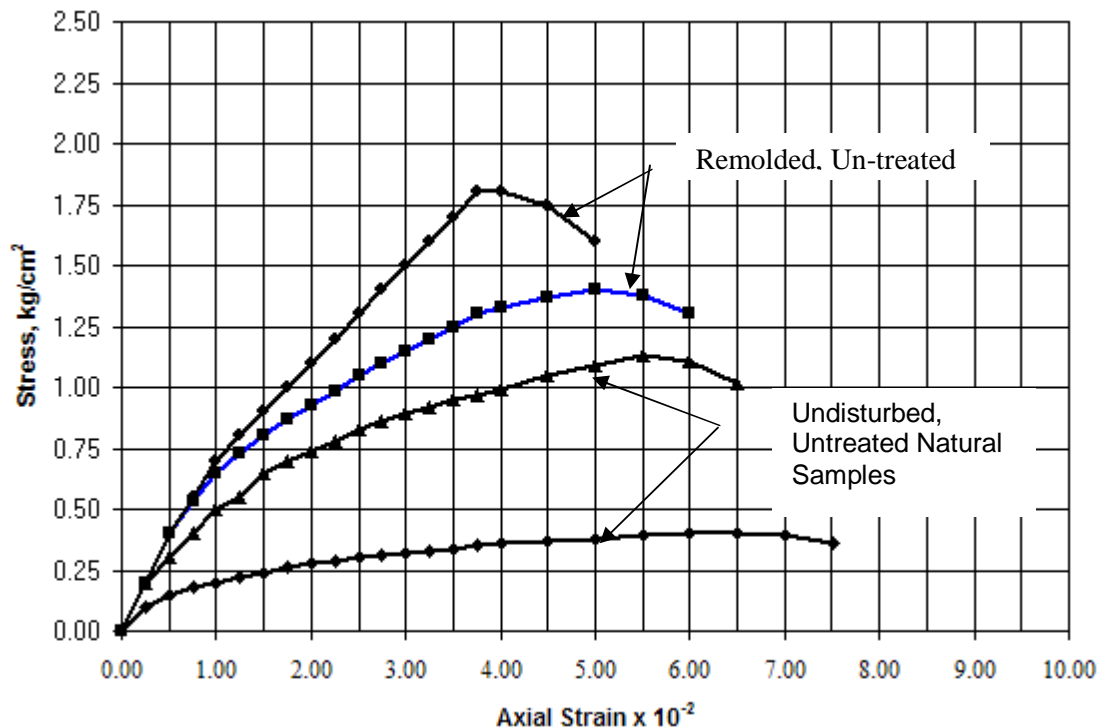


Fig. 4: Stress–strain relationship for undisturbed un-treated and remolded un-treated samples

• Dry Density

Curves (2 & 3) in figure (3) represented the upper and lower limits of the dry density-moisture content relationship of five tests. It can be shown that the average dry density for lime-soil treatment is obviously less than that for remolded un-treated soil. On the other hand optimum moisture content for lime-soil treatment is more than that for un-treated soil. The decrease in dry density can be attributed to the ion exchange that produces water-stable aggregates with high permeability and coarser grained compared to the original soil. The increased in optimum moisture content is considered a result of lime-hydration that needs more water to complete.

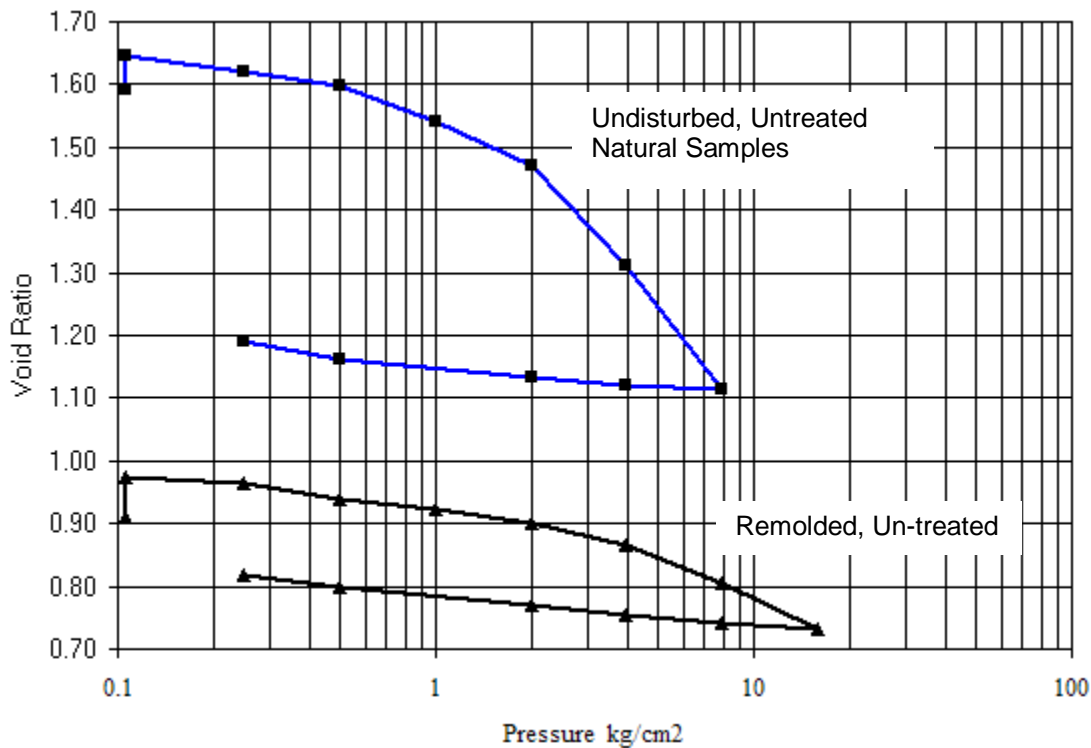


Fig. 5: Consolidation test results for undisturbed un-treated and remolded un-treated samples

<p>Undisturbed, Untreated Natural Samples: Initial water content % = 49 Initial bulk density (g/cm³) = 1.48 Initial void ratio = 1.59 Degree of saturation % = 79 Specific gravity (assumed) = 2.58 Compression Index, Cc = 0.66</p>	<p>Remolded, Un-treated Samples: Initial water content % = 31 Initial bulk density (g/cm³) = 1.770 Initial void ratio = 0.91 Degree of saturation % = 87.9 Specific gravity (assumed) = 2.58 Compression Index, Cc = 0.24</p>
--	---

• **Unconfined Compressive Strength**

Figure (6) shows stress-strain relationship for undisturbed un-treated samples and lime-treated samples. The properties of lime-treated samples are represented by curves (2 & 3) in figure (3). For unconfined compressive strength, tests were carried out on samples after different curing time similar to 2 hour, 12 hour, 3 days, 7 days and 28 days. It can be observed that the increasing in shear strength just after 2 hour from lime mixing was more than double the upper limit of shear strength for natural soil as shown in figure (6-1). The shear strength started to increase with time so that it reached after 28 days to eight times that for natural soil as shown in figure (6-2). In general the failure occurred at smaller strain for the harder samples and the mode of failure is brittle as long as the sample is more hard. So lime-treatment changed cemented collapsing-swelling clay from a consistency of medium stiff to hard consistency within very short time less than 12 hour.

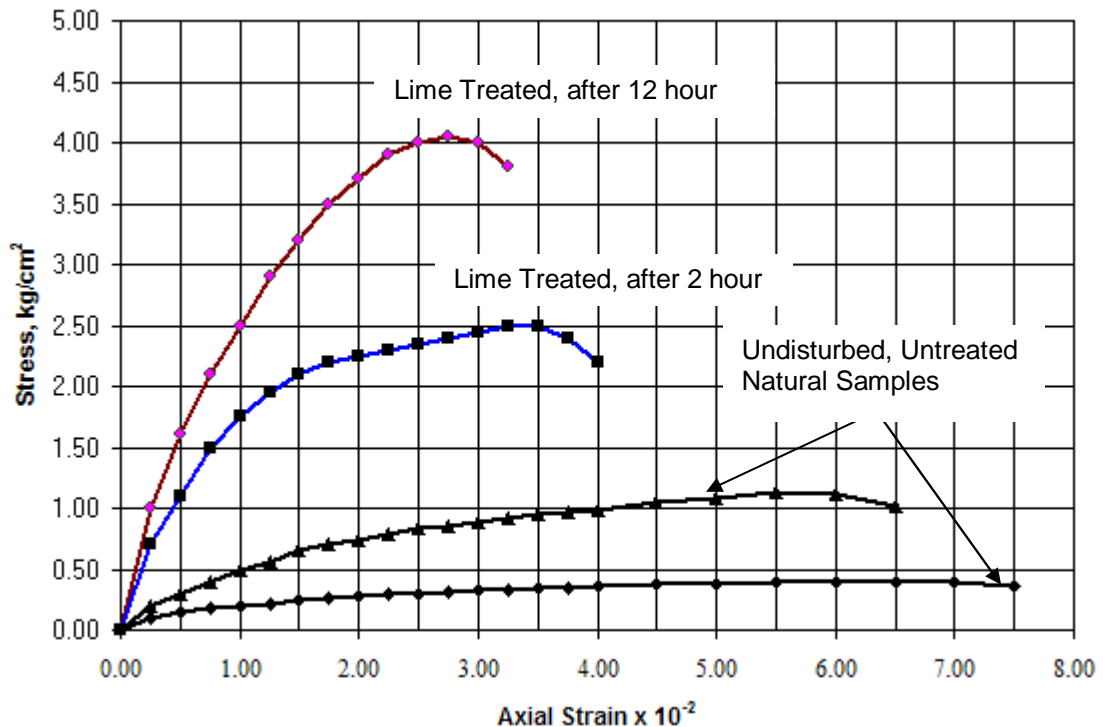


Fig. 6-1: Stress – strain relation shows soil improvement by lime-treated

• Volume Change

Volume change is considered the most difficult behavior of unsaturated clay that still challenges the geotechnical engineer. To study the effect of lime on this property consolidation tests were performed on lime-treated samples. To perform the consolidation test, modified proctor tests were carried out for lime-treated soil as shown in figure (3) curves (2 & 3) then samples were taken from proctor mold with suitable dimensions for the oedometer. This test was carried out according to ASTM D 2435-96 with sample dimensions equal to 63.5mm diameter and 20mm thickness. Figure (7) shows a semi log relationship between the pressure and void ratio for undisturbed un-treated natural cemented collapsing-swelling clay and lime-treated samples. It can be seen that the lime completely changed the compressibility properties of the treated soil. Void ratio decreased due to increase of bulk density, moreover compression index significantly decreased due to increase of soil stiffness. Also no swelling potential was observed for lime-treated soil.

FIELD STABILIZATION

• Field Grouting Program

After finishing the experimental lab tests, a comprehensive design was suggested to suit the properties of soil and to guarantee successful stabilization and soil improvement. Boreholes were drilled to a depth of 8.0m below foundation level – that already excavated to 5.0m below ground surface level – with diameter of 73mm. The distance between boreholes was 2.0m from all directions to divide the area to small squares with dimensions 2.0m x 2.0m. After drilling, P.V.C pipes with 50mm diameter were installed inside the boreholes. P.V.C pipes with end closed have holes with diameter 5mm covered about 25% from surface area of the whole length of the pipe. After pipe installing, cement-lime mortar was poured in-between borehole side and P.V.C pipe. Then after 2 hours, lime grouting was pushed in P.V.C under pressure to guarantee that 5mm holes always opened. The main grouting started after 24 hours.

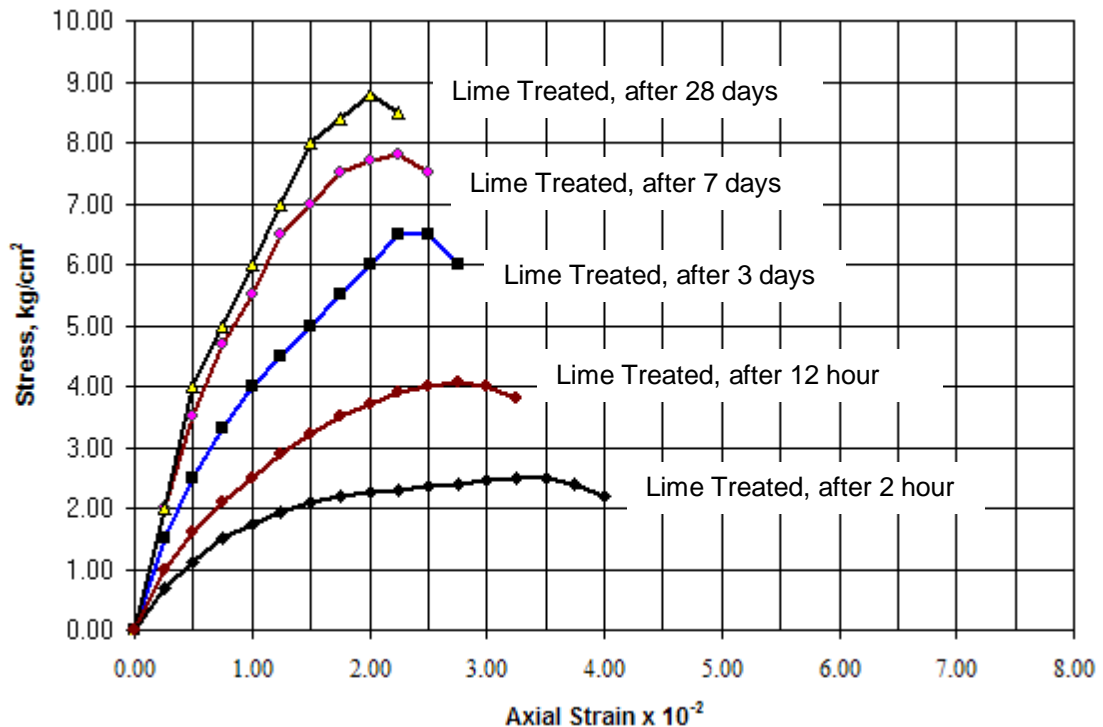


Fig. 6-2: Stress – strain relation for lime-treated soil after different time

• Lime Grouting Preparing

To prepare grouting materials, 550kg to 600kg of hydrated high calcium lime - $\text{Ca}(\text{OH})_2$ – was mixed with 1000kg drinking water to produce lime solution with 55% to 60% concentration. This solution was prepared in the field during the time of grouting and grouted through P.V.C pipe under suitable pressure with grouting pump. Grouting continued for each pipe until reaching to one of two criteria. These are the volume of grouting should be about 13% of volume of grouted soil or grouting pressure reached 10 Par (Par $\approx 1.00 \text{ kg/cm}^2$) for each point.

• Quality Control Tests

Standard penetration test was considered a reasonable field test to check the quality and soil improvement. Undisturbed samples were also extracted from boreholes to measure soil properties after lime-treatment and to examine the soil improvement. Unconfined compressive strength and consolidation tests were performed and comparisons were achieved between these tests for un-treated and lime-treated cemented collapsing-swelling clay.

• Standard Penetration Tests, S.P.T

Standard penetration tests were carried out during drilling the boreholes after about 15 day from the end of filed works of lime-treatment. Figure (8) shows comparison between S.P.T for soil before treatment and after lime-treatment. S.P.T for untreated soil ranged between 3 and 13 which indicated that soil stiffens in the range of soft to stiff. For lime-treated soil, S.P.T ranged between 13 and 34 which indicated that soil stiffens in the range of stiff to hard. The scatter in S.P.T values was expected and it is an axiomatic result of this procedure of grouting, but the lime-treatment still generally fulfilled a good results.

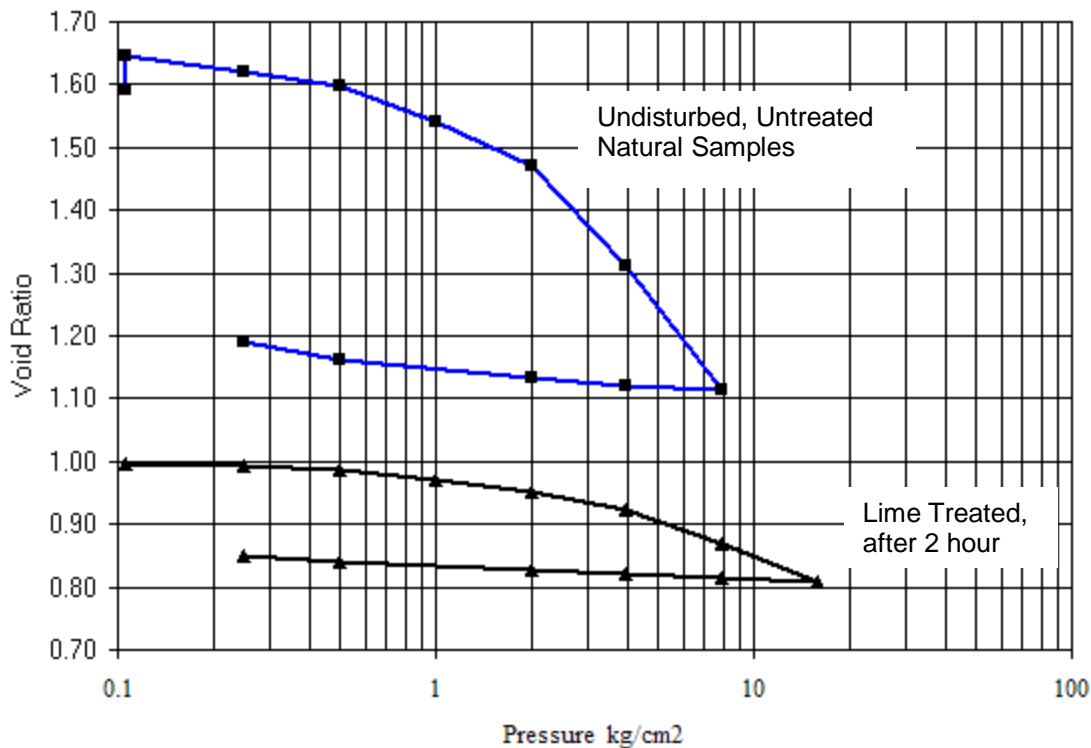


Fig. 7: Consolidation test for undisturbed un-treated and lime-treated samples

Undisturbed, Untreated Natural Samples:	Lime Treated Samples, after 2 hour:
Initial water content % = 49	Initial water content % = 34
Initial bulk density (g/cm ³) = 1.48	Initial bulk density (g/cm ³) = 1.754
Initial void ratio = 1.59	Initial void ratio = 1.00
Degree of saturation % = 79	Degree of saturation % = 89
Specific gravity (assumed) = 2.58	Specific gravity (assumed) = 2.62
Compression Index, Cc = 0.66	Compression Index, Cc = 0.20

• **Unconfined and Consolidation Behavior**

Figure (9) shows a comparison between unconfined compressive strength for un-treated undisturbed samples and lime-treated undisturbed samples. It can be seen that the results for undisturbed samples after field stabilization ranged between 1.53 kg/cm² and 3.10 kg/cm² which indicated that the gain in compressive strength reached to triple the original values. These results represent the upper and lower limits of about 20 unconfined tests for samples at different depths. There is no obvious relation between the compressive strength and depth of the sample. This phenomenon reflects the non-homogeneity of lime treatment all over the total thickness of soil strata but the lime-treatment still generally fulfilled a good results. Another comparison was achieved between lab and field lime-treatment to estimate at what level lab results or lab program can be applied in the practical field, as shown in figure (10). The acquired field compressive strength is still too much smaller than that of the lab. The average value of the compressive field strength represents about 25% of the maximum lab value. It can be said that the field stabilization succeeded to achieve actual compressive strength with factor of safety equal to 4.0 relatively to the lab or the design compressive strength.

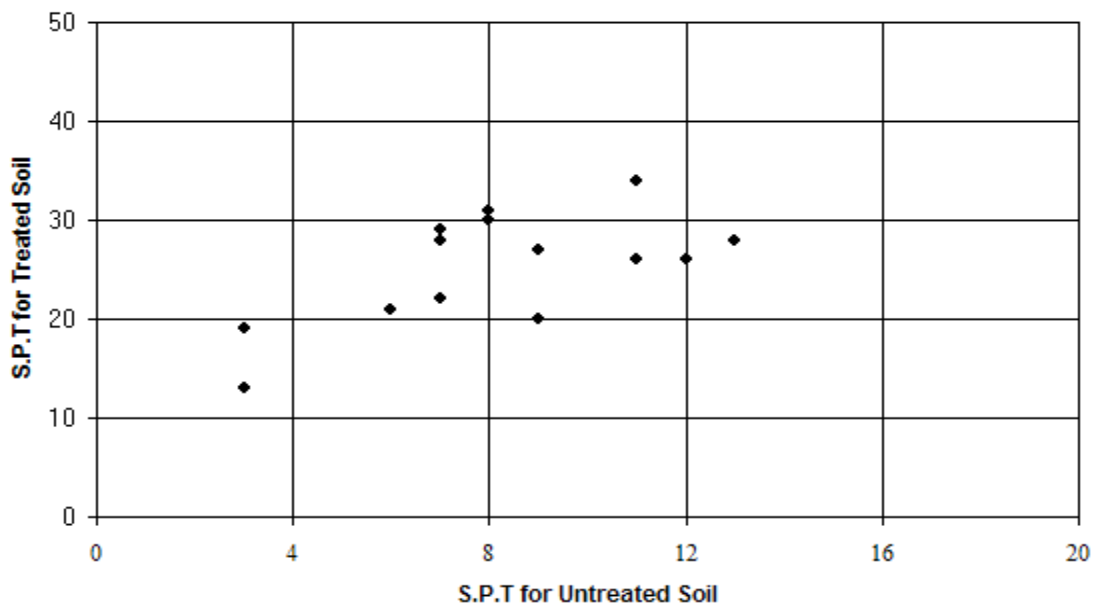


Fig. 8: Comparison between S.P.T results for treated and un-treated soil

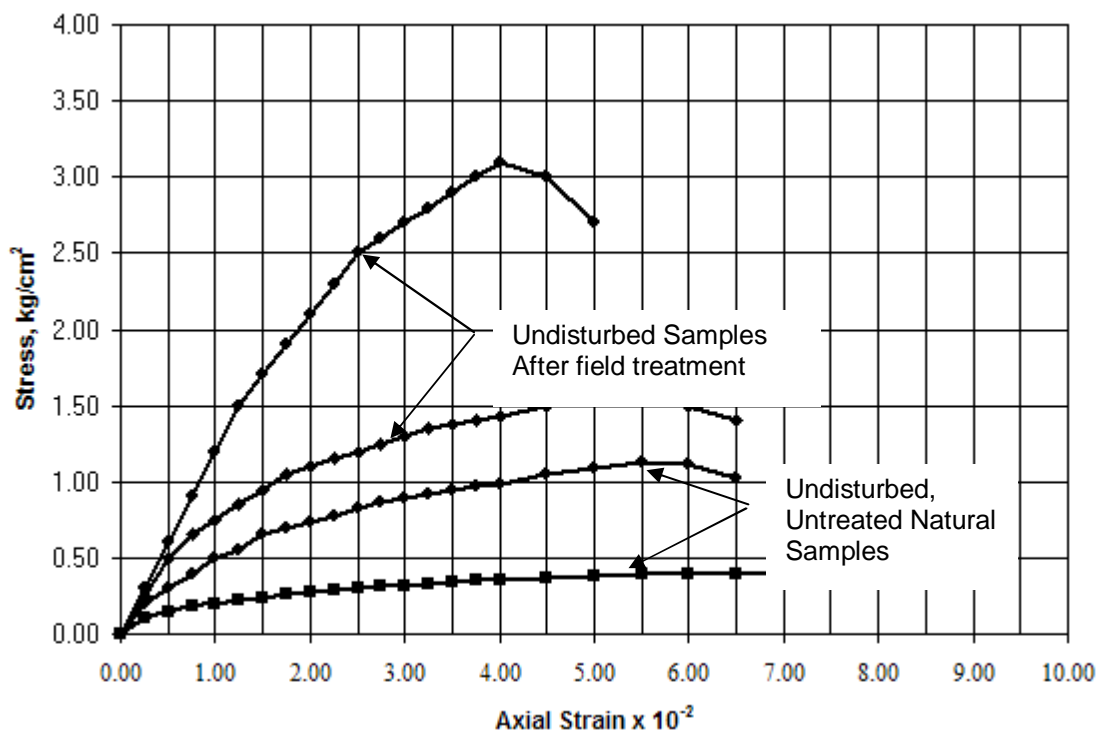


Fig. 9: Stress – strain relation for improved soil (after field treatment)

Figure (11) shows the upper and lower limits of consolidation behavior for 6 tests carried out on undisturbed samples at different depths. Figure (12) shows comparison between the properties of consolidation curves for original soil and that after field stabilization. The stabilized soil has been significantly improved and the lime-treatment succeeded to change the problematic characteristics of cemented collapsing-swelling clay to water stable soil. Figure (13) shows comparison between the consolidation tests for lab and field lime-treated samples. Good agreement was actualized and high confidence level was fulfilled during applying the lab results on the practical field.

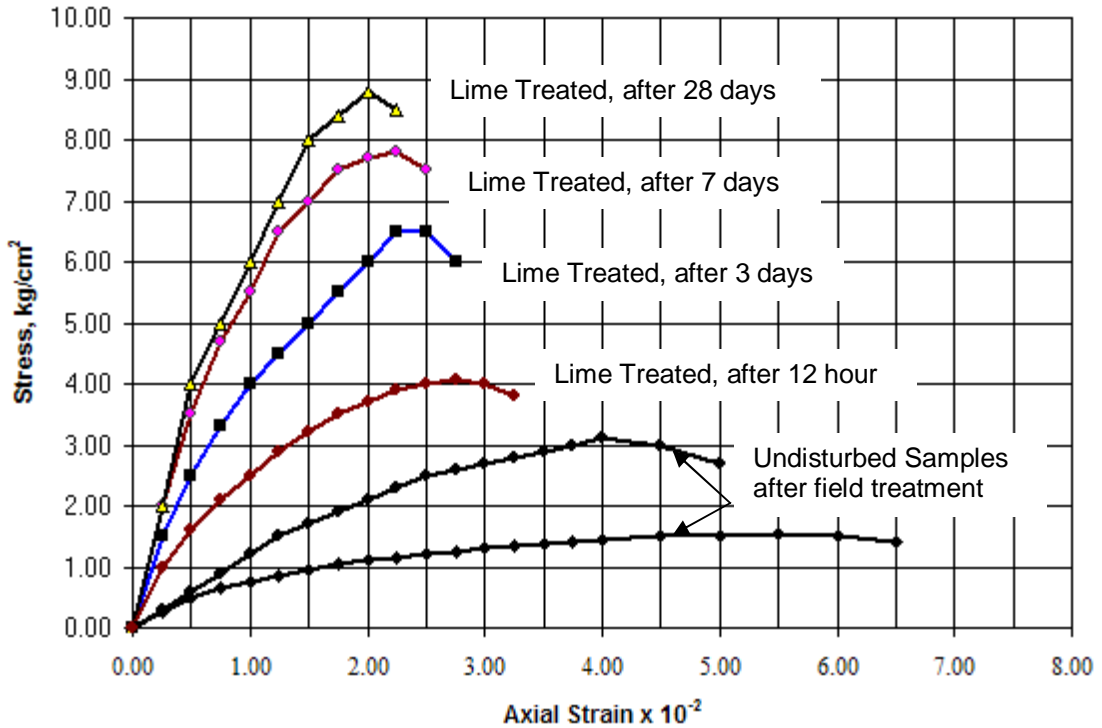


Fig. 10: Comparison between stress-strain relationship for lab treated soil and the field improved soil

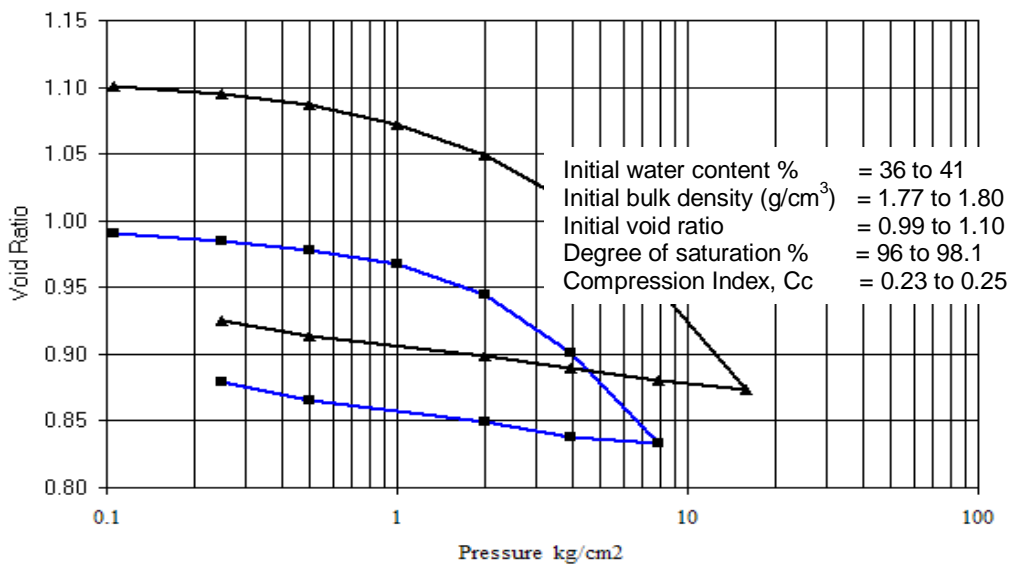


Fig. 11: Consolidation tests after field treatment (upper and lower limits)

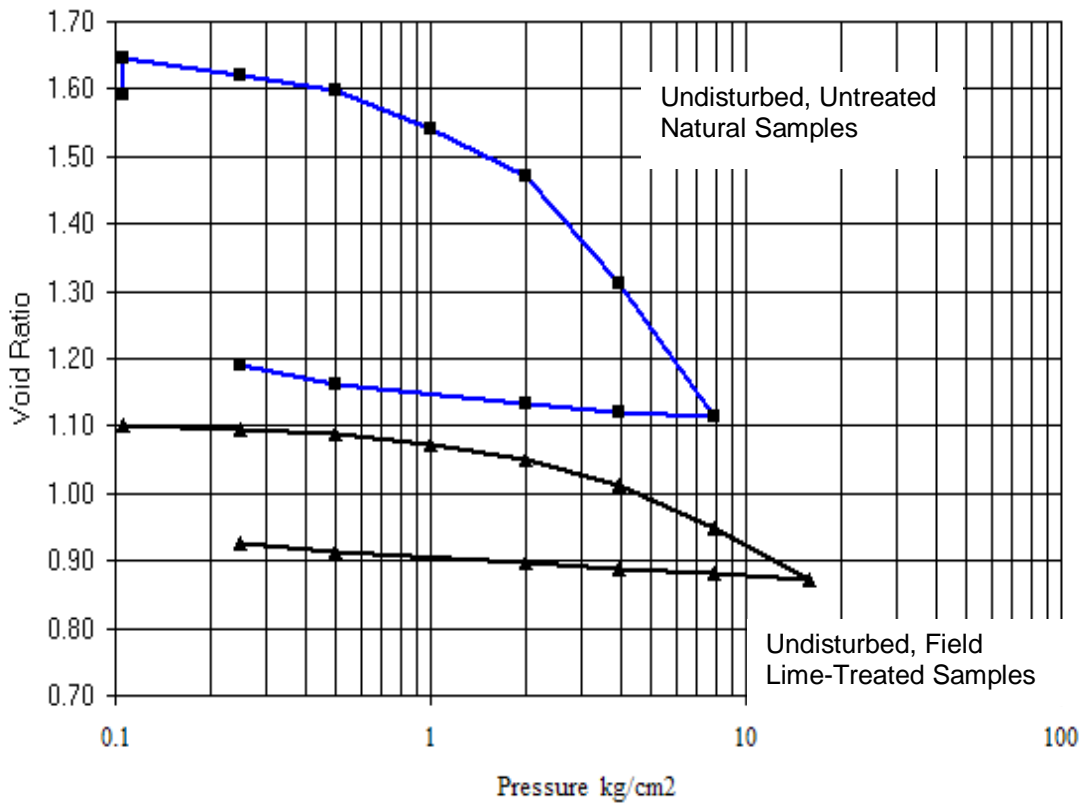


Fig. 12: Shows soil improvement after field treatment in comparison to un-treated soil

Undisturbed, Untreated Natural Samples:	
Initial water content %	= 49
Initial bulk density (g/cm ³)	= 1.48
Initial void ratio	= 1.59
Degree of saturation %	= 79
Specific gravity (assumed)	= 2.58
Compression Index, Cc	= 0.66

Undisturbed, Field Lime-Treated Samples:	
Initial water content %	= 41
Initial bulk density (g/cm ³)	= 1.770
Initial void ratio	= 1.10
Degree of saturation %	= 98.1
Specific gravity (assumed)	= 2.64
Compression Index, Cc	= 0.25

CONCLUSIONS

Cemented collapsing-swelling clay that was found at Al-Madinah Al-Munawarah in Saudi Arabia was stabilized by using lime treatment. Lab program was designed to check the validity, quantity and suitability of lime to improve this type of soil. 8% of lime by dry weight was suggested to be added to the natural soil and dry-mixed to prepare the different lab tests. The important results can be summarized as follows:

- Atterberg limits for treated-soil were obviously affected so that liquid limit decreased while plastic and shrinkage limits increased.
- Treated soil has not any swelling potential and the free swell significantly decreased.
- Unconfined compressive strength for lab tests was highly increased and reached after 28 day about 10 times that for original soil. While the compressive strength after field stabilization reached about 3.0 times.
- Consolidation characteristic for treated soil was highly improved so that void ratio and compression index significantly decreased while bulk and dry density increased.
- In spite of using simple grouting technique for soil stabilization the achievement results were very good according to the lab results.

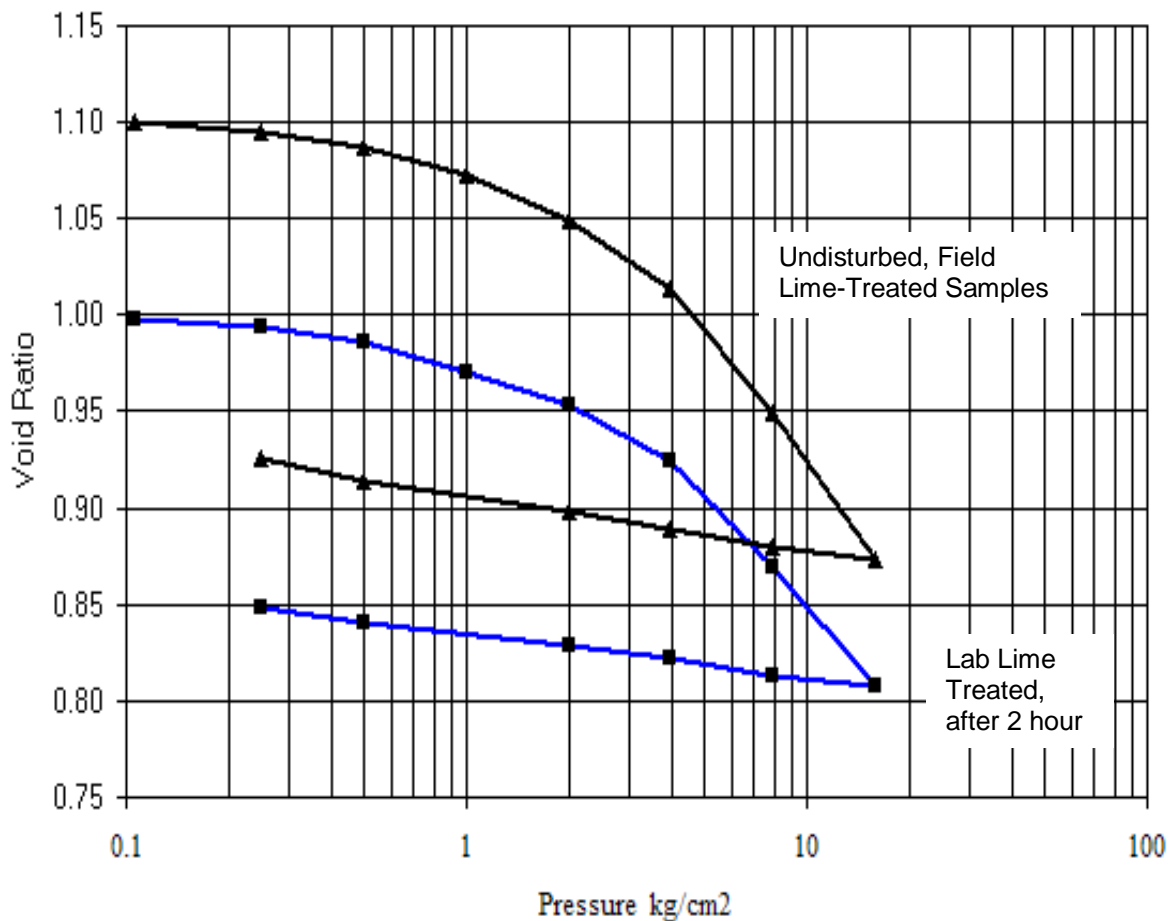


Fig. 13: Shows soil improvement after field treatment in comparison to lab treatment

Lime Treated Samples, after 2 hour:	Undisturbed, Field Lime-Treated Samples:
Initial water content % = 34	Initial water content % = 41
Initial bulk density (g/cm ³) = 1.754	Initial bulk density (g/cm ³) = 1.770
Initial void ratio = 1.00	Initial void ratio = 1.10
Degree of saturation % = 89	Degree of saturation % = 98.1
Specific gravity (assumed) = 2.62	Specific gravity (assumed) = 2.64
Compression Index, Cc = 0.20	Compression Index, Cc = 0.25

ACKNOWLEDGEMENTS

The author would like to thank the staff of AL-JAZZAR consulting engineers, Al-Madinah branch, Saudi Arabia for their assistance during carrying out the field and lab tests.

REFERENCES

1. AL-JAZZAR consulting engineers, K.S.A (2002), technical report # R-02-202 and its supplementary.
2. Canadian Foundation Engineering Manual (1992), Third Edition, Canadian Geotechnical Society.
3. Hammam, A.H and Abdul Salam, A.I (2008), "Effect of geotechnical & structural problems on failure of structures", Symposium disasters` management & safety of buildings in Arab Countries, Riyadh, Saudi Arabia, March 29 – April 01.
4. Hammam, A.H, et al (2007), "Properties of cemented collapsing-swelling clay", Journal of the Egyptian Geotechnical Society, Vol. 18, part 2.
5. Hoda Abd Elhady (2007), "Properties of treated expansive soil", 12th International colloquium on structural and geotechnical engineering, Ain Shams Univ., Egypt.
6. Abdel-Aziz A.A.Senoon (2006), "Effect of lime admixture on the properties of compacted sandy soil", Journal of the Egyptian Geotechnical Society, Vol. 17, part 2.
7. Awad, T. and Abdel-Hady, H. (2005), "Movement of laboratory footing model resting on treated expansive soil", 11th Int. colloquium on structural and geotechnical Engineering, Ain Shams Univ., Egypt.
8. El-Hoseiny, K. E., Youssef, A. A. and Samaan, E. H. (2005), "Improving of expansive soil behavior using different techniques", 11th Int. colloquium on structural and geotechnical Engineering, Ain Shams Univ., Egypt.
9. Muntohar, A.S. (2002), "Improvement of the bearing of soil by using lime-rice husk ash", 2nd International conference on geotechnical and geo-environmental engineering in arid lands, Riyadh, Saudi Arabia.
10. Moseley, M.P. (1996), "Ground improvement", Blackie Academic & Professional, first edition.
11. Mohamed, A.M.O., et al (1991), "Soil improvement using chemical treatment", 1st geotechnical engineering conference, Cairo Univ., Sept. 30 – Oct. 3.
12. Bowles, J.E. (1996), "Foundation Analysis and Design", 5th edition, McGraw-Hill, New York.
13. NAVY and Air Force, Department of the Army, USA (1994), "Manual of soil stabilization for pavement".
14. Mossaad, M.E et al (2008), "A study on collapsing soil in Egypt", National Academy for Scientific Research and Technology, final report.
15. Evans, G. L., and Bell, D. H. (1981), "Chemical stabilization of Loess, New Zealand", 10th International conference on Soil Mechanics and Foundation Engineering
16. El-Sakhawy, R. (1999), "Stabilization of Collapsible Soil with Slag", Journal of the Egyptian Geotechnical Society.
17. El-Sakhawy, R. (2000), "Treatment of Collapsible Soil by Cement Dust", Journal of the Egyptian Geotechnical Society.
18. Al-Hamoud, A. S., Khedaywi, T., and Al-Ajlouni M. (1995), "Studies on the control of swell and collapse potential of selected Jordanian soils using asphalt stabilization", Soils and Foundations, 35(2), 15-23.

19. Gulsah Yesilbas (2004), "Stabilization of expansive soils using aggregate waste, rock powder and lime", M.Sc., Natural and applied sciences of the Middle East Technical Univ.
20. Egyptian Code for Soil Mechanics and Foundation Design & Construction (2001), "Foundations on Problematic Soils", Vol. 5.
21. Radwan, A.M. (1994), "Practical Principles & Fundamentals of Soil Mechanics", Scientific Book House, Cairo, Egypt (Arabic).

STRENGTHENING OF HOLLOW CONCRETE MASONRY WALLS WITH OR WITHOUT OPENING USING DIFFERENT TECHNIQUES

Mohamad M. El-Attar, Ahmed A. El-Nady

Structural Engineering Department, Faculty of Engineering, Cairo University, Cairo, Egypt

Hossam Z. El-Karmoty*, Amal A. Ibrahim

Housing and Building National Research Center, Cairo, Egypt

ABSTRACT

Egypt possesses a wealth of old unreinforced masonry (URM) buildings, most of them are of historic significance. Many of these masonry structures need to be retrofitted either because of increasing loads and/ or durability problems, change in seismic requirements, lack of maintenance and conversion of old buildings to new houses or occupancies. In the last 25 years many achievements have been developed in the strengthening techniques and retrofitting of buildings. The application of modern materials in strengthening and repairing techniques is now rapidly growing in many types of structures. This paper presents an experimental study on retrofitting of the unreinforced concrete masonry walls by using some techniques which are grout injection, ferrocement overlays, ordinary plastering and glass fiber polymers sheets (GFRP). Eleven wall panels were subjected to uniform vertical loads. Different parameters were taken into consideration during this study; namely; type of retrofitting techniques, the presence and absence of the wall openings and finally the shape of the opening. Different properties were observed, measured and compared in this investigation; such as crack pattern, failure mode, the cracking and failure loads, maximum strain, initial stiffness, and toughness. In general; the experimental results demonstrated that the using of these techniques of strengthening achieve better cracking behavior and mode of failure. Also, the axial load capacity, initial stiffness and toughness of the wall were relatively enhanced. It was found that the application of the grout injection greatly enhances the overall behavior of the wall panel. The strength of the walls was directly affected by presence of the opening and its dimensions. Many conclusions, relations, and recommendations that may be useful for designers were obtained and introduced.

Keywords: Unreinforced Masonry Buildings, Ferrocement, Grout, GFRP.

INTRODUCTION

Masonry is one of the oldest forms of construction known to humanity. The term masonry refers generally to brick, stone, concrete-block, etc., or combination therefore, bonded with mortar. Masonry can be define as "construction usually in mortar, of natural building stone or manufactured units such as brick, concrete block, adobe, glass, block tile, manufacture stone, or gypsum block". Many of the masonry structures need to be retrofitted either because of inadequate design criteria, deterioration of the structural materials as a consequence of age and inadequate maintenance, uneven settlements, or because of increase in seismic load demand. There are several techniques that are commonly used for strengthening the masonry walls and the choice of the sustainable technique depends on some reasons such as the type of masonry, the geometry of the wall, the type of stresses which the wall is subjected to and the required level of upgrading.

* Corresponding author
Received Date: 3/9/08
Acceptance Date:23/10/08

Several conventional rehabilitation techniques for masonry walls (both clay and concrete) have been developed and presented by many researches ^{1,2,3,4,5,6,7,8}. These techniques considered include epoxy injection, shotcrete, external reinforcement, ferrocement center core technique, grouting, bonding FRP strips to the face of masonry wall and injection of epoxy mortar. The current study aims to investigate the behaviour of concrete blocks unreinforced masonry walls with or without openings under uniform vertical loads. Four techniques were used for strengthening: ferrocement overlays, grout, ordinary plastering and GFRP laminate. To achieve the aim of the current study, an experimental program consisting of testing eleven wall panels 1600 by 1200 mm under uniform vertical load was conducted. The type of strengthening technique and the presence & geometry of the opening are the main key variables studied in the current research.

RESEARCH PROGRAM

The experimental test program was designed to achieve the research objectives of the study. Eleven wall panels 1600 by 1200 mm were manufactured for this experimental program as shown in Table 1 and Figure 1 using hollow concrete blocks. All wall panels were constructed using the same mason to maintain the same level of workmanship. The mortar joint thickness was kept 10 mm throughout all panels. The joint thickness was controlled by wooden bar 10 mm square section. The mortar joint were used on both faces of the panel. Water curing process was applied for about 7 days using sprinkler to wet the wall panels by fresh water once a day. As shown in Table 1, two shapes of openings were used, square (400 * 400 mm) or rectangular (400 * 800 mm). The effect of the four strengthening techniques were studied and compared in the study: ordinary plastering, GFRP laminates, ferrocement overlays and grout.

Table 1: Details of the Tested Walls

Wall	Geometry of opening	Technique of strengthening
W1	Non	Non
W2	Square	Non
W3	Rectangular	Non
W4	Non	Grout
W5	Square	Grout
W6	Rectangular	Grout
W7	Non	Ferrocement Overlays
W8	Square	Ferrocement Overlays
W9	Rectangular	Ferrocement Overlays
W10	Non	Ordinary Plastering
W11	Square	GFRP Laminates (Two Faces)

MATERIALS PROPERTIES

The structural behavior of masonry walls depends on the properties of the material which used in construction of the walls such as (brick, mortar, cement ...etc.). So several tests were carried out on these materials during the phases of the construction of the walls in order to control the quality of walls construction to minimize the variation in quality that may appear in the construction and strengthening processes.

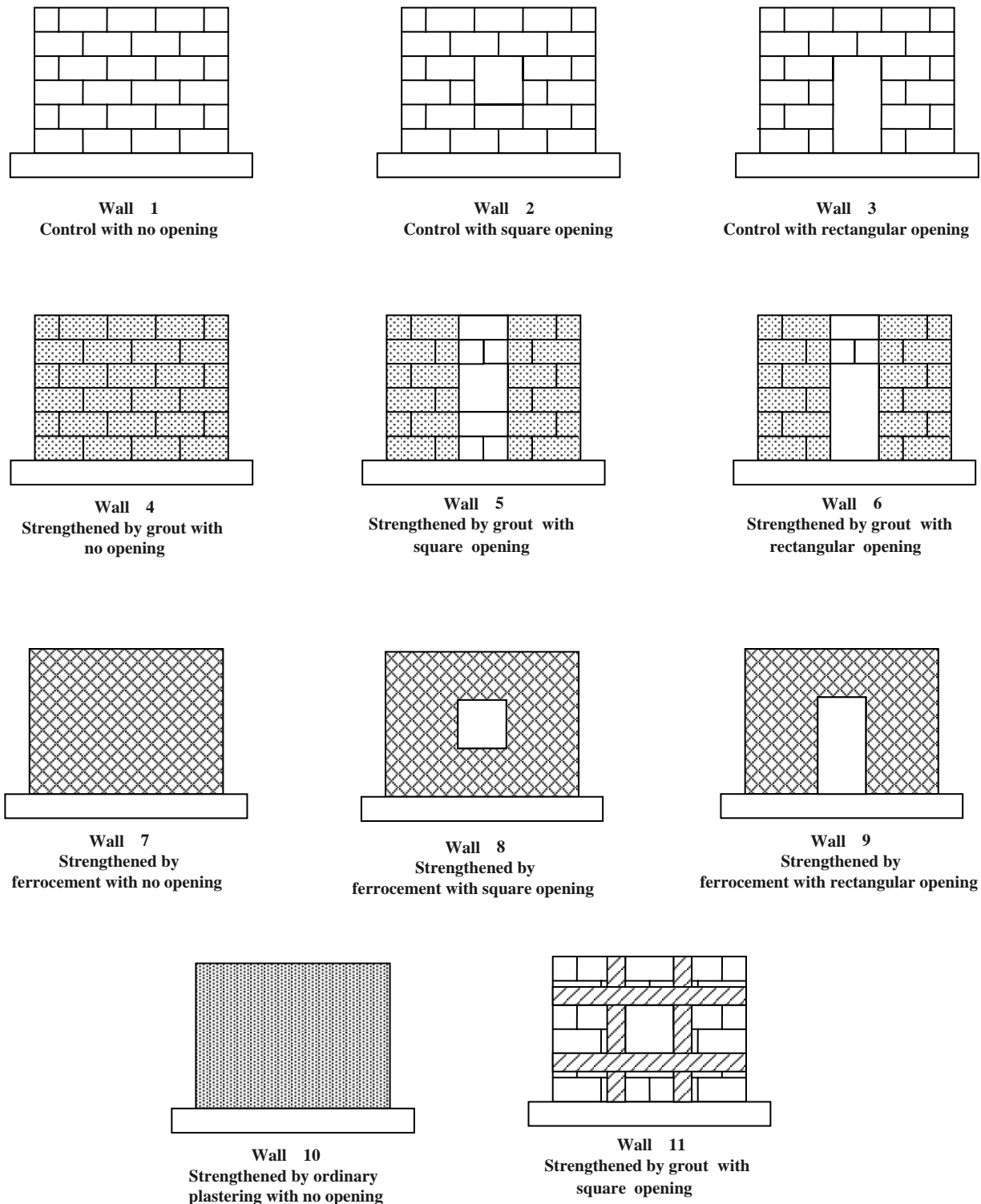


Figure 1 Tested Walls in the Experimental Program

Concrete hollow blocks with dimensions (400*200*200) mm were used; quality control tests were carried on a sample of three individual blocks according to the Egyptian standard specifications (ESS 1292-1/2005)⁹. The average compressive strength of concrete hollow blocks was 140.56 kg/cm². Unit weight of concrete hollow blocks was 1.22.

Local sand from natural sources complied with Egyptian standard specification (ESS 1109-2001)¹⁰ was used for masonry mortar, ferrocement mortar and plaster. The sand used was free from any impurities and the maximum permissible weight percent of deleterious substances did not exceed 1%. Sieve analysis was carried out on the sand; and the sand grading was found to be between the limits of Egyptian standard specification.

CEM I 42.5 N produced by Egyptian Cement Company was used in this research work. The physical and mechanical tests were done as per (ESS No. 2421/ 2005)¹¹. The physical and mechanical properties are complying with (ESS. No. 4756 -1/2007)¹².

GFRP laminates of 0.11-mm thickness and 100 mm width were used for strengthening walls W11, W12. The tensile strength and modulus of elasticity of the laminates were (2250 MPa) and (70 GPa), respectively as reported by the manufacturing company. Epoxy resin was used to bond the GFRP laminates to the face of the wall.

Galvanized steel wire mesh-fabric of the woven form with 20 mm square openings was used, with plastering layer, to form a ferrocement overlay. This steel wire mesh is locally produced in the form of rolls (1.2 wide and 10 m long). The wires were 1.9 mm diameter and their yield strength was 380 N/mm². Steel anchors of nominal diameter 8.5 mm at spacing 400 mm in vertical and horizontal directions were used for fixing the steel wire mesh to the masonry wall panel before plastering.

MORTAR AND GROUT MIXES

A type No. 1 mortar, fulfilling the Egyptian Code of Masonry (ECM 2005)¹³, was used in the construction of the wall panels. This type has been widely used in Egypt by most masons, with mix proportions (by weight of cement) as follows:

Cement : Sand : Water
1 : 2.5 : 1

According to ECM, (2005), these proportions have a guide minimum compressive strength value equal 15· Kg / cm². The water was established by the mason's requirements for suitable workability. The mortar used was mixed by hand on a steel plate and then used within five minutes directly after mixing. In order to determine an important property of the plastic mortar properties, several measures of workability in the laboratory were made on the masonry mortar by the flow test, using standard flow table, to control the mason's requirements. In this test, the flow of mortar is measured by the increase in diameter of a cone of mortar after 25 drops on the standard flow table. The flow table as a measure of mortar consistency is used during the construction of all walls; the suitable flow as found was about 100% depending on the day temperature, relative humidity, and materials conditions. Further more, compressive strength of masonry mortar was measured. Nine cubes (50*50*50 mm) per each wall were cast in a nonabsorbent mould. These cubes were tested in axial compression at 3,7,28 days respectively and at the same age of testing of the corresponding wall. The results show that the average compressive strength for the masonry mortar at the age of 28 days was 175.58 kg/cm². This value exceeded the guide value required by ECM, (2005), which equals 150 kg/cm² for mortar type N0.1. The mix which used in the ferrocement mortar has to get appropriate mortar consistency to ensure proper application of the mortar on the steel mesh-fabric overlay. The appropriate flowability was found to be in the ranges from 130 to 160 % on the standard flow table test. This mix has a target compressive strength 400 kg / cm², had cement content of 650 kg per cubic meter, and its mix proportions (by weight of cement) were as follows :

Cement: Sand: Water
1 : 2.0 : 0.4

Compressive strength for the ferrocement mortar was measured by using control cubes (100*100*100 mm) were tested in compression. The results show that the average compressive

strength for the masonry mortar at the age of 28 days was 460 kg/cm². This value exceeded the target compressive strength.

According to the Egyptian Code of Masonry (ECM), (2005), second type of grout mortar (grouting for thickness more than 50 mm) was used in strengthening the masonry walls this type has a minimum compressive strength 140 kg / cm², its mix proportions (by weight of cement) were as follows:

Cement: Sand: Gravel: Water
1 : 2.5 : 1.5 : 1

This grout mortar was mixed and poured in the holes of the masonry walls and compacted well with an electrical vibrator. A slump test was done on the grout mortar to measure its slump using the slump cone within 5 minutes of obtaining the final portion of the mortar. The slump test result gives a slump about 200 mm. Further more, compressive strength of grout mortar was measured. Nine cubes (100*100*100 mm) per each wall were cast in a nonabsorbent mould. These cubes were tested in axial compression at 3,7,28 days respectively. The results show that the average compressive strength for the grout mortar at the age of 28 days was 180.12 kg/cm². This value exceeded the guide value required by ECM, (2005), which equals 140 kg/cm² for this type of grout mortar.

PRISM TESTS AND RESULTS

Three prisms, one for each mortar mix during wall construction were built using the same mortar mix for the walls. The height to thickness ratio for all prisms was about three, which fulfill the ASTM C1314¹⁴ and ACI 530-(MSJC)¹⁵ requirements. Prisms were built consisting of a single wythe specimen laid in stack bond of three concrete blocks. The prisms were cured in the same conditions of the corresponding walls. Gypsum-capping layers were applied on the top and bottom of the prisms in order to achieve good leveling under loading and avoid local stresses.

The prisms were placed on the testing machine with capacity 50 tons after measuring the dimensions. The load increased gradually with constant rate up to failure. The masonry compressive strength (f_m') was calculated according to the Equation (2-1) from ACI 530-(MSJC). Correction factor was taken according to the height to thickness ratio.

$$f_m' = [P_{\max} / (l * t_{\min})] * C.F$$

Where:

f_m' : masonry prism compressive strength

P_{\max} : Max. Crushing load of prism

l: prism min. width

C.F: Correction factor

It was found that masonry compressive strength was about 62.79 kg/cm².

APPLICATION OF STRENGTHENING TECHNIQUES

Ordinary plastering was applied to the masonry wall as follows: at first, the wall was spattered with 2:1 cement: sand slurry after 28 days from the construction of the wall, then the plastering mortar that was mixed with proportions with 1.0 cement, 2.0 sand, and 0.4 water was applied to the wall from the two faces with about 20 mm thickness. The plastering mortar layer was cured by water for 7 days.

Ferrocement overlays were applied to the strengthened masonry walls as follows : the walls were spattered with 2:1 cement : sand slurry after 28 days from the construction , then drilling through holes at steel anchors places (40 spacing in both vertical and horizontal directions) was carried out. The steel mesh –fabric was fixed over the anchors using washers and tying nuts. Finally, plastering mortar was applied with about 20 mm thickness. The ferrocement overlay was cured by water for 7 days.

GFRP laminates were attached to the wall after the wall mortar had reached an age of 28 days. The strengthening procedure was applied according to the instructions of the manufacturing company of the laminates. The wall surface was prepared by removing the weak elements. The mixed resin was applied to the prepared surface using a trowel in a quantity of approximately 1.0 to 1.2 kg/m² depending on roughness of the surface. The GFRP laminates were attached to the wall and rolled by special laminating roller to ensure that GFRP laminates are saturated in the epoxy resin and there is no air voids between the fibers and the wall surface. The glued vertical and horizontal GFRP strips around the opening had length 1600 mm in horizontal direction and 1200 mm in vertical direction from the two faces.

A Grout mortar was mixed with a proportion 1 cement: 2.5 sand: 1.5 gravel: 1 water and poured in the holes of the concrete blocks with a distance about 600mm from the right and left of the openings along the overall height of the wall. This mix was compacted very well during pouring by using an electrical vibrator.

WALL PANEL TESTING SETUP AND MEASUREMENTS PROCEDURES

The wall panels were tested using a compression hydraulic jack with a maximum capacity 300 tons. The walls were constructed on a reinforced concrete beams with a dimensions 2000mm long and with a cross-section 200mm * 300 mm to be rested on it and to help in hanging them during transportations. For testing the walls, they were transported using a wire crane to a large frame and placed on it. In order to simulate uniform loading a (C channel) steel beam was rested on the top on the wall in addition with a steel rigid I-beam with a depth 400 mm welded with 7 stiffeners at a distance 320 mm between them.

Two Linear Voltages Displacement Transducers (LVDT) were fixed on the surface of the wall panels' faces with appropriate length, using steel angles for fixation. The type of (LVDT) used has a maximum displacement 25 mm (tension and compression). These two (LVDT) were fixed to measure vertical strains with gage length 80 cm. Also two dial gauges were fixed on the walls near the (LVDT) to take vertical measurements in case of (LVDT) not functioning.

After fixing the specimen wall panels in the test setup, the load was increased gradually with constant rate up to failure. The deformations and the loading sequence were directly recorded and collected by a data acquisition system, and processed by computer. For each panel the first cracking load and the failure load were observed and recorded. Also the crack pattern was mapped on the panels to determine its cracking behavior.

DISCUSSION OF EXPERIMENTAL RESULTS

Table 2 summarizes the outcome of the experiments: the maximum ultimate load P_{max} , maximum strain, initial stiffness and toughness. There are two main variables for the testing program: the first variable is the four strengthening techniques which are used (Grout mortar, GFRP laminates, ferrocement overlays and plastering layers) and the second variable is the effect of presence of opening and its dimensions. Also, Figure 2 shows the failure modes of all walls.

Table 2: Experimental Results

Wall No	Strengthening Technique	Ultimate Load (KN)	Strain at Ultimate Load (mm/mm)	Initial Stiffness (KN.mm/mm)	Toughness (KN.mm/mm)
1	Control	920	0.0042	142910	2.72
2	Control	820	0.0058	115605	2.35
3	Control	660	0.0056	98360	1.85
4	Grout	2300	0.013	404614	23.36
5	Grout	1850	0.012	241154	14.3
6	Grout	1800	0.014	212882	17.8
7	Ferrocement	1400	0.012	305480	11.73
8	Ferrocement	1100	0.0066	212566	3.99
9	Ferrocement	1000	0.0078	158865	5.29
10	Plastering	1210	0.006	180600	5.7
11	GFRP	970	0.0054	158559	2.81

EFFECT OF PRESENCE AND GEOMETRY OF OPENINGS

The effect of presence and geometry of openings on the ultimate capacity and behavior of the walls can be reflected by comparing similar walls which have the same properties such as presence of the same strengthening techniques or which unstrengthened with different geometry of opening.

Figure 3 shows the load-strain relationship of walls W1, W2, W3 which are tested as control walls as illustrated in Table 1. W1 has no opening while W2 and W3 have square (400 mm * 400 mm) and rectangular (400 mm * 800 mm) openings, respectively. As shown from Figure 3 the wall without opening W1 recorded an ultimate capacity of 920 KN while the wall that possessed opening resulted in a significant reduction in ultimate capacity of 10.8 % (Pult = 820 KN) in case of presence of square opening W2 and 28.3 % (Pult = 660 KN) in case of presence of rectangular opening W3.

In other words, presence of opening in the tested walls displayed less stiffness and strength so it was noticed also from the result calculations in Table 2 that the stiffness was reduced from 142910 KN.mm/mm for W1 to 115605, 98360 for W2 and W3 respectively, and the toughness was reduced from 2.72 KN.mm/mm for W1 to 2.35, 1.85 for W2, W3 respectively. Moreover, rectangular opening weakened the stiffness, the toughness and the strength of the tested walls than square opening. This is attributed to the reduction in the cross section of the tested wall, i.e. less moment of inertia.

As shown in Figure 2, failure cracks of W1 were mainly due to splitting in the bricks and passing through the joints. Cracks appeared near the top and propagated to the bottom. On the other hand, presence of openings in the walls W2 & W3 changed the mode of failure. Major straight cracks appeared beside the openings and propagated to the bottom and the top of the walls.

The same trend can be shown in Figure 4 and Figure 5 which present the load-vertical strain relationships of walls W4, W5, W6 which are strengthened by grout mortar and W7, W8, W9 which are strengthened by ferrocement overlays.

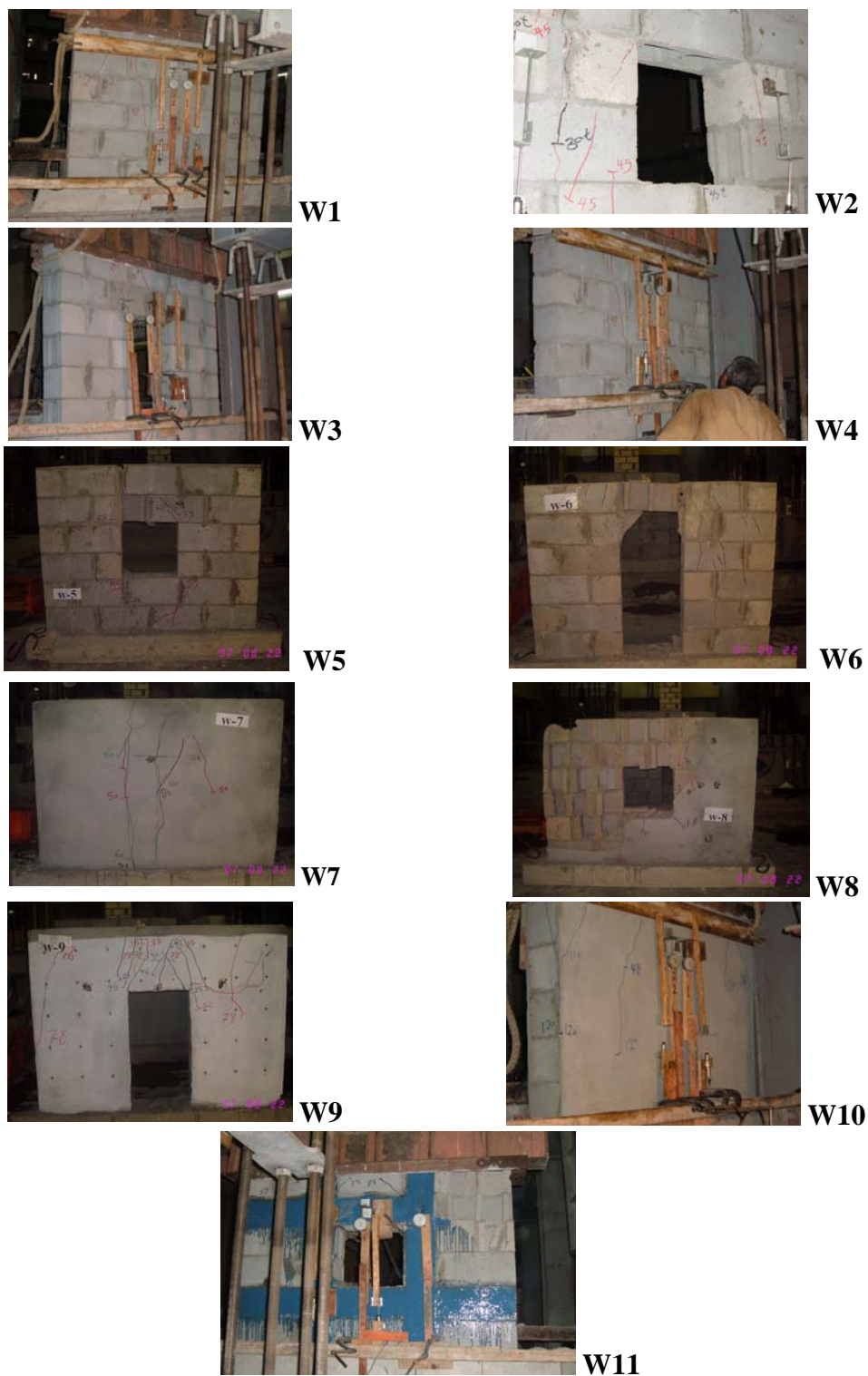


Figure 2 Failure Modes of Walls

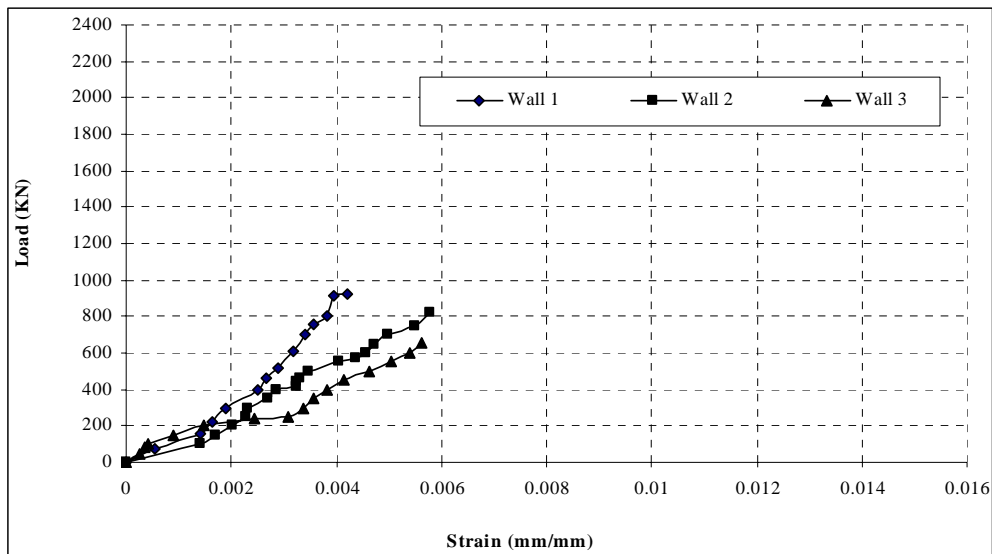


Figure 3 The Load-Strain Relationship of Walls W1, W2, W3

From Figure 4, W4 which has no opening recorded an ultimate capacity of 2300 KN while the wall W5, W6 that possessed square and rectangular opening showed lower ultimate capacity when comparing to wall W4. The decrease was about 20 % (Pult = 1850 KN), and 22 % (Pult = 1800 KN), respectively. On other hand ,the stiffness was reduced from 404614 for wall W4 to 241154, 212882 for walls W5,W6 and the toughness was 23.36 for wall W4 and reduced to 14.3 , 17.8 for walls W5, W6 respectively. No failure cracks appeared in wall W4 such that it failed suddenly at its maximum load in contrast with walls W5, W7 which have square and rectangular openings lead to changing their mode of failure. Very few cracks appeared above and under the openings in the regions without grout mortar. Also there was a very few cracks on the right and left of the opening in wall W6 propagated through the mortar joints.

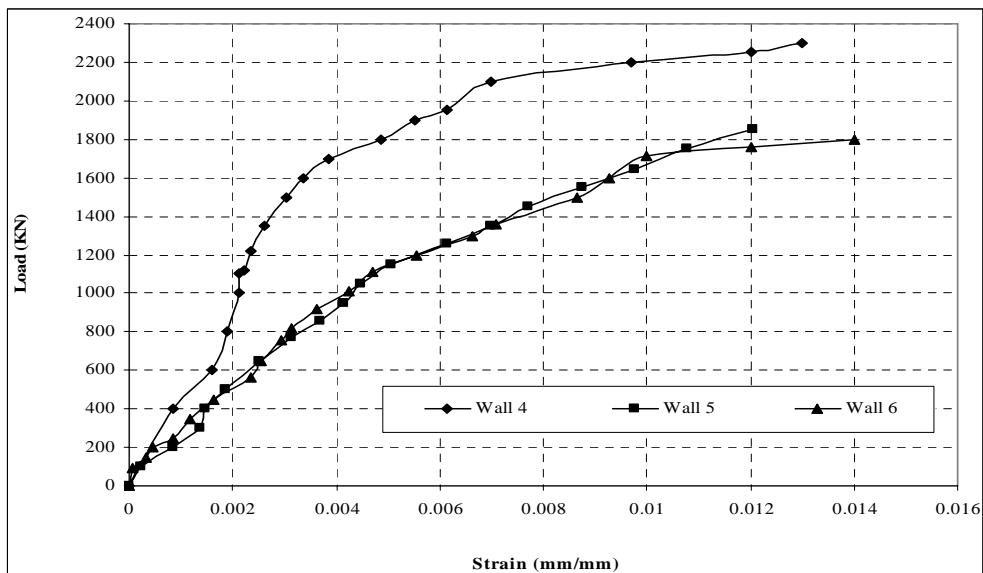


Figure 4 The Load-Strain Relationship of Walls W4, W5, W6

In Figure 5, it is shown that W7 which has no opening recorded an ultimate capacity of 1400 KN while the wall W8, W9 that possessed square and rectangular openings showed lower ultimate capacity when compared to wall W7 about 21% (Pult = 1100 KN) , 28.5 % (Pult = 1000 KN), respectively. On other hand ,the stiffness was reduced from 305480 for wall W7 to 212566, 158865 for walls W8, W9 and the toughness was 11.72 for wall W7 and reduced to 3.99 , 5.29 for walls W8, W9 respectively. As shown in Figure 8, failure cracks of W7 were

mainly due to crushing in the layers of ferrocement plastering in the middle of the wall. Cracks appeared near the top and propagated to the bottom. On the other hand, presence of openings in the walls W8 & W9 changed the mode of failure; Major straight cracks appeared beside the openings and propagated to the bottom and the top of the walls and a crushing in the ferrocement overlays was found.

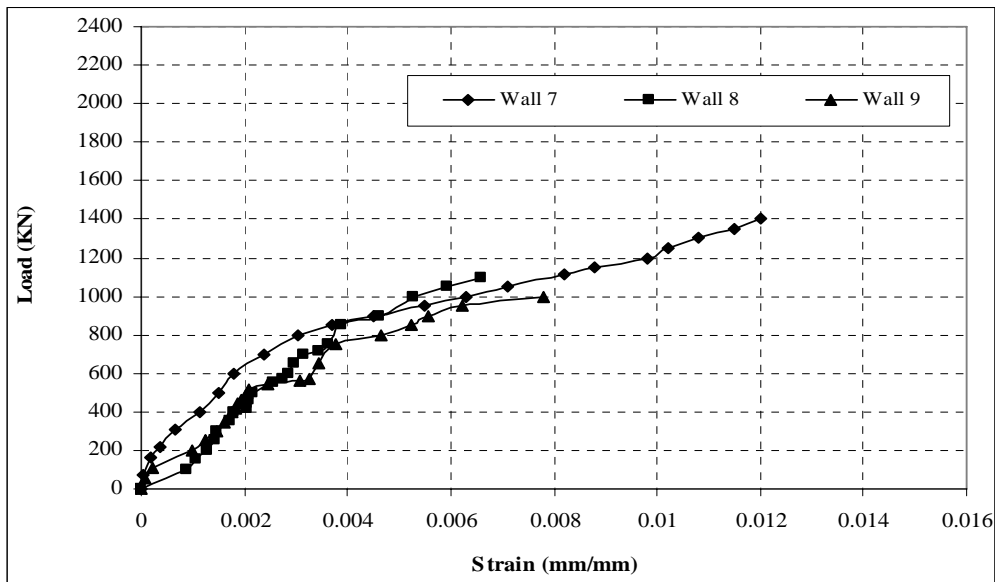


Figure 5 The Load-Strain Relationship of Walls W7, W8, W9

EFFECT OF STRENGTHENING TECHNIQUES

As mentioned before, the present study aims to investigate the effect of four strengthening techniques for upgrading the ultimate bearing capacity of masonry walls.

Figure 6 shows the load-strain relationships of walls that have no openings which are W1, W4, W7, W10; such that wall W1 was the control specimen (unstrengthened) while walls W4, W7, W10 were strengthened with different techniques; W4 was strengthened by grout mortar in the holes of the blocks along 600 mm from each end of the wall, W7 was strengthened by ferrocement overlays from two faces and W10 was strengthened by a layers of plastering. It was shown from Figure 6 that the wall strengthened by a grout mortar W4 gives the highest ultimate bearing capacity and the highest toughness value, while the wall W7 which is strengthened by ferrocement overlays give the highest stiffness value. Figure 6 also showed that all of the used strengthening techniques increased the ultimate capacity of the tested walls when compared to the control wall W1. Wall W4 which was strengthened by a grout mortar showed the highest increase in the ultimate bearing capacity (150 %). Failure of W4 was a sudden failure and there was a very few cracks appeared in the middle part of the wall which have no grout in its holes. On other hand, wall W7 which was strengthened by ferrocement overlays from the two faces recorded an ultimate capacity equal 1400 kN, i.e. the increase in the capacity was 52.2 %. Failure of wall W7 occurred due to increasing the cracks and crushing in the ferrocement overlays.

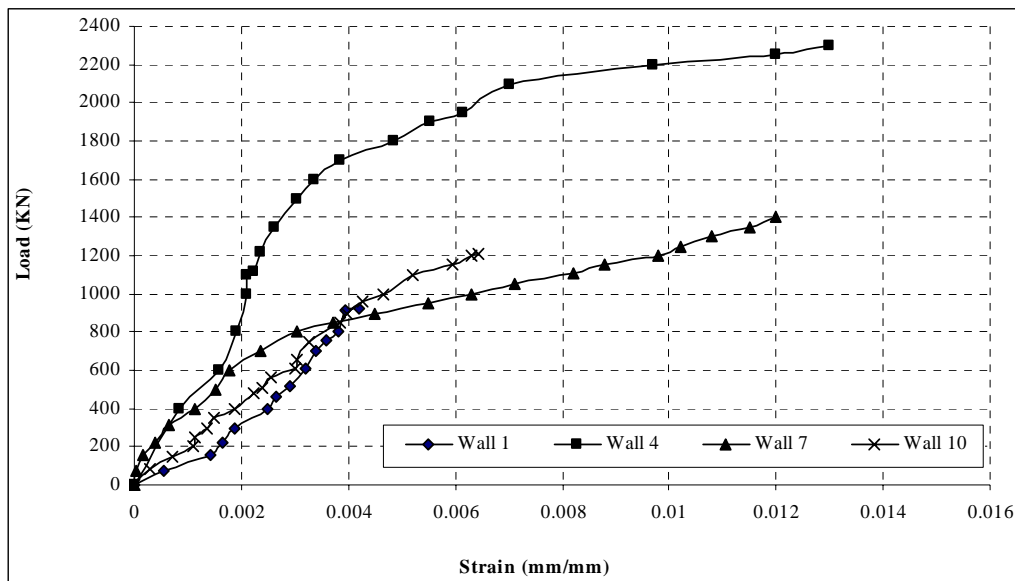


Figure 6 The Load-Strain Relationship of Walls W1, W4, W7, W10

Also, the strengthening using ordinary plastering layers didn't achieve a significant increase for the bearing capacity of the tested wall. The recorded ultimate load for W10 was 1000 KN, i.e. the increase in the capacity was 9 % only. Failure of wall W10 was due to depending of mortar plastering followed by a propagation of cracks. It can be observed also that the capacities of the walls strengthened with a grout mortar and ferrocement overlays techniques, W4 & W7 respectively, were shown to be much higher than the wall strengthened by ordinary plastering only, W10 by about 90 % and 16 % respectively.

Figure 7 show a comparison between using of strengthening techniques in walls W2, W5, W8, W11 which have square openings (400 mm * 400 mm); such that wall W2 was the control specimen (unstrengthened) while walls W5, W8, W11 were strengthened with different techniques; W5 was strengthened by grout mortar in the holes of the blocks along 600 mm from each end of the wall beside the opening, W8 was strengthened by ferrocement overlays from two faces and W11 was strengthened by GFRP laminates around the opening. The same sequence as illustrated in case of walls with no opening. Wall W5 that strengthened by a grout mortar give the highest ultimate bearing capacity and the highest toughness value, while the wall W8 which strengthened by a ferrocement overlays give a higher stiffness value, on other hand wall W11 which strengthened by GFRP laminates give a lowest value of ultimate bearing capacity, stiffness and toughness.

Figure 7 also showed that all of the used strengthening techniques increased the ultimate capacity of the tested walls when compared to the control wall W2. Wall W5 which was strengthened by a grout mortar showed the highest increase in the ultimate bearing capacity (126 %). Failure of W5 was a sudden failure and there was a very few cracks above and under the opening. On other hand, wall W8 which was strengthened by a ferrocement overlay from the two faces recorded an ultimate capacity equal 1100 KN, i.e. the increase in the capacity was 34 %. Failure of wall W8 occurred due to propagation of the cracks and crushing in the ferrocement overlays around the opening. The using of GRFP for strengthening in wall W11 didn't increase its bearing capacity of the tested wall compared with the control wall W2 so much. The recorded ultimate load for W11 was 970 KN, i.e. the increase in the capacity was 18.3 % only. Failure of wall W11 occurred due to propagation of cracks around the opening followed by rupture of GFRP laminates, then a part of the masonry blocks was fell down.

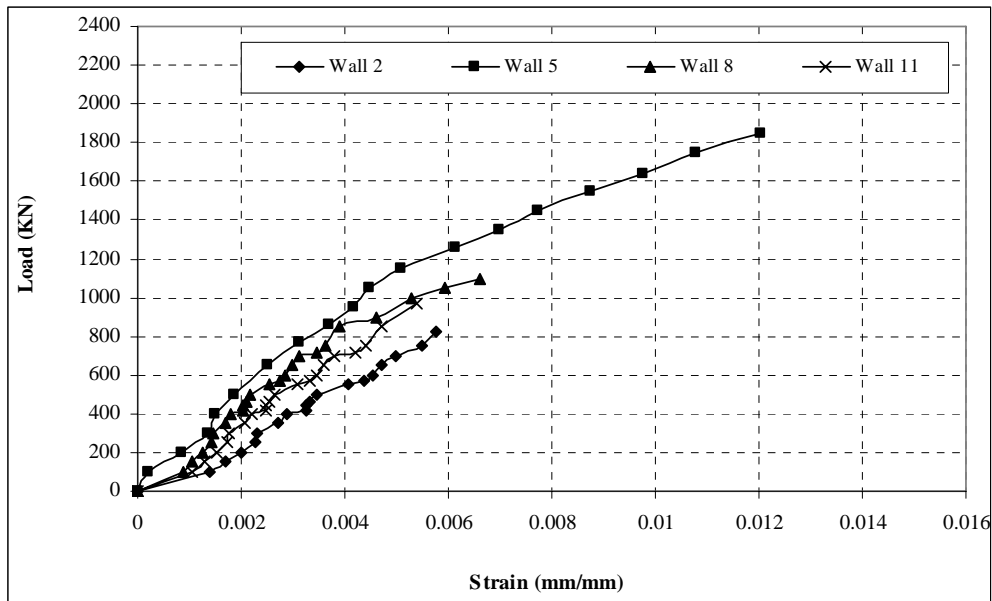


Figure 7 The Load-Strain Relationship of Walls W2, W5, W8, W11

From the last results, it can be observed that the capacities of the walls strengthened with a grout mortar and ferrocement overlays techniques, W5 & W8 respectively, were higher than the wall strengthened by GFRP laminates, W11 by about 91 % and 13.4 %, respectively.

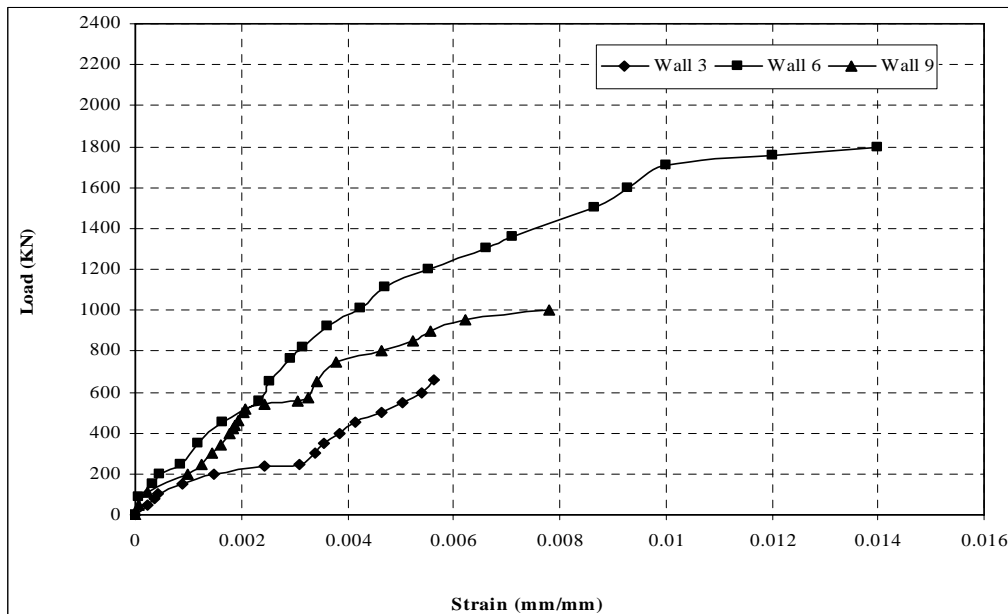


Figure 8 The Load-Strain Relationship of Walls W3, W6, W9

The last comparison which studies the effect of using different strengthening techniques can be observed from Figure 8 which shows the load-strain relationships of walls which have rectangular openings (800 mm * 400 mm), W3, W6, and W9.

The wall W3 is the control specimen of this group of walls while walls W6, W9 are strengthened by a grout mortar and ferrocement overlays respectively. It was noticed that Wall W6 that strengthened by a grout mortar give the highest ultimate bearing capacity, the highest stiffness and the highest toughness values, followed by wall W9 which strengthened by ferrocement overlays and give a lowest value of ultimate bearing capacity, stiffness and toughness. Using of

the strengthening techniques, grout mortar and ferrocement overlays increase the ultimate bearing capacity of the tested walls when compared with the control wall W3. The walls W6, W9 have an increase in ultimate bearing capacity by about 173 % compared with the wall W3.

As shown in Figure 2, failure of wall W6 was a sudden failure and there was a very few cracks above and under the opening. On other hand, failure of wall W9 occurred due to propagation of the cracks and crushing in the ferrocement overlays above the opening. Finally, it can be observed that the capacity of the wall strengthened with a grout mortar W6, was much higher than the wall strengthened by ferrocement overlays, W9 by about 82 %.

CONCLUSIONS

From the analysis and discussion of the test results obtained from this research, the following conclusions can be drawn:

1. In general, presence of opening in the tested walls decreased the ultimate capacity and displayed less stiffness and Toughness.
2. Using the same widths of rectangular and square openings, rectangular opening weakened the stiffness, the toughness and the strength of the tested walls than square opening. This is attributed to the reduction in the cross section of the tested wall, i.e. less moment of inertia.
3. Failure cracks in the walls were mainly due to splitting in the bricks and passing through the joints. On the other hand, presence of openings in the walls changed the mode of failure such that the major straight cracks appeared beside the openings and propagated to the bottom and the top of the walls.
4. All of the used strengthening techniques increased the ultimate capacity of the tested walls when compared to the control walls.
5. The walls strengthened by a grout mortar give the highest ultimate bearing capacity and the highest toughness value.
6. The wall which was strengthened by a grout mortar showed the highest increase in the ultimate bearing capacity (150 %) while the wall which was strengthened by ferrocement overlays showed an increase in the ultimate bearing capacity by (52.2 %).
7. The wall which strengthened by GFRP laminates gives a lowest value of ultimate bearing capacity, stiffness and toughness.
8. Failure of wall strengthened by GFRP laminates occurred due to propagation of cracks around the opening followed by rupture of GFRP laminates, then a part of the masonry blocks fell down.

RECOMMENDATIONS

1. The walls strengthened with a grout mortar technique give a highest value of ultimate bearing capacity compared with the walls strengthened with other techniques.
2. The walls strengthened with ferrocement overlays technique showed more ductile failure compared with the walls strengthened with other techniques.

REFERENCES

1. El-Dakhkhni W.W., Hamid A.A., and Elgaaly M., "GFRP Reinforcing of Concrete Masonry Infill Walls" 3rd International Conference on Composites in Infrastructures, San Francisco, USA, June 2002, Paper No. 4, on CD-ROM.
2. Elkarmouty .H. Z. and Khafaga .M.A., "Strengthening of Masonry Walls with Openings Using Different Techniques", The Fourth Middle East Symposium on Structural Composites for Infrastructure Applications, Alexandria, Egypt, May 20-23, 2005.
3. EL Nawawy O. A. M., Ezzeldin Y. S. Ahmed, EL-Mostafa M.H., and Sami A.S.F., "Behavior of Retrofitted Ureinforced Hollow Concrete Masonry Walls", The Third Middle East Symposium on Structural Composites for Infrastructure Applications, Aswan, Egypt, Dec 17-20, 2002.

4. Fouad M. Khalaf, Arnold W. Hendry, and Daniel R. Fairbairn, "Study of The Compressive Strength of Blockwork Masonry", ACI Structural Journal, V.91, No.4, July-August 1994.
5. Glanville, J. I., Hatzinikolas, M. A., and Ben-Omran, H. A., "Engineered Masonry Design" Limit State Design, Winston House Winnipeg, 1996.
6. Hadad S. H., Mahmoud, A.S., and Abou Elmagd S. A., "Behavior of Strengthened Masonry Shear Walls With Openings Using GFRP", The Third Middle East Symposium on Structural Composites for Infrastructure Applications, Aswan, Egypt, Dec 17-20, 2002.
7. Sabrah. T., "Rehabilitation of Masonry Walls Using Ferrocement Overlays", M.Sc Thesis, Cairo University, (2003).
8. Salama A. E., Ganem G. M., Abd El Wahab. W. R. and Elsayed T. A., "Retrofitting Multiwythe Historic Stone Masonry Walls in Egypt Using Grout Injection Technique", The Fourth Middle East Symposium on Structural Composites for Infrastructure Applications, Alexandria, Egypt, May 20-23, 2005.
9. Egyptian Standard Specification, "Concrete Masonry Units Part1: Load bearing Concrete Masonry Units", No. 1292-1/2005.
10. Egyptian Standard Specification, "Concrete Aggregates from Natural Sources", No 1109-2001.
11. Egyptian Standard Specification, "Standard Methods of Physical and Mechanical Tests for Cement", No. 2421/2005.
12. Egyptian Standard Specification, "Portland Cement", No. 4756 -1/2007.
13. Egyptian Code of Practice for Design of Masonry Buildings (ECP 204-2005), Ministry of development, New Communities, Housing and Utilities, Housing and Building National Research Center.
14. ASTM C1314-99 "Standard Specification Method for Constructing and Testing Masonry Prisms Used to Determine Compliance with Specified Compressive Strength of Masonry".
15. ACI committee 530, "Building Code Requirement for Masonry Structure" American Concrete Institute, 2005.

PERFORMANCE OF REACTIVE POWDER CONCRETE PRODUCED USING LOCAL MATERIALS

Assem Abdelalim

Professor of Materials, Dean of Faculty of Engineering, Shoubra, Banha University, Egypt

Mohamed Ramadan

Associate Professor, Faculty of Engineering, Shoubra, Banha University, Egypt

Tarek Bahaa*

Associate Professor, Housing & Building National Research Center, Cairo, Egypt

Wael Halawa

Assistant Lecturer, Faculty of Engineering, Shoubra, Banha University, Egypt

ABSTRACT

Reactive Powder Concrete (RPC) is a new family of high strength cement based composites that achieves high levels of compressive strength. The introduction of the RPC opened new applications for engineers and researchers.

This paper presents an experimental program of two phases. The first phase included 36 mixes to investigate the possibility of producing RPC using materials available in the local Egyptian market. Also, optimizing the content of the constituent materials of RPC was studied. Key variables were water/cement ratio, quartz, silica fume and steel balls. The second phase included six mixes, M1 to M6, to evaluate the structural properties of reactive powder concrete. In addition, the effect of curing regime and some durability aspects, such as drying shrinkage and sulphate attack, were investigated.

The results demonstrated that reactive powder concrete can be produced using materials available in the local Egyptian market. A compressive strength up to 160 N/mm^2 and a flexural strength up to 46 N/mm^2 were achieved. The reactive powder concrete showed better durability in terms of resistance to sulphate attack and drying shrinkage. The dominant role of the curing regime on the performance of reactive powder concrete was highlighted.

Keywords: RPC, Reactive Powder Concrete, Quartz, Silica Fume, Cement Based Composites.

INTRODUCTION

In the last decades, construction industry was developed and concretes with much higher levels of strength and more durability have been introduced to serve different structural purposes. Recently, Reactive Powder Concrete (RPC) was developed in France in 1994 as a new category of high strength cement based composites. RPC achieves compressive strength level in the range of $120\text{-}200 \text{ N/mm}^2$ and flexural strength in the range of $30\text{-}60 \text{ N/mm}^2$. Moreover, it is characterized by its high durability. If needed, the RPC can achieve compressive strength values exceeding 200 N/mm^2 by applying special conditions: post set heat treatment and external pressure before or during setting, Richard and Cheyrezy [1&2]. The RPC was applied for the first time in the area of construction in 1997 in Canada.

Development of RPC is based on the principle that a material with minimum inner voids will possess a greater load-carrying capacity and display better structural performance. Accordingly, the coarse aggregate was eliminated and the RPC mix is composed of fine sand,

* Corresponding author
Received Date:27/10/08
Acceptance Date:23/11/08

high content of cement, silica fume, quartz, and super Plasticizer. The absence of the coarse aggregate reduced the heterogeneity between the cement matrix and the aggregate and hence enhanced the microstructure and the performance, Collepardi et al. [3]. Despite that the matrix does not contain coarse aggregate, RPC is widely recognized as concrete not as mortar.

The cement content has a dominant role in determining the strength of RPC. The effect of this factor was investigated by Kurdi et al. [4]. They used cement content varying from 800-1090 kg/m³ and achieved a maximum compressive strength of 132 N/mm². This range of cement content was adopted in the current study.

Silica fume in RPC serves the three-fold function of increasing density, pozzolanic reaction and strengthening the interfacial transition zone between cement matrix and sand. Kurdi et al. [4] studied the effect of silica fume content. The results of their experimental study illustrated that the optimum silica fume content for RPC is about 25% of the cement weight. Chan and Chu [5] studied the effect of silica fume contents ranging from 0% to 40% on steel fiber bond characteristics in reactive powder concrete. It is found that the incorporation of silica fume can effectively enhance the fiber-matrix interfacial properties.

El-Hefnawy and Abbas [6] studied the effect of curing on performance of RPC. Their results concluded that applying heat-treatment at 100 °C on RPC for three hrs, after 24 hrs of casting, enhanced the compressive strength four times more than the untreated one. This improvement increased to six times when the heat-treatment was extended to 24 hrs.

A preliminary study of RPC as a new repair material was conducted by Lee et al. [7]. The test results showed that the RPC displays excellent repair and retrofit potentials in compressive and flexure strengthening and possesses high bond strength, and high adhesion with steel as compared with other concretes.

OBJECTIVES

There has been little information in the literature on production and performance of reactive powder concrete made from materials available in the local Egyptian market. The research reported in this paper tries to partially fill this void and has the following objectives:

- Producing RPC using materials available in the Egyptian market.
- Optimizing the content of the constituent materials of RPC: water/cement ratio, quartz, silica fume and steel balls.
- Evaluating the structural performance and some durability aspects of RPC: curing, sulphate attack and drying shrinkage.

EXPERIMENTAL PROGRAM

The experimental program has two phases. The first phase included 36 trial mixes to investigate the possibility of producing and optimizing the RPC mix using materials available at the Egyptian market. The second phase included six mixes to evaluate the structural performance of RPC. In addition, the curing effect and some durability aspects, such as drying shrinkage and sulphate attack, were investigated. The following sub-sections will summarize the details of the program, however more details can be found in Halawa [8].

Materials

The RPC mix was made from natural siliceous sand, seawater cement, silica fume, quartz powder, tap drinking water, and super-plasticizer. Testing of these materials was carried out according to the Egyptian standard specifications. Natural siliceous sand with a specific gravity of 2.7 and a grain size distribution ranging from 150 µm to 600 µm was used in all mixes. The sand

particles finer than 150 µm were excluded to avoid the interference with the coarse cement particles (100 µm) as recommended by Kurdi et al. [4].

The cement used in this investigation was seawater cement locally produced by Helwan Company. The cement had a Blaine fineness of 3300 cm²/gm, a specific gravity of 3.15 and a 7-days compressive strength of 36 N/mm². Silica fume locally produced by the Egyptian Ferro Alloy Company was used. It had a SiO₂ content of 96.5%, a specific gravity of 2.10 and a specific surface area of 20000 cm²/gm. Locally produced quartz powder with a SiO₂ content of 98%, Blaine fineness of 3100 cm²/gm, and a specific gravity of 2.85 was used.

A super-plasticizer namely Viscocrete 5400 produced by Sika Egypt Company was used. Viscocrete 5400 is an aqueous solution of modified polycarboxylate. It complies with ASTM C494 Type F. In some mixes, steel balls with specific gravity of 7.85 were incorporated. The steel balls were screened on sieves to obtain a grain size range similar to that of the used sand, i. e. from 150 µm to 600 µm. Magnesium sulphate (Mg₂SO₄) was used as a source of sulphates ions. The purity of magnesium sulphates was 99.9%. A solution of 4% Mg₂SO₄ concentration was prepared for studying the effect of sulphate attack on the compressive strength and length change.

Mix Proportions

In the first phase of the experimental program 36 trial mixes were made. The mixes were evaluated by their compressive strength values to determine the optimum mix design. Table 1 shows the mix proportions. Most of proportions for mixes 1 to 32 are similar to those reported by Kurdi et al. [4] to provide reference comparison. The cement content of the RPC mixes ranged from 800 kg/m² to 1000 kg/m³. The investigated parameters were water/cement ratio, silica fume content, quartz content, combined effect of silica fume and quartz and incorporation of steel balls.

Table 1: Mix Proportions for Phase 1 Mixes

Mix No.	C:	W:	S:	SF:	Q:	SB
1	1	0.21	1.10	-	-	-
2	1	0.19	1.10	-	-	-
3	1	0.17	1.10	-	-	-
4	1	0.15	1.10	-	-	-
5	1	0.5	3	-	-	-
6	1	0.21	1.10	0.15	-	-
7	1	0.19	1.10	0.15	-	-
8	1	0.17	1.10	0.15	-	-
9	1	0.15	1.10	0.15	-	-
10	1	0.21	1.10	0.25	-	-
11	1	0.19	1.10	0.25	-	-
12	1	0.17	1.10	0.25	-	-
13	1	0.15	1.10	0.25	-	-
14	1	0.19	1.50	0.25	-	-
15	1	0.21	1.10	-	0.20	-
16	1	0.19	1.10	-	0.20	-
17	1	0.17	1.10	-	0.20	-
18	1	0.21	1.10	-	0.40	-
19	1	0.19	1.10	-	0.40	-
20	1	0.19	0.88	-	0.32	-
21	1	0.21	1.10	0.15	0.20	-
22	1	0.19	1.10	0.15	0.20	-
23	1	0.17	1.10	0.15	0.20	-
24	1	0.21	1.10	0.25	0.20	-
25	1	0.19	1.10	0.25	0.20	-
26	1	0.17	1.10	0.25	0.20	-
27	1	0.21	1.10	0.15	0.40	-
28	1	0.19	1.10	0.15	0.40	-
29	1	0.17	1.10	0.15	0.40	-
30	1	0.21	1.10	0.25	0.40	-
31	1	0.19	1.10	0.25	0.40	-
32	1	0.17	1.10	0.25	0.40	-
33	1	0.19	0.90	0.25	0.40	.58
34	1	0.19	0.70	0.25	0.40	1.17
35	1	0.19	0.50	0.25	0.40	1.67
36	1	0.19	0.56	-	0.32	0.94

"C" Cement

"W" Water

"S" Sand

"SF" Silica Fume

"Q" quartz

"SB" Steel Balls

As shown in Table 1, the water/cement ratio ranged from 0.15 to 0.21, with 0.02 increments. The amount of sand was varied from 50% to 110% of cement weight. Different percentages of silica fume (0.0, 0.15, and 0.25 of cement weight), and quartz (0.0, 0.2, .32 and 0.4 of cement weight) were examined. The content of super-plasticizer was kept around 4% of cement weight in all mixes except mix 5 that was not provided by super-plasticizer. The workability of the mixes was measured using the mortar flow table. The flowability ratios for different RPC mixes were in the range 115% to 130%.

Based on the results of phase (I), five optimum designed RPC mixes, M2 to M6, were selected. Moreover, Mix M1 was used as a control mix as it represents a common conventional mix. Mix proportions and quantities required for one cubic meter are shown in Table 2. These mixes were studied to evaluate the structural performance and durability of RPC.

Table 2: Mix Proportions for Phase 2 Mixes

Mix No.	Mix Proportions						Quantities Required for One Cubic meter (kg)					
	C:	W:	S:	SF:	Q:	SB	C	W	S	SF	Q	SB
M1	1	0.5	3	-	-	-	515	258	1546	-	-	-
M2	1	0.19	0.88	-	0.32	-	1018	193	895	-	326	-
M3	1	0.19	1.10	0.25	0.40	-	815	155	895	203	326	-
M4	1	0.19	0.70	0.25	0.40	1.17	815	155	571	203	326	954
M5	1	0.19	1.50	0.25	-	-	815	155	1200	203	-	-
M6	1	0.19	0.56	-	0.32	0.94	1018	193	571	-	326	954

"C" Cement "W" Water "S" Sand "SF" Silica Fume "Q" quartz "SB" Steel Balls

Test Specimens

In phase 1, the measured property was the compressive strength. For the 36 mix, compression tests of three 50×50×50 mm cubes at ages 7, 28 and 56 days were performed.

In phase 2, the compressive strength and flexural strength were measured for Mixes M1 to M6. For each mix, compression tests of three 50×50×50 mm water cured cubes at ages 7, 28, 56, 90 and 180 days were performed. Also, flexural tests of three 40×40×160 mm prisms at ages 7, 28 and 56 days were performed according to ASTM C348. Additional six cubes for mixes M1 to M4 were tested at ages 28, 56, 90 & 180 days. Three of them were cured in air while the remaining three cubes were exposed to sulphate attack. Length change due to drying shrinkage and sulphate attack was measured for mixes M1, M3 & M4 using 25×25×285 prisms. The latter test was performed according to ASTM C490.

Fabrication of Specimens

Mixing was performed in a high speed-mixer to ensure the homogeneity of the RPC mixes. The mixing sequence was similar to the one introduced by Bonneau et al. [9]. The total mixing time is 7 minutes as follows:

- Dry mixing of cement, sand, and powders for 1.5 minute at a slow speed (140 ± 5 rpm).
- mixing water containing half of the super-plasticizer was added and mixing continued for 2 minutes.
- One minute rest then the second half of super-plasticizer, diluted in an equal volume of water, was added followed by 1.5 minutes mixing at the slow speed.
- Final mixing was applied for one-minute at a high speed (285± 10 rpm).

The mix was cast in the moulds and mechanically compacted using vibrating table for 30 seconds. The specimens were covered by plastic sheets for 24 hours prior to demolding. Two curing regimes were used in this investigation: air curing and water curing. For air curing, specimens were left in the room temperature until the age of testing. For water curing, specimens were immersed in the water curing tanks until the age of testing. On the other hand, specimens used to evaluate the effect of sulphate attack on strength were maintained in pure water for 28 days before immersion in sulphate solution.

RESULTS AND DISCUSSION OF PHASE 1

Achieved Compressive Strength Values for RPC

Compressive strength of RPC mixes of phase 1 at different ages (7, 28 & 56 days) are presented in Table 3. As seen in Table 3, the conventional mixes achieved a 56 days compressive strength ranging from 36.6 to 58.8 N/mm². The incorporation of the quartz into the mix increased the strength to range from 55.9 to 92.5 N/mm². The incorporation of the silica fume into the mix significantly increased the strength to range from 76.5 to 99.5 N/mm².

Mixes contain both quartz and silica fume displayed higher strength values that range from 81.0 to 151.0 N/mm². The maximum achieved compressive strength at 56 days is 158.0 N/mm² for Mix 34 that contains quartz, silica fume and steel balls. This level of compressive strength is greater than that of high strength concrete. The typical values of compressive strength of high strength concrete are in the range of 60.0-100.0 N/mm². It can be concluded that RPC can be produced using materials available in the local Egyptian market.

Table 3: Compressive Strength for Mixes of Phase 1

Mix No.	Comp. Strength N/mm ²			Notes
	7 days	28 days	56 days	
1	32.5	43.4	47.7	Conventional mixes
2	34.3	45.2	50.2	
3	41.0	53.0	58.8	
4	38.0	47.8	52.3	
5*	26.9	34.6	36.6	
6	44.1	65.0	76.5	Mixes contain silica fume
7	51.8	77.0	87.0	
8	60.2	87.5	91.5	
9	58.3	84.5	90.0	
10	59.0	86.0	91.0	
11	61.3	89.5	95.2	
12	61.9	93.5	99.5	
13	60.5	89.2	97.0	
14	60.0	85.0	94.0	Mixes contain quartz
15	34.3	51.0	60.0	
16	35.7	52.0	63.5	
17	304.5	45.0	58.5	
18	32.9	50.0	55.7	
19	39.9	58.5	66.5	
20*	55.0	82.0	92.5	
21	50.4	72.8	81.0	Mixes contain quartz & silica fume
22	54.6	79.5	93.5	
23	502.5	76.5	86.3	
24	59.5	86.2	95.0	
25	81.0	107.8	120.7	
26	63.0	91.5	112.9	
27	502.5	76.5	91.9	
28	64.5	97.5	102.3	
29	58.5	85.5	96.1	
30	75.0	125.2	128.7	
31*	103.5	140.0	151.0	
32	79.0	128.5	130.0	
33	97.5	125.0	140.0	
34*	104.3	147.0	158.0	Mixes contain steel balls
35	95.0	119.0	133.2	
36*	60.0	82.8	95.2	

* Mixes Selected for Phase 2

As estimated from the compressive strength values in Table 3, the rate of increase in compressive strength between ages 7&28 days ranged from 25% to 55%. This rate is greater than that occurred between ages 28&56 days. The latter ranged from 10% to 21%. This is similar to the results reported by Richard and Cheyrezy [2].

Optimization of Water/Cement Ratio

In order to determine the optimum water cement ratio (w/c) for the RPC mixes which contain quartz, three mixes (15, 16 & 17) were made with w/c ratios of 0.17, 0.19, and 0.21, respectively. These mixes had quartz content equal 20% of cement weight. The relationship between the w/c ratio and compressive strengths of the mixes at 7, 28, and 56 days is illustrated in Figure 1. The figure shows that the RPC mix with w/c ratio of 0.19 had higher compressive strengths than those mixes with 0.17 and 0.21 w/c ratios.

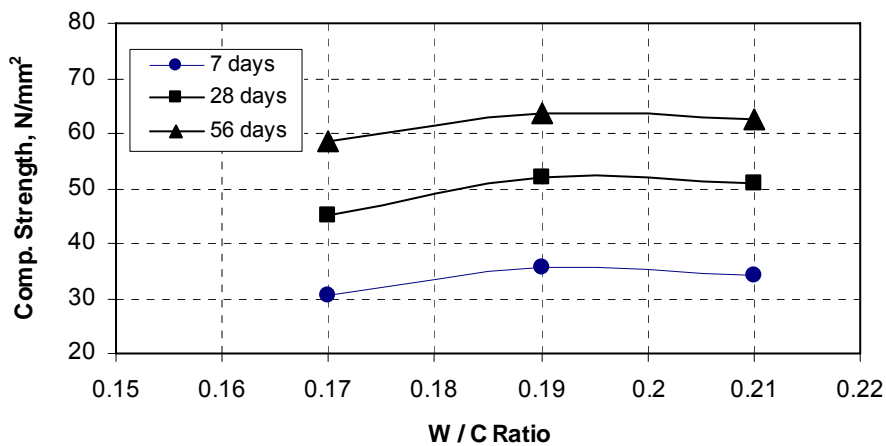


Fig. 1: Relationship of Compressive Strength & W/C Ratio for Quartz Mixes

To investigate the effect of w/c ratio on silica fume mixes, eight mixes with various w/c ratios (0.15, 0.17, 0.19, 0.21) were made. Four mixes (6, 7, 8 & 9) contained 15% silica fume while the other four mixes (10, 11, 12 & 13) contained 25% silica fume. Figures 2-a & 2-b present the relationship between the w/c ratio and 7, 28 and 56 days compressive strengths for the mixes.

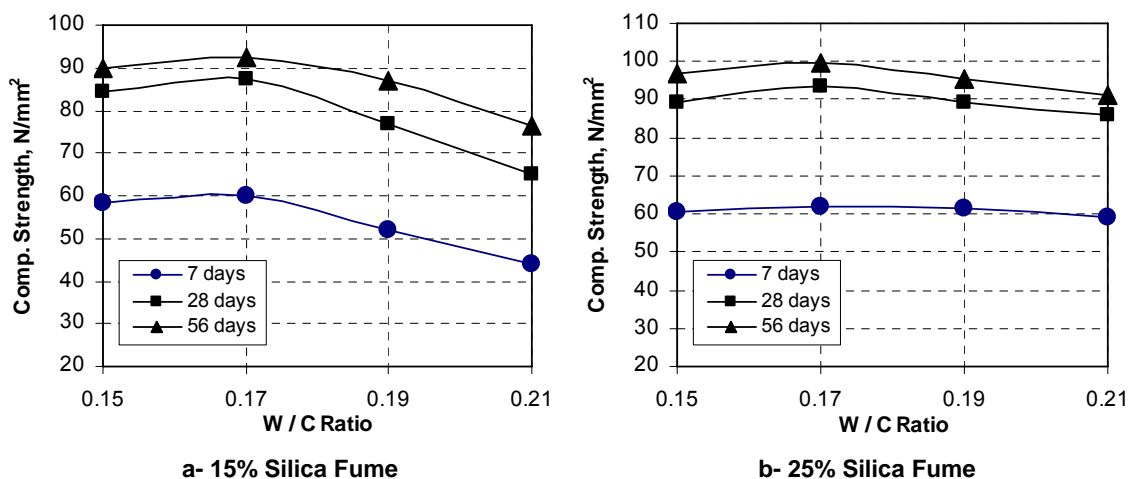


Fig. 2: Relationship of compressive Strength & W/C Ratio for Silica Fume Mixes

The results demonstrate that increasing the w/c ratio from 0.15 to 0.17 resulted in an enhancement in the compressive strength of silica fume mixes. This is because water cement ratio below 0.17 was not adequate for efficient hydration of cement in the matrix. Further increase of w/c ratio beyond 0.17 reduced the compressive strength due to the increase in the porosity of the mix. These results are in line with the results reported by Richard and Cheyrezy [1].

The optimum w/c ratio for RPC mixes containing 15% or 25% silica fume was found to be 0.17. When quartz was introduced in the silica fume mixes, the optimum w/c ratio increased from 0.17 to 0.19. This trend was observed for different contents of silica fume or quartz, see Figure 3. The increase in the optimum w/c ratio for quartz mixes was to overcome the friction of the quartz grains which are characterized by their rough and irregular surface.

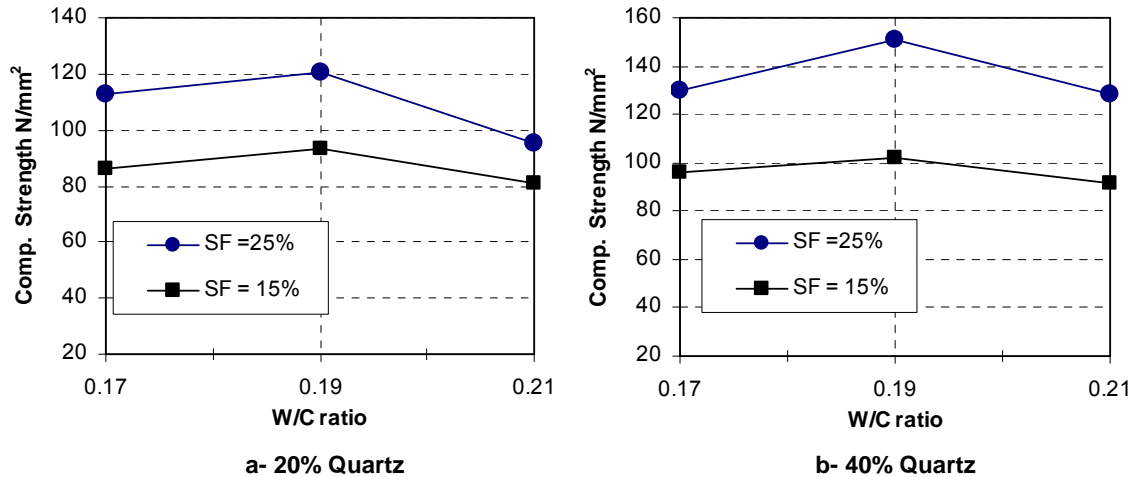


Fig. 3: Relationship of Comp. Strength & W/C Ratio for Silica Fume Mixes Containing Quartz

Based on the previous findings, it is concluded that the optimum value of water cement ratio for reactive powder concrete mixes ranges from 0.17 to 0.19 based on the matrix composition.

Optimization of Quartz and Silica Fume Contents

The effect of quartz content on the compressive strength of RPC made with 0.19 w/c ratio and cured in water is demonstrated in Figure 4. It can be seen that the compressive strength values at 7, 28, and 56 days increases with the increase of the quartz content in the RPC mix till the quartz content equals 32% of cement weight. At this value, mix 20 shows the highest 56-days compressive among the quartz mixes that equaled 92.5 N/mm². The incorporation of quartz powder into the mix filled the grade between the cement and sand particles. Accordingly, the matrix becomes denser and the compressive strength improved. However, increasing the quartz content to 40%, reduced the 56-days compressive strength by 28%, Mix 19. So, It can be concluded that quartz is necessary for producing RPC provided that the appropriate content is utilized.

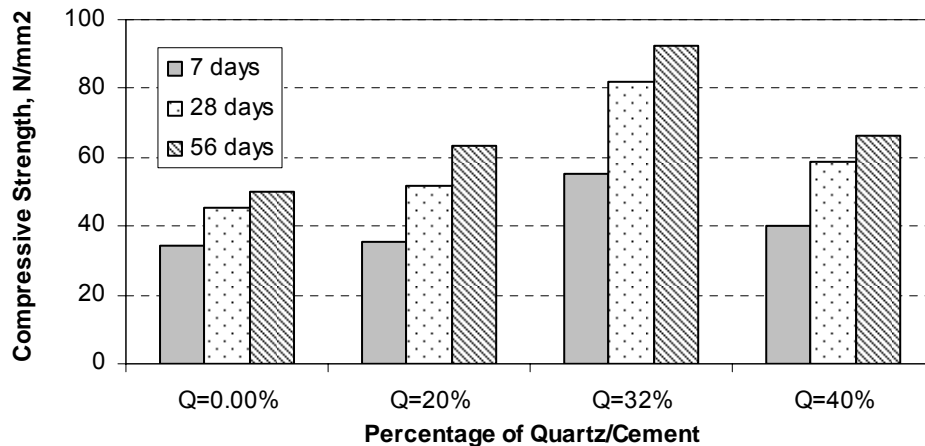


Fig. 4: Effect of Quartz Content on Compressive Strength of RPC

Figure 5 presents the effect of using 15% and 25% silica fume on the compressive strength of RPC made with 0.17 w/c ratio and cured in water. The compressive strength of RPC at 7, 28, and 56 days increased with increasing the amount of silica fume in the RPC mix. The improvement, in the 56 days compressive strength of RPC reached 56% and 69%, when silica fume of 15% and 25% of cement weight was used, respectively. It should be mentioned that the utilization of 15% silica fume resulted in significant improvement in the compressive strength. When silica fume content was raised by 10% to reach a 25%, the extra added silica fume produced less significant improvement. This may be due to that the amount of calcium hydroxide developed through the cement hydration process is not sufficient for the pozzolanic reaction of the extra silica fume.

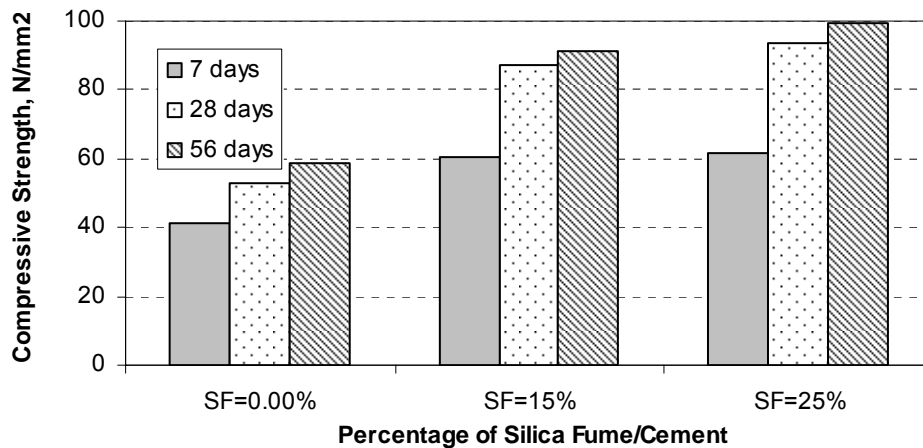


Fig. 5: Effect of Silica Fume Content on Compressive Strength of RPC

On the other hand, a positive interaction between the quartz and silica fume was observed. Introduction of quartz into mixes with either 15% or 25% silica fume enhanced the compressive strength. A high strength level of 151 N/mm² was recorded for mix 31 that contains 40% quartz and 25% silica fume.

It can be said that the utilization of silica fume and quartz together is indispensable for producing RPC. The optimum contents for silica fume and quartz are in the ranges of 15-25% and 30-40% of the cement weight, respectively.

Optimization of Steel Balls Content

The effect of using steel balls, as a replacement of sand, in the RPC mixes was investigated through evaluating the compressive strength of mixes 33 to 36. As seen in Table 3, using steel balls content equals 58% of the cement weight, mix 33, did not produce beneficial effect. However, using 117% steel balls resulted in a marginal improvement in the compressive strength of 5%. This improvement is due to the higher stiffness of the steel balls that enabled the matrix to sustain higher levels of loading.

RESULTS AND DISCUSSION OF PHASE 2

Based on the results of phase 1, six mixes were selected for further assessment of the structural performance and durability of RPC and will be presented in the following subsections.

Development of Compressive Strength for RPC

The compressive strengths for mixes M1 to M6 were measured at ages 7, 28, 56, 90 & 180 days, see Table 4. As can be seen, the conventional mix M1 displayed the lowest strength

values, while the RPC Mix M4 had the highest strength. Figure 6 shows, the development of the compressive strength with the age for mixes M1 to M6.

For the conventional mix M1, the rates of enhancement in the compressive strength are 28%, 6%, 1% and 0.5% at ages of 28, 56, 90 and 180 days, respectively. Each value was estimated relative to the preceding age. Accordingly, the major part of the compressive strength of the conventional mix was developed at age 28 days. This agrees with the known background about conventional concrete where the 28 days compressive strength is used for estimating the characteristic strength.

Table 4: Compressive versus Flexural Strengths for Mixes of Phase 2

Mix No.	Compressive Strength N/mm ²					Flexural Strength N/mm ²			Strength Ratio		
	7 days	28 days	56 days	90 days	180 days	7 days	28 days	56 days	7 days	28 days	56 days
M1	29.9	34.6	36.6	37.0	37.2	5.1	6.5	7.0	0.171	0.188	0.191
M2	57.4	82.0	92.5	93.6	93.9	13.0	18.8	20.5	0.226	0.229	0.222
M3	103.5	140.0	151.0	155.0	157.0	40.0	43.0	44.5	0.386	0.307	0.295
M4	104.3	147.0	158.0	161.0	162.5	41.5	45.0	46.1	0.398	0.306	0.292
M5	75.0	95.5	110.0	120.5	123.6	32.5	36.0	38.5	0.433	0.377	0.350
M6	65.0	85.8	98.0	101.0	101.7	30.5	33.0	36.0	0.469	0.385	0.367

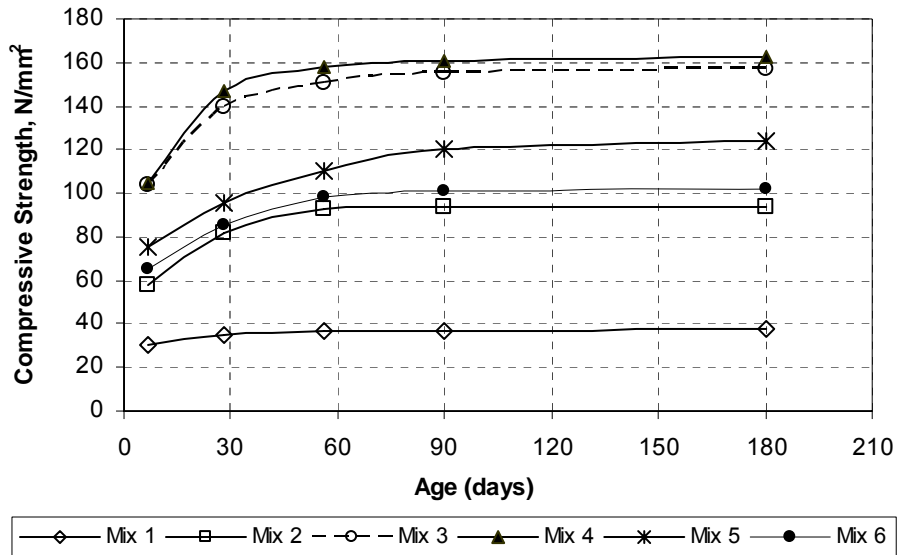


Fig. 6: Development of Compressive Strengths for Mixes of Phase 2

On the other hand, the rates of enhancement in the compressive strength of the RPC mix M2 are 43%, 13%, 1.2% and 0.3% at ages 28, 56, 90 and 180 days, respectively. Most of the compressive strength was gained at age 56 days. After that no significant enhancement at ages 90 & 180 days was observed. Other RPC Mixes M3 to M6 showed similar trend to that of M2. So, it will be more convenient to evaluate the compressive strength of RPC based on its 56 days age and not based on 28 days as conventional concrete.

Flexural Strength of RPC

The flexure strengths for mixes M1 to M6 were measured at ages 7, 28 and 56 days. As seen in Table 4, the conventional mix had the lowest flexural strength values of 5.1, 6.5 and 7.0 N/mm² at 7, 28, 56 days respectively. Compared to the conventional mix, the RPC mixes showed improvement in the 56-day flexural strength ranged from 193% for mix M2 that contains quartz only to 560% for Mix M4 the contains quartz, silica fume and steel balls.

The strength ratio (flexural strength / compressive strength) of RPC mixes showed significant enhancement, refer to Table 4. For instance, the strength ratio of the RPC Mix M4 is 0.292 which is 53% higher than that of the conventional mix. The improvement in the flexural strength and strength ratio of RPC is due to better homogeneity and denser matrix of the RPC.

Effect of Curing

To evaluate the curing effect on the strength of RPC mixes, specimens from mixes M1 to M4 were subjected to two curing regimes: air curing and water curing. Figure 7 shows that air curing adversely affected the performance and did not allow the RPC mixes to achieve the strength levels that recorded with water curing.

It can be noticed that most of the reduction in the strength of air cured specimens with respect to their counter part water cured specimens occurred at the age of 56 days. The strength reduction in the RPC mixes, especially mix M4, is higher than that experienced by the conventional mix. This can be referred to the fact that w/c ratio in the RPC mixes is much lower than that of the conventional mix. Thus, with no water from curing, the remaining water in the RPC mix is not sufficient for the hydration of cement and for the pozzolanic reaction.

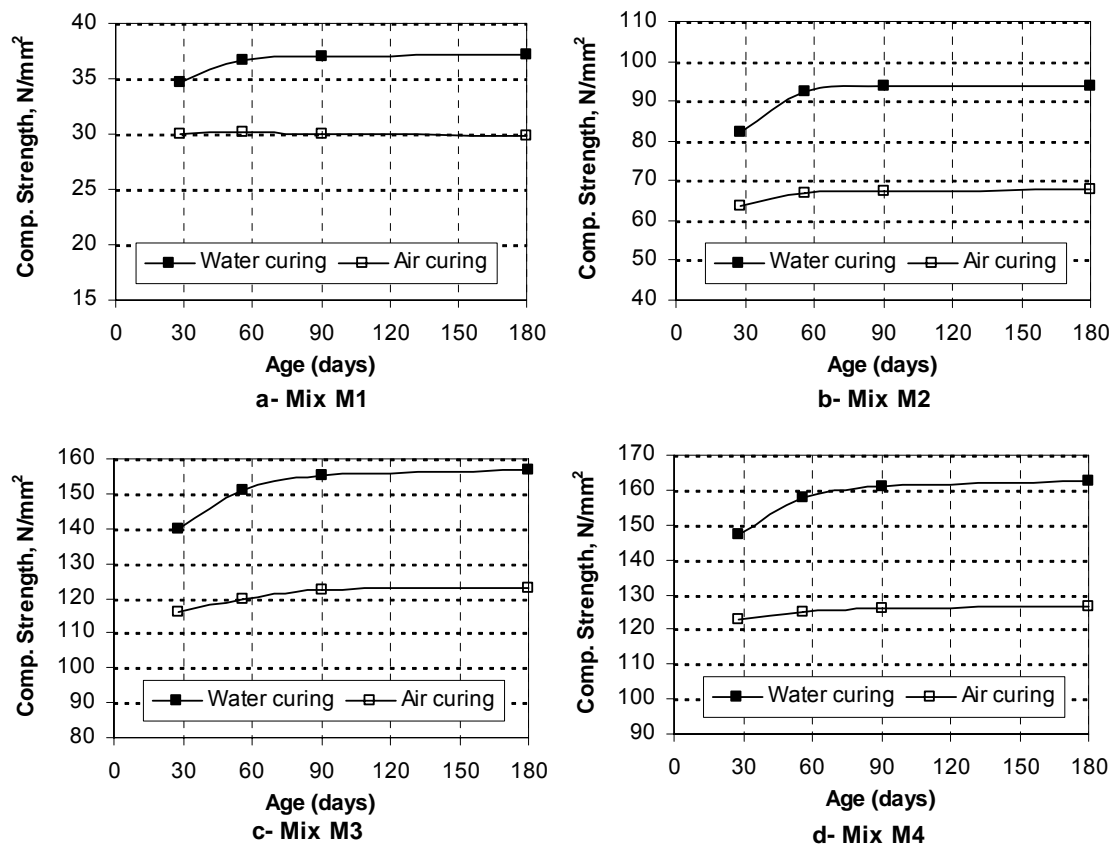


Fig. 7: Effect of Curing Regime on Compressive Strength

It can be concluded that curing regime plays a dominant role in determining the concrete strength. However, it is more crucial for the RPC than the conventional concrete. These results agree with Yazıcı et al. [10].

Strength Reduction due to Sulphate Attack

Sulphate attack causes deterioration in concrete in the shape of expansion, cracking and corrosion, which lead to strength reduction. In order to investigate this effect for RPC, two sets of cube specimens from mixes M1 to M4 were prepared and tested. Each set included three cubes from each mix. One set was cured in pure water, while the other was cured in pure water for 28 day then exposed to sulphate solution till age of testing. The reduction in the strength due to sulphate attack is shown in Figure 8.

The conventional mix suffered from strength reduction of 15% at 180 days age, while the RPC mix M2 experienced lower reduction of 9% at 180 days. On the other hand, negligible strength reduction of about 1% was recorded for the RPC mixes M3 and M4. The latter two mixes contain silica fume that consumed most of calcium hydroxide which is necessary for the chemical reaction of sulphate attack. In addition, the silica fume mix is much denser with less permeability and hence prevents the sulphate ions from penetrating the RPC. So, RPC has much higher resistance to sulphate attack than that of the conventional concrete.

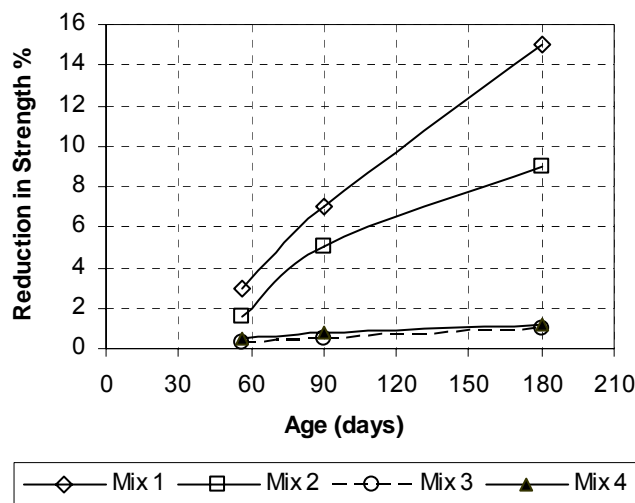


Fig. 8: Effect of Sulphate Attack on Compressive Strength

Length Change due to Drying Shrinkage

Prisms from three mixes M1, M3 and M4 were cast and cured in water for two days then left in air. Figure 9, shows the length change measurements due to drying shrinkage for the specimens of the three mixes. At the beginning, all mixes showed expansion but the expansion of the conventional mix was much higher than that of the RPC mixes. Then specimens started to display shrinkage.

The overall length change was 0.16% for the conventional mix while the RPC mixes M3 & M4 showed lower values of .094% and .066%, respectively. This is due to the better microstructure of the RPC mixes. The superiority of the RPC mix M4 is due to the presence of the steel balls that created restraints inside the matrix and resisted the shrinkage strains.

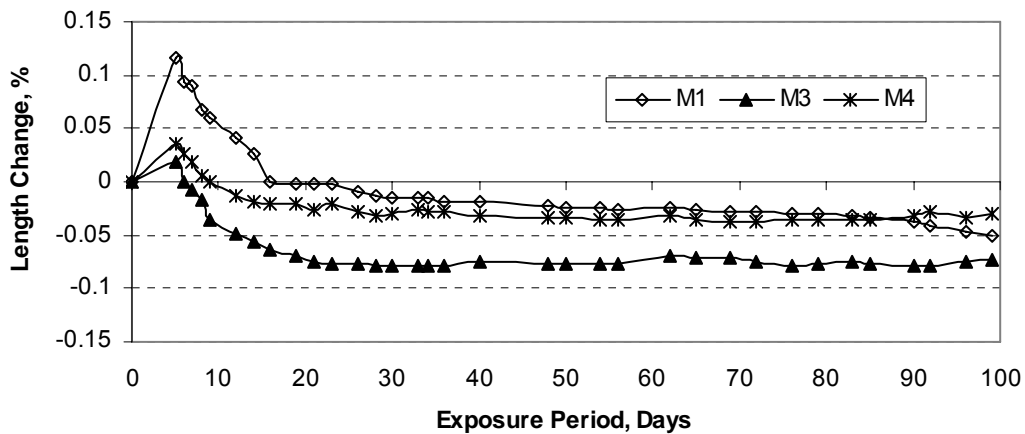


Fig. 9: Length Change due to Drying Shrinkage

Length Change due to Sulphate Attack

Prisms from three mixes M1, M3 and M4 were cast and cured in water for 28 days before immersion in the sulphate solution. Length change measurements are presented in Figure 10. It is clear that the conventional mix showed a high expansion of .057% at 100 days age. Moreover, the conventional mix prisms displayed notable hair cracks.

On the contrary, the RPC mixes M3 and M4 showed much lower expansions equaled .004% and .01%, respectively. The reduction in the expansion of RPC due to sulphate attack can be attributed to the filler effect of silica fume and quartz that prevented the penetration of the sulphate ions. Also, the introduction of silica fume compensates most of the calcium hydroxide and hence reduces the formation of gypsum and ettringite.

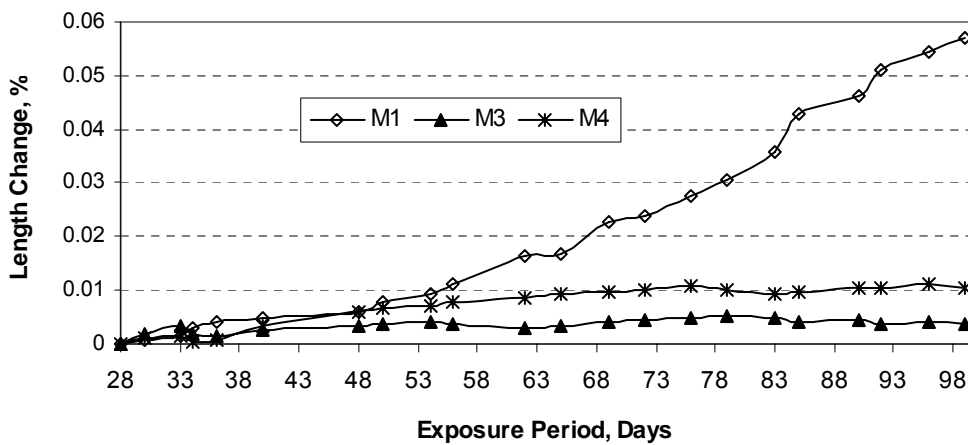


Fig. 10: Length Change due to Sulphate Attack

CONCLUSIONS

Based on the test results and discussion and within the scope of the investigated parameters, the following conclusions were drawn:

- 1- Reactive powder concrete can be produced using materials available in the local Egyptian market.

- 2- Reactive powder concrete has superior structural properties. A compressive strength up to 160 N/mm² and a flexural strength up to 46 N/mm² were achieved.
- 3- The optimum value of water/cement ratio for reactive powder concrete mixes ranges from 0.17 to 0.19 based on the matrix composition.
- 4- The utilization of silica fume and quartz is indispensable for producing RPC. The optimum contents for silica fume and quartz are in the ranges of 15-25% and 30-40% of the cement weight, respectively.
- 5- It will be more convenient to evaluate the compressive strength of RPC based on its 56 days age rather than the 28 days used for conventional concrete.
- 6- Curing regime plays a dominant role in determining the strength of RPC. Air curing adversely affected the performance and did not allow the RPC to achieve its target strength level.
- 7- Reactive powder concrete possesses superior durability compared to conventional concrete. It has higher resistance to sulphate attack and drying shrinkage.
- 8- The presence of steel balls improves the resistance of RPC against drying shrinkage. Also, minor enhancement in the compressive strength was observed.

REFERENCES

1. Richard, P., Cheyrezy, M. (1994), "Reactive Powder Concretes with High Ductility and 200-800 MPa Compressive Strength", proceedings of V.M. Malhotra Symposium on "Concrete Technology: Past, Present, and Future", SP-144, ACI, pp.507-518.
2. Richard, P., Cheyrezy, M. (1995), "Composition of Reactive Powder Concrete", Cement and Concrete Research, Vol. 25, No. 7, pp.1501-1511.
3. Collepardi, S., Coppola, L., Troli, R., Collepardi, M. (1997), "Mechanical Properties of Modified Reactive Powder Concrete", proceedings of the 5th CANMET/ACI International Conference on Super plasticizers and other Admixtures in Concrete , SP-173, ACI, Farmington Hills, Mich., pp.1-21.
4. Kurdi, A., Khoury, S., Abbas, R. (2001), "A new concrete for the 21 century: reactive powder concrete", Alexandria Engineering Journal Vol. 40 , No. 6, pp. 893-909.
5. Chan, Y., Chu, S. (2004), "Effect of Silica Fume on Steel Fiber Bond Characteristics in Reactive Powder Concrete", Cement and Concrete Research, Vol. 34, pp. 1167-1172.
6. El-Hefnawy, A., Abbas, R. (2003),"Effect of Curing Conditions on The Performance Of Reactive Powder Concrete", Proceeding of The International Conference on Performance of Construction Materials in The New Millennium, Cairo, Egypt, February 18-20.
7. Lee, M.G., Wang, Y. C., Chiu, C.(2007), "A Preliminary Study of Reactive Powder Concrete as a New Repair Material", Construction and Building Materials, Volume 21, Issue 1, pp.182-189.
8. Halawa, W. S. M., (2008) "Producing Reactive Powder Concrete by using Local Materials", M.Sc. Thesis, Faculty of Engineering, Banha University, Egypt.
9. Bonneau, O., Lachemi, M., Dallaire, E., Dugat, J., Aitcin P.C. (1997), "Mechanical and Durability of Two Industrial Reactive Powder Concretes", ACI Material Journal, Vol. 94, Issue 4, pp. 286-290.
10. Yazıcı, H., Yardımcı, M. Y., Aydina, S., Karabulut A. (2008), "Mechanical properties of reactive powder concrete containing mineral admixtures under different curing regimes" Construction and Building Materials Journal, available online since September 2008.

BOND STRESS-SLIP RELATIONSHIP AND DEVELOPMENT LENGTH OF FRP BARS EMBEDDED IN CONCRETE

Ehab Ahmed

Dept. of Civil Engineering, Univ. of Sherbrooke, Sherbrooke, Quebec, Canada, J1K 2R1

Ehab El-Salakawy*

Dept. of Civil Engineering, Univ. of Manitoba, Winnipeg, Manitoba, Canada, R3T 5V6

Brahim Benmokrane

Dept. of Civil Engineering, Univ. of Sherbrooke, Sherbrooke, Quebec, Canada, J1K 2R1

Corresponding author, Email: Ehab.Ahmed@USherbrooke.ca

ABSTRACT

The bond characteristics of reinforcing bars is one of the most critical issues in the design of reinforced concrete structures. This study presents the bond strength and stress-slip relationships of fiber-reinforced polymer (FRP) reinforcing bars embedded in normal strength concrete. The study included pullout testing of 40 FRP and steel reinforcing bars embedded in concrete blocks (200×200×200 mm) with $5d_b$ embedment length. The test parameters were: reinforcing bar material (Glass FRP, Carbon FRP, and Steel) and bar diameter (6.4, 9.5, 12.7, and 15.9 mm GFRP bars – 9.5 and 12.7 mm CFRP bars – 10M and 15M steel bars). The bond strength of GFRP and CFRP reinforcing bars, on average, was 64% and 71% that of steel bars, respectively. The measured bond-slip was modeled using well-known bond slip constitutive laws and employed in the calculation of the development length. The development length was evaluated and compared with the CSA S806-02, CSA S6-06, and ACI 440.1R-06 provisions.

Keywords: FRP, Bond, Bond-slip, Development length, Embedment length, Pullout.

INTRODUCTION

The anticipated service life of many steel-reinforced concrete structures is shortened due to corrosion of steel reinforcement and related deteriorations. Climatic conditions may have a hand to accelerate the corrosion process in environments where large amounts of salts are used for ice removal during winter months. These conditions normally result in costly repairs and may lead to catastrophic failure. Therefore, replacing steel reinforcement with non-corrodible FRP reinforcement reduces the potential for corrosion and the associated deterioration and can increase the service life of RC structures. However, the direct replacement of steel with FRP bars is not possible due to various differences in the mechanical properties of the FRP materials compared to steel especially higher tensile strength, lower modulus of elasticity, and the absence of a well-defined yield plateau in their characteristic stress-strain relationships.

The resisting mechanisms under bending, shear, and torsion are related to the development of adequate bond. Besides, many serviceability checks, such as control of crack width and of member deflections, involve the evaluation of the effects of tension stiffening, which is a phenomenon directly arising from bond behavior [1]. Due to the lack of well-established standards, a wide variety of FRP bars are currently commercialized, ranging from the simple smooth and helical deformed bars to bars treated with external features such as sand-coating. Therefore, a better understanding of the mechanical properties and bond behavior is needed for a rational approach to the design of FRP-reinforced structures. A number of bond tests have been conducted by several authors on FRP bars [2-7]. However the bond behavior of FRP bars in concrete has not been rationally established due to the numerous available FRP products.

* Corresponding author
Received Date:2/11/08
Acceptance Date:13/11/08

Cosenza et al. [8] reported that the sand-coated continuous fiber rebars show good bond resistance; however, the interface between sand grains and bars detaches abruptly leading to a brittle failure. Thus, the current study was planned to investigate the bond behavior of commercially available sand-coated carbon and glass FRP bars embedded in normal strength concrete using pullout test method in accordance with ACI 440.3R-04 [9]. Although, the pullout testing does not represent the actual case of stress in beam specimen, it gives an idea about the mode of bond failure and bond strength of FRP bars compared to the conventional steel bars. Beside, by using such type of testing the strength of the coating material which may be provided to the FRP bars to enhance the bond performance can be evaluated. Moreover, it represents the highest performance of bond because of the confinement of the concrete surrounding the bar and develops the local bond-slip relationship [1]. The test parameters included diameter and type of FRP and steel reinforcing bars. The experimental results such as bond strength, mode of failure, and bond stress-slip relationship of the reinforcing bars are presented and discussed. The bond-slip models for FRP bars presented by Cosenza et al. [8] and Malvar [10] were utilized to evaluate the bond-slip relationships for the test specimens. Furthermore, an analytical solution of the problem of FRP bar embedded in a concrete block and tested in pullout [8] was used to evaluate the development length of FRP bar embedded in concrete. The development length was predicted using the CSA S806-02 [11], CSA S6-06 [12] and ACI 440.1R-06 [13] and was compared to the values obtained from the analytical solution of the problem.

EXPERIMENTAL PROGRAM

This study focuses on the bond behavior of two different types of sand-coated FRP bars (glass FRP bars of 6.4, 9.5, 12.7 and 15.9 mm-diameter and carbon FRP bars of 9.5 and 12.7 mm diameter) and deformed steel bars (11.3 and 15.9 mm-diameter). The study compares the bond strength, bond stress-slip relationships, and mode of failure for the FRP bars and the conventional steel bars and predicts the development length based on the bond-slip model. A total of 40 pullout specimens, including 5 replicates for each bar type and diameter, were constructed and tested to failure. The embedment length was kept constant, equals to $5d_b$ for all test specimens, where d_b is the bar diameter. The pullout testing for FRP bars with short embedment length ($5d_b$) was selected to get approximately uniformly distributed bond stress and to develop the bond-slip model for the tested FRPs. Besides, by using such type of testing, the strength of the surface layers which may be added to the FRP bars to improve the bond performance was evaluated. Table 1 gives the details of the experimental program and test specimens.

Table 1: Details of Test Specimens

Material	Group	FRP bar number	Diameter (mm)	No. of specimens	Surface characteristics
GFRP	1	No. 6	6.4	5	Sand-coated
	2	No. 10	9.5	5	
	3	No. 13	12.7	5	
	4	No. 16	15.9	5	
CFRP	6	No. 10	9.5	5	wire wrapping covered by sand-coated
	7	No. 13	12.7	5	
Steel	8	No. 10M	11.3	5	Deformed
	9	No. 15M	15.9	5	

Materials

Reinforcing Bars (GFRP, CFRP and Steel)

Sand-coated FRP reinforcing bars were used in the current study. These bars are manufactured by combining the pultrusion process and an in-line coating process for the outside surface. These bars are made of E-glass fibers (for GFRP bars) and continuous carbon fibers (for CFRP bars) with a fiber content of 77.5% (by weight) in a vinyl ester resin. Both types of FRP bars

have the sand-coating layer, but the CFRP ones have additional helical wire wrapping on the surface within the sand-coating layer as shown in Fig. 1. In accordance with the ACI 440.3R-04 [9] test methods, the measured mechanical properties of the FRP bars used in the current investigation are listed in Table 2 as well as the properties of the steel bars (10 M and 15M) that were used for comparison.

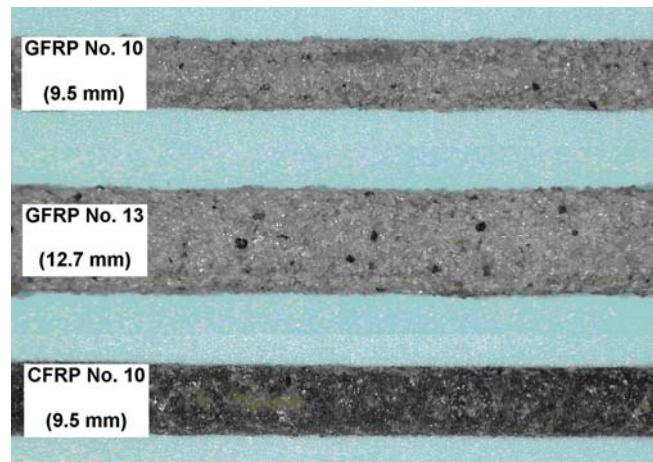


Fig. 1: Surface Configuration of FRP Bars

Table 2: Properties of Sand-Coated FRP and Steel Bars

Property	GFRP bars				CFRP bars		Steel bars	
	No. 6	No. 10	No. 13	No. 16	No. 10	No. 13	10M	15 M
Diameter (mm)	6.4	9.5	12.7	15.9	9.5	12.7	11.3	15.9
Tensile strength (MPa)	864 ± 23.0	836 ± 10.6	813 ± 38.7	802 ± 24.4	1305 ± 88.0	1204 ± 75.0	$f_y=450$	$f_y=460$
Tensile modulus (GPa)	46.09 ± 1.89	45.83 ± 1.06	45.84 ± 1.47	46.48 ± 1.00	132.10 ± 4.14	133.6 ± 9.65	200	200
Strain (%)	1.87	1.82	1.77	1.73	1.00	0.91	$\epsilon_v=0.23$	$\epsilon_v=0.23$

Concrete

The test specimens were cast in the laboratory using normal weight concrete (concrete type V, MTQ) with targeted compressive strength of 35 MPa after 28 days. The actual compressive strength was determined from standard tests, which were carried out on the day of specimen testing (after about 35 days of casting). The average compressive strength of the standard cylinders was 38 MPa.

Test Specimens

For the determination of the bond strength and local bond-slip relationship between the reinforcing bar and concrete, pullout tests with concentric rebar in 200 mm concrete cube was used. The FRP and steel bars were cut to the desired length. Plastic tubes for de-bonding were installed on the bars using silicon filling at their ends. The reinforcing bars were placed in the formwork and the bars were adjusted vertically using lateral supporting bars in both directions and finally, the concrete was cast.

The specimens were cured with water for seven days and then kept in the laboratory environment (room temperature) for three weeks. Following those four weeks and using epoxy grout, steel tubes (sleeves) were installed on the free-end of the FRP bars as a grip for the testing machine head (Fig. 2a). These sleeves were used to overcome the problem of low transverse strength of the FRP bars. Finally, the test specimens were allowed one week for the curing of the epoxy grout before testing. Each specimen is designated by a set of symbols and numbers to be uniquely identified. The first letter denotes the reinforcing bar material (G for

Glass; C for Carbon; S for steel) followed by the bar size number and ended by the replicate number. Each bar type and size was addressed through five replicates to get some measure of uncertainty.

Test Setup and Procedure

The tests were performed using a universal testing machine (BALDWIN) with a capacity of 300 kN. A prefabricated steel plate of 15 mm-thickness provided with four holes of 22 mm-diameter at the corners was attached to the fixed head of the machine. Then, a hollow stem circular cylinder with a side opening was placed directly on the steel plate. Figure 2 shows the details of a test specimen as well as the complete test setup and instrumentations. This hollow cylinder allows for the slip measurements of the free-end using a linear variable displacement transducer (LVDT). The concrete block is placed over the hollow cylinder (eccentric with the cylinder and the steel plate). Finally, a second steel plate (identical to the first one) was placed over the concrete cube and the plates were attached together through four threaded bars of 19 mm-diameter with two nuts each. The loaded-end slip was measured using three LVDTs as shown in Fig. 2.c and the slip was considered as an average of the three LVDT readings. The applied load was measured with the machine load cell. The output from the testing machine and the four LVDTs were recorded using data acquisition system connected to a computer.

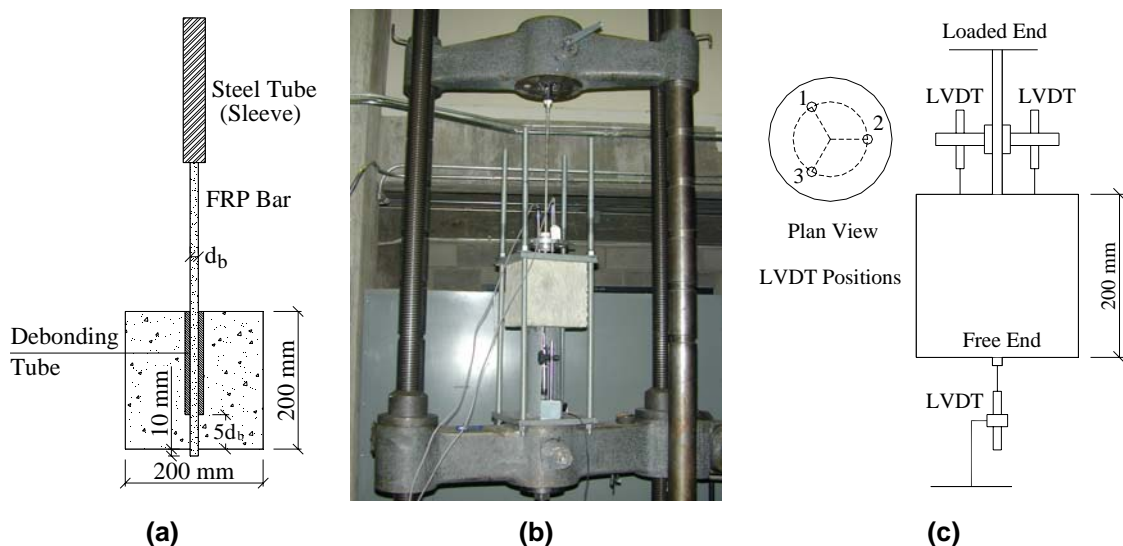


Fig. 2: Specimen and Test Setup Details: (a) Dimensions of the Test Specimen; (b) Test Setup and Instrumentation; (c) Positions of the LVDTs

TEST RESULTS AND DISCUSSION

Mode of Failure

The observed mode of failure for all of the test specimens is given in Tables 3 to 5. The FRP specimens all failed by pullout of the FRP (glass and carbon) bars due to the de-bonding of the sand-coating layer (peeling off the coating layer). This observed mode of failure occurred due to the high bond stress exerted at the FRP sand-coating surface and surrounding concrete that exceeded the corresponding bond strength at the interface between the sand-coating layer and the FRP bar core. On the other hand, the failure mode of steel bars was referred to pullout due to the concrete-bar interface because the surface deformation in this case is a part of the bar itself. Therefore, the bond strength of coated bars may be limited to the bond strength between the bar-core and the coating layer even though higher bond is attainable at the surface layer-concrete interface. It should be mentioned that the splitting of concrete cover did not occur due to thick cover to bar diameter ratio (c/d_b) which was 15.1, 10, 7.4 and 5.8 for FRP bars No. 6,

10, 13 and 16, respectively, whereas this ratio was 8.3 and 5.8 for steel bars No. 10M and 15M, respectively.

Table 3: Test Results of GFRP Bars

Specimen	Diameter (mm)	Surface area (mm ²)	Pullout load (N)	Bond strength (MPa)	Average bond strength (MPa)	Failure mode
G-6-1	6.4	643.07	15352	23.87	20.15 ± 3.078	P
G-6-2			12326	19.17		P
G-6-3			11481	17.85		P
G-6-4			14729	22.90		P
G-6-5			10902	16.95		P
G-10-1	9.5	1416.93	22027	15.55	17.57 ± 2.085	P
G-10-2			27500	19.41		P
G-10-3			24652	17.40		P
G-10-4			28301	19.97		P
G-10-5			22027	15.55		P
G-13-1	12.7	2532.25	33997	13.43	14.12 ± 2.227	P
G-13-2			40938	16.17		P
G-13-3			29858	11.79		P
G-13-4			42451	16.76		P
G-13-5			31549	12.46		P
G-16-1	15.9	3969.12	50728	12.78	13.61 ± 0.755	P
G-16-2			58293	14.69		P
G-16-3			54733	13.79		P
G-16-4			54733	13.79		P
G-16-5			51618	13.00		P

Table 4: Test Results of CFRP Bars

Specimen	Diameter (mm)	Surface area (mm ²)	Pullout load (kN)	Bond strength (MPa)	Average bond strength (MPa)	Failure mode
C-10-1	9.5	1416.93	31238	22.05	18.39 ± 3.811	P
C-10-2			28078	19.82		P
C-10-3			29769	21.01		P
C-10-4			23095	16.30		P
C-10-5			18111	12.78		P
C-13-1	12.7	2532.25	46723	18.45	17.94 ± 0.732	P
C-13-2			46278	18.28		P
C-13-3			47168	18.63		P
C-13-4			42896	16.94		P
C-13-5			44053	17.40		P

Table 5: Test Results of Steel Bars

Specimen	Diameter (mm)	Surface area (mm ²)	Pullout load (kN)	Bond strength (MPa)	Average bond strength (MPa)	Failure mode
S-10M-1	11.3	2004.73	48058	23.97	23.84 ± 0.46	P
S-10M-2			48503	24.19		P
S-10M-3			46278	23.08		P
S-10M-4			48503	24.19		P
S-10M-5			47613	23.75		P
S-15M-1	15.9	4019.20	112580	28.01	27.17 ± 0.761	P
S-15M-2			105461	26.24		P
S-15M-3			106796	26.57		P
S-15M-4			109465	27.24		P
S-15M-5			111690	27.79		P

Bond Strength

The average bond strength is calculated from the following equation:

$$\tau_{av} = \frac{F_u}{\pi d_b l_b} \quad (1)$$

From the test results (Table 3 and 4) it can be seen that the GFRP bars of 6.4 mm-diameter showed the highest bond strength, 20.15 MPa, whereas the GFRP bars of 15.9 mm-diameter showed the lowest bond strength, 13.61 MPa. On the other hand, there was no significant difference between the bond strength of CFRP bars of 9.5 and 12.7 mm-diameters (only 2%), whereas the GFRP bars No. 13 showed 19% reduction in the bond strength compared to No.10 bars. Figure 4 shows a comparison between the bond strength for all test specimens (GFRP bars No. 6, 10, 13 and 16, CFRP bars No. 10 and 13, and steel bars No. 10M and 15M). The CFRP bars showed an average increase of 11% in the bond strength in comparison to the GFRP bars. This may be due to the helical wire wrapping configuration within the sand-coating layer and the higher modulus of elasticity compared to the GFRP bars. Moreover, on average, the bond strength of GFRP and CFRP bars was about 64% and 71% that of the steel bars, respectively.

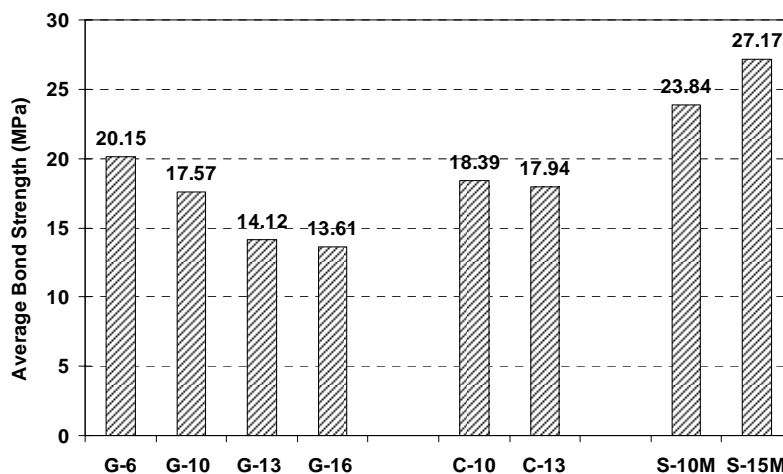


Fig. 4: Comparison between the Bond Strength of Test Specimens

From Table 3 and Fig. 4, it can be noticed that the greater the GFRP bar diameter, the lower the bond strength of GFRP bars. Results of Benmokrane et al. [4] confirm the preceding finding since GFRP bars of 12.7, 15.9, 19.1 and 25.4 mm showed bond strength values equal 10.6, 7.3, 6.6 and 6.4 MPa, respectively. Achillides and Pilakoutas [14] referred the decrease in bond strength of FRP with the increase in bar diameter to: i) Embedment length: the larger diameter bars require longer embedment lengths to develop the same bond stress ii) Poisson effect: the Poisson effect can lead to a reduction in bar diameter as a result of longitudinal stress. This reduction increases with bar diameter increase. Wang [15] pointed out the possibility of defects (voids created by concrete shrinkage or water bleeding) as another important factor that may cause lower bond strength of bigger bars.

BOND-SLIP RELATIONSHIP AND ANALYTICAL MODELING

While the bond stress was evaluated using Eq. 1, the free-end slip is directly recorded during the test through the LVDTs readings. Figures 5 and 6 show the bond stress-free-end slip relationship for the GFRP (No. 6 and No. 10) and CFRP (No. 10), respectively. Similarly, Figure 7 shows the bond stress-free-end slip relationship for 15M steel bars. The average peak values (maximum bond stress, τ_m , and the corresponding free end slip, s_m) for FRP bars are listed in Table 6.

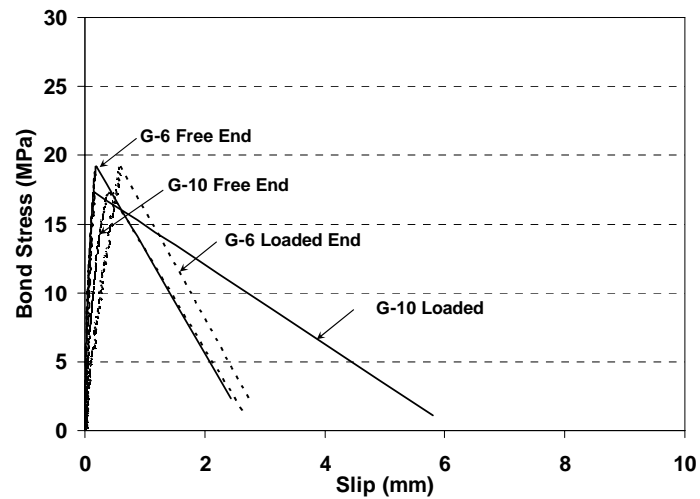


Fig. 5: Bond Stress-Slip Relationship for GFRP Bars No. 6 and No. 10

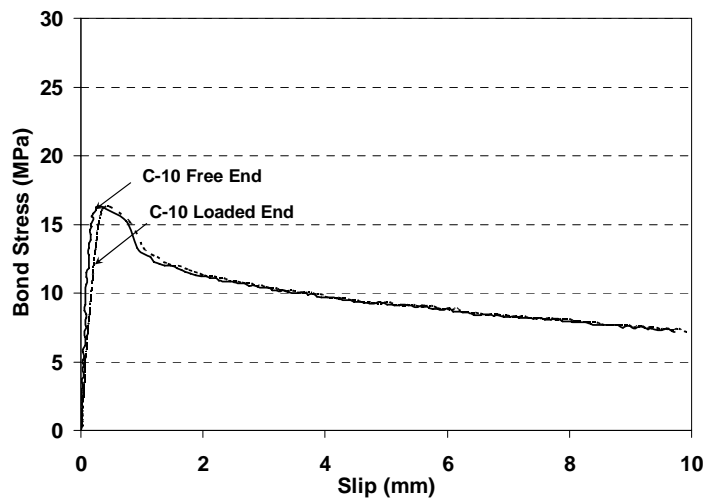


Fig. 6: Bond Stress-Slip Relationship for CFRP Bars No. 10

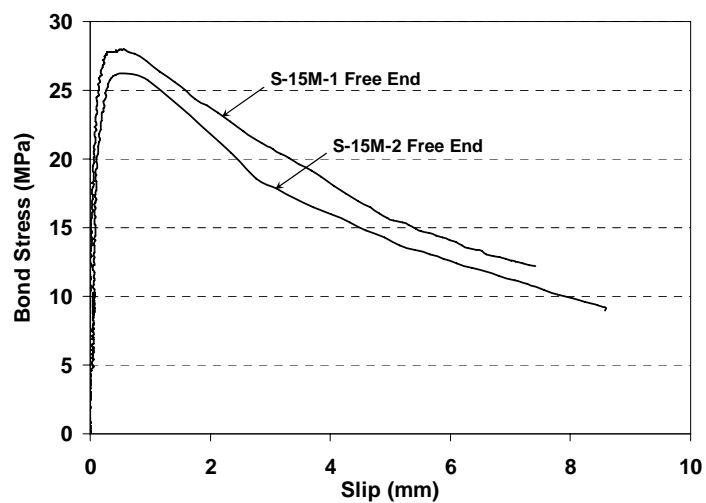


Fig. 7: Bond Stress-Free End Slip Relationship for Steel Bars No. 15M

Table 6: The Average Peak Values (τ_m and s_m) for Bond Stress and Free End Slip

Specimen	G-6	G-10	G-13	G-16	C-10
τ_m (MPa)	20.15	17.57	14.12	13.61	18.39
s_m (mm)	0.261	0.222	0.330	0.216	0.287

The measured loaded-end slip is adjusted for the elastic elongation of the bar within the distance from the end of the embedment length to the point where the LVDTs are attached, as follows:

$$s_{le} = s_{av} - s_e \tag{2}$$

$$s_e = \frac{F_u l}{E_{frp} A_b} \tag{3}$$

As the bond-slip (τ - s) constitutive law is need to investigate the behavior of reinforced concrete members considering the interaction between concrete and reinforcement, an analytical law representing the experimental results is to be investigated and validated. The currently available analytical models for τ - s identify general law which has to be adjusted to simulate the experimental results through determining its parameters by curve fitting. Two models are to be employed and analyzed to simulate the test results namely Malvar [10] and Modified BEP models [8]. Those models are calibrated using the experimental results to determine their constants to represent the bond-slip law for the tested FRP bars.

Malvar Model

Through an extensive experimental research on GFRP bars with different configurations of the outer surface, Malvar [8] proposed a refined model of the overall bond behavior, depending on two empirical constants (F and G) to be determined by curve fitting of the experimental bond-slip (τ - s) curves. This model is represented as follows:

$$\frac{\tau}{\tau_m} = \frac{F(s/s_m) + (G - 1)(s/s_m)^2}{1 + (F - 2)(s/s_m) + G(s/s_m)^2} \tag{4}$$

This model was used to simulate the behavior of the tested FRP bars considering the peak values from the experimental results (τ_m and s_m). The F and G constants are determined through the best fitting of the experimental bond-slip values for different FRP bars. The values of F and G are listed in Table 7. Figure 8 shows the comparison between these theoretical relationships and the experimentally obtained values. Figure 9 shows a comparison between τ - s relationships using Malvar model for different FRP bars. From this figure, Malvar [8] model seems to be able to reproduce the entire bond slip laws by means of a unique solution of the governing equation.

Modified BPE Model

A version of the Eligehausen, Popov and Bertero law (BPE) [16] modified (mBPE) by Cosenza et al. [8] was employed in the current study as the constitutive relationship because this relationship is very suitable for reproducing test results in case of FRP bars [8]. The aforementioned modified bond-slip constitutive law is shown in Fig. 10.

This modified constitutive law is represented by the ascending part (A) for $s < s_m$ which is formally coincident with first branch of BPE [16] and is given by:

$$\tau(s) = \tau_m \left(\frac{s}{s_m} \right)^\alpha \tag{5a}$$

The descending part of the curve (B) for $s_m < s < s_u$ and it is known as the softening branch and given by:

$$\tau(s) = \tau_m \left(1 + p - P \frac{s}{s_m} \right) \tag{5b}$$

Pecce et al. [1] used an identification procedure for determining the values of the parameters defining the mBPE constitutive law (τ_m , s_m , α and p). However, in the current study the values of α and p were determined based on the best fitting of the test results but considering the measured values of τ_m and s_m . Table 7 gives the values of α that controls the constitutive bond-slip law for tested FRP bars. However, for the descending portion an average value for the

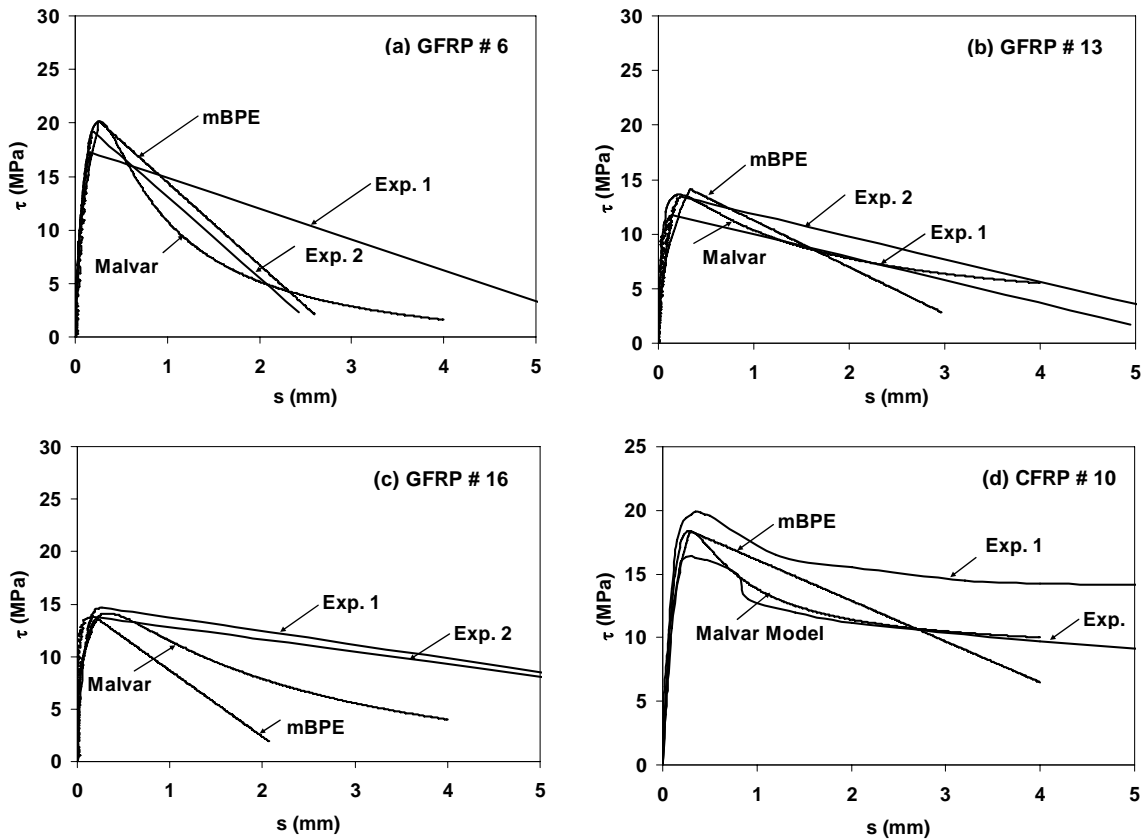


Fig. 8: Comparison between the Experimental and Analytical Bond-Slip Relationships

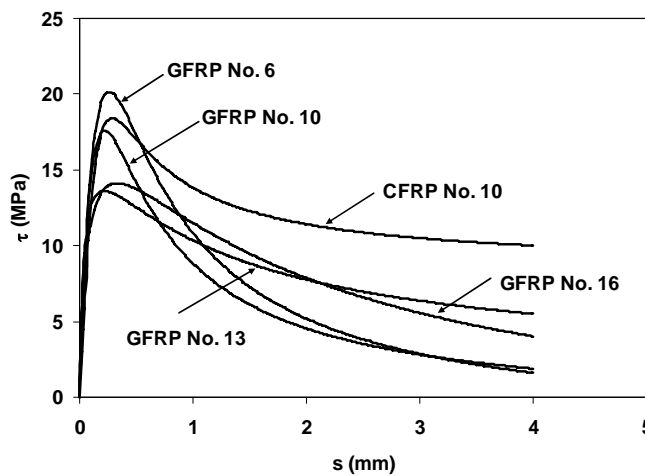


Fig. 9: Comparison between Malvar Models for FRP Bars

p factor equals 0.1 was used. Figure 9, also, shows the comparison between the measured bond-slip values and the theoretical mBPE model for different FRP bars. On the other hand Fig. 11 shows a comparison between the mBPE models for the different FRP bars.

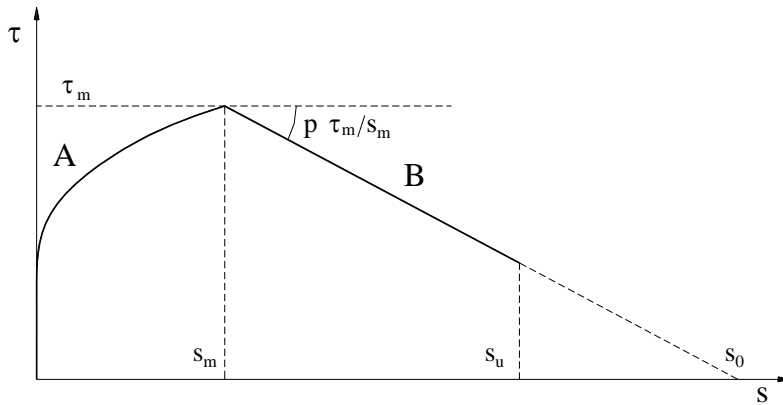


Fig. 10: Bond-Slip Law: Modified BPE Model

Table 7: Values of α for mBPE Model and F and G for Malvar Model

Specimen	G-6	G-10	G-13	G-16	C-10
α	0.458	0.388	0.437	0.271	0.413
F	2.85	3.02	6.59	8.29	2.38
G	0.89	0.94	0.79	1.16	1.86

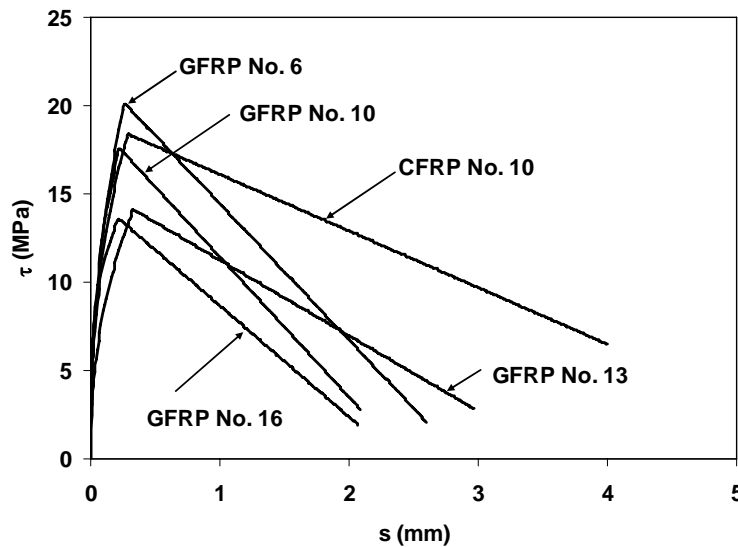


Fig. 11: Comparison between mBPE Models for FRP Bars

THE DEVELOPMENT LENGTH

Development length is the shortest length of bar in which the stresses can increase from the initial zero to the ultimate strength, f_{frpu} . Therefore the straight development length can be calculated as:

$$l_d \pi d_b \tau_{av} = A_{frp} f_{frpu} \tag{6}$$

Code Provisions for the Development Length

CAN/CSA S806 [11]

The CAN/CSA S806-02 [11] code provides the following expression for calculating the development length (Provided that the clear cover and clear spacing of the bars being developed are at least 1.5 db and 1.8 db, respectively):

$$l_d = 1.15 \frac{k_1 k_2 k_3 k_4 k_5 f_F A_{frp}}{d_{cs} \sqrt{f'_c}} \quad (7)$$

CHBDC - CAN/CSA S6-06 [12]

The Canadian Highway Bridge Design Code, CHBDC - CAN/CSA S6-06 [12], specifies the following expression to calculate the development length of FRP bars:

$$l_d = 0.45 \frac{k_1 k_5}{d_{cs} + k_{tr} \frac{E_{frp}}{E_s}} \left(\frac{f_{frpu}}{f_{cr}} \right) A_{frp} \quad (8)$$

where $k_{tr} = A_{tr} f_y / 10.5sn$ and the term $d_{cs} + k_{tr} E_{frp} / E_s$ should not be taken greater than $2.5 d_b$.

ACI 440.1R-06 [13]

The ACI 440.1R-06 [13] introduces the following expression for development length:

$$l_d = \frac{\alpha \frac{f_{fr}}{0.083 \sqrt{f'_c}} - 340}{13.6 + \frac{c}{d_b}} d_b \quad (9)$$

where c/d_b should not be taken larger than 3.5.

Development Length Based on Bond-Slip Model

Cosenza et al. [17] presented an analytical approach to evaluate the development length. The analytical study was based on the problem of a rebar embedded in a concrete block and pulled-out by means of a tensile force applied at one end. However, the solution of such problem requires actual bond-slip constitutive law of FRP bar to be defined. Considering the well-representing bond-slip constitutive model for the tested FRP bars the development length will be evaluated the aforementioned approach. Through the following lines, the analysis of the problem of a rebar embedded in a concrete block and pulled-out by a tensile force will reviewed as introduced by Cosenza et al. [17]. The schematic representation of the studied case is shown in Fig. 12. The differential equation that governs the bond problem [18] is obtained by considering:

The equilibrium of the bar:

$$\frac{\pi d_b^2}{4} d\sigma = \pi d_b \tau dx \quad (10)$$

A linear elastic behavior for the bar that is given by (neglecting the concrete in tension):

$$\sigma = E\varepsilon \cong E \frac{ds}{dx} \quad (11)$$

where E and ε are the elastic modulus of elasticity and the strain of the bar, respectively.

From Eqs. (10) and (11) the following differential equation is obtained:

$$\frac{d^2 s}{dx^2} - \frac{4}{E d_b} \tau(x) = 0 \quad (12)$$

Considering the Eligehausen et al. [16] modified by Cosenza et al. [8] shown in Fig. 10 (illustrated earlier and its constants were determined to represent the results of the studied FRP bars) when integrating Eq. (12), two cases have to be separately considered (Case A ($s \leq s_m$) and Case B ($s > s_m$)).

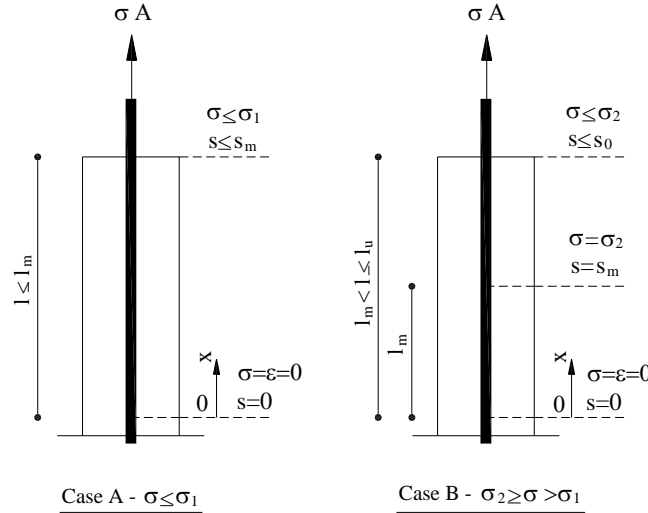


Fig. 12: Schematic Representation of the Pullout Problem [17]

Case A ($s \leq s_m$)

Integrating the governing equation in this case yielded two characteristic limit values: The limit tensile stress in the FRP bars (σ_1) which corresponds to a slip equals s_m :

$$\sigma_1 = \sqrt{\frac{8E \tau_m s_m}{d_b (1+\alpha)}} \tag{13}$$

The limit development length (l_m) which represents the upper bond of the development length related to the ascending part of the bond-slip law (Fig. 10) corresponds to a stress applied to the FRP bars equals to σ_1 :

$$l_m = \sqrt{\frac{E d_b s_m (1+\alpha)}{2 \tau_m (1-\alpha)^2}} \tag{14}$$

and it can also be represented by the following:

$$l_m = \frac{\sigma_1 (1+\alpha)}{4\tau_m (1-\alpha)} = l_{0m} \frac{(1+\alpha)}{(1-\alpha)} \tag{15}$$

where l_{0m} is the development length evaluated for $\sigma = \sigma_1$ and $\tau = \tau_m$.

For $\sigma < \sigma_1$ the development length can be evaluated as follows:

$$l_d = l_m \left(\frac{\sigma}{\sigma_1} \right)^{(1-\alpha)/(1+\alpha)} \tag{16}$$

Case B ($s \leq s_m$)

Considering the equation of the descending part of the bond-slip model (Eq. 5b), Eq. (12) becomes as follows:

$$\frac{d^2s}{dx^2} - \frac{4p\tau_m}{E d_b s_m} s = \frac{4(1+p)\tau_m}{E d_b} \tag{17}$$

Thus, the development length l_d can be obtained by:

$$l_d = l_m \left\{ 1 + \sqrt{\frac{(1-\alpha)^2}{2p(1+\alpha)}} \left[\arcsin \sqrt{\frac{A_{r2}}{A_{r\max}}} \right] - \arcsin \sqrt{1 - \frac{d_b \sigma^2}{8EA_{r\max}}} \right\} \quad (18)$$

where l_m is given by Eqs. (14) or (15), while:

$$A_{r2} = \frac{\tau_m S_m}{2p}; \quad (19a)$$

$$A_{r\max} = \frac{\tau_m S_m}{1+\alpha} + \frac{\tau_m S_m}{2p} \quad (19b)$$

Eq. (18) provides the development length for values of $\sigma \geq \sigma_1$ however for $\sigma = \sigma_1$ ($s = s_m$) Eq. (18) yields $l_d = l_m$.

Cosenza et al. [17] recommended neglecting the softening branch of the bond-slip curve due to the unstable nature in the design purposes. This is evident for tested FRP bars because the descending portion of the τ - s relationship varies greatly even within the replicates of the same parameter. Neglecting the contribution of the softening branch, the above-mentioned value σ_1 can be seen as an upper threshold for the normal stress σ . In particular, σ_1 represents a limit beyond which-even though it is possible to anchor the rebar it is necessary to rely on the descending branch of the bond-slip law. Therefore, it is possible to define σ_1 as the limit condition [17].

Considering the aforementioned procedure as well as the bond-slip relationships for different FRP bars, the development length is calculated and presented in Table 8. The development length (without considering any factors of safety) ranged from 7 to 15 times the bar diameter for GFRP bars and 17 to 20 times the bar diameter for CFRP bars. The development length was also calculated using the code provisions using the same stress level in the FRP bars (σ_1) and assuming a concrete cover to bar diameter ratio of 2.5 to minimize the probability of the concrete cover splitting. Comparison between code predication and the theoretical calculation is presented in Table 9 and Figure 13. From this table, it can be seen that the both S806-02 [11] and S6-06 [12] showed almost the same development length values which ranged from 11 to 21 d_b for GFRP bars and 24 to 28 d_b for CFRP bars. Corresponding to the estimated development length, the average bond stress was 5.40 and 5.52 MPa for CSA S806-2 [11] and CSA S6-06 [12], respectively. On the other hand, the ACI 440.1R-06 [13] showed very high estimation in comparison and development length ranged from 7 to 33 d_b for GFRP bars and 43 to 53 d_b for CFRP bars and the corresponding average bond stress was 4.58 MPa. It worth mentioning that the ACI 440.1R-06 [13] showed un-conservative prediction for GFRP No. 16. The ACI equation under estimated the development length that was required to achieve a stress in the GFRP No. 16 equals 0.29 of its tensile capacity. Thus, this equation may lead to under estimated development length when the limiting stress for the FRP bars is less than 30% of its tensile strength.

Table 8: Predicted Development Length (l_d) Based on The Bond-Slip Model

	Area (mm ²)	E (GPa)	f_u (MPa)	τ_m (MPa)	S_m (mm)	α	σ_1 (MPa)	σ_1/f_{frpu}	l_d (mm)	l_d/d_b
G-6	32.15	46.09	864	20.15	0.261	0.458	455.87	0.53	97.4	15.0
G-10	70.85	45.83	836	17.57	0.222	0.388	329.33	0.40	101.0	11.0
G13	126.61	45.84	813	14.12	0.33	0.437	305.99	0.38	175.6	14.0
G16	198.46	46.48	802	13.61	0.216	0.271	232.57	0.29	118.4	7.0
C-10	70.85	132.1	1305	18.39	0.287	0.397	648.29	0.50	194	20.0
C-13	126.61	133.6	1204	17.94	0.262	0.397	532.12	0.44	218.2	17.0

Table 9: Predicted Development Length Corresponding to Specified Stress Limit (σ_1)

	d_b (mm)	σ_1 (MPa)	CSA-S806-02 [11]		CSA-S6-06 [12]		ACI-440-06 [13]	
			l_d	l_d/d_b	l_d	l_d/d_b	l_d	l_d/d_b
G-6	6.4	455.9	135.0	21.0	132.0	21	214.5	34.0
G-10	9.5	329.3	144.7	15.0	141.6	15.0	174.3	18.0
G13	12.7	306.0	179.8	14.0	175.9	14.0	197.5	16.0
G16	15.9	232.6	171.1	11.0	167.3	11.0	107.3	7.0
C-10	9.5	620.6	272.7	29.0	266.8	29.0	505.8	53.0
C-13	12.7	533.1	313.2	25.0	306.4	24.0	543.1	43.0

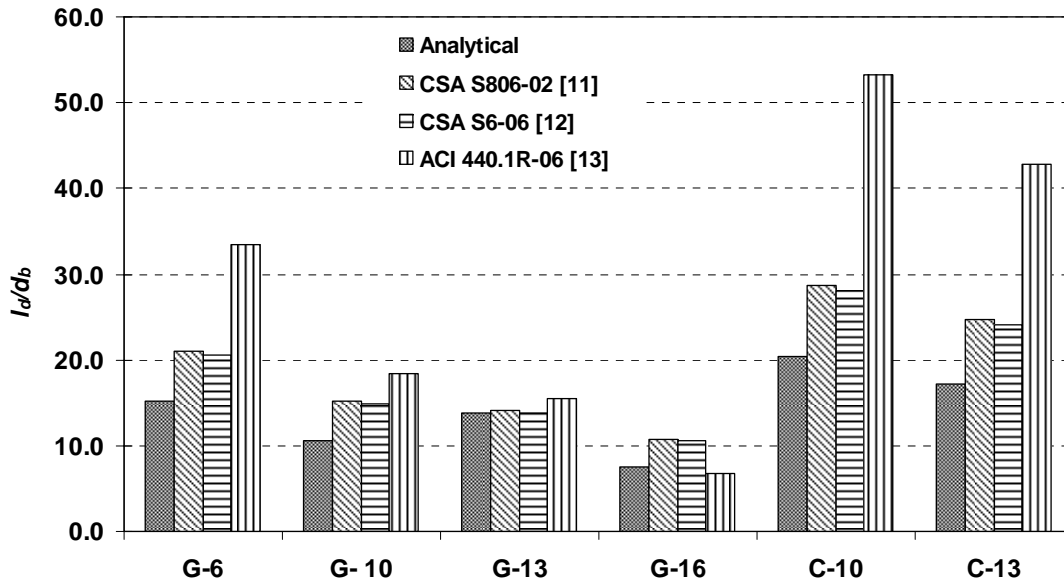


Fig. 13: Predicted Development Length for Different FRP Bars

The development length was re-calculated using the tensile strength of FRP as maximum limit and the results are listed in Table 10. As expected, Both CSA S806-2 [11] and CSA S6-06 [12] showed the same values for the development length with an average of 38 and 57 d_b for GFRP and CFRP, respectively with a corresponding average bond stress equals 5.46 MPa. The ACI estimation for the development length was very high in comparison with CSA S806-2 [11] and CSA S6-06 [12]. The average development length was 78 and 129 d_b for the GFRP and CFRP bars, respectively with a corresponding average bond stress equals 2.58 MPa. The ACI estimated values was 2.1 and 2.26 times the CSA S806-2 [11] and CSA S6-06 [12] values for the GFRP and CFRP bars, respectively.

Table 10: Predicted Development Length Corresponding to the Strength of FRP Bars

	d_b (mm)	f_{FRP} (MPa)	CSA-S806-02 [11]		CSA-S6-06 [12]		ACI-440-06 [13]	
			l_d	l_d/d_b	l_d	l_d/d_b	l_d	l_d/d_b
G-6	6.4	864.0	255.8	40.0	250.2	39.0	527.5	82.0
G-10	9.5	836.0	367.4	39.0	359.4	38.0	751.1	79.0
G13	12.7	813.0	477.6	38.0	467.2	37.0	969.1	76.0
G16	15.9	802.0	589.9	37.0	577.0	36.0	1192.3	75.0
C-10	9.5	1305.0	573.5	60.0	561.0	59.0	1285.0	135.0
C-13	12.7	1204.0	707.3	56.0	691.9	55.0	1564.1	123.0

Belarbi and Wang [19] specified design bond value corresponding to a slip at the free end equals 0.005 mm. from the analytical prediction, the average bond stress corresponding to 0.005 mm slip value was 8.72 MPa. Considering the general equation that represents the development length as follows:

$$l_d = \frac{f_{frpu}}{K\sqrt{f'_c}} d_b \quad (20)$$

Solving both equations (6) and (20) the K value can be obtained from the following equation:

$$K = \frac{4\tau_{av}}{\sqrt{f'_c}} \quad (21)$$

From Eq. (21) and considering a factor of safety equals 1.4, K value equals 4 is obtained. Calculating the development length from Eq. (20) considering K value equals 4 lead to an average development length equals 33 and 50 d_b for GFRP and CFRP bars, respectively. Thus, the bond stress corresponding to 0.005 mm slippage at the free end could be an appropriate value as design bond strength.

SUMMARY AND CONCLUSIONS

The current study presents the bond strength of fiber-reinforced polymer (FRP) reinforcing bars embedded in normal strength concrete. The study compares the bond strength, bond stress-slip relationships, and mode of failure for the FRP bars and the conventional steel bars. A total of 40 pullout specimens of GFRP, CFRP, and conventional steel bars embedded in concrete cubic blocks with embedment depth equals five times the bar diameter ($5d_b$) were constructed and tested. The experimental bond-slip relationships were modeled using Malvar [10] and Cosenza et al. [8] models. The bond-slip constitutive law was utilized in the analytical solution of the development length of FRP bars embedded in concrete and compared with the CSA S806 [11], CSA S6-06 [12] and ACI 440.1R-06 [13] predictions. Based on the results of this study the following can be concluded:

1. The bond strength of the sand-coated GFRP and CFRP bars was 64% and 71%, respectively, that of the steel bond strength for pullout failure mode.
2. The bond strength of GFRP bars decreases as the reinforcing bar diameter increases, this assure the previous findings from literature, however, both tested CFRP diameters showed almost the same bond strength. This may be referred to the helical wire wrapping that was provided before the sand coating and the high modulus of the bars as well.
3. At the same stress level in the FRP bars, the code predictions for the development length were higher than the analytically calculated development lengths using bond-slip models. The code equations provided a conservative estimation of the development length, however, at the low stress level (as observed in GFRP No. 16); the ACI 440.1R-06 [13] equation gives un-conservative prediction of the development length.
4. The ACI 440.1R-06 [13] equation gives a longer development length compared to the CAN/CSA S806-02 [11] and CAN/CSA S6-06 [12].
5. The bond stress corresponding to 0.05 mm slippage at the free end may be considered as design bond strength for FRP bars.

ACKNOWLEDGMENTS

The authors wish to express their gratitude and sincere appreciation to the Natural Science and Engineering Research Council of Canada (NSERC), Pultrall Inc., (Thetford Mines, Quebec, Canada) for financing this research work.

NOTATIONS

A_{frp} cross-sectional are of FRP bar (mm^2);
 A_{tr} cross-sectional area of the transverse reinforcement (mm^2);

c	concrete cover (mm);
d_b	bar diameter (mm);
d_{cs}	the smaller of the distance from the closest concrete surface to the center of the FRP bar being developed or two-third the center-to-center spacing of the FRP bars being developed (mm);
E_{frp}	modulus of elasticity of FRP bar (MPa);
E_s	modulus of elasticity of steel bar (MPa);
F, G	empirical constants determined for each FRP bar type;
f'_c	concrete compressive strength (MPa);
f_{cr}	concrete cracking strength (MPa);
f_F	design stress in FRP at ultimate limit state (MPa);
f_{fr}	developed stress in the FRP bars (MPa);
f_{frpu}	ultimate tensile strength of FRP bar (MPa);
F_u	failure load (N);
f_y	yield stress of the reinforcing steel bars (MPa);
k_1	bar location factor;
k_2	concrete density factor;
k_3	bar size factor;
k_4	bar fiber factor;
k_5	bar surface factor;
k_{tr}	transverse reinforcement index;
l	the length between the end of embedment length to the point of attachment of the LVDTs on the bar (mm);
l_{om}	development length evaluated for $\sigma = \sigma_1$ and $\tau = \tau_m$ (mm);
l_b	bonded length (embedment length) (mm);
l_d	development length (mm);
l_m	the limit development length which represents the upper bond of the development length related to the ascending part of the bond-slip law corresponds to a stress applied to the FRP bars equals to σ_1 (MPa);
n	number of FRP bars being developed;
p	coefficient defines the descending (softening) branch;
s	center-to-center spacing of the transverse reinforcement (mm);
s_{av}	average measured slips (mm);
s_e	elastic elongation (mm);
s_{le}	loaded-end slip (mm);
s_m	slip at peak bond strength;
s_u	ultimate slip (mm);
α	coefficient describes the ascending branch;
α	bar location modification factor;
σ_1	the limit tensile stress in the FRP bars which corresponds to a slip equals s_m (MPa);
τ_{av}	average bond strength (MPa);
τ_m	bond strength (peak) (MPa).

REFERENCES

1. Pecce, M., Manfredi, G., and Realfonzo, R., & Cosenza, E. (2001), "Experimental and Analytical Evaluation of Bond Properties of GFRP Bars", ASCE Journal of Materials in Civil Engineering 13(4), pp 282-290.
2. Ehsani, M. R., Saadatmanesh, H., & Tao, S. (1995), "Bond of hooked glass fiber reinforced plastic GFRP reinforcing bars to concrete", ACI Material Journal, 92(4), pp 391-400.
3. Ehsani, M. R., Saadatmanesh, H., & Tao, S. (1996), "Design recommendations for bond of GFRP rebars to concrete", ASCE Journal of Structural Engineering, 122(3), pp 247-254.
4. Benmokrane, B., Tighiouart, B., & Chaallal, O. (1996), "Bond strength and load distribution of composite GFRP reinforcing bars in concrete", ACI Material Journal, 93(3), pp 246-253.

5. Benmokrane, B., Zhang, B., Laoubi, K., Tighiouart, B., & Lord, I. (2002), "Mechanical and bond properties of new generation of carbon fibre reinforced polymer reinforcing bars for concrete structures", *Canadian Journal of Civil Engineering*, 29(2), pp 338–343.
6. Okelo, R. & Yuan, R.L. (2005), "Bond Strength of Fiber Reinforced Polymer Rebars in Normal Strength Concrete", *ASCE Journal of Composites for Construction*, 9(3), 203-213.
7. Tastani, S. P., & Pantazopoulou, S. J. (2006), "Bond of GFRP Bars in Concrete: Experimental Study and Analytical Interpretation", *ASCE Journal of Composites for Construction*, 10(5), pp 381–391.
8. Cosenza, E., Manfredi, G., & Realfonzo, R. (1997), "Behavior and Modeling of Bond of FRP Rebars to Concrete", *ASCE Journal of Composites for Construction*, 1(2), pp 40-51.
9. ACI Committee 440. (2004), "Guide Test Methods for Fiber-Reinforced Polymers (FRPs) for Reinforcing or Strengthening Concrete Structures", ACI 440.3R-04, American Concrete Institute, Farmington Hills, Mich., USA, 40p.
10. Malvar, L. J. (1995), "Tensile and Bond Properties of GFRP Reinforcing Bars", *ACI Material Journal*, 92(3), pp 276–285.
11. Canadian Standard Association (CSA). (2002), "Design and Construction of Building Components with Fibre Reinforced Polymers", CAN/CSA S806-02, Canadian Standards Association, Rexdale, Ontario, Canada.
12. Canadian Standard Association (CSA). (2006), "Canadian Highway Bridge Design Code", CAN/CSA-S6-06, Canadian Standards Association, Rexdale, Ontario, Canada.
13. ACI Committee 440. (2006), "Guide for the Design and Construction of Concrete Reinforced with FRP Bars", ACI 440.1R-06, American Concrete Institute, Farmington Hills, Mich., 41p.
14. Achillides, Z. & Pilakoutas, K. (2004), "Bond Behavior of Fiber Reinforced Polymer Bars under Direct Pullout Conditions", *ASCE Journal of Composites for Construction*, 8(2), pp 173-181.
15. Wang H. (2005), Discussion of "Bond Behavior of Fiber Reinforced Polymer Bars under Direct Pullout Conditions By Achillides, Z. and Pilakoutas, K.", *ASCE Journal of Composites for Construction*, 9(5), pp 468.
16. Eligehausen, R., Popov, E. P., & Bertero, V. V. (1983), "Local Bond Stress-Slip Relationships of Deformed bars under Generalized Excitations", Report No. 83/23, Earthquake Engineering Research Center, University of California, Berkeley, Calif., USA.
17. Cosenza, E., Manfredi, G., & Realfonzo, R. (2002), "Development Length of FRP Straight Rebars", *Composites: part B*, Elsevier, Vol. 33, pp 493-504.
18. Rehm, G. (1961), "Über die Grundlagen des Verbundes zwischen Stahl und Beton", *Deutscher Ausschuss für Stahlbeton*, Heft 138. Berlin: Verlag Wilhelm Ernst & Sohn.
19. Belarbi, A. & Wang, H. (2004), "Bond-Slip Response of FRP Reinforcing Bars in Fiber Reinforced Concrete under Direct Pullout", *Proceedings of the International Conference on Fibre Composites, High-Performance Concretes and Smart Materials*, Chennai, India, January 8-10, Vol. I, pp 409-419.

LONG TERM DEFLECTION OF REINFORCED HIGH STRENGTH CONCRETE BEAMS

Mohamed S. Issa*

Housing and Building National Research Center, Giza, Egypt.

Mohamed R. Mahmoud, Akram M. Torkey, and Mohamed T. Mostafa

Faculty of Engineering, Cairo University, Giza, Egypt.

ABSTRACT

High strength concrete is characterized by low creep strains compared with normal strength concrete. This means that its long-term deflection is expected to be less than that of normal strength concrete. This fact needs to be accounted for by the long-term deflection multiplier of the ACI Code [1].

This paper deals with the long-term deflection of reinforced concrete beams made of high strength concrete. Five simply supported beams were loaded for about one year. The experimental work was carried out to investigate the effects of concrete strength, reinforcement yield stress, span/depth ratio and loading type on the long-term deflection. The long-term deflection multiplier of the ACI Code is re-evaluated to account for the effect of concrete strength.

Keywords: beams, deflection, high strength concrete & sustained load deflection

EXPERIMENTAL PROGRAM

The experimental program consisted of testing five simply supported beams. The ratio of the compression reinforcement to the tension reinforcement was 0.36. The tension reinforcement ratio was 1.43% with yield stresses of 280 MPa and 400 MPa. Span to effective depth ratio of tested beams ranged from 18.18 to 27.27. Three types of loading were applied: midspan load, third-points loads and six equally spaced loads equivalent to uniform load. Data of the tested beams are given in Table (1) and data of beams reinforcement are given in Table (2). Full details are available in reference [2].

Test specimens

The beams cross-sections were (10*14) cm. The effective spans were either 200 cm or 300 cm. Each beam was reinforced by two bars as tension reinforcement and two bars as compression reinforcement. The details of these bars are found in Tables (1) and (2). The transverse reinforcement (stirrups) was Ø8 each 6-cm center-to-center for all the tested beams.

Material properties

Steel: Normal mild steel bars of 6, 8, and 10 mm diameter in addition to high tensile steel bars of 10 mm diameter were used in these experiments. Mechanical properties were determined from the standard tension tests. The measured yield stress of these bars is shown in Table(2). Concrete: A mix of ordinary Portland cement, natural sand, crushed dolomite, and water was used. Admixtures such as ADDICRETE BVF and silica fume were also used. The proportions by weight of the concrete mix are given in Table (3).

* Corresponding author
Received Date:26/8/08
Acceptance Date:4/11/08

Table (1): Details of the tested beams

Beam	Effective depth, d (mm)	Cross section, b × h (mm)	Clear span, L (mm)	Load type	Span / depth	Reinforcement	
						Bottom A _s	Top A _s
B1	110	100 × 140	3000	Third points	27.27	2Ø10	2 Ø 6
B2	110	100 × 140	3000	Mid-span	27.27	2Ø10	2 Ø 6
B3	110	100 × 140	3000	Third points	27.27	2Ø10 plain	2 Ø 6
B4	110	100 × 140	2000	Third points	18.18	2Ø10	2 Ø 6
B5	110	100 × 140	3000	Uni-form (6loads)	27.27	2Ø10	2 Ø 6

Table(2): Reinforcement data

Beam	Reinforcement ratio ρ (%)	∞	Bottom reinforcement		Top reinforcement	
			Nominal f _y (MPa)	Measured f _y (MPa)	Nominal f _y (MPa)	Measured f _y (kg/cm ²)
B1	1.43	0.36	400.0	443.8	280.0	-
B2	1.43	0.36	400.0	443.8	280.0	-
B3	1.43	0.36	280.0	-	280.0	-
B4	1.43	0.36	400.0	443.8	280.0	-
B5	1.43	0.36	400.0	443.8	280.0	-

where; $\rho = A_s/bd$, $\infty = A_s/A_s$

Table (3): Mix design quantities for 1 m³ of concrete

Portland Cement	550 kg
Silica fume	80 kg
Water	165 kg
Crushed dolomite	1125 kg
Natural sand	550 kg
ADDICRETE BVF	22 kg
Water/cement	0.3

Beam fabrication

For each tested beam the steel reinforcement cage was put together in wooden forms. Before installing this cage, the sides of the form were brushed by oil to avoid any bond between the concrete and form.

A mechanical rotary mixer of vertical axis and pan type was used to mix the constituent materials in the laboratory. The concrete components were weighed, and the dry mix were blended in the mixing bowl. Hence, water was gradually added to the mixing bowl until the paste had formed. Then, beams were cast. At the same time, control standard specimens (cubes and cylinders) were cast in order to determine the mechanical properties. Beams were moist cured for eight days. It was then removed and stored in laboratory environment until the testing day. The test was carried out when the age of the concrete was at least one month.

The average concrete cube (150*150 mm) strength (f_{cu}) is 82.3 MPa and the average concrete cylinder (150mm diameter and 300mm height) strength f'_c is 64.3 MPa. The initial modulus of elasticity E_c of the produced concrete is 25.95 GPa and the splitting tensile strength is 4.32 MPa.

Test set up

All beams were tested in the Concrete Research Laboratory, Cairo University. Initial testing of the beams was done in a 500-ton capacity hydraulic machine. At each load increment, the vertical deflections along the span as well as the strains through the depth of the beam at midspan, were recorded. The deflections of the beams were measured using dial gages with 0.01 mm accuracy. The strains were measured using Demec gauges with gauge length of 200mm on both faces of the beams.

This initial short-term testing was under load of maximum value equals to approximately 0.7 of the theoretical ultimate load of each beam, which is the beams service load. Then blocks of weight equal to the value of the service load were fitted to each beam and kept in place for around one year (see Figure 1). Deflection measurements were taken regularly during this long-term testing. Blocks were then removed while deflection measurements continued for close to one month so that the recovered deflection is determined.



Figure (1): Sustained loading of Beam B5

TEST RESULTS

Crack patterns

A summary of the short-term test results is given in Table (4). The table includes the cracking load, the maximum load and the corresponding deflections at midspan. Similar characteristics were noticed for the cracking patterns of the different beams. All beams were cracked in a flexural type mode starting by hair cracks which join and widen as the load increases.

Table (4): Short-term test results of studied beams

Beam	f_{cu} (N/mm ²)	Cracking stage		Maximum stage (0.7 of ultimate load)	
		load (kN)	deflection (mm)	load (kN)	deflection (mm)
B1	83.0	2.00	1.98	11.14	15.18
B2	83.0	2.50	2.45	7.4	13.33
B3	81.5	3.60	2.63	8.48	11.24
B4	81.5	5.10	1.02	16.48	7.39
B5	81.5	3.75	2.88	16.00	17.61

Long-term deflection

Initial elastic beam deflections and measured total deflections are given in Table (5). The relationship between the total deflections and the initial deflections is presented in Table (6). The ratio of the total deflection at 6 months, for example, to the initial deflection ranges from 1.2 to 1.34 and the ratio of the span to the deflection at 6 months of loading ranges from 168.2 to 287.4 .

For beam B1, Figure (2), which was subjected to third-points loads, the initial deflection was 11.07 mm. It was followed by a steady increasing deflection to a total deflection of 14.64 mm before unloading. The recovered deflection was 10.58 mm.

Reinforced concrete beams made of high strength concrete showed good elastic recovery of deflection on unloading but only limited creep recovery as shown in Figure (2). The elastic recovery included almost the entire instantaneous deflection. This behavior indicates the largely elastic/brittle nature of high strength concrete.

Table (5): Results of long term tests

Beam	Initial deflection Δ_i (mm)	Total long term deflection (mm)				L/Δ_{6m}
		1 month Δ_{1m}	3 months Δ_{3m}	6 months Δ_{6m}	9 months Δ_{9m}	
B1	11.07	12.17	13.03	13.29	14.40	225.7
B2	8.65	10.13	11.05	11.56	12.01	259.5
B3	7.92	9.52	10.22	10.44	11.20	287.4
B4	7.35	8.27	8.70	8.86	8.83	225.7
B5	13.60	15.13	16.32	17.84	18.64	168.2

Table (6): Relationship between the total deflection and the initial deflection

Beam	Δ_{1m} / Δ_i	Δ_{3m} / Δ_i	Δ_{6m} / Δ_i	Δ_{9m} / Δ_i
B1	1.10	1.18	1.20	1.30
B2	1.17	1.28	1.34	1.39
B3	1.20	1.29	1.32	1.41
B4	1.13	1.18	1.21	1.20
B5	1.11	1.20	1.31	1.37

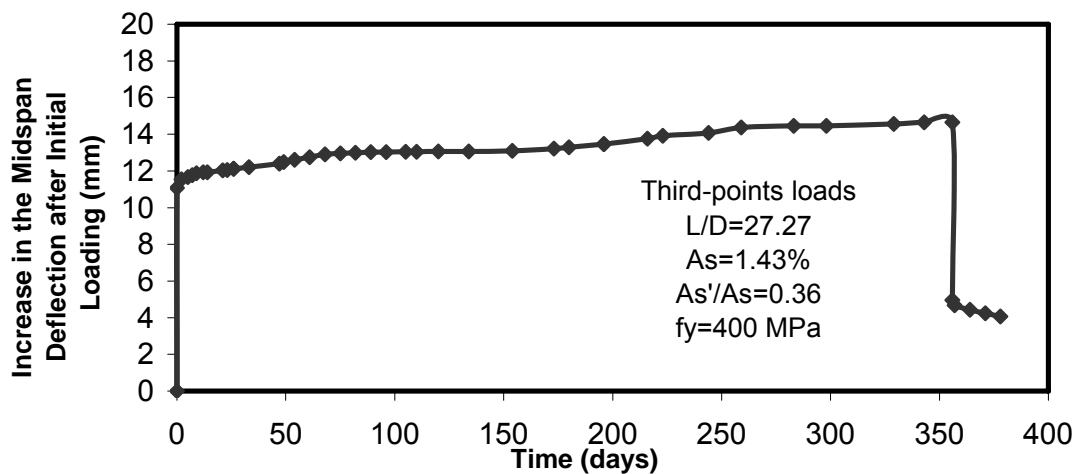


Figure (2): Variation of total deflection for Beam B1 with time

Effect of loading type on the long-term deflection

The long-term (shrinkage+creep) deflection curves for beams under different loading types are shown in Figure (3) from which we can see that the sustained load deflection reduces with the increase in the number of loads. From Table (6), the ratio between the total long term deflection and the initial deflection decreases with the increase in the number of loads. For beam B1 subjected to third-span loads, this ratio ranges from 1.10 to 1.30, while for beam B2 subjected to midspan load, this ratio ranges from 1.17 to 1.39.

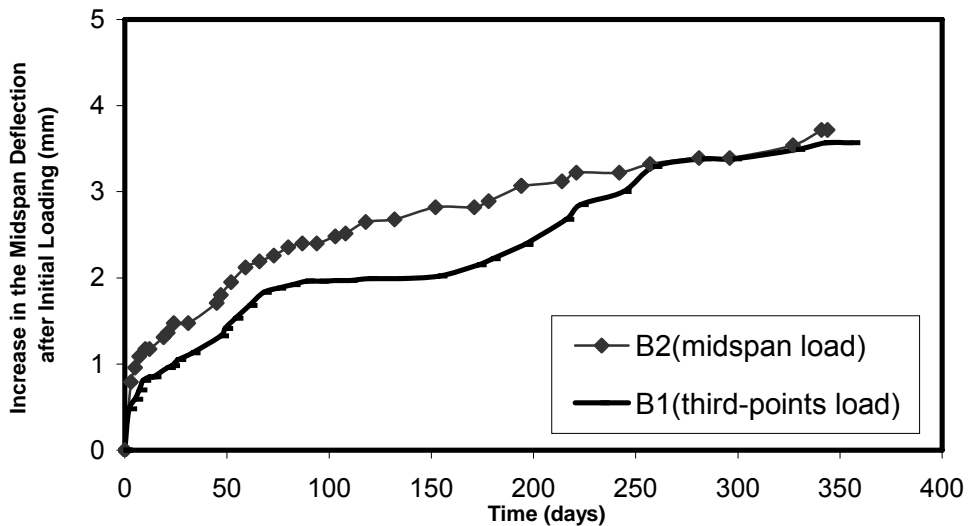


Figure (3): Effect of loading type on the sustained load deflection

Effect of yield stress of tension reinforcement on the long-term deflection

It is expected that beams reinforced with plain, mild steel will have higher long-term (shrinkage+creep) deflection. This was the case in this research as shown in Figure (4) for beams B1 and B3. From Table (6), the ratio between the total long term deflection and the initial deflection is higher for beam B3 with mild steel. This ratio ranges between 1.20 and 1.41 for beam B3 and ranges between 1.10 and 1.30 for beam B1.

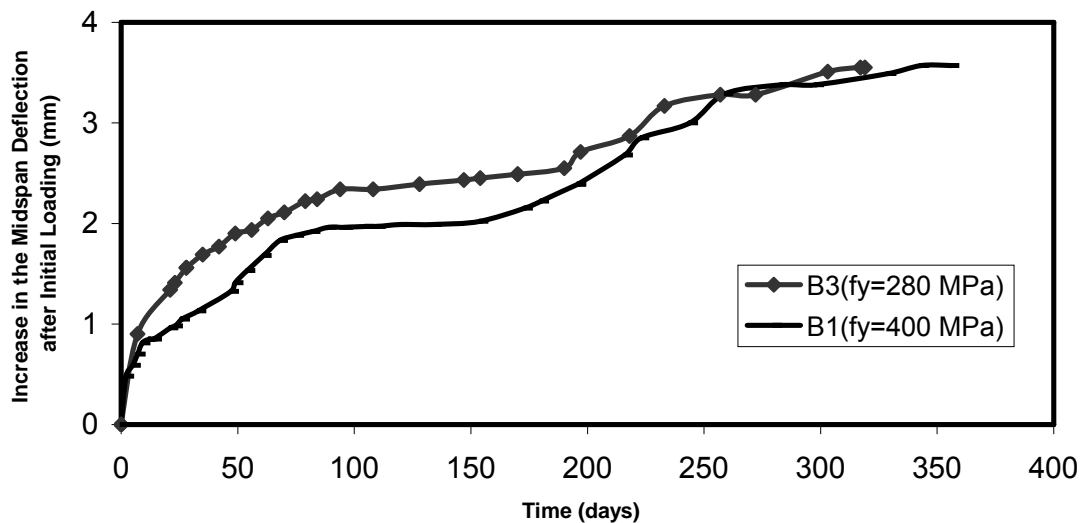


Figure (4): Effect of yield stress of tension reinforcement on sustained load deflection

Effect of span/depth ratio on the long-term deflection

Beams B1 and B4 of Figure (5) demonstrate that beams with less span/depth ratio show stiffer response under load.

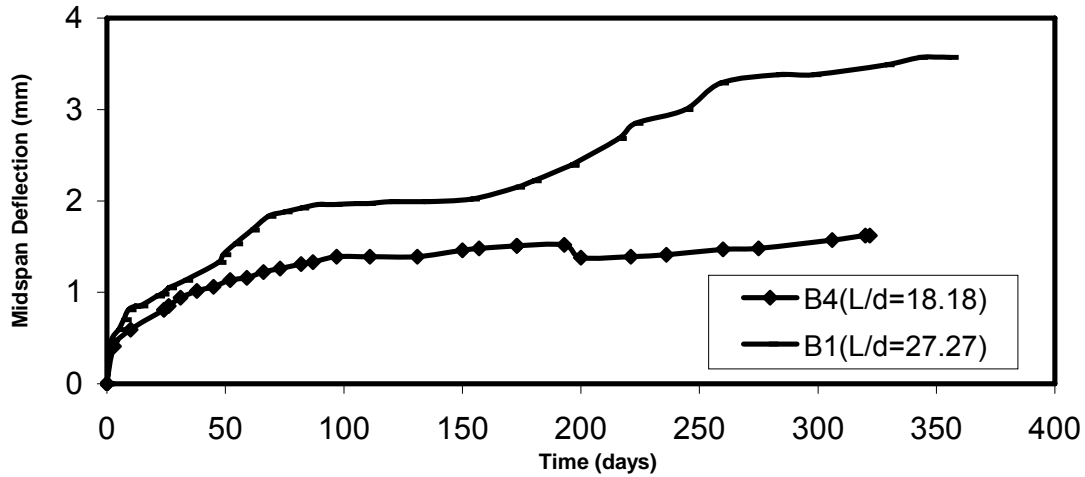


Figure (5): Effect of span/depth ratio on sustained load deflection

EVALUATION OF LONG-TERM DEFLECTION MULTIPLIER OF THE ACI CODE

There is a large experimental evidence now that high-strength reinforced concrete beams exhibit significantly less long-term deflections than normal-strength concrete members. This is mainly due to the lower creep strain of high strength concrete. Also, the influence of compression steel is less pronounced for high strength concrete beams. This is because the force transfer from the compression concrete to compression reinforcement is reduced for high strength concrete beams, for which creep is lower than normal strength concrete (references [3], [4], [5] and [6]). The experimental work of this research revealed that long-term deflections are influenced by the bond between steel and concrete. The use of plain reinforcement increases the sustained load deflection. These three observations are not accounted for in the long-term deflection multiplier of the ACI Code which will be modified in the coming paragraphs.

Proposed form for the long-term deflection multiplier

To account for the concrete compressive strength, and for the decreasing influence of the compression reinforcement in the case of high strength concrete beams, the creep and shrinkage deflection multiplier is written in the following form .

$$\lambda = \frac{F_1 \zeta}{1 + 50F_1 \rho'} \tag{1.0}$$

Where F_1 = correction factor.

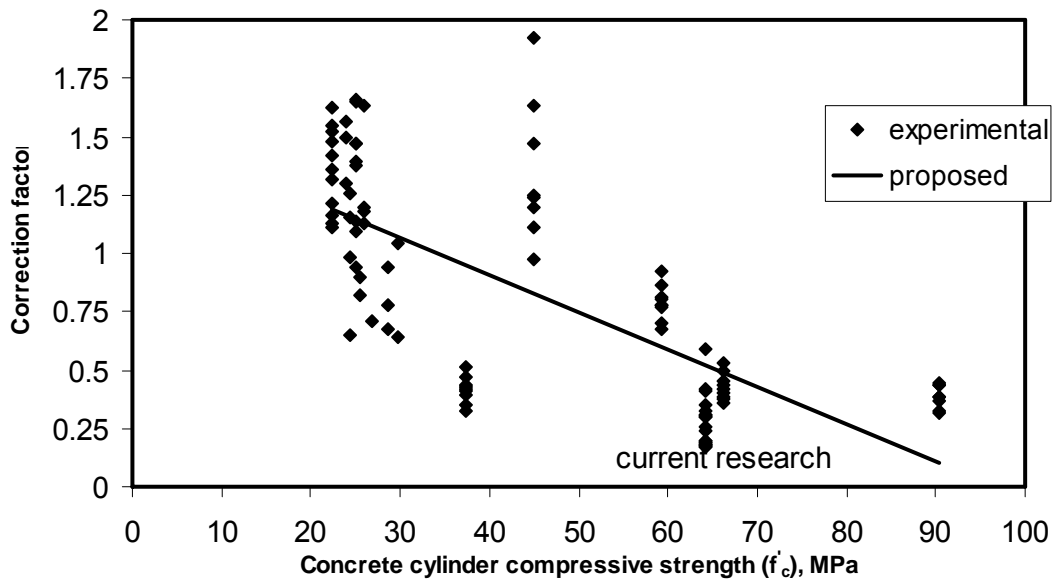
ζ =factor depending on the duration at which long-term deflection is to be calculated

ρ' =ratio of compression reinforcement

The ratio, λ , of the sustained load deflection to the immediate deflection was calculated from the experimental results of the beams of this research and plotted along with the experimental results of other researchs as reported by reference [7] (Figure 6). A curve fitting was made to obtain the following form of the correction factor

$$F_1 = 1.55 - 0.016 * f'_c \tag{2.0}$$

where f'_c is in MPa.



Figure(6): Relationship between the correction factor F_1 and the concrete cylinder compressive strength f'_c , data extracted from reference [7]

CONCLUSIONS

Based on the results of the experimental investigation, the following conclusions are drawn:

1. The increase in the span-to-depth ratio is associated with an increase in the sustained load deflections.
2. The use of plain mild steel as main reinforcement results in larger long-term deflections when compared with a beam of the same reinforcement area but using deformed high tensile steel.
3. A proposed modification for the ACI long-term deflection multiplier is recommended. It accounts for the strength of concrete. The form of the modified long-term multiplier is:

$$\lambda = \frac{F_1 \xi}{1 + 50F_1 \rho}$$

where $F_1 = 1.55 - 0.016 * f'_c$

REFERENCES

- 1) ACI Committee 318 (2002), "Building Code Requirements for Structural Concrete (ACI 318M-02) and Commentary (ACI 318RM-02)", American Concrete Institute, Detroit, USA.
- 2) Issa, M. S. (2003), "Immediate and Sustained Deflection of High Strength Reinforced Concrete Beams", PhD Thesis, Cairo University, Faculty of Engineering.
- 3) ACI Committee 435 (1995), "Control of Deflection in Concrete Structures", Reported by ACI Committee 435, pp.2-77.
- 4) Ganeswaran, R. and Rangan, B.V. (1996), "Long-Term Deflections of High-Strength Concrete Beams and One-Way Slabs", ACI Publication SP-161-11 "Recent Developments in Deflection Evaluation of Concrete", Editor: Nawy, Edward G., pp.243-266.
- 5) Paulson, Kent A., Nilson, Arthur H. & Hover, Kenneth C. (1991), "Long-Term Deflection of High-Strength Concrete Beams", ACI Materials Journal, V.88, No.2, pp.197-206.

- 6) Nilson, Arthur H. (1985), "Design Implications of Current Research on High-Strength Concrete", ACI Special Publication 87-7 "High-Strength Concrete", Editor: Russell, Henry G., pp.85-118.
- 7) Sherif, Alaa G. and Dilger, Walter H. (1998), "Critical Review of CSA A23.3-94 Deflection Prediction For Normal and HSC Beams", Can. J. Civ. Eng., V.25, pp.474-489.

NATURAL VENTILATION OF A SINGLE FLAT BUILDING

Mahmoud A. Hassan ^{1*}, Nabil M. Guirguis¹, Ali. A. Abd El-Aziz²

¹ Housing and Building National Research Center- Cairo – Egypt

² Faculty of Engineering- Shoubra- Banha University- Egypt

ABSTRACT

This paper illustrates experimental and theoretical results of a naturally ventilated building model. The test model was fabricated using perspex glass to simulate actual single flat building model with a scale 1: 30. This model was provided with a heating plate at the roof to simulate the heat gain by the solar radiation. The model was subjected to air flow in a wind tunnel to study the effect of the different air flow directions with the main façade of the model (natural ventilation through openings) on the average temperature and convective heat transfer coefficient of the heated ceiling. The reduction of average temperature of the ceiling indicates the good ventilation (good air flow) inside the model. A smoke tunnel visualization technique was used to give a viewer white smoke lines inside the model, also a CFD computer software package was used to predict the velocity distribution inside the models in a contour form for different air flow direction. The results present the importance of natural ventilation in reduction of the ceiling temperature and in turns reduce the indoor temperature.

KEYWORDS : Wind tunnel, Smoke tunnel, Natural ventilation , CFD Package, ANSYS software, Building model

INTRODUCTION

Saving of energy nowadays became very important after depletion of conventional sources of energy. Natural ventilation is unavoidable now as it helps to maintain a healthy indoor environment of acceptable standards; proper natural ventilation is a function of external and internal conditions (Outdoor& indoor conditions). The ventilation conditions inside a building are among the primary factors determining human health, comfort and well being. They have a direct effect on human body through the physiological effect of air purity and motion, and an indirect effect through their influence on the temperature and humidity of the indoor air and surface. Ventilation serves three distinct functions. The first is to maintain the quality of the air in the building above a certain minimum level by replacing indoor air, vitiated in the process of living and occupancy, by fresh outdoor air. This requirement may be termed health ventilation and should be ensured under all climatic conditions. The second function is to provide thermal comfort by increasing the heat loss from the body and preventing discomfort due to moist skin; this may be termed thermal comfort ventilation. The third is to cool the structure of the building when the indoor temperature is above that outdoors, and this may be termed structural cooling ventilation.

The relative importance of each of these functions depends on the climatic conditions prevailing in different seasons and regions, and each involves air flow of a different order of magnitude and their satisfactory use sometime calls for different design details.

Most regions have various requirements during the various seasons, so that details of design should have provisions to satisfy all the above requirements. Ventilation problems can be studied from measurements taken in full scale buildings under natural conditions or by model studies in a wind tunnel.

* Corresponding author
Received Date:2/1/08
Acceptance Date:12/10/08

The ventilation in full-size buildings varies continually with the fluctuations in external wind direction and velocity. Therefore it is necessary to repeat measurements over a period of time, in order to obtain a reliable assessment of the conditions. Ventilation conditions in a building are also affected by near by structures, and therefore it is difficult to isolate the effect of one given factor from the influence of the surroundings. Because of these difficulties most investigations of ventilation problems are conducted in a wind tunnel using models.

In aeronautical studies, it is normally required that the Reynolds number must be the same for the model and the body it represents. In this way air velocity is increased in accordance with their size ratio and similar flow patterns are achieved around the model and the full scale body. However, it was proved by several investigations that the flow pattern for building is independent of the Reynolds number. And those even wide variations in air velocity do not affect flow and pressure distribution over the surfaces.

Therefore normal air velocities were used when investigating building ventilation problems. For every model there is a critical air velocity above which the latter does not affect the flow pattern. Under such conditions the flow pattern around buildings can then be inferred from scale model observation.

There are some previous investigations in the natural ventilation field, many researches were published, and these researches are done in four distinct categories as follows:

1- Field work conducted on real buildings covering published materials on natural ventilation tests in such buildings (commercial or others) with emphasis on evaluation of thermal comfort indicators for occupants present in the investigated building and under prevailing natural conditions

2-Laboratory work, covering published materials that give result of tests carried out on experimental rooms of prototype or model scale. In such experiments certain measurements were made to evaluate the natural ventilation characteristics under various conditions and openings

3-Theoretical investigation (including computations), covering published materials related to attempts of theoretical modeling of natural ventilation.

4- Combined investigation, covering published materials containing a mix of the above categories. I.e. material containing field /theoretical work together or field/ laboratory work or theoretical/ laboratory work, or all combined.

Previous Work

Aynsley [1] have shown a detailed characteristic of air flow from large ceiling fans are analyzed, ceiling fans offer an including spectral density of gusts that indicate the presence of desirable gusts in the frequency range of 0.3 hz to .5 hz. The results indicate that ceiling fans offer an energy-efficient option for providing indoor comfort in warm, humid, environment. Larger, high volume, low-speed, ceiling fans at 0.019 W/m² of floor area served, offer a 93% increase in energy efficiency over smaller higher-speed ceiling fans at 0.35 W/m².

Bae and Chun [2] thermal environment was measured and residents' subjective thermal comfort in apartments' living rooms was investigated during summer. The measurement was conducted during 60 days from July 3rd to August 31st in 2004 in rooms of six apartment buildings rooms where air-conditioners were located. Questionnaire surveys was also conducted to investigate residents' subjective indoor environment sensation for the living rooms. It is concluded that, the range of residents' acceptance comfort temperature can be defined as 23.70 °C ~ 28.89 °C of SET* (standard new Effective Temperature). Finally, it is illustrated that if the indoor climate could be kept to satisfy these zones by such passive architectural schemes as promoting natural ventilation or shadings, the energy consumption resulting from running the air conditioners would be reduced.

Cettina [3] obtained a case study of Taranto city council including active-passive energy saving systems, in particular building right orientation, cross ventilation, cooling pipe, chimney walls and utilization of eco friendly materials causing low environmental impact. The dimensions of the building are created East to West in order to take full advantage of the sun throughout the winter and ventilation throughout the summer. The south-facing perspectives comprise large windows to capture solar energy throughout the winter and are protected by a skin that is

attached to the wall at a distance of around 2 m and thereby protects the façade from the sun during the summer. The north-facing perspectives comprise smaller windows and the skin is attached to the walls to protect the north-facing façade from the heat dispersion in the winter and do not screen sun rays during the summer.

Colombari [4] presented a series of advanced façade solutions which have been realized in conjunction with innovative environmental system, and is continuously monitored in terms of energy consumption and indoor environment. The measurements were carried out in 14 full-scale test rooms located in San Vendemiano, Italy, and provide a direct comparison between different solutions exposed to identical climatic conditions and yield the basis for validation of both simplified and detailed engineering tools. The building envelope configurations comprise double skin façade (naturally and mechanically ventilated), demonstrating stand-alone systems as well as integration between façade and environmental systems, which comprise variations of radiant system as well as displacement ventilation. A comparison between the innovative solutions is installed side-by-side with conventional systems adopting high performance glazing and fan coil cooling/heating. The results show that, the main difference between the two most important advanced systems described as follows: the active façade is preferred in climates where occupant comfort close to the façade during cold period is a concern. The interactive façade is preferred when cooling loads are a major concern.

Dear [5] explores recent performance rating schemes currently undergoing revision in Australia (national housing energy rating scheme) and the Netherlands (ATG). The application of adaptive thermal comfort principles in various contexts has been discussed with particular attention being paid to the way in which the outdoor meteorological and climatic context of a building should be represented in the adaptive algorithms. The default representation is an actual measurements or a climatologically monthly mean air temperature. The time-lagged correlations between clothing insulation and outdoor weather were examined and used these as the basis of defining exponentially decaying weights in a running weekly mean outdoor temperature. Finally, the ways in which these adaptive concepts could applied were illustrated, including algorithms for the control be of mixed-mode building management systems and building performance rating schemes.

Hasselaar's [6] a description of the microclimate in the bedroom was established and the measurements are focused on the moisture balance, air flow patterns and change rate and house dust mite allergen. Home inspection visits and interviews result in a data base with 333 cases. The relations between occupancy, use of ventilation openings, moisture production and mould problems are analysed on the basis of these data. The moisture balance study shows that ventilation with cool fresh air is important and that high peaks some where in the house will affect the moisture level in bedroom that likely to be occurring and poorly ventilated with fresh air. Good ventilation during sleep reduces the allergen concentration in the bedroom air, but does not prevent exposed to dust blown from under the covers to the breathing area.

Medhat and Khalil [7] devoted to investigate the Egyptian thermal comfort variables that affect the building design requirements; supply fresh air, indoor temperature and relative humidity, local air velocities, turbulent flow regimes, mean radiant temperatures and infiltration levels. Also, the non-thermal variables, such as, health, age, activity, clothing, sex, nutrition, location, season and acclimatization for any of the occupants were considered. The results show that, the study leads to change the acceptable limits of indoor conditions in the new rural developed arid zones in upper-egypt. Also, the use of the standard vapor compression cycles at hot and dry climates affect the thermal heat gain due to fresh air which will be reduced greatly as the load represents about 20% to 25% of the grand total load. Adding to the above increasing indoor dry bulb temperature by 5 °C will reduce the total thermal loads by about 8% to 12%. The results obtained indicated that, all men over 45 years of age preferred an effective temperature one degree higher than other below this age.

Robert [8] demonstrates possibilities to evaluate thermal comfort near windows in office rooms in winter time in Scandinavian climate. Results in the form of PPD at different distances from a window are compared based on measurements made by a thermal comfort meter and computer calculations with a program for energy and indoor climate. Also, the influence of different room conditions were measured and analysed. The results demonstrate how thermal loads close to windows can be quantified. It is shown that, the windows in cold climates, with low surface temperatures and potential air leakage, are of particular interest for the thermal indoor climate.

The results indicated that, measurements and computer calculation can be used to quantify the thermal climate in different ways.

EXPERIMENTAL WORK AND TEST MODEL

The present section is devoted to presenting the constructional details of a wind-tunnel test facility that was designed, built and tested at the Housing & Building National Research Centre (HBRC). The facility as it stands is considered as an asset for research work on building models and can be utilized for commercial testing that may be required by building designers in various sectors of the country.

Wind tunnel Constructional Details:

The tunnel consists of, as shown in Figure 1-a four major sections: the inlet section, the working section, the diffuser section and the coaxial fan section. The fan is driven by an AC motor (4.2kw and 640rpm) and gives a maximum velocity of 12m/s in the working section. The quantity of air is controlled by means of a controller unit that allows for five fan speeds (corresponding to air speed ranging from 3m/s up to 12m/s). The use of a standard streamlined intake at tunnel duct inlet results in a low turbulence flow in the working section. However, in practice, prevailing winds are either of moderate or high turbulence intensity. Consequently, to obtain turbulent wind in the working section it would be necessary to use turbulence generating devices in the form of grids of varying geometry and positioned suitably upstream of the working section. On the other hand, an atmospheric boundary layer type of flow must be generated in the working section in order to simulate ground-affected turbulent winds. For this purpose, logarithmic-profile-generating devices again in the form of a grid must be mounted some distance ahead of the test model. Figure 1-b show a photo of the wind tunnel and the driven unit.

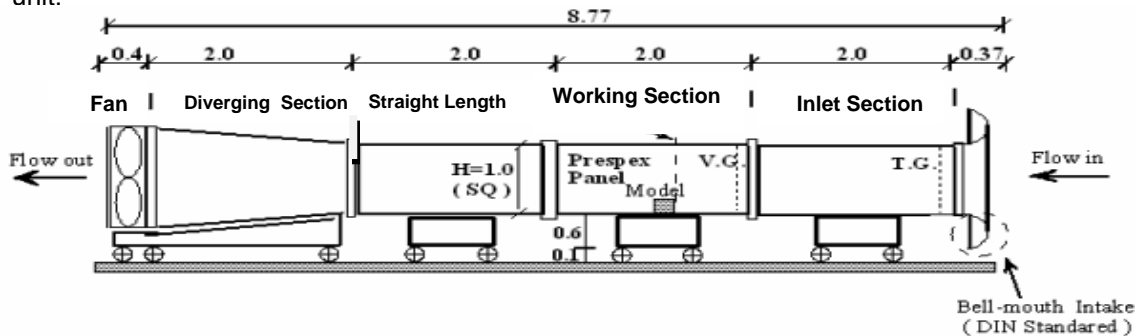


Figure 1-a Wind Tunnel Layout showing location of Different Test Facility Sections.



Fig 1-b A photograph of the Wind Tunnel and driven Section

Smoke tunnel constructional details:

It was necessary to use a smoke tunnel to observe and photograph the airflow configuration inside the model. The smoke tunnel provides a simple picture of turbulence, stagnation and reattachment zones around and inside building.

(i) Smoke generator:

The smoke generator is a glass bottle filled with kerosene; condense return glass tube, heater, vapor container, blower and smoke rake. These are all connected to each other using rubber tubing.

(ii) Smoke tunnel working section:

The working section of the smoke tunnel is of rectangular cross section of dimension 10 x10x20 cm. Laminar airflow is obtained through the test section using honeycomb attached at the tunnel duct inlet. As the heater is switched on the heated kerosene vapor passed through the smoke rake and streaks of kerosene vapor flow through the working section and over the test model. The model was supported in the working section and clear streamlines of flow inside the model were observed and photographed for different air flow directions. Fig. 2 show a schematic diagram and photo of the smoke tunnel.

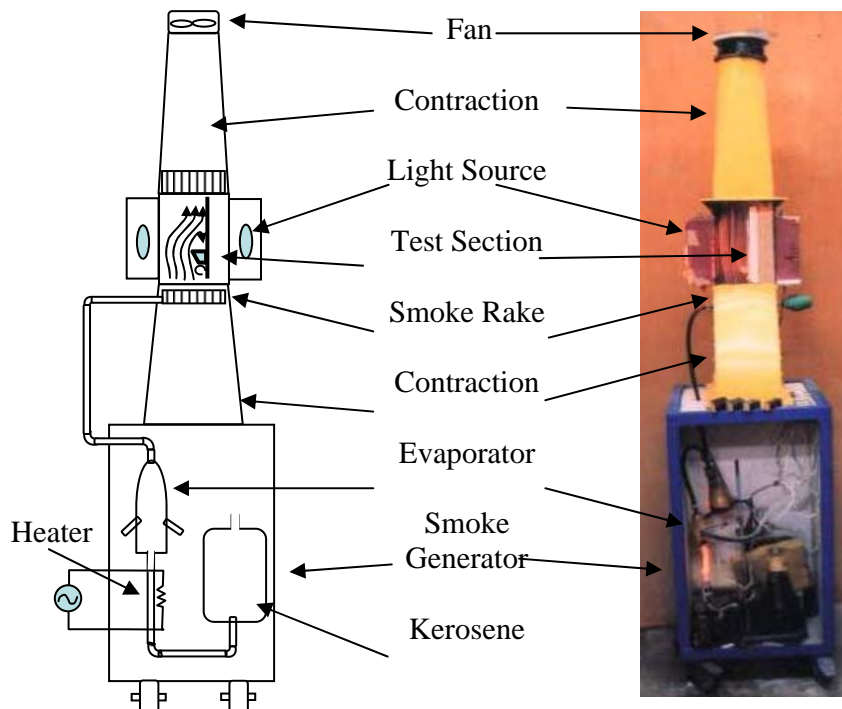


Fig. 2: Smoke Tunnel

Test models:

In order to study the ventilation inside buildings, two test models were constructed to simulate a single flat house. This model consists of 2 bed rooms (BR1&BR2), kitchen (Kt), bath room (BT) and big hall (H) as shown in Figure 3-a. The first test model, was made from plastic sheet (Plexiglass 3mm thick) of dimensions (30 x 33 x 10 cm height) each bedroom contains two adjacent windows. The kitchen and bathroom each contains one window and the hall contains two opposite doors and one window. The ceiling of the model was provided with a heating plate of resistance 160 ohm. The heating plate was constructed as follows a Ni-Cr wire, 0.3mm diameter was wound around a ceramic plate (30 x 33 x 0.05 cm thickness) with a pitch of 5mm sandwiched between two Formica plates. The pitch of winding the wire was small enough to

give a uniform heat flux to the heating plate. A rheostat was used to regulate the power supply to the heater.

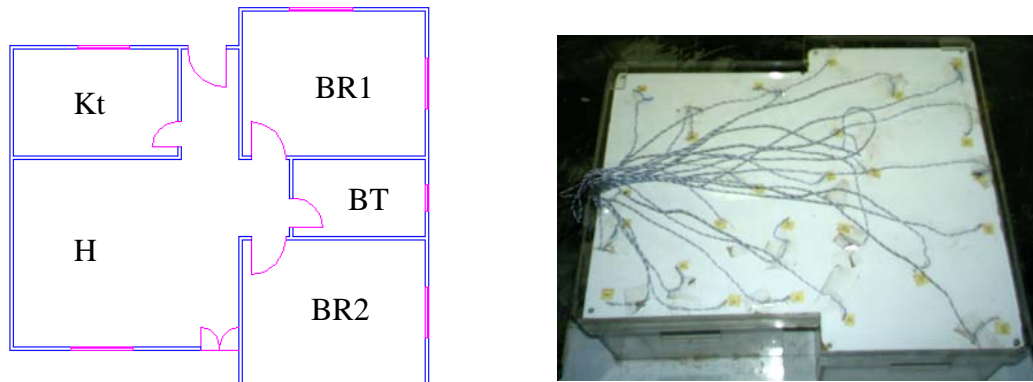


Fig. 3 shows the Test Model and Measuring points.

The thermocouples were mounted on the exterior surface of the heated surface and connected to a data-logger to measure the temperature at different points of the surface. The heating plate was insulated at the top to study the effect of indoor ventilation on the ceiling temperature.

The second test model of dimensions (13.5 x12.5 x 5 cm height) and its base was painted black to see and photograph the visualization of the smoke flow inside it in the smoke tunnel.

To analyze the thermal behavior of the test model under various aerodynamic conditions, thermal measurements were needed. For this purpose, calibrated Cooper-Constantan thermocouples were utilized in conjunction with a data logger. The data logger contains 32 channels; it is used for measuring, plotting and recording any electrical signals, coming from the test models are connected to the data logger who provided with cold junction compensation; the temperature values can be displayed in degree centigrade or degree Fahrenheit.

The experimental work

The experimental work was carried out for two types of tests:

(i) Thermal behavior tests :

For which the model was provided with electric heater at the roof with thermocouples mounted at 25 points for measuring the temperature of each room of the model to be studied in the wind tunnel for different orientation (angle of attack) every 30°.

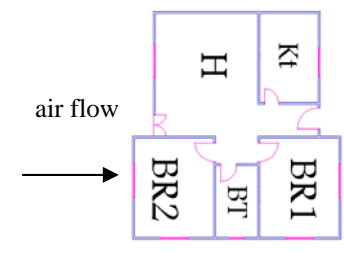
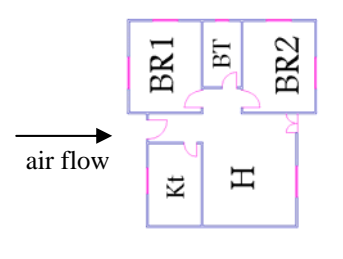
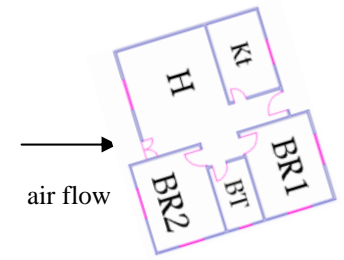
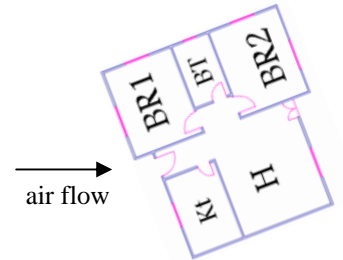
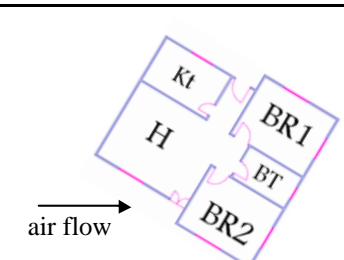
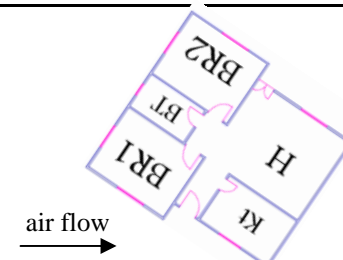
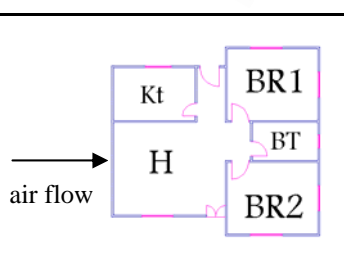
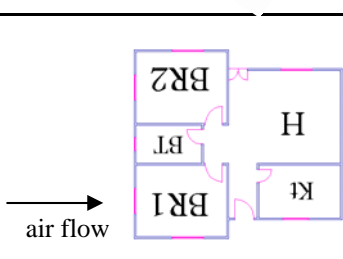
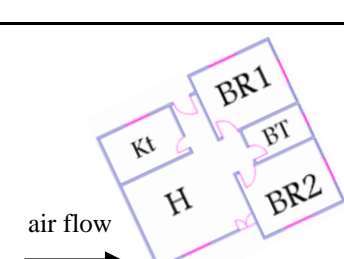
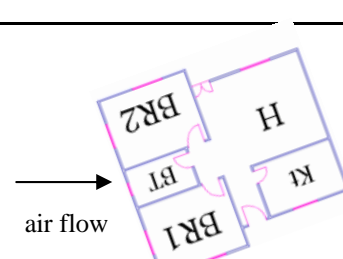
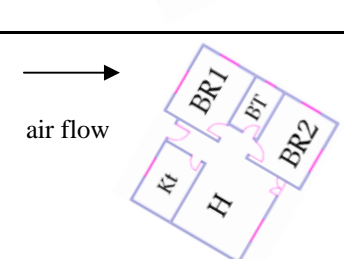
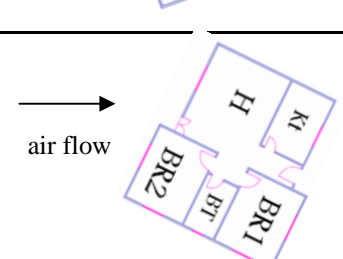
(ii) Flow visualization tests :

In which a smaller size model was tested in the smoke tunnel for a visualized picture of the flow inside the model

THEORITICAL WORK

In the present work an investigation is carried out using a computational fluid dynamics (CFD) computer program ANSYS which is based on the finite element method and solves both flow and thermal fields in any domain to examine the effect of the combinations of inlet and outlet windows on thermal comfort in ventilated space in buildings. A typical model of a building with openings in various combinations was considered for computation under a given thermal load. The results of ANSYS consisted of (i) local velocity inside the ventilated space, which is averaged, (ii) average temperature inside the ventilated space, (iii) local temperature on building walls which are averaged. Table 1 shows the different air flow angles with respect to the main facade for the experimental and theoretical study.

Table 1 : Different Air Flow directions Used For the Experimental & Theoretical Study.

Case No	Angle	Sketch	Case No	Angle	Sketch
1	0°		7	180°	
2	30°		8	210°	
3	60°		9	240°	
4	90°		10	270°	
5	120°		11	300°	
6	150°		12	330°	

RESULTS AND DISCUSSION

Cross ventilation of some spaces is usually needed to allow natural ventilation to take place at night time, with the intention of removing heat gains accumulating through ceiling during day time. Inlet and outlet openings allow air to flow over the exposed ceiling.

The study of the natural ventilation may be done in many forms and shapes, there may be a change in the construction, the position of openings, orientation of the building or material used in insulation and shading to the building.

In this work a study of the effect of natural ventilation inside a one floor building was carried out. Firstly there was an experimental study using a test model with scale 1:30 to be studied in the wind tunnel. This model was studied for different air flow directions (angles) from 0° to 330° with interval 30° as shown in table 1. The plate temperature for different points location (25 points) were measured and the normalizes average temperature for each zone (room) was calculated using the equation;

$$T_{norm} = (T_{avs} - T_{air}) / T_{air} \tag{1}$$

where T_{avs} is the average temperature of the heated plate and T_{air} is the air flow temperature. The convective heat transfer coefficient was calculated using the equation;

$$h = q / (T_s - T_{as}) \tag{2}$$

where, h is the convective heat transfer coefficient (W/m²·°C), T_s : surface temperature, (°C), T_{as} : air temperature adjacent to plate or thin film temperature, (°C).
 , q=heat flux, (W/m²). And is expressed by :

$$q=Q / A = (V^2 / R) / A \tag{3}$$

where;

Q= Heater Power, (watt).

V=power supply voltage, (volt)

R=resistance of the heater, (ohm).

A=model floor (or ceiling) area (m²).

The experimental results were expressed as normalizes average temperature (Tnorm) and normalizes convective heat transfer coefficient (h / h_o) where h_o is the convective heat transfer coefficient in case no wind (i.e. all windows are closed) and were calculated for different Zones (rooms) and air flow direction, the normalized plate temperature were also expressed in surface contours using surfer mapping program.

Before carrying out the heat transfer measurements on the ceiling of the test model, all the model openings were closed and the normalized temperature for each zone was calculated.

The experiments were carried out to move fresh air through one opening at both inlet and outlet.

As shown in Figure 4-a in case no 1, when the angle of attack $\alpha=0^\circ$ and all windows were opened, the normalized temperature was minimum in the bedroom no.2 and the bedroom no.1 also. But it was maximum in the kitchen. These results occurs because the air flow pass directly from bedroom no.2 and entered bedroom no.1 directly and some of it was divided and enter the bathroom and the hall and finally going to the kitchen. The figure show that the variation of normalized heat transfer coefficient h/h_{closed} . In which h_{closed} is the case of no wind or all windows are closed (Bad Case)

As shown in Figure 4-b, when the angle of attack $\alpha=30^\circ$, the normalized temperature was minimum for the bedroom no.2 and the hall and they have a maximum h/h_{closed} . But the other zones have a maximum normalized temperature and a minimum h/h_{closed} .

Figure 4-c, when the angle of attack $\alpha=60^\circ$, show that the same trend as at $\alpha=30^\circ$, was occurred. In Figure 4-d, when the angle of attack $\alpha=90^\circ$, all regions Have nearly the same value of the normalized temperature and h_{av} .

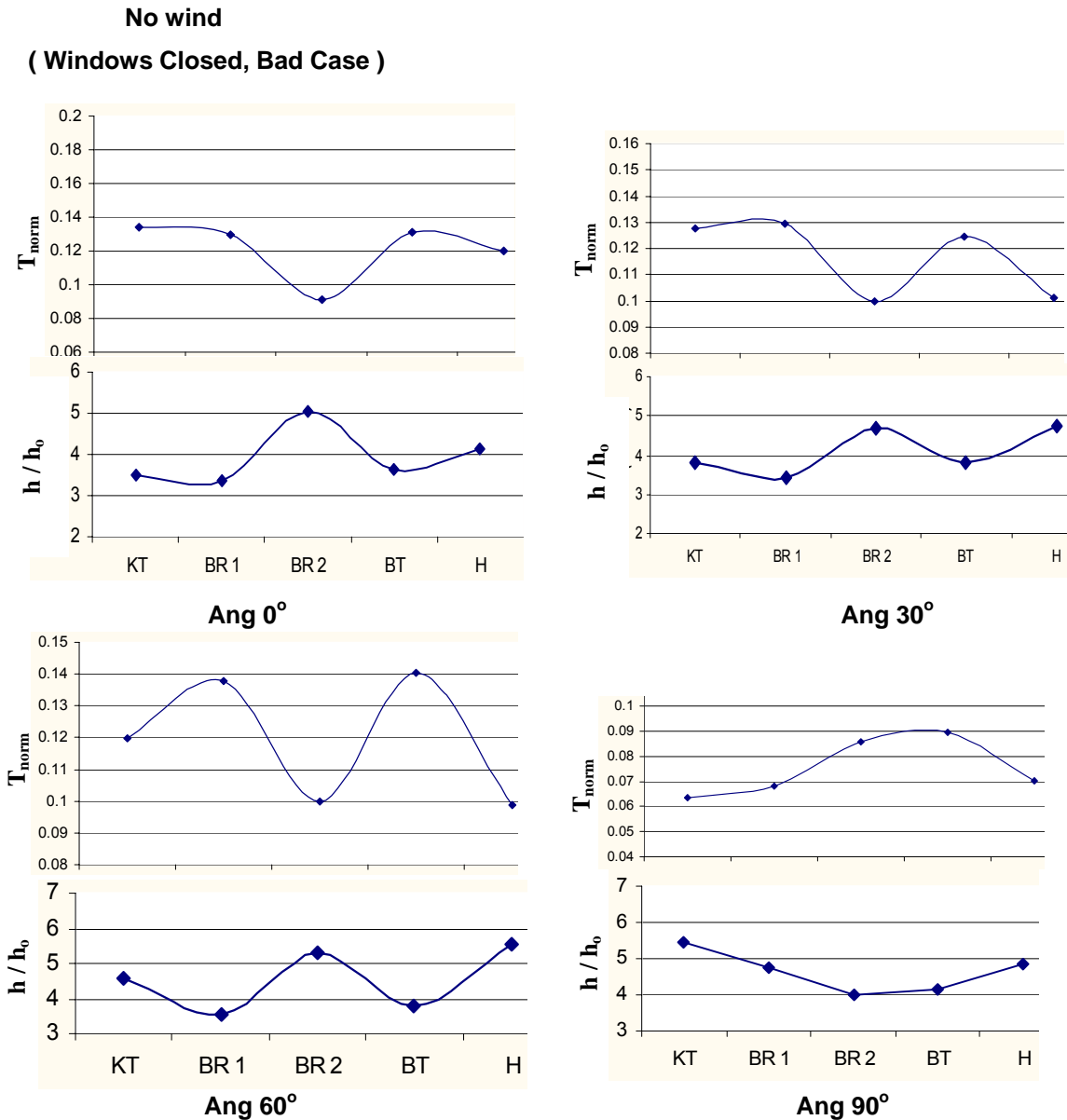


Fig. 4 : Normalized average temperature and convective heat transfer coefficient for the ceiling of different rooms for different air flow directions, (0°, 30°, 60°, 90°)

Figure 5-a shows that, the variation of normalized temperature and h_{av} at $\alpha=120^\circ$. The bedroom no.2 and the bathroom have a maximum normalized temperature and a minimum h_{av} , however, the other flat regions have a minimum normalized temperature and a maximum h_{av} . In Figure 5-b at $\alpha=150^\circ$, the same trend as in the case of $\alpha=120^\circ$, was occurred. At angle $\alpha=180^\circ$, the difference in the zone normalized temperature is very small and the value of h_{av} was closed to each other. As shown in Figure 5-d at $\alpha=210^\circ$, all normalized temperature and h_{av} were increased by 2% for all zone. Figure 6-a shows the effect of the change of the angle of attack to $\alpha=240^\circ$, the bedroom no.2 still have a maximum normalized temperature and a minimum h_{av} . But when the angle become $\alpha=270^\circ$ as shown in Figure 6-b the kitchen and the hall have a maximum normalized temperature and a minimum h_{av} and the other zones have a minimum normalized temperature and a maximum h_{av} . At $\alpha=300^\circ$ as shown in Figure 6-c, the bedroom no.2 has a minimum normalized temperature and a maximum. Finally at $\alpha=330^\circ$ as shown in Figure 6-d, the same trend as in the case of $\alpha=300^\circ$ was occurred.

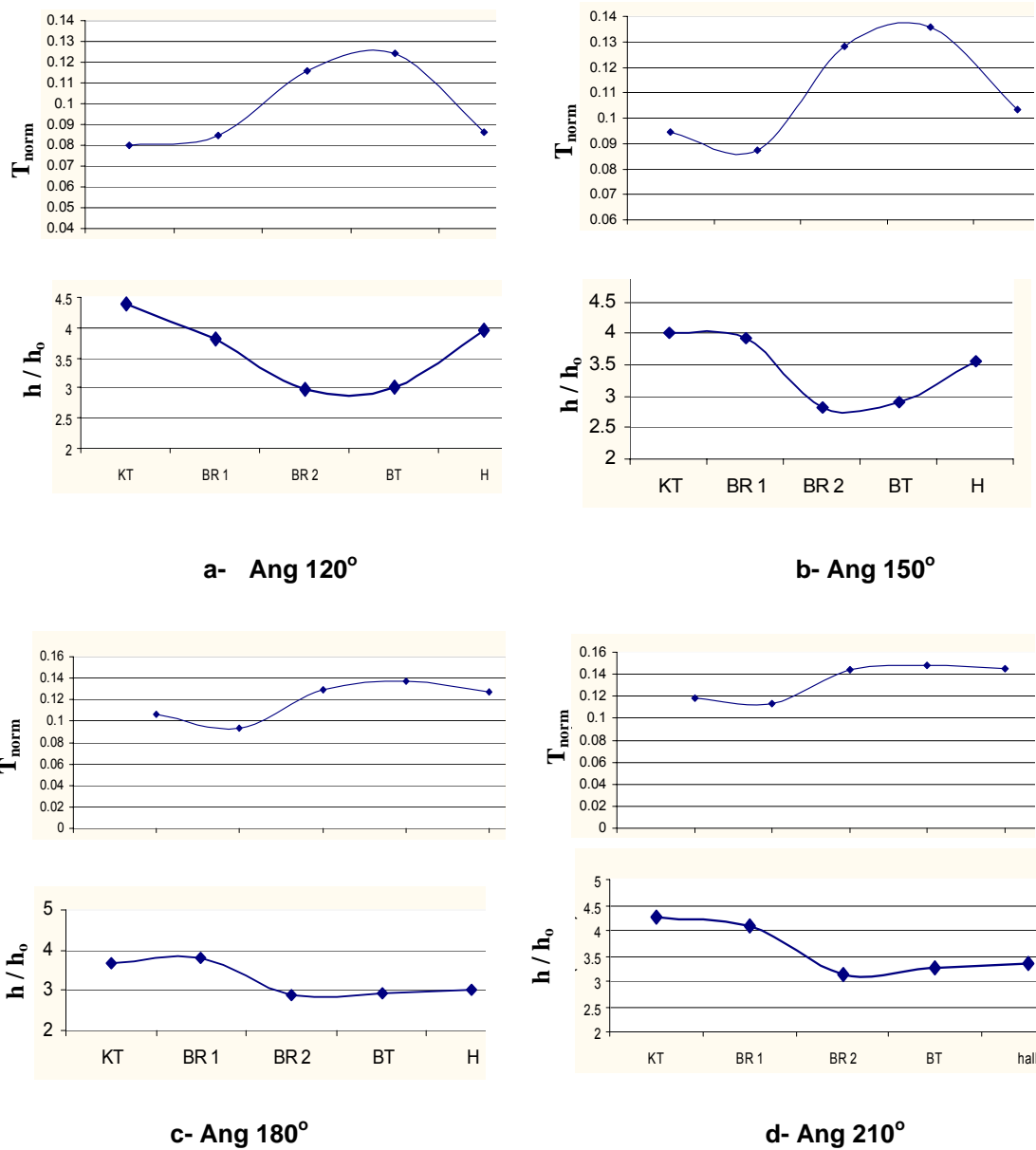


Fig. 5 : Normalized average temperature and convective heat transfer coefficient for the ceiling of different rooms for different air flow directions, (120° , 150° , 180° , 210°)

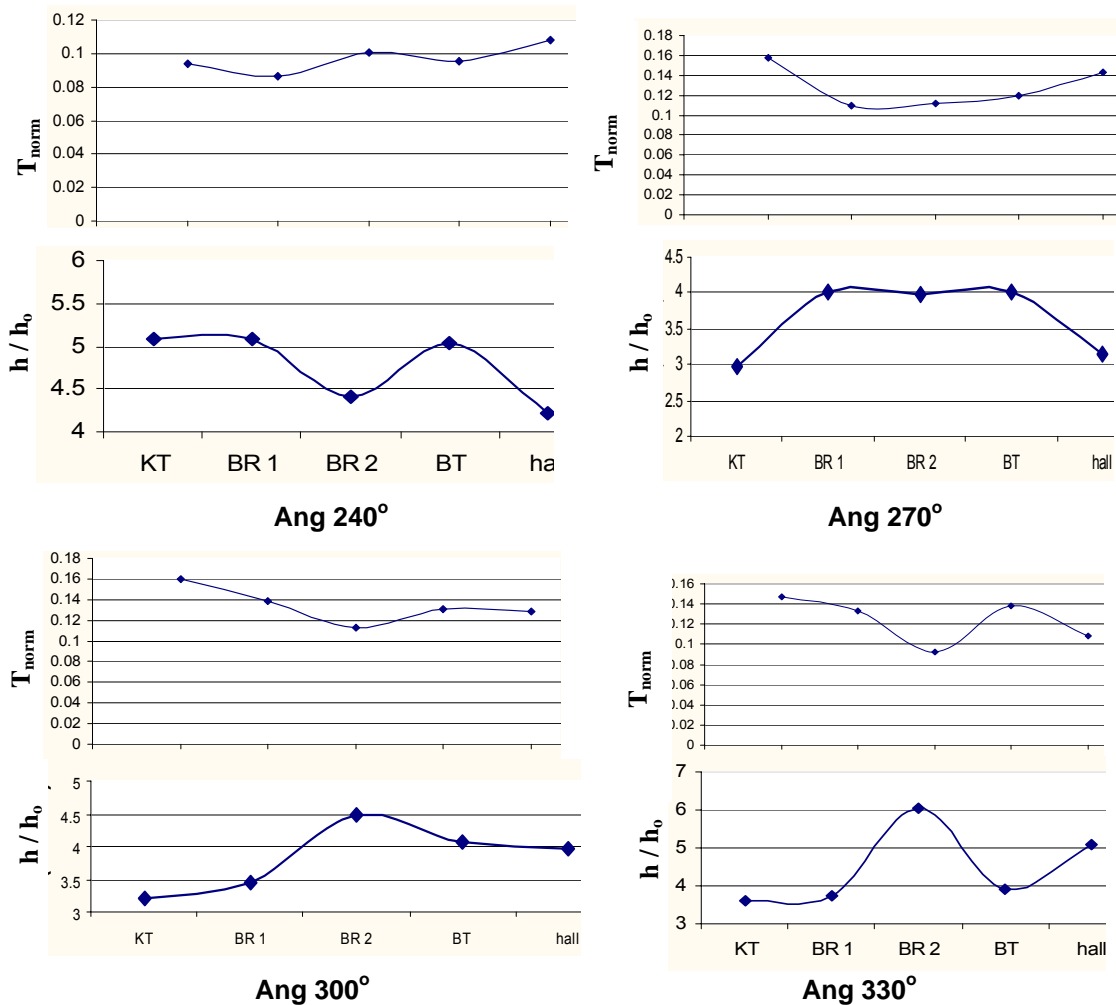


Fig. 6 : Normalized average temperature and convective heat transfer coefficient for the ceiling of different rooms for different air flow directions, (240°, 270°, 300°, 330°)

Figure 7 a-b shows a comparison between the experimental and computed results for air flow and temperature contours for angles $\alpha=0^\circ$, 30° , 60° , and 90° . It can be illustrated that more circulation was occurred and therefore, the temperature inside the room lower than the temperature inside bedroom no.1. also, it could be concluded that sufficient circulation of the flow inside the bathroom and the hall so their temperature is slightly higher than the temperature of bedroom no.2. it can be concluded that, for this position of the building with the prevailing wind the location of the bedroom, the bathroom and the hall were a good ventilated. Figure 7-b when the angle was changed to $\alpha=30^\circ$, it is observed that larger area of the hall and the bedroom no.2 were covered by smoke compared with the other rooms. Also, it was illustrated that the kitchen and bathroom have no chance for a ventilation. Finally it is clear that the ventilation inside the test model was weaker than that at $\alpha=0^\circ$. Figure 7-c show the variation of the flow pattern at $\alpha=60^\circ$, it is shown that there is a good enhancement for the flow pattern inside the kitchen and therefore at this angle the kitchen will be in a good ventilation. At $\alpha=90^\circ$ as shown in Figure 7-d, the flow inside all rooms has low eddies in which the temperature was not removed and the thermal comfort was not achieved meaning bad ventilation was occurred at this angle.

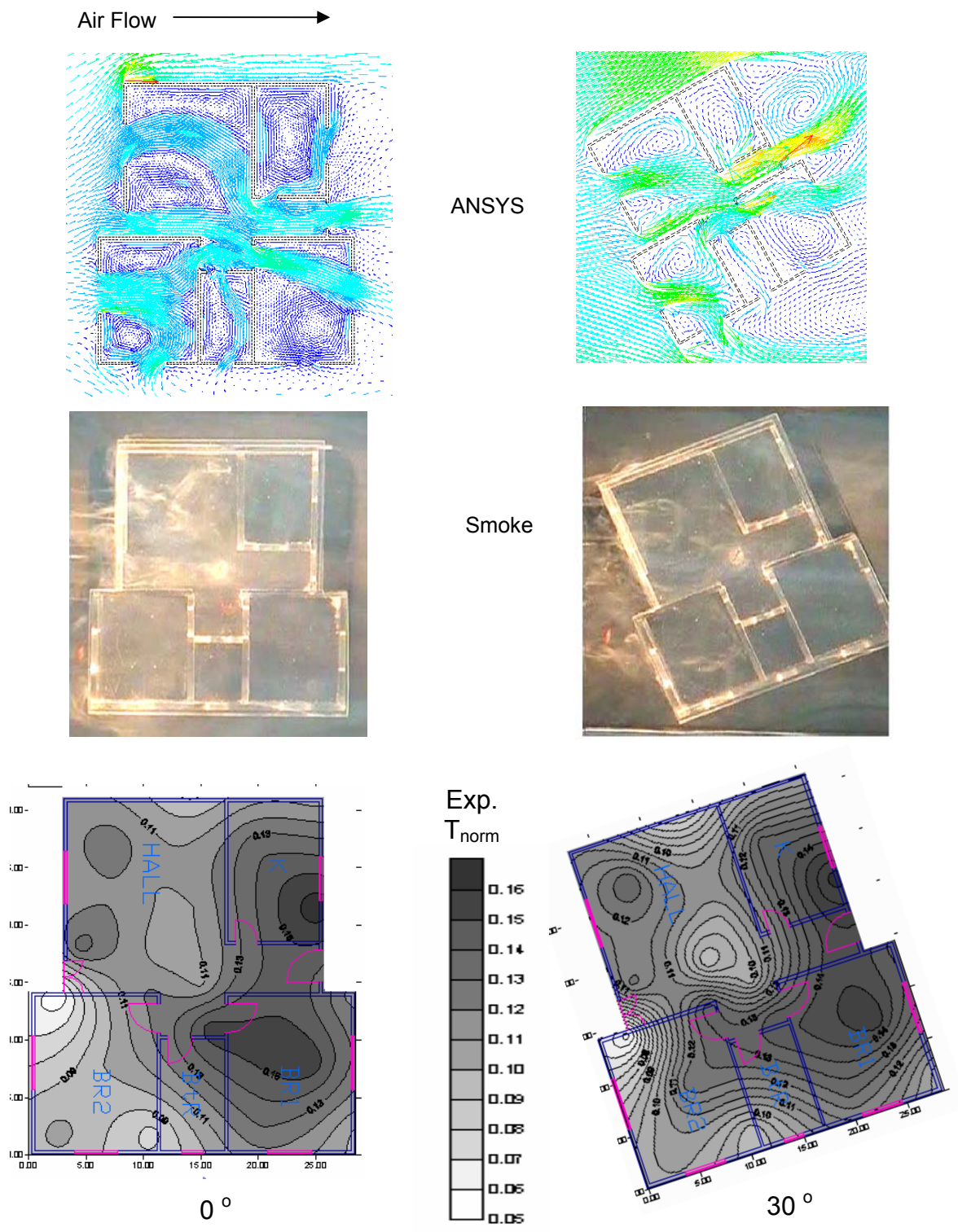


Fig. 7- a : Experimental and computed results for air flow and temperature contours for different air flow angles (0°, 30°)

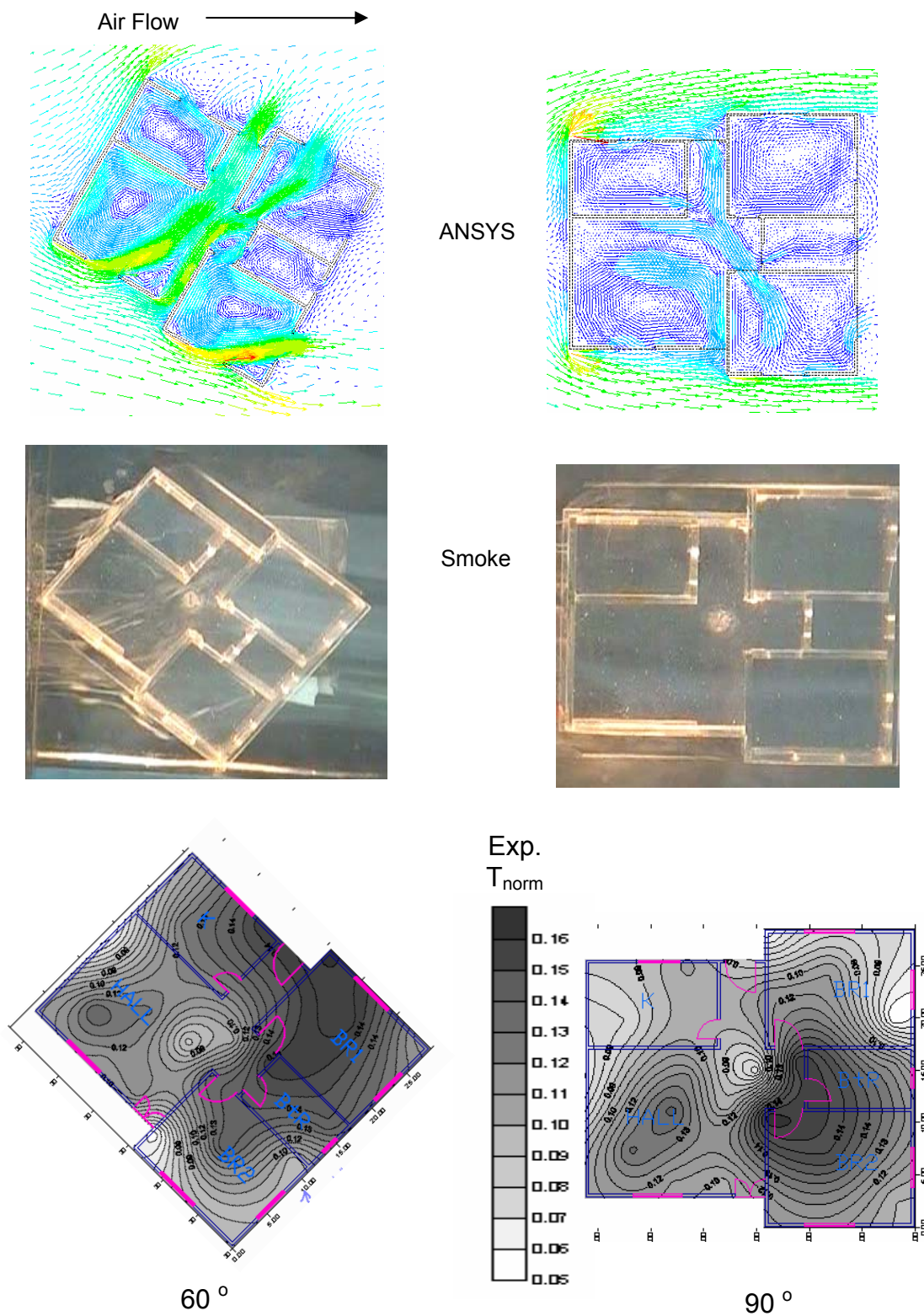


Fig. 7 - b : Experimental and computed results for air flow and temperature contours for different air flow angles (60°, 90°)

Figures 8 - a,b shows a comparison between the visualization results using the smoke tunnel and the computational using the ANSYS CFD with the contours lines from the experimental for angle $\alpha=120^\circ$, it is observed that the flow pattern for the bedroom no.1 and the hall is larger than the flow pattern for the bedroom no.2 and the kitchen. For the bathroom the flow being very small so it is clear that for this situation the bathroom will be bad ventilated. For $\alpha=150^\circ$, it is observed that the same behavior as the case of $\alpha=120^\circ$. For $\alpha=180^\circ$ as shown in Fig. 8-b it can be concluded that, finally the last comparison in the case of $\alpha=210^\circ$ in which the hall, the bedroom no.2 and kitchen have larger flow pattern and more circulation of the smoke than the bedroom no.1 and the bathroom.

Figures 9 - a,b shows a comparison between the visualization results using the smoke tunnel and the computational using the ANSYS CFD with the contours lines from the experimental for angles $\alpha=240^\circ$ to $\alpha=330^\circ$. For the case of $\alpha=240^\circ$, only the bedroom no.1 has a little flow pattern and some circulation and therefore it is bad ventilated in this angle of attack. For angle $\alpha=270^\circ$, all zones have a good ventilation which resulted in the flow pattern and the smoke circulation. At angle $\alpha=300^\circ$ only the kitchen has a little ventilation compared to the other zones which have a good ventilation. Finally, at angle $\alpha=330^\circ$ only the kitchen and the bathroom would be in bad ventilation and the other zones(the two bedrooms and the hall) have good ventilation (low temperature and good air flow).

CONCLUSIONS

- The experimental and computed results show the effect of natural ventilation in reduction of the ceiling temperature which yields to reduction in indoor temperature.
- When the building orientation is located at 270 degree of air flow direction, better flow pattern and heat transfer enhancement from the heated ceiling are observed at bedrooms
- The average ceiling temperature was normalized with the outdoor air temperature. While the heat transfer coefficient was normalized with the heat coefficient transfer at closed case. The trend of curves at these angles have nearly the same pattern, it was noticed that every 90° the temperature distribution had thun C:\WINDOWS\shinhem.scr
-
- same trend.
- The cross ventilation for building orientation at 300 degree angle is desirable in summer.
- It should be easier to give an optional strategy for the building orientation and thus a contribution on improvement in indoor air quality.
- Good visual comparison is obtained from computational results and visualization results.

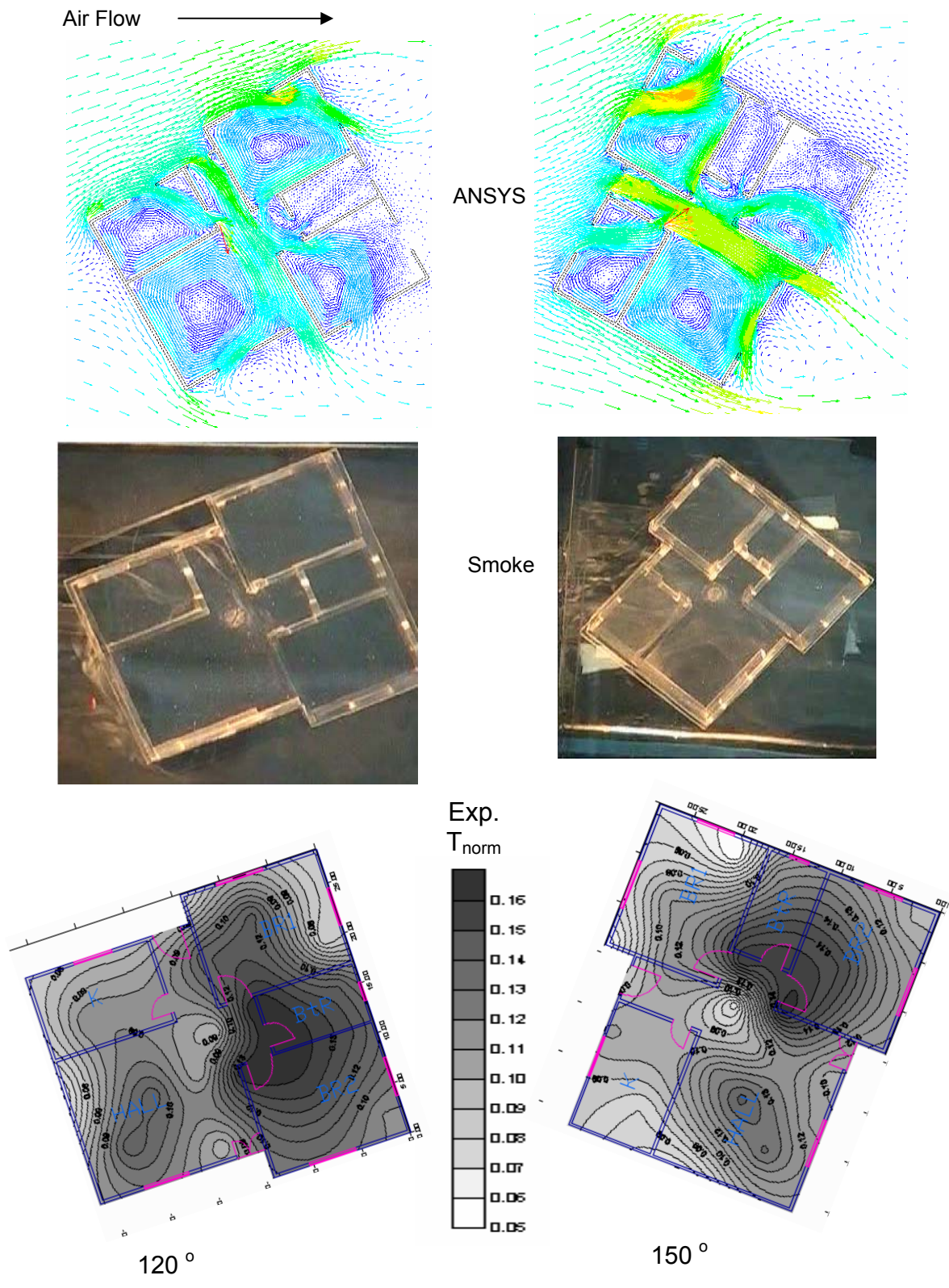


Fig. 8-a : Experimental and computed results for air flow and temperature contours for different air flow angles (120°, 150°)

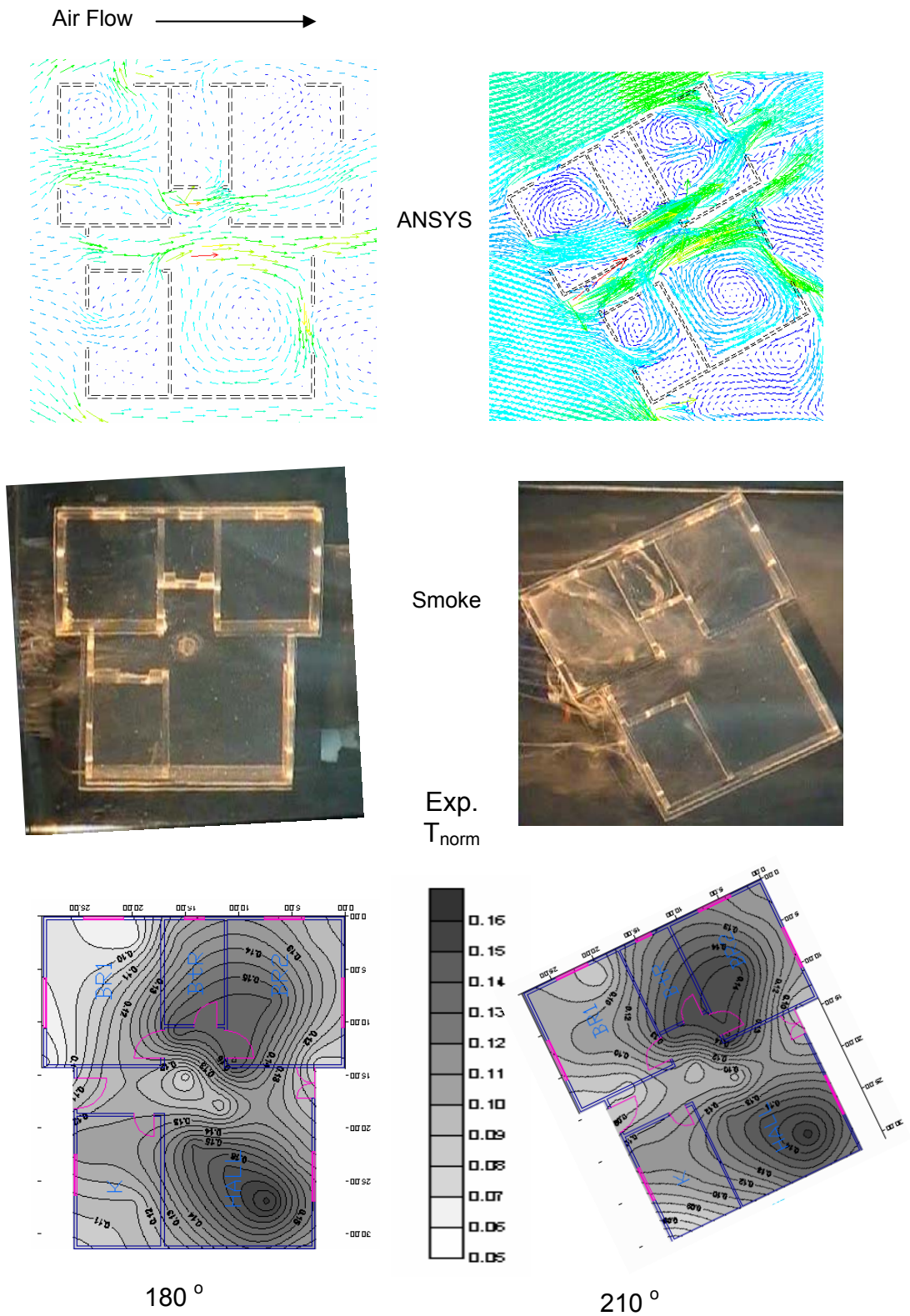


Fig. 8-b : Experimental and computed results for air flow and temperature contours for different air flow angles (180°, 210°)

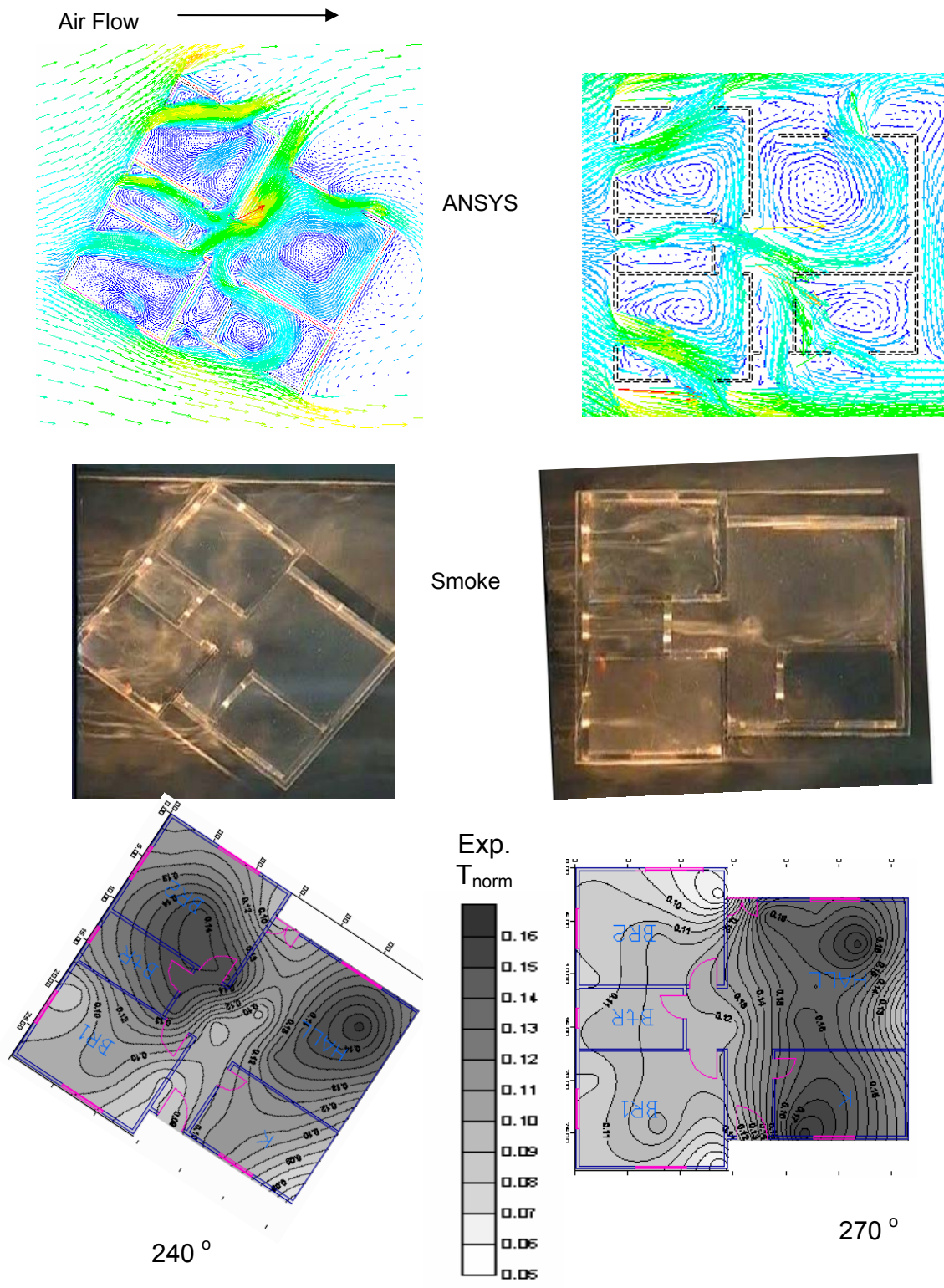


Fig. 9 - a : Experimental and computed results for air flow and temperature contours for different air flow angles (240°, 270°)

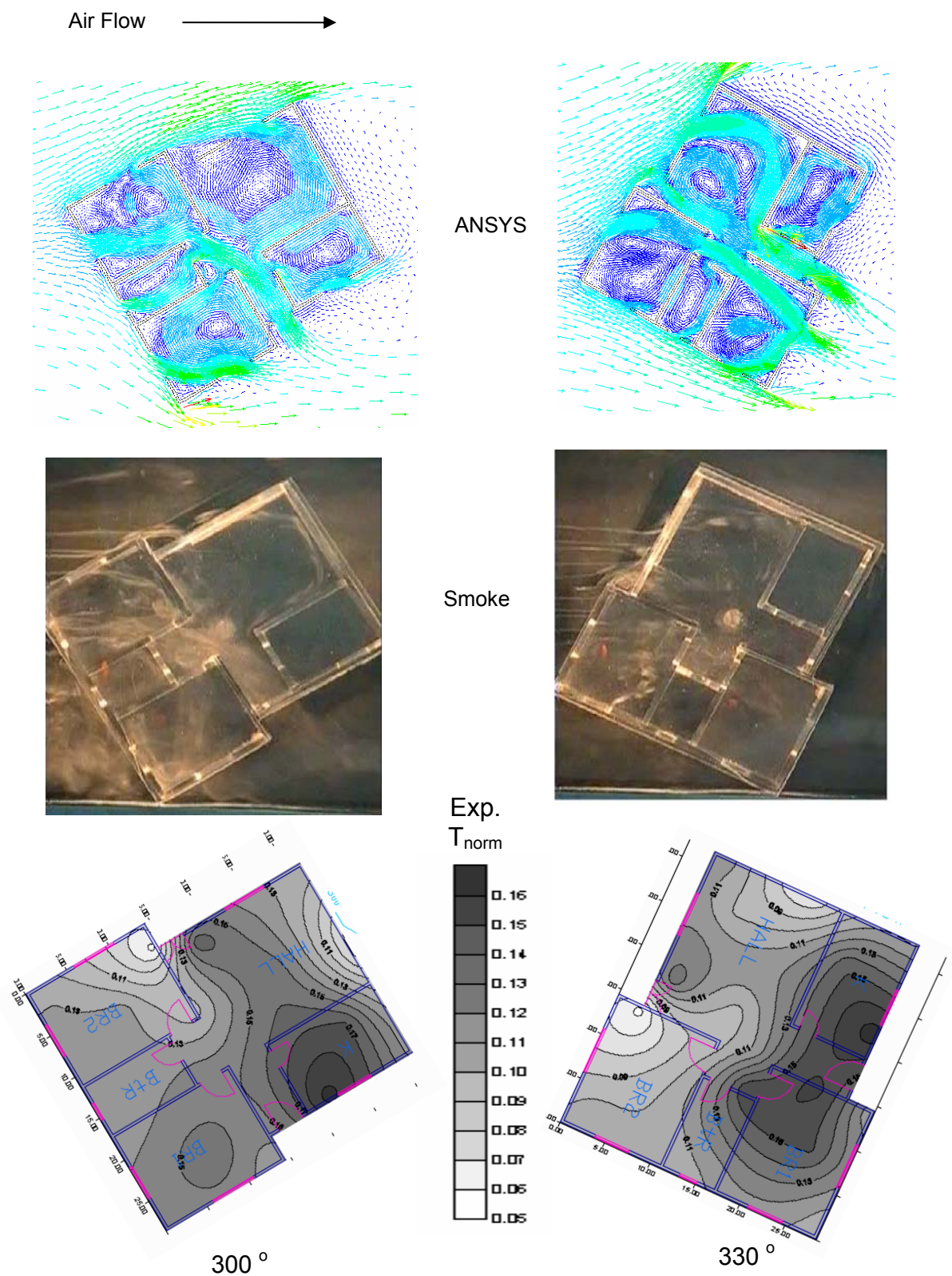


Fig. 9 - b : Experimental and computed results for air flow and temperature contours for different air flow angles (300°, 330°)

REFERENCES

1. Aynsley R. & W. Thain, (2002) " Air Flow for Energy-Efficient Comfort", World Renewable Energy Congress, Germany.
2. Bae N. & Chun C., (2002)," A Study on Acceptable Thermal Comfort Zone and Resident Behavior of Operating Cooling Devices in Apartments" Healthy Building 2006
3. Cettina G., (2002),"ITALY: An Example of Environmental Building Policy; World Renewable Energy Congress, Germany.
4. Colombari, M. , Kragh M., & Zobec M., (2002)" Introduction of Advanced Façade Technology", World Renewable Energy Congress, Germany.
5. Dear R.J. (2006),"adaptive thermal comfort in building management and performance", proceeding of healthy building ,Portugal.
6. Hasselaar E. & Van Ginker J.T., (2006), "how Healthy is the Bed Room", proceeding of healthy building ,Portugal.
7. Medhat A.A. & E. E. Khalil, (2006), " Thermal Comfort Meets Human Acclimatization in Egypt", proceeding of healthy building ,Portugal.
8. Robert O. & Antonios S.,(2006), " Thermal Comfort near Windows Measurements and Computer calculations for an office rooms", proceeding of healthy building ,Portugal.

THE USE OF RICE STRAW FOR MANGANESE ADSORPTION FROM GROUND WATER

Maha. M. El Shafei^{1*}, Ashraf. A. Karakish¹, Ahmed. Abd El Maguid²

1- Associate Professor, Housing & Building National Research Center, Cairo, Egypt

2- Researcher, Housing & Building National Research Center, Cairo, Egypt

ABSTRACT

The increased spread of rice straw burning process in rural areas has added the level of air pollution. Therefore, finding suitable methods for using rice straw rather than burning is considered a national aim.

Several researcher were concerned about the different uses of rice straw, among them was the use of rice straw as an adsorbent material for the removal of metals from water like manganese which is present in ground water.

Manganese is present in high amount in the earth context and that explains its presence in ground water in amounts that exceed the permissible limit for using it as a drinking Water source. These limits were put according to certain considerations related to technical aspects to limit certain problems such as an unacceptable taste, change in color of clothes or the color of water itself or precipitates in water networks and others. Therefore, several methods for iron & manganese removal from ground water were developed.

In this research rice straw was used as an adsorbing material for manganese as substitute for the high cost already used material. Practical application of this method will be considered one of the cheapest ways in construction and operation. The proposed method can be applied in Egyptian villages and societies that depend on ground water containing manganese and don't have the financial abilities or technical experiences in operating and maintenance.

All experiments were done on the laboratory using combined water. Batch analysis method was applied for studying the adsorption process with the control of all the different surrounding circumstances of the experiments. Different sizes and textures of rice straw were used plus applying different methods of rice straw activation.

It was concluded that manganese adsorption process at rice straw surface is affected with the change in temperature, where the higher adsorption level occurred at 25°C temp, it was also found that manganese adsorption efficiency (MAE) increases with the decrease of straw grain size i.e increased smoothers and the best (MAE) occurred at the surface or rice straw activated with NaOH.

Keywords: Rice Straw, Manganese, Adsorption, Activation, Batch, Analysis, Compound Water

INTRODUCTION

Rice husk was selected as a pioneer material in the process of adsorption due to its stable chemical composition, high mechanical force, its particular composition, its insolubility in water and its low cost (1). Many previous researches were interested in using activated and inactivated rice husk as an adsorbent material for removal of pollutants (2-4).

Inactivated rice husk has the ability to bind with heavy metals ions and its removal as mentioned in researches (5-9). Other researches discussed the effect of rice husk activation on the improvement of its adsorption power for metals ions and pollutants (10-13).

* Corresponding author
Received Date:29/7/08
Acceptance Date:20/11/08

Many researches studied a solution for this subject e.g. research (14) which used tartaric acid modified rice husk in removal of Cu and Pb from an aqueous solution contained concentrations from 100 to 400 mg/lit of the two elements and it was found that the amount of removal increased with the increase in mixing and decreased with the increase in the size of the used husk particles and the percentage of removal for lead (Pb) is higher than for copper (Cu). Also, researches (15-19) discussed same subject.

Research (20) showed the ability of rice husk in removing heavy metals such as chromium (Cr) from wastewater. Also, research (21) used green algae and ground rice husk for removal of heavy elements such as manganese (Mn).

Research (22) used rice husk activated with potassium phosphate for removal of (Cd II) from wastewater using columns with continuous flow method also fixed volume method (batch analysis) it was found that columns method achieved higher removal percentage and the amount of removal is effected with the concentration of the solution and its pH, temperature and contact time, it was found that the adsorption process has an endothermic nature.

Research (23) used rice husk in removal of some inorganic elements with low concentrations like cyanide which is highly toxic on men and animal.

Research (24) used inactivated rice husk and potassium hydroxide rice husk for removal of some heavy elements which are (iron, manganese, zinc, copper, cadmium, and lead) with 100% removal for all elements. Research (25) discussed burned rice husk in presence of nitrogen to form active carbon and activated with potassium hydroxide in removal of (Cr V) from a solution of concentration 5-60 mg/lit and pH less than 5 and husk volume 0.8 gm/lit, it was found that there was a great decrease in adsorption amount at pH higher than 5 also the adsorption increases with the increase in temperature, size and volume of the pores. Generally speaking the researches of using rice husk in the adsorption (26) are more than the researches of using rice straw (27).

Research (28) discussed the removal of some toxic heavy metals like (copper, lead, zinc and cadmium) using rice husk and other agricultural wastes (garlic, onion papers, sugar cane and flower petals) applying columns with constant flow method. The removal percentage for copper using agricultural wastes is 80%, using rice husk is 66%, for lead using agricultural wastes is 74%, using rice husk is 91% and for zinc using agricultural wastes is 26%, using rice husk is 56% and for cadmium using agricultural wastes is 71% and using rice husk is 92.5%.

The aims of the research are divided into general and special aims; the general aims are strengthening the use of rice straw as an agricultural waste, protection of environment from pollution resulting from bad methods of removal of rice straw through burning it and also find low cost methods to remove manganese from ground water. While special aims are as follows:

- Studying manganese adsorption at rice straw surface.
- Studying the effect of physical properties of rice straw on the process of manganese adsorption.
- Studying the effect of rice straw activation on the process of manganese adsorption.

MATERIALS & METHODS

All experiments were done on the laboratory using synthetic water in the laboratory. Batch analysis method was applied for study of adsorption process with the control of all the different and surrounding circumstances of the experiment. Different sizes and textures of rice straw were used plus different methods of rice straw activation were applied.

Rice Straw Grain Size

Rice straw was used after being prepared into different sizes as follows:

- Size (A): rice straw was horizontally cut into 2-4 cm using grinder without grinding or vertical cutting of the straw.
- Size (B): rice straw was grounded using sharpening machine to obtain needle shapes of the straws then passed through a strainer 8mm in size. This size is

different than size (A) in the more surface exposure of the internal surface to the adsorption process.

- Size (C): similar to size (A) but was cut into about 0.5-1cm.
- Size (D): in this type rice straw was grounded and prepared in medium coarse pattern and passed through graduated strainers, the straws passed through strainer size 0.16mm were used.
- Size (E): rice straw was grounded into high degree of softness and passed through a strainer size 0.16mm.

Figures (1- 5) show types of rice straw used in the experiments.

Rice Straw Washing

Rice straw was prepared into two different ways:

- The first way rice straw was prepared and cut as in the previous paragraph but without washing.
- The second way rice straw was washed after cutting it, washing was done using distilled water through submerging rice straw in distilled water for 60 min. then water was removed and changed with another amount of water enough for submerging the straw.

This process was repeated several times until the yellow color resulting from the washing process was completely removed.

This is followed by dryness process in a drying oven over a metallic surface for 24 hrs in 105 c temperature, after that rice straw is kept in a closed place until being used in the experiment.

Rice Straw Activation

Rice straw was chemically activated following the steps of previous researches. The activation was done using tartaric acid (14) and sodium hydroxide (24) with the addition of acetic acid due to its cheap price although it has never been used before.

The activation was done on prepared rice straw type (D) and all the experiments were done on it. Different degrees of the activation process were applied with the use of solutions with different concentrations and different volumes in relation to the activated rice straw volume. In all cases the activation was done by submerging rice husk in a solution of all the chemicals used with certain volume and certain concentration, it was left for 24 hrs then washed with distilled water by submerging it for several times with measuring of the pH of washing water until the pH reached value 7. This was followed by dryness at 50°C temperature for enough time, while for tartaric acid and acetic acid rice straw was dried at 180°C temperature for 10 min after drying at 50°C temperature. (Tables 1, 2, and 3 show different degrees of activation using NaOH, tartaric acid and acetic acid).

Used Water

Solutions with different concentrations of manganese ion and manganese salts were used as a source of manganese ions. This was after their solubility with different volumes in distilled water in order to obtain different concentrations.

Laboratory Experiments

1.00 lit capacity glass bottles were used to perform the batch analysis with the addition of 1000ml manganese solution to the glass bottles with the required concentration, and then rice straw was added to start the experiment. The bottles were put on a mixing surface with changing speed inside an incubator to stabilize the temperature at the required temperature for the experiment. A control sample was used in all the experiments to know the different effects on the experiment and this was after the addition of rice straw to the sample.

All the experiments were done at about 10mg/lit concentration of manganese.



Fig. 1: Rice Straw Size A



Fig. 2: Rice Straw Size B



Fig. 3: Rice Straw Size C



Fig. 4: Rice Straw Size D



Fig. 5: Rice Straw Size E

Table (1): Degrees of Rice Straw Activation Using NaOH (1)

Degree of activation	straw weight (gm)	Solution volume (ml)	Solution concentration (mol)
A	50	1000	0.02
B	50	1000	0.01
C	50	1000	0.05
D	50	300	0.01
E	50	500	0.01
F	50	1500	0.01

Table (2): Degrees of Rice Straw Activation Using Tartaric Acid (2)

Degree of activation	straw weight (gm)	Solution volume (ml)	Solution concentration (mol)
A	50	1000	0.6
B	50	1000	1.2
C	50	1000	2.2
D	50	300	1.2
E	50	500	1.2
F	50	500	1.2

Table (3): Degrees of Rice Straw Activation Using Acetic Acid (3)

Degree of activation	straw weight (gm)	Solution volume (ml)	Solution concentration (mol)
A	50	1000	0.1
B	50	1000	0.3
C	50	1000	0.6
D	50	1000	1.2
E	50	1000	2.2
F	50	300	1.2
G	50	500	1.2
H	50	1500	1.2

Analysis

An analysis to manganese concentration in experimental water was carried out following the laboratorial plan using colorimetric method by using spectrometer model Cecilce 3021 using ready made chemicals from Hanna HI 93709.

Research Parameters

The experiments were carried out under different circumstances to study the adsorption process as follows:

Straw Weight: The experiments were carried out with straw weights 2, 5, 10 and 20 gm

Temperature: The experiments were carried out at temperatures 10, 25, and 40°C

Mixing Speed: The experiments were carried out at mixing speeds 50, 100, and 200 rpm

pH: The experiments were done at pH values 3, 7, and 9

Activation degrees: The experiments were carried out at the previously mentioned activation degrees (A, B, C, D, E, and F) for all different chemicals.

RESULTS

The experiments were carried out following a research plan and its results according to research parameters were as follows:

Results at Different Straw Weights

Figure no (6) shows residual manganese concentration at different straw weights and this was for washed, as received and types (1, 2, and 3) husk. The results showed that about 90% Of the adsorption process happened in the first 5 min, from the figure we find that the amount of adsorbed manganese increased with the increase of straw weight and it kept on increasing sharply until 10 gm straw weight then it greatly decreased at 20 gm straw weight, and this was for 1 lit manganese solution. The average removal percentage for manganese was 60% at 2gm straw weight, and 75% at 5gm straw weight, and 88% at 10gm and 20gm straw weight.

Results at Different Temperatures

Figure no (7) shows manganese concentration at different temperatures (10°C, 25°C, and 40°C) and this was for washed, as received and types (1, 2, and 3), the results showed decrease in manganese adsorption efficiency at 10°C temperature more than at 25°C temperature and 40°C temperature and this was for activated rice straw. The adsorption efficiency decreased to a lower extent at 40°C temperature for washed and as received rice straw, the efficiency at 10°C temperature was not clearly influenced compared to it at 25°C temperature. The efficiency greatly decreased at 40°C temperature. In the two cases the greatest efficiency occurred at temperature 25°C.

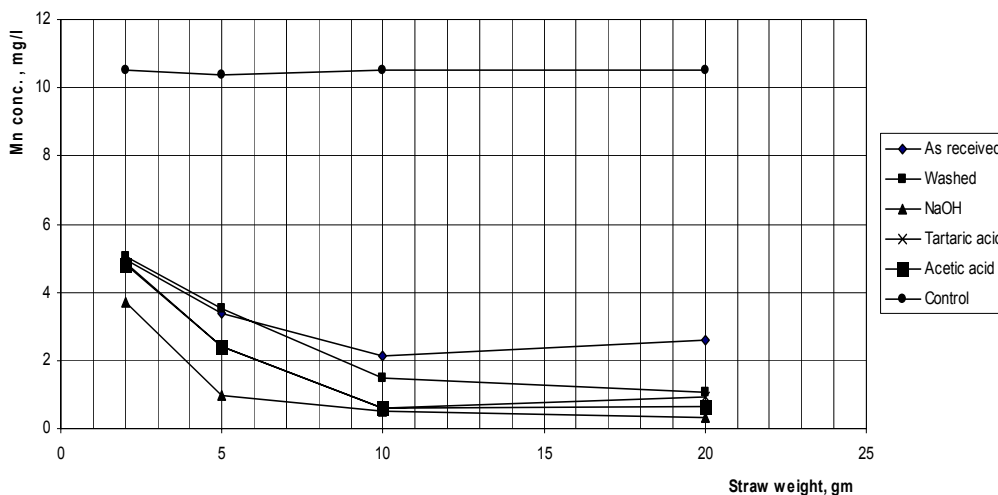


Fig.6: Manganese Concentration at Different Straw Weights

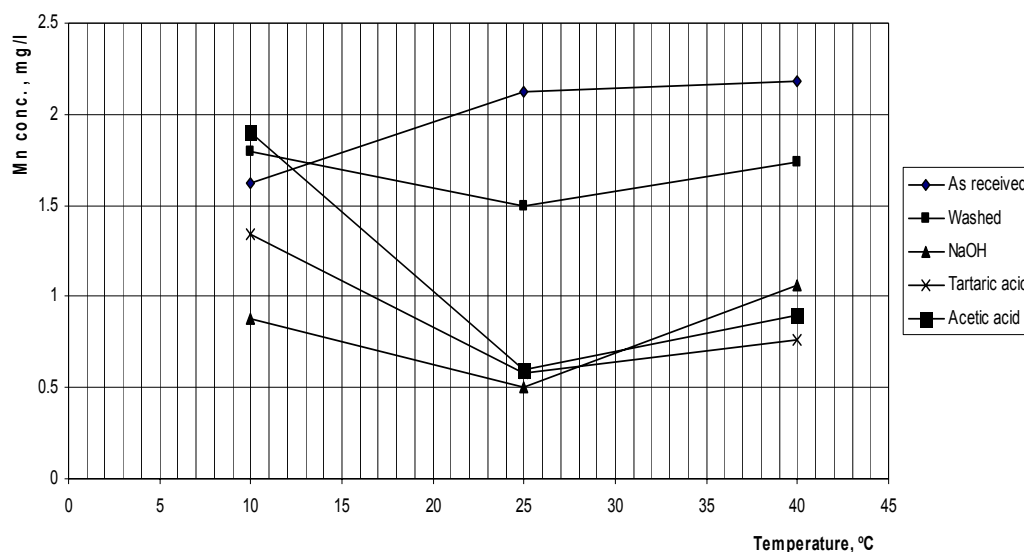


Fig.7: Manganese Concentration at Different Temperatures (10°C, 25°C, and 40°C)

Results at Different Mixing Speeds

Figure no (8) shows manganese concentration at different mixing speeds (50, 200, and 100 rpm) and this was for washed, as received and types (1, 2, and 3), the results showed remarkable decrease in manganese adsorption efficiency at mixing speed 200 rpm more than at mixing speed 100 rpm also the adsorption efficiency at mixing speed 50 rpm was decreased more than at 100 rpm but to a lesser extent.

Results at different pH

Figure no (9) shows manganese concentration at different pH values (3, 7, and 9) and this was for washed, as received and types (1, 2, and 3), the results showed decrease in manganese adsorption efficiency at pH value 3 to a higher extent than at pH value 7, and the adsorption process was slightly affected when raising the pH value to 9.

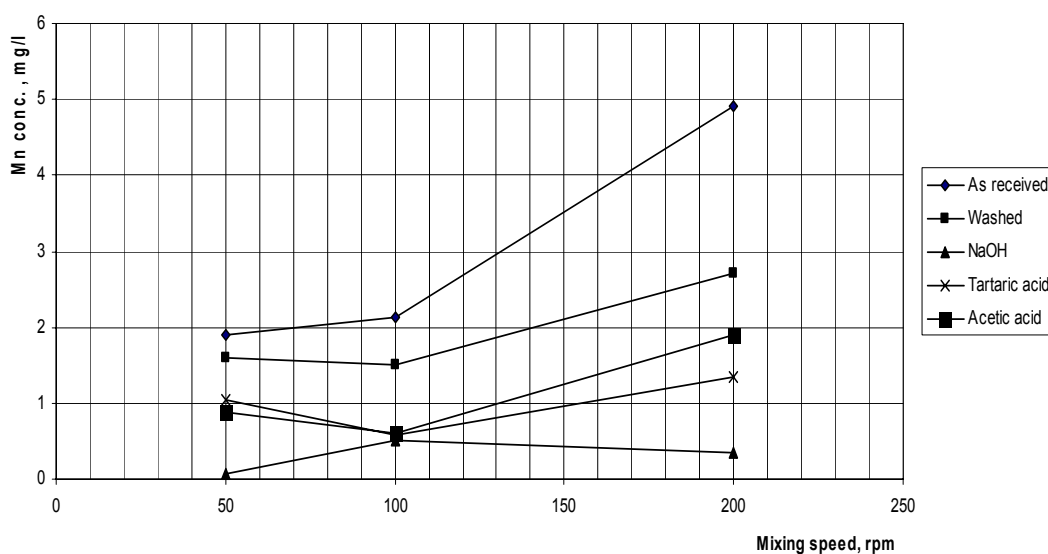


Fig. 8: Manganese Concentration at Different Mixing Speeds (50, 200, and 100 rpm)

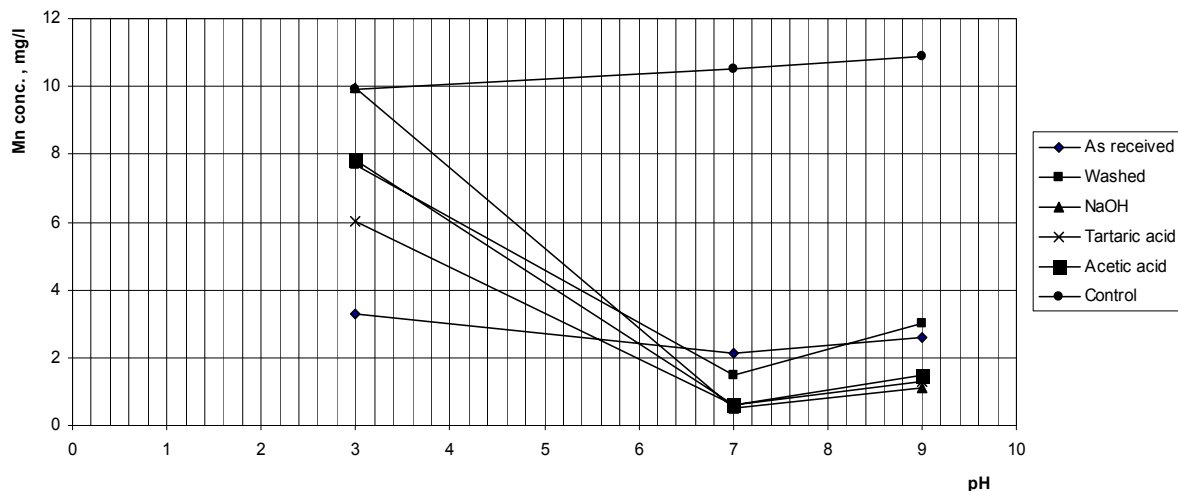


Fig. 9: Manganese Concentration at Different Ph Values (3, 7, and 9)

Results at Different Straws Grain Sizes

Figure no (10) shows manganese concentration at different staying times and that for different straw grain sizes (A, B, C, D, and E) and the figure shows manganese concentration at different straw grain sizes. The results showed that size H gave higher efficiency in manganese adsorption and it's the smoothest straw size. The efficiency decreased in husk size B, D, and A and the most decrease was at size C. In all cases the efficiency of adsorption process is affected by the smoothness of the straw grain size, the efficiency increases with the increase in smoothness and vice versa although with the previous results, this result is not of a great value.

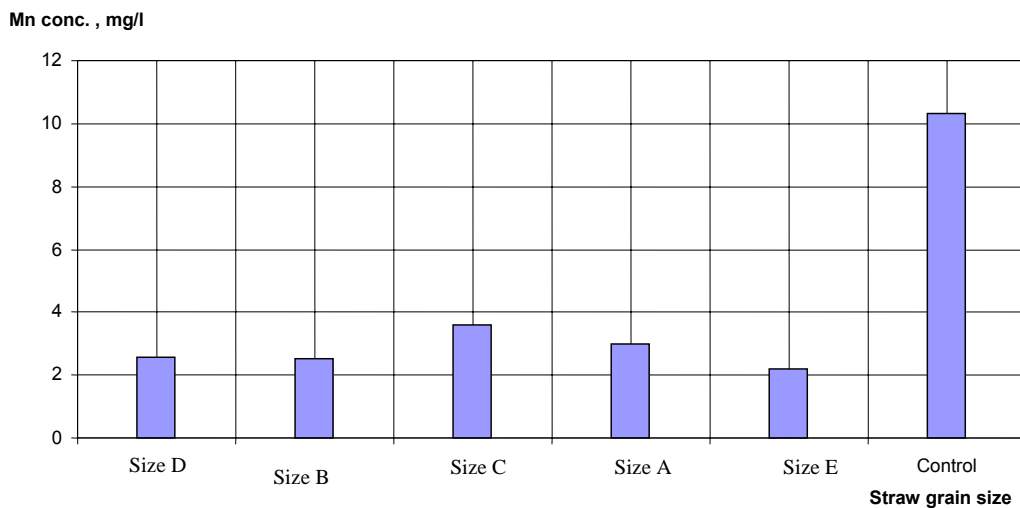


Fig.10: Manganese Concentration at Different Straw Grain Sizes

Results at Different Activation Degrees

It was previously mentioned that the activation process was studied using two different operating conditions which were the volume of the used chemicals solution in activation and its concentration.

The Effect of Solution Volume

Figures 11, 12, and 13 show manganese concentration at different solution volumes for each of NaOH, tartaric acid and acetic acid, from the results we found that for NaOH solution the highest efficiency occurred at 1 lit solution volume for every 20 mg of straw weight and that agrees with previous researches (14) at that field, regarding tartaric acid solution was directly proportional with the increase in the used solution volume and it reached at greatest volume used which was 1.5 lit, and for acetic acid the efficiency was also directly proportional with increase in the volume of the solution but with descending increase and that appeared from lines slopes in demonstrating figures.

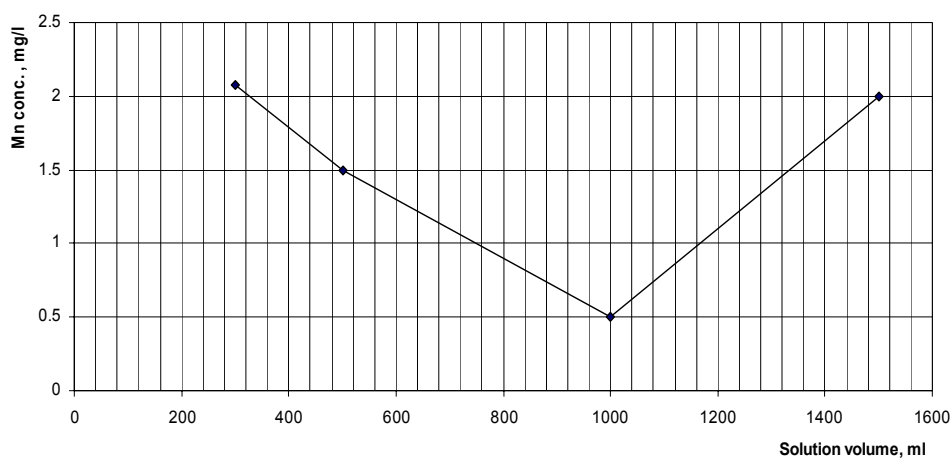


Fig. 11: Manganese Concentration at Different Solution Volumes for Each of NaOH

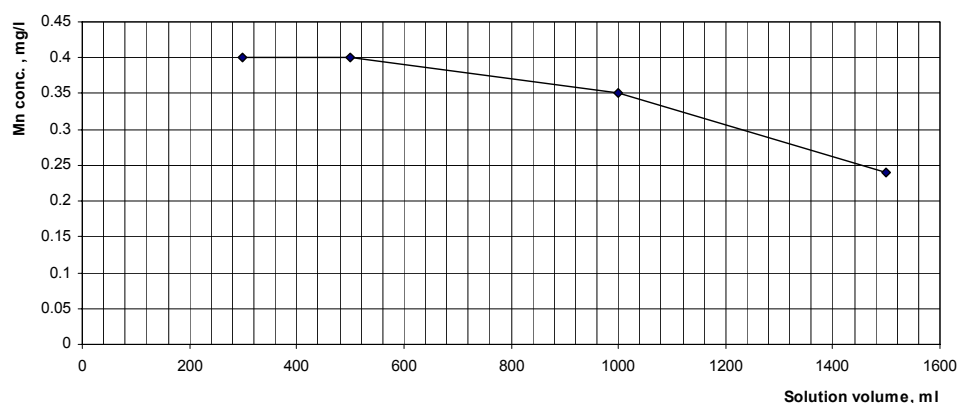


Fig. 12: Manganese Concentration at Different Solution Volumes for Each of Tartaric Acid

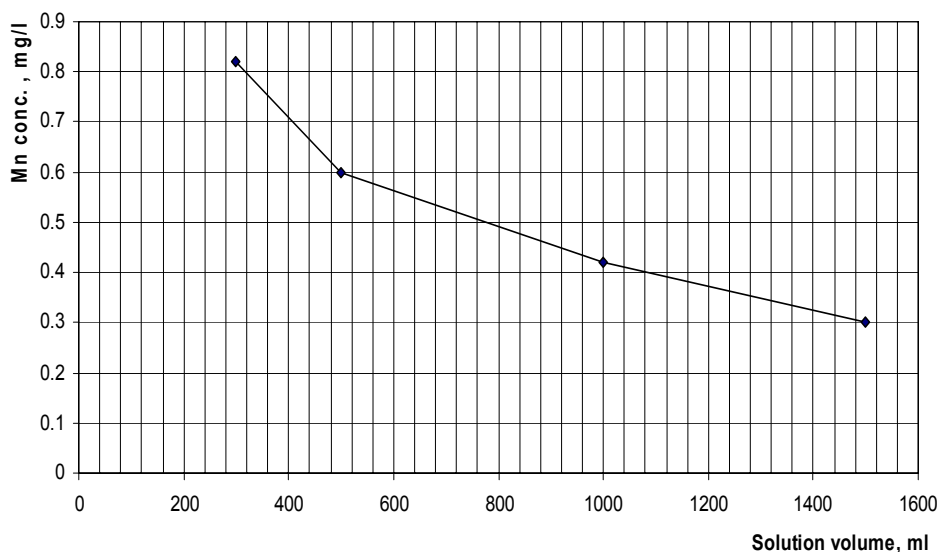


Fig. 13: Manganese Concentration at Different Solution Volumes for Each of Acetic Acid

The Effect of Solution Concentration

Figures (14, 15, and 16) show manganese concentration at different solution concentrations for each of the used three chemicals. From the results we found that for NaOH the highest efficiency found occurred at 0.1 mol concentration, and for tartaric acid the efficiency was decreased with the increase in concentration from 0.6 mol to 1.2 mol then it stayed constant with the increase to 2.2 mol and this goes with the behavior of efficiency with the increase in solution volume that reflects the increase in efficiency with the decrease in the amount of acid to straw percentage. For acetic acid the efficiency decreased with the increase in solution concentration and the efficiency increased with the increase in solution volume and that means increase in efficiency with the decrease in the amount of acid to straw percentage.

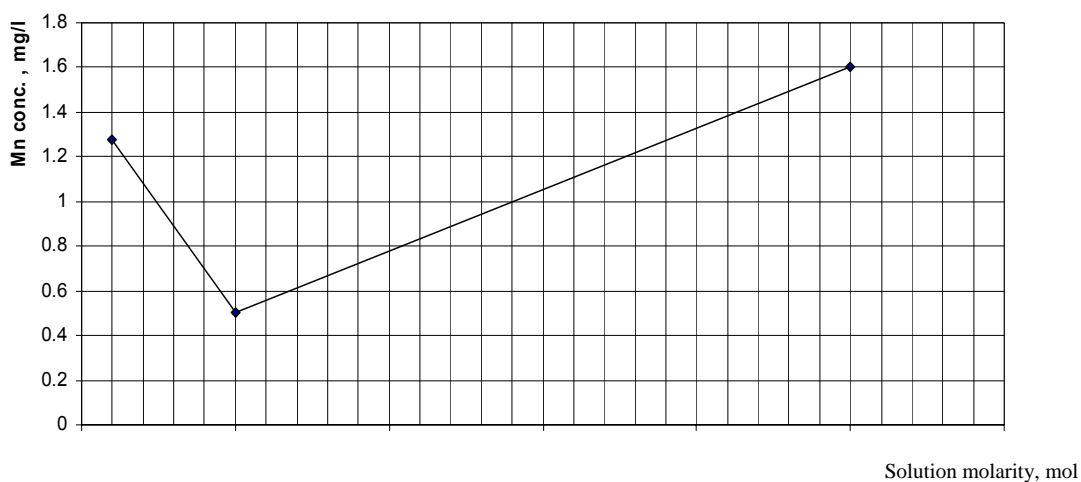


Fig. 14: Manganese Concentration at Different Solution NaOH Concentration

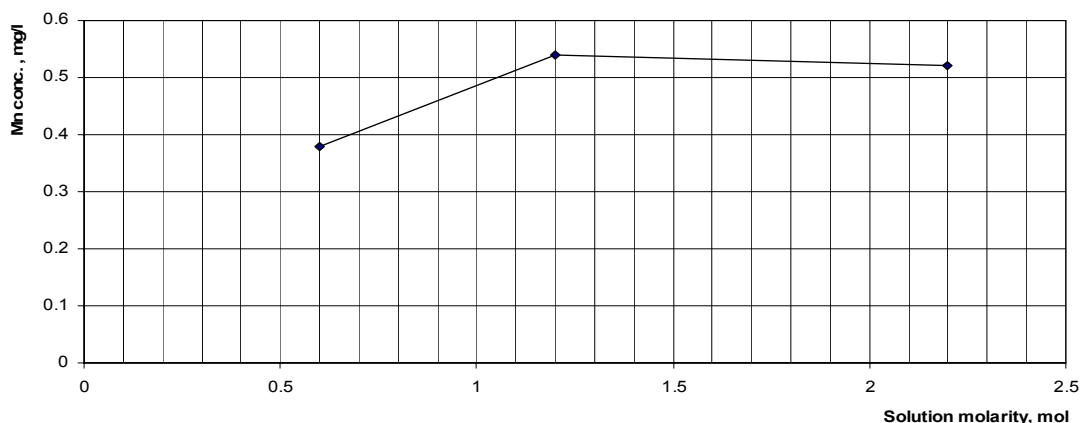


Fig. 15: Manganese Concentration at Different Solution Tartaric Acid Concentration

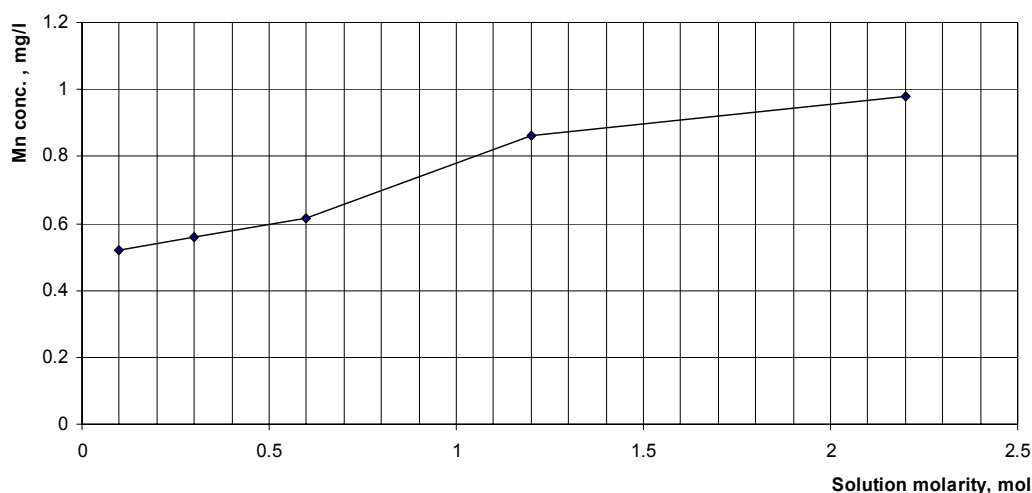


Fig.16: Manganese Concentration at Different Solution Acetic Acid Concentration

CONCLUSION

The amount of adsorbed manganese at rice straw surface increases with the increase in straw weight added to the solution, the percentage removal was 80% from the manganese concentration at the beginning of the experiment at 10gm straw weight at manganese concentration 10mg/lit.

Manganese adsorption process at rice straw is affected with the change in temperature where it decreased at 10° c and 40° c temperatures more than at 25° c temperatures at which the highest adsorption efficiency occurred.

Manganese adsorption efficiency greatly decreases with the increase in mixing speed and the most efficiency is at mixing speeds 100 and 50 rpm where the efficiency is not greatly different between these two speeds.

Manganese adsorption efficiency greatly decreases at acidic media at pH value 3 more than at pH value 7, and it weakly decreases at pH value 9 more than at pH value 7.

Manganese adsorption efficiency increases with decrease in straw grain size i.e. increased smoothness and vice versa, although this effect is not of great influence; therefore only the economical studies can determine the straw grain size of the straw to be used.

The best adsorption efficiency for manganese at the surface of straw activated with NaOH occurred at 1 lit solution volume and 0.1 mol concentration, and for straw activated with tartaric acid and acetic acid the efficiency increased with the increase in the volume of the solution used in the activation and the decrease in the acid concentration to the limit of the value used in the research.

REFERENCES

1. El-Azab, A.M.M., Ph.D. thesis, (1992), Cairo University.
2. Upendra, K. and Manas B. (2006) "Sorption of cadmium from aqueous solution using pretreated rice husk". *Bioresource Technology* 97 : pp.104:109.
3. Dadhlich, A.S. , Beebi, S.K. and Kavitha, G.V., (2004) " Adsorption of Ni(II) using agro waste, rice husk", *J. Environ. Sci. Eng.*, 46, PP, 179–185.
4. Narsi R.B., Mini B., Nivedita S. and Asha G., (2004), "Adsorption of Cr(VI) on activated rice husk carbon and activated alumina", *Bio-resource Technology*, pp.305–307.
5. Marshall, W.E., Champagne, E.T., Evans, J.E., (1993), "Use of rice milling by- product (hulls and bran) to remove metal ions from aqueous solution", *J. Environ. Sci. Health A* 28 (9), PP 1977 – 1992.
6. Singh , K.K. , Rastogi , R. and Hasan, S.H. (2005) , "Removal of Cr(VI) from wastewater using rice bran". *Journal of Colloid and Interface Science* 290 : pp.61:68.
7. Singh , K.K. , Rastogi , R. and Hasan, S.H., (2005) "Removal of cadmium from wastewater using agricultural waste 'rice polish'". *Journal of Hazardous Materials A* 121 : pp.51:58.
8. A.S. Dadhlich, S.K. Beebi, G.V. Kavitha, Adsorption of Ni(II) using agro waste, rice husk, *J. Environ. Sci. Eng.* 46 (2004) 179–185.
9. D. Roy, P.N. Greenlaw, B.S. Shane, Adsorption of heavy metals by green algae and ground rice hulls, *J. Environ. Sci. Health A* 28 (1993) 37–50.
10. Suemitsu, R. Uenishi, R., Akashi, I., Nakanom, M., "The Use of dyestuff – treated rice hulls for removal of heavy metal from wastewater", (1986), *J. Appl. Polym. Sci.* 31 (1) 75 – 83.
11. Lee, C.K., Low, K.S., Mah, S.J., "Removal of a gold (III) complex quaternized rice husk", (1998), *Adv. Environ. Res.* 2 (3) 351- 359.
12. Low, K.S, Lee, C.K., "Quaternized rice husk as sorbent for reactive dyes", (1997), *Biores. Technol.* 61 (2) 121 – 125.
13. Upendra, K. and Manas B. (2006) "Sorption of cadmium from aqueous solution using pretreated rice husk". *Bioresource Technology* 97 : pp.104:109.
14. Wog, K.K., Lee, C.K, Low, K.S, Haron, M. J., "Removal of Cu and Pb by tartaric acid modified rice Husk from aqueous solutions", (2003), *Chemo Sphere* 50 (23 – 28).
15. Gupta, V.K., Mittal, A., Jain, R., Mathur, M., Sarwar, S., 2006b. Adsorption of Safranin-T from wastewater using waste materials activated Carbon and activated rice husks. *J. Colloid Interf. Sci.* 303 80–86.
16. S. Kumagai, Y. Noguchi, Y. Kurimoto, K. Takeda, Oil adsorbent produced by the carbonization of rice husks, *Waste Manage.* 27 (2007) 554–561
17. S. Kumagai, K. Ikawa, K. Takeda, Ammonia gas adsorption by carbonized rice husk, *Int. J. Mater. Eng. Resour.* 13 (2006) 92–95.
18. D.H. Lataye, I.M. Mishra, I.D. Mall , Pyridine sorption from aqueous solution by rice husk ash (RHA) and granular activated carbon (GAC): Parametric, kinetic, equilibrium and thermodynamic aspects , *Journal of Hazardous Materials* 154 (2008) 858–870
19. D. Mohan, K.P. Singh, S. Sinha, D. Ghosh, Removal of pyridine from aqueous solution using low cost activated carbons derived from agricultural waste materials, *Carbon* 42 (2004) 2409–2421.
20. Munaf, E., Zein. R., "The use of rice husk for removal of toxic metals from wastewater", (1997), *Environ. Technol.* 18 (3). 359 – 362 .
21. Roy, D., Greenlav, P.N Shane. B.S., "Adsorption of heavy metals by green algae and ground rice husks", (1993) *J. Environ. Sci. Health A* 28 (1) 37 (1) , 37 – 50.
22. Ajmal , M., Khan Rao, R.A., Anwar, S., Ahmed , J. Ahmad, R. "Adsorption studies on rice hunk : Removal and recovery of Cd (II) from wastewater", (2003), *Bioresource Technology* 86 (147 – 149).
23. Srinivasan, "Evaluation of rice husk carbon for the removal of trace inorganic from water", (1986), Ph.D. Dissertation, Indian Inst. Technol. Madras.
24. Daifullah, A.A., Girgis, B.S., Gad, H.M., "Utilization of agro-residues (Rice Husk) in small wastewater treatment plant Materials ", (2003) *letters* 57 (1723 – 1731).
25. Guo, Y. Qi, J, Yang, S., Yu, K., wong, Z., Xu. H., "Adsorption of Cr (VI) on micro – and mesoporous rice husk – based active carbon", (2002), *Materials and Physics* 87 (132 – 137)

26. M. Akhtar, M.I. Bhangar, S. Iqbal, S.M. Hasany, Sorption potential of rice husk for the removal of 2,4-dichlorophenol from aqueous solutions: kinetic and thermodynamic investigations, *J. Hazard. Mater.* 128 (2006) 44.
27. Shan-Li Wang, Yu-Min Tzoua, Yi-Hsien Lua, Guangyao Sheng "Removal of 3-chlorophenol from water using rice-straw-based carbon", *Journal of Hazardous Materials* 147 (2007) 313–318
28. Kumar, P., Dara, S., "Removal of toxic Heavy metal ions from wastewaters using modified agricultural waste materials", (1980), *Prog. Wat. Tech.* Vol. 13 Brighton (353 – 361)